POLITECNICO DI TORINO

Collegio di Ingegneria Chimica e dei Materiali

Master of Science Course
in Materials Engineering

Master of Science Thesis

3D printing of bioactive glass scaffolds for bone tissue repair

Tutors

Prof. Enrica Verné
Prof. Francesco Baino

Candidate

Jacopo Barberi

March 2018

Index

Sommario

1. Introduzione

Sin dall'inizio della sua storia, l'uomo ha cercato di sviluppare tecniche e materiali in grado di riparare, rigenerare o sostituire parti di corpo o organi affetti da malattie o traumi. In ambito ortopedico questo significa riuscire ad ottenere dispositivi che possono essere impiantati in zone di frattura o di difetto e che siano in grado di integrarsi nell'osso, legarsi al tessuto e sostenerlo durante il processo di guarigione. Materiali moto promettenti in questo campo sono i vetri bioattivi, che dal 2000 si sta cercando di utilizzare per la produzione di strutture tridimensionali porose, chiamate scaffold, che possano essere impiantate. Questa tesi ha come primo obbiettivo la fabbricazione di scaffold tramite la tecnica di *additive manufacturing* nota come *robocasting*, cercando di ottenere strutture con porosità adeguata alla rigenerazione ossea (≈100-200 μm), e la loro caratterizzazione. Successivamente è stata effettuata un'indagine sugli effetti della porosità sulle proprietà degli scaffold, specialmente sulla bioattività.

I vetri bioattivi appartengono alla seconda generazione dei biomateriali e sono stati sviluppati a partire dalla fine degli anni '70 grazie al lavoro di Larry Hench. I biomateriali sono definiti come "sostanze non viventi utilizzate nella fabbricazione di un dispositivo medico che presenta, in una qualche zona, un'interfaccia con tessuto vivente". Essi sono suddivisi in tre categorie, a seconda della loro interazione con il corpo umano:

- Prima generazione (1950-1975): sono i primi materiali scoperti e hanno la caratteristica di essere inerti rispetto all'ambiente fisiologico. Quindi sono progettati per non generare reazioni avverse dal corpo ma non riescono nemmeno a legarsi con i tessuti circostanti;
- Seconda generazione (1975-2000): sono materiali bioattivi, cioè sono in grado di modificarsi a contatto con il tessuto e di stimolare una reazione voluta da parte del corpo. Viene definito il concetto di bioattività come "l'abilità di un materiale di esercitare la sua funzione stimolando una risposta appropriata dal sistema vivente che lo ospita";
- Terza generazione (2000-oggi): il materiale è in grado di mandare segnali biochimici e biologici al corpo per stimolare una risposta specifica, essi sono in gradi di sostituire in modo funzionale il tessuto vivente.

I biovetri, assieme ad altri materiali come leghe metalliche, bioceramici e polimeri, sono utilizzati principalmente in campo ortopedico e presentano la capacità di legarsi saldamente all'osso circostante tramite la precipitazione di idrossiapatite sulla sua superficie.

L'idrossiapatite è un sale doppio di fosforo e calcio ($Ca_{10}(PO_4)_6(OH)_2$) e costituisce la parte minerale dell'osso umano, valendo per il 60% del peso dell'osso stesso. Le ossa umane sono un esempio di tessuto connettivo duro e presentano una complessa struttura gerarchica (**Fig. 2.1**). Quando queste vengono danneggiate in modo tale che la naturale funzione autorigenerativa dell'osso è compromessa, la chirurgia ortopedica moderna ricorre all'utilizzo di materiali sostitutivi, per rimpiazzare localmente l'osso e supportarne la guarigione. Esistono tre principali categorie di sostituti ossei: autograft (viene prelevato osso autologo, cioè dal paziente stesso, in una zona diversa da quella del danno e reimpiantato); allograft e xenograft (viene utilizzato osso estraneo al paziente, sia umano che non. Può dare problemi di rigetto e trasmissione malattie); impianto sintetico (viene impiantato un dispositivo realizzato in materiali sintetici, uno scaffold).

Gli scaffold sono dispositivi tridimensionali che hanno il compito di sostenere e incentivare la rigenerazione ossea. Per questo sono fatti in modo tale da imitare il più fedelmente possibile la struttura e le proprietà meccaniche dell'osso. I materiali utilizzati per la produzione di questi sostituti sono diversi. Oltre ai già menzionati biovetri, vengono utilizzati altri tipi di bioceramici, ad esempio idrossiapatite sintetica, e biopolimeri. Sono stati creati anche scaffold compositi ceramico-polimerici, per sfruttare le ottime caratteristiche di biocompatibilità dei bioceramici ma limitarne la fragilità grazie ai biovetri.

I vetri bioattivi sono tra i materiali più studiati per applicazioni di rigenerazione ossea. Infatti, grazie alla facilità con cui si può variarne la composizione, è possibile ottenere una grande variazione delle proprietà, sia per quanto riguarda la bioattività e altre funzioni espletabili all'interno del corpo umano, sia sul fronte del processo produttivo degli scaffold.

La bioattività dei vetri è fortemente legata alla struttura amorfa del reticolo vetroso e alla composizione, in particolare è fondamentale la presenza di ioni che possano facilmente diffondere fuori dal reticolo. I primi biovetri prodotti appartengono ai sistemi silicatici, in particolar modo al sistema SiO_2-Na_2O-CaO. I meccanismi di bioattività di questi vetri sono stati ampiamente studiati e sono basati principalmente sullo scambio ionico tra il vetro e l'ambiente biologico che lo circonda. È possibile andare ad identificare alcuni passaggi che avvengono sia in vitro, cioè immersi in soluzioni che mimano l'ambiente biologico, che in vivo:

- Scambio di cationi: il primo step è il rilascio di cationi da parte del vetro, in particolare cationi mono- e bivalenti (Ca^{2+} e Na^{+}), e l'assorbimento di ioni H^{+} dalla soluzione. Questo porta alla creazione di silanoli sulla superfice del vetro e all'aumento del pH;
- Rilascio di silice solubile: col procedere delle reazioni di scambio e della formazione di silanoli, unito all'aumento del pH, i legami ossigeno pontanti del vetro vengono attaccati e si assiste alla formazione di tetraedri di silice "slegati" ($Si(OH)_4$) che vengono disciolti in soluzione;
- Polimerizzazione della silice solubile: dato il gran numero di silanoli che si sono generati sulla superfice, avvengono reazioni di condensazione tra la superficie del vetro e i tetraedri di silice in soluzione. Ciò porta alla formazione di uno strato di gel di silice povero di ioni;
- Diffusione di Ca^{2+} e PO_4^{3-}: ioni calcio e fosforo diffondono nello strato di gel di silice, provenendo sia dal vetro sottostante che dall'ambiente circostante. Si forma uno strato di fosfato di calcio amorfo;
- Cristallizzazione di idrossiapatite: quando le concentrazioni di ioni calcio e fosforo nello strato amorfo raggiungono livelli adeguati, questo inizia a cristallizzare dando forma all'idrossiapatitie.

Ai passaggi osservabili in vitro se ne aggiungono e sovrappongo altri che avvengono solo se il biovetro è impiantato in un corpo vivente (**Tab. 2.2**).

I biovetri si possono suddividere in tre famiglie, a seconda dell'ossido formatore:

- Vetri silicati: sono stati i primi biovetri ad essere prodotti, a partire dal 45S5 Bioglass di Hench (45% SiO_2, 24,5% Na_2O, 24,5% CaO, 6% P_2O_5, mol%). L'ossido formatore utilizzato è la silice e principalmente vengono aggiunti ossidi di calcio, sodio e fosforo, per ottenere composizioni simili all'osso. Sono attualmente i vetri più studiati e utilizzati, principalmente perché rimangono i vetri più bioattivi tra quelli prodotti per fusione;
- Vetri fosfati: i vetri fosfati, ottenuti utilizzando il fosforo come ossido formatore, hanno la proprietà di essere completamente riassorbibili dall'organismo, grazie alla bassa stabilità del reticolo vetroso. Questo è molto allettante perché permetterebbe una completa rigenerazione del tessuto osseo, senza alcun residuo esterno;
- Vetri borati: i vetri borati o boro-silicati, ottenuti tramite sostituzione della silice con l'ossido di boro, presentano livelli di bioattività più alti rispetto a i vetri silicati e una velocità di conversione in idrossiapatite più alta. Inoltre, data la bassa temperatura di transizione vetrosa dei vetri borati, offrono vantaggi anche dal punto di vista di fabbricazione degli scaffold.

Oltre agli ioni classici (Si, Ca, Na, P), sono stati creati biovetri introducendo nel reticolo una moltitudine di altri ioni per ottenere o controllare diverse proprietà, ad esempio antibattericità (Ag, Cu) o angiogenesi (Cu, Co).

Per poter essere funzionali come materiali sostitutivi per l'osso, gli scaffold hanno la necessità di avere una struttura e delle proprietà il più simile possibile all'osso stesso, in modo che il corpo percepisca meno differenza possibile e che il tessuto possa rigenerarsi nella maniera corretta. Durante la progettazione di uno scaffold, bisogna tenere in conto delle seguenti caratteristiche:

- Biocompatibilità: è necessario che lo scaffold vada a stimolare una reazione appropriata del tessuto circostante, limitando al massimo i processi infiammatori che potrebbero portare alla

formazione di una capsula fibrosa e alla dislocazione della protesi stessa. Inoltre, il materiale dev'essere in grado di sopravvivere all'interno del corpo senza modificarsi, a meno che la modifica non sia voluta, come per gli scaffold bioriassorbibili. In caso di degradazione voluta dello scaffold, i prodotti di degradazione non devono essere nocivi per l'organismo;

- Struttura gerarchica e porosità: l'impianto deve riuscire a imitare al meglio la struttura dell'osso in cui viene impiantato, spesso l'osso trabecolare. Quindi bisogna riuscire ad andare a generare una struttura che presenta un'alta percentuale di porosità aperta, minimo il 40-50%, di dimensione variabile, dai 100 ai 300 μm circa. Questo consente all'osso di popolare in modo corretto le cavità. La presenza di mesoporosità può risultare utile per la diffusione di elementi nutritivi e per lo smaltimento dei prodotti di scarto delle cellule;
- Proprietà meccaniche: per il periodo in cui lo scaffold sostituirà l'osso è necessario che fornisca anche sostegno meccanico. Quindi gli scaffold, specialmente se pensati per l'utilizzo in zone che devono sostenere dei carichi, devono presentare proprietà meccaniche almeno pari a quelle dell'osso sano. Inoltre, l'osso è un tessuto meccano-recettivo, cioè risponde ai carichi esterni crescendo in base all'entità di essi. Quindi i suoi sostituti non possono avere proprietà troppo superiori all'osso stesso per non rischiare il riassorbimento dovuto a mancanza di stimolo meccanico:
- Proprietà di superficie: la superficie dello scaffold è il luogo principale di interazione tra l'impianto e il tessuto. Questa va ad avere una forte influenza sull'assorbimento di sostanze dai fluidi biologici e sulla conseguente adesione di cellule sulla superficie. Pertanto è necessario che la superficie abbia adeguate caratteristiche morfologiche e chimiche.

I primi tentativi di produzione di scaffold in vetri bioattivi risalgono al 2002 e le prime tecniche utilizzate sono state prese in prestito dal campo della fabbricazione di materiali ceramici cellulari. Da allora molteplici tecniche sono state messe a punto e, con l'avvento dell'additive manufacturing, il loro numero è incrementato ulteriormente. Le tecniche di fabbricazione degli scaffold si possono quindi dividere in due grandi rami: le tecniche tradizionali e le tecniche di prototipazione rapida (*additive manufacturing*) (**Tab. 3.1**).

All'interno delle tecniche tradizionali collocano diversi metodi molto usati:

- I metodi delle schiume: sono metodi che prevedono di ottenere la struttura porosa andando a generare una schiuma all'interno di uno *slurry* o una soluzione che vengono poi consolidate tramite trattamento termico. È possibile utilizzare questo metodo con uno *slurry* composto da polvere di vetro, tensioattivi e monomeri, da polimerizzare per fissare la schiuma ottenuta, oppure si può andare a schiumare una soluzione sol-gel, durante le reazioni di produzione del vetro per metodo sol-gel appunto.
- Consolidamento termico di particelle: in questa classe di tecniche vengono utilizzati dei trattamenti termici per consolidare, tramite sinterizzazione controllata, polveri di vetro pre-formate. In questi casi la porosità è ottenuta tramite controllo dell'avanzamento della densificazione oppure grazie all'uso di particelle porogene organiche che vengono mescolate assieme alle polveri e poi rimosse tramite *burning-out.*
- Replica di polimeri porosi: grazie alle tecniche odierne è possibile produrre delle spugne polimeriche con porosità facilmente controllabile e variabile, che risultano molto simili all'osso trabecolare. Infiltrando la spugna con uno *slurry* vetroso è possibile utilizzarla come templante per l'ottenimento di scaffold a struttura controllata. Si possono produrre materiali compositi o ceramici a seconda che la parte polimerica venga rimossa o meno.
- *Freeze-drying*: questi metodi di produzione prevedono l'utilizzo di cristalli di ghiaccio come formatori delle porosità, al posto di agenti porogeni organici. Una soluzione colloidale di particelle di vetro viene fatta congelare, dopo di che il solvente è rimosso tramite evaporazione, lasciando la struttura porosa. Alla fine le particelle vengono consolidate termicamente.

Le tecniche di *additive manuafcturing* sono estremamente invitanti per la realizzazione di scaffold data la loro estrema versatilità, sia nel controllo della microstruttura che della forma finale del dispositivo. Principalmente sono tecniche che prevedono la costruzione del prodotto *layer-by-layer*, cioè uno stato alla volta. Alcune di queste tecniche sono:

- *Selective laser sintering*: in questa tecnica viene utilizzato un fascio laser per sinterizzare localmente delle polveri. Viene preparato uno strato di polveri ceramico all'interno di un contenitore, quindi il fascio laser scansiona la superficie secondo il percorso voluto, scaldando e sinterizzando solo le polveri che ne vengono investite, formando il primo strato. Altre polveri vengono depositate su quelle già sinterizzate per aggiungere gli strati successivi.
- Stereolitografia: questo metodo, molto comune nella stampa 3D di polimeri, prevede di utilizzare un laser per far reticolare selettivamente delle resine polimeriche liquide, costruendo l'oggetto finale strato per strato. È possibile utilizzarlo per generare scaffold se si usa una miscela di polveri e resine polimeriche oppure utilizzando la tecnica per produrre modelli polimerici da infiltrare successivamente con *slurry* vetrosi.
- *Direct ink writing*: a questa famiglia appartengono diverse tecniche che sono basate sulla deposizione di inchiostri di diverso tipo. L'inchiostro può essere depositato sotto forma di goccia e può essere puramente polimerico, come nel *3D-printing*, oppure può essere una miscela di legante polimerico e polvere vetrosa, nel caso del *ink-jet printing*. Nel primo caso l'inchiostro, che è un legante, viene depositato su un letto di polveri per formare la struttura strato per strato, nel secondo l'inchiostro contiene già sia il legante che il vetro e la struttura viene formata dalla deposizione delle gocce. Il *robocasting*, tecnica utilizzata in questa tesi, prevede invece la deposizione di un filamento di inchiostro continuo, composto anch'esso da legante e polvere di vetro. La struttura dello scaffold risulta essere simile ad una serie di griglie sovrapposte.

1.1 2. Materiali e metodi

2.1 Produzione degli scaffold in vetro bioattivo

Per poter andare a fabbricare gli scaffold in biovetro tramite *robocasting* è stato necessario iniziare dalla preparazione delle materie prime come vetro e inchiostro e, successivamente, ottimizzare il processo produttivo. Dopo di che, gli scaffold sono stati caratterizzati dal punto di vista strutturale, meccanico e della bioattività in vitro.

Per la produzione di scaffold per la rigenerazione ossea, il primo passaggio è stata la scelta della composizione del vetro. Si è usato il vetro denominato 47.5B, sviluppato al Politecnico di Torino, e appartenente al sistema SiO_2-P_2O_5-CaO-MgO-K_2O-Na_2O, la composizione è riportata in **Tab. 4.1**. È stato scelto questo vetro per la sua comprovata bioattività e per la presenza dell'ossido di magnesio che incrementa la lavorabilità, andando ad aumentare la differenza tra la temperatura di transizione vetrosa e quella di cristallizzazione.

L'inchiostro per la stampa 3D è composto da una miscela di polvere di vetro e legante polimerico. Perciò la prima fase del lavoro è stata incentrata sull'ottenimento delle polveri con dimensioni volute (<32 μm). Il vetro è stato ottenuto tramite fusione di ossidi precursori e colata in acqua distillata per ottenere una fritta di vetro, facile da macinare. La fritta così ottenuta è stata poi macinata utilizzando un macinatore a palla singola in zirconia. Infine le polveri sono state setacciate per ottenere la taglia richiesta. Quelle troppo grandi sono state rimacinate e in seguito rifuse, per poter ottenere efficienze di macinazione accettabili.

Il processo di stampa avviene tramite l'uso di una stampante che presenta una testa a cui viene assicurata la cartuccia con l'inchiostro e una base metallica su cui viene appoggiato il substrato utilizzato per stampare gli scaffold. Per ottenere un processo di stampa stabile e preciso è necessario ottimizzare diversi parametri, la composizione dell'inchiostro è stato il primo ottimizzato.

L'inchiostro è composto da una miscela tra polveri di vetro e una soluzione acquosa di Pluronic F-127, che funge da legante. Il Pluronic è un copolimero a blocchi che presenta un comportamento termoreversibile. Infatti a basse temperature, attorno a 0°C, la sua viscosità è estremamente bassa, infatti si presenta allo stato liquido, mentre ad alte temperature, circa 40°C, gelifica. Inoltre ha comportamento pseudoplastico. Questo comportamento peculiare viene sfruttato per avere facilità nella fabbricazione dell'inchiostro, mescolando legante e vetro a basse temperature, ma per ottenere buona resistenza durante il processo di stampa, evitando il collasso della struttura. Il comportamento da fluido non newtoniano favorisce l'estrusione dall'ugello della stampante.

La composizione dell'inchiostro, cioè il rapporto volumico tra vetro e soluzione di F-127 e la concentrazione di Pluronic nella soluzione stessa, è stata ottimizzata per ottenere un inchiostro lavorabile ma resistente, per mantenere le caratteristiche strutturali volute. La preparazione dell'inchiostro prevede di miscelare, utilizzando un agitatore a vortice, le polveri di vetro e la soluzione di Pluronic raffreddata in una boccetta. Una volta ottenuto un composto omogeneo e dopo aver rimosso il più possibile l'aria intrappolata, l'inchiostro viene trasferito nella cartuccia di stampa con l'ausilio di una siringa.

Quando l'inchiostro è pronto si può procedere al processo di stampa. La cartuccia viene caricata sulla macchina e collegata ad una linea che porta l'aria compressa utilizzata per spingere lo stantuffo della siringa e estrudere l'inchiostro. La pressione dell'aria è un parametro fondamentale per ottenere un buon risultato finale. Infatti una pressione troppo elevata porta all'estrusione di troppo materiale e alla formazione di linee ingrossate che chiudono le porosità più piccole, mentre pressioni troppo basse, e un conseguente scarso flusso di inchiostro, generano filamenti sottili che tendono a rompersi. Anche la velocità relativa tra la testa e la base ha un effetto importante, simile a quello della pressione. Se la velocità è troppo elevata il filamento viene allungato, assottigliandosi fino a rompersi. Se è troppo bassa viene depositato un eccesso di materiale e le linee si ingrossano. Quando la pressione e la velocità sono state impostate la stampa degli scaffold può essere avviata e l'ugello depone il filamento seguendo un percorso che viene definito tramite un codice. La struttura finale dello scaffold dipende dal programma impostato, per quanto riguarda la disposizione dei filamenti sul piano orizzontale, mentre l'altezza dei filamenti, quindi quella dei pori, è dettata dal diametro dell'ugello che definisce quello del filamento stesso. Durante questo lavoro sono stati prodotti scaffold con due strutture differenti, uno con porosità costante, ottenuta deponendo filamenti dritti a distanza costante, e uno con gradiente di porosità, ottenuta infittendo le linee nella parte centrale dello scaffold. Il percorso del filamento è rappresentato in **Fig. 4.11**. Entrambi sono stati stampati utilizzando un ugello di diametro 410 μm.

Finito il processo di stampa gli scaffold sono lasciati asciugare e poi vengono sinterizzati per un'ora a 600°C. La rampa termica di salita prevede degli step a temperatura costante per ottenere la rimozione del legante polimerico.

2.2 Caratterizzazioni

Le caratterizzazioni sono state fatte in due momenti distinti, all'inizio, sui materiali di partenza, specialmente sul vetro, per ottenere informazioni utili all'ottimizzazione del processo produttivo, e alla fine, dopo aver prodotto gli scaffold, per valutarne le proprietà sotto i punti di vista utili per applicazioni ortopediche. Una visione di insieme di tutte le caratterizzazioni effettuate è presente in **Tab. 4.5**.

Il vetro è stato caratterizzato per valutarne le proprietà termiche e la morfologia delle polveri ottenute. Inoltre ne è anche stata misurata la densità per poter ottenere l'inchiostro. Sulle polveri di vetro sono state quindi effettuate analisi al microscopio elettronico per avere indicazioni sulla forma e sulle dimensioni delle particelle. Contestualmente è stata effettuata un'analisi composizionale tramite EDS per avere conferma della composizione. La presenza di una struttura completamente amorfa è stata indagata tramite diffrazione di raggi X (XRD).

Per poter ottimizzare il processo di sinterizzazione, ma comunque evitando la formazione di fasi cristalline all'interno del materiale, è stato necessario effettuare un accurata caratterizzazione termica del vetro. Informazioni di base sono state acquisite effettuando analisi di calorimetria differenziale (DSC) a scansione e microscopio riscaldante (HSM), mentre informazioni più precise sul comportamento dopo trattamenti ad alta temperatura sono stati ottenuti tramite analisi DSC e XRD sequenziali. Il materiale è stato trattato per un'ora a diverse temperature, ogni 10°C tra 560°C e 640°C, e per ogni trattamento è stata eseguita un'analisi DSC e una XRD. Questo ha permesso di valutare il comportamento di cristallizzazione del vetro e di individuare la corretta temperatura di sinterizzazione.

Dopo che gli scaffold sono stati prodotti ne è stata analizzata la struttura, sono state valutate le proprietà meccaniche e la bioattività. La morfologia dei due tipi di scaffold, quello con gradiente di porosità e quello con porosità costante, è stata valutata tramite analisi al microscopio ottico, al microscopio elettronico e tramite indagini svolte utilizzando tecniche di micro-tomografia computerizzata (micro-CT). La porosità totale degli scaffold è stata misurata sia utilizzando l'analisi micro-CT che il metodo empirico delle densità.

Un'indagine preliminare delle proprietà meccaniche è stata effettuata per capire se gli scaffold prodotti in questo modo possono essere adatti per la rigenerazione di porzioni d'osso soggette a carichi. Perciò gli scaffold di entrambe le tipologie sono stati testati a compressione. Inoltre, è stato testato un numero sufficientemente elevato (20) di scaffold con gradiente di porosità da calcolare il modulo di Weibull. Ciò è utile per avere un'indicazione della riproducibilità dell'intero processo di produzione, in particolare della fase di preparazione dell'inchiostro, la più critica essendo la meno automatizzata.

Infine è stata testata la bioattività in vitro per valutare eventuali differenze tra le due diverse strutture. Gli scaffold sono stati immersi in SBF per tempi variabili (6h, 24h, 48h, 72h, 1 e 2 settimane) per valutare il rilascio ionico da parte dei campioni. La concentrazione degli ioni in soluzione è stata determinata tramite spettroscopia ad emissione atomica con sorgente al plasma accoppiato induttivamente (ICP-OES). Di interesse è anche l'evoluzione del pH della soluzione. Scaffold prelevati dopo diversi tempi di immersione sono stati analizzati tramite SEM per valutare l'evoluzione morfologica del campione, la formazione dello strato di gel di silice e la precipitazione di apatite sulla superficie delle trabecole. L'analisi EDS, eseguita contemporaneamente, è servita per evidenziare il rilascio ionico del campione e per valutare la composizione dell'idrossiapatite formatasi. L'evoluzione dello strato superficiale dello scaffold e la precipitazione di apatite sono anche state osservate tramite analisi XRD. Inoltre, altri campioni sono stati immersi in SBF per 2 e 4 settimane e successivamente testati a compressione per valutare l'evoluzione delle proprietà meccaniche nel tempo.

1.2 3. *Risultati e discussione*

Le polveri di vetro ottenute dopo la setacciatura, operata utilizzando setacci con una mesh a 32 μm, sono state analizzate al microscopio elettronico per ottenere informazioni sulla morfologia e la taglia delle particelle. Si è visto che le particelle presentano un'ampia distribuzione dimensionale, dai 32 μm fino a particelle submicrometriche. Inoltre hanno forme irregolari ma abbastanza equiassiali, come si può vedere in **Fig. 5.1**. Questo tipo di distribuzione dimensionale è utile da inserire nell'inchiostro per *robocasting* in quanto assicura un migliore impacchettamento delle particelle ed una migliore scorrevolezza del composto all'interno dell'ugello. Le analisi composizionali hanno confermato che la composizione ottenuta è coerente con quella nominale e non ci sono zone di disomogeneità. La struttura appare completamente amorfa.

La densità è stata misurata pari a 2.640±0.002 g/cm^3, in linea con i vetri che non presentano elementi pesanti al loro interno.

Le analisi termiche sono state condotte per ottenere le informazioni necessarie ad ottenere scaffold completamente amorfi dopo il trattamento di sinterizzazione. Grazie all'analisi DSC è stato possibile ottenere le temperature caratteristiche del vetro, quali temperatura di transizione vetrosa, onset di cristallizzazione, picco di cristallizzazione e temperatura di fusione. I risultati ottenuti sono in buon accordo con quelli presentati da Vernè et al. nell'articolo di presentazione di questa particolare composizione di vetro bioattivo e sono riportati in **Tabella 1**.

Tabella 1 Temperature caratteristiche del vetro 47.5B

Transizione vetrosa (T_g)	**Onset di cristallizzazione (T_x)**	**Picco di cristallizzazione (T_c)**	**Fusione (T_m)**
547°C	760°C	806°C	1004°C

Informazioni sul comportamento del materiale dal punto di vista del ritiro durante trattamento termico sono state acquisite tramite il microscopio riscaldante. La curva ottenuta, presentata in **Fig. 5.4**, non presenta il plateau che di solito indica il raggiungimento del massimo ritiro, che precede la fusione del campione. Le ipotesi sviluppate per spiegare questo fatto sono due. L'assenza del plateau può essere dovuta ad una lenta cinetica di cristallizzazione, rispetto alla rampa di temperatura. Questo comporta che i cristalli che si formano non sono abbastanza grandi da fermare il flusso viscoso delle particelle e quindi il ritiro del campione. L'altra ipotesi è legata alla grande distribuzione dimensionale delle particelle. La dimensione delle particelle influenza il comportamento durante il riscaldamento. Particelle più piccole presentano eventi come la cristallizzazione e la fusione a temperature minori rispetto a

particelle più grandi. È possibile che le particelle più piccole, submicrometriche, fluiscano quando le grandi raggiungono il massimo ritiro, causando un ritiro continuo del materiale nella sua totalità. È comunque possibile ricavare le temperature associate a determinati valori di viscosità (primo ritiro, rammollimento, sfera, mezza sfera e fusione) grazie all'analisi dell'evoluzione della forma del campione. I risultati sono elencati in **Tab. 5.3**.

Dal confronto tra i dati ricavati dalla DSC e quelli ricavati dal HSM è possibile andare ad individuare un intervallo in cui ricercare la giusta temperatura di sinterizzazione, all'incirca tra la T_g e la temperatura di rammollimento.

Per assicurare l'ottenimento di scaffold vetrosi completamente amorfi, il comportamento di cristallizzazione del vetro è stato indagato ulteriormente tramite simulazioni del processo di sinterizzazione a temperature diverse e successiva analisi con DSC. Le analisi sono state condotte su campioni trattati termicamente per un'ora a: 560°C, 570°C, 580°C, 590°C, 600°C, 610°C, 620°C, 630°C, 640°C. Dall'analisi delle curve ottenute (**Fig. 5.6**) si può notare come, sin dai trattamenti a basse temperature, si formi una seconda fase basso-fondente ma che non ci siano effetti sulla temperatura di transizione vetrosa. Dall'analisi dell'area sotto il picco di cristallizzazione, che è inversamente proporzionale alla quantità di materiale che è cristallizzato durante il trattamento termico, si può notare come la cristallizzazione rimane praticamente invariata fino ai trattamenti a più alta temperatura, 630°C e 640°C. La cristallizzazione rimane comunque abbastanza bassa da non essere rilevata da analisi condotte mediante XRD, i quali spettri non presentano picchi (**Fig. 5.8**). Grazie a questo tipo di analisi è possibile anche ottenere informazioni riguardo all'andamento della velocità di nucleazione, osservando la variazione della temperatura del picco di cristallizzazione. Infatti è possibile costruire una curva che ha lo stesso andamento della velocità di nucleazione utilizzando il metodo Marotta e plottando $[(1/T_c-1/T_c^0)]$, dove T_c è la temperatura di cristallizzazione dopo il trattamento e T_c^0 quella del vetro tal quale, rispetto alla temperatura di trattamento. Dal grafico ottenuto (**Fig.5.7**) si deduce che il massimo della velocità di nucleazione si raggiunge a 600°C.

Tenendo conto di tutte le informazioni ricavate dalle analisi termiche, è stato deciso di sinterizzare gli scaffold a 600°C. Il valore è conservativo ed è stato scelto per avere la certezza di ottenere scaffold completamente vetrosi, anche se altre proprietà, come quelle meccaniche, possono risentirne.

Dopo la caratterizzazione delle polveri di vetro è stato necessario, prima di procedere alla stampa vera e propria degli scaffold, ottimizzare il processo di *robocasting*, iniziando dalla messa a punto della composizione dell'inchiostro. Sono stati provati diversi inchiostri, in termini di rapporto volumico vetro/soluzione di F-127 e diverse concentrazioni di Pluronic in soluzione. I diversi inchiostri sono stati valutati in base a due differenti parametri:

- Processabilità: questo parametro valuta la facilità di preparazione dell'inchiostro stesso, riguardo alla fase di mescolamento dei componenti e alla rimozione dell'aria. La processabilità aumenta al diminuire della frazione vetrosa e della concentrazione di F-127;
- Forza dell'inchiostro: la forza dell'inchiostro è definita come la capacità del filamento di rimanere diritto e non curvarsi sopra lo spazio tra due filamenti dello strato sottostante. Serve una forza elevata per mantenere una struttura regolare. Inoltre limita la deformazione delle trabecole dovute al peso dello scaffold stesso. La forza è proporzionale alla quantità di vetro e di Pluronic all'interno della soluzione.

La composizione degli inchiostri provati è la seguente (espressa in forma XX-YY, con XX frazione volumica di vetro e YY concentrazione di legante in soluzione): 30-25, 35-25, 30-30, 35-30, 35-27.5. La scelta è ricaduta sul 35-27.5, in quanto offriva il miglior compromesso tra processabilità e forza.

Una volta scelto l'inchiostro si è proceduto alla definizione dei parametri di stampa, quali pressione, velocità di scansione e progettazione del disegno degli scaffold. Pressione e velocità vanno aggiustate contemporaneamente, dato che agiscono in modo analogo sulla struttura finale e dipendono dalla viscosità dell'inchiostro, mentre il progetto, in particolar modo la distanza tra i filamenti, dipende dal ritiro del vetro durante sinterizzazione. Poiché l'inchiostro è molto sensibile a parametri come umidità e temperatura, che non sono stati controllabili durante il lavoro, le condizioni ottimali di stampa variano leggermente da sessione a sessione a causa della variazione di viscosità. Questo implica che prima di poter stampare gli scaffold è necessario fare qualche tentativo per trovare i settaggi giusti. Dato che la

velocità di scansione è inclusa nel codice di progetto, non è facilmente modificabile quindi viene fissata. La pressione, invece, è facilmente controllabile e si agisce su di essa per trovare le giuste condizioni per procedere ad una stampa regolare e continua. Per la produzione degli scaffold si è usata una velocità pari a 2 mm/s e una pressione variabile tra 18 e 22 psi.

Per ottenere la porosità di dimensione voluta sono state effettuate diverse prove, variando la distanza di deposizione tra i filamenti e poi misurando il risultato finale dopo sinterizzazione. La distanza è stata calcolata valutando anche lo spessore del filamento stesso. È risultato che per ottenere pori "grandi" (≈200 μm) la distanza tra filamenti dev'essere di 636 μm, mentre per i pori "piccoli" (≈100 μm) è stato necessario ridurre lo spazio a 510 μm. Le dimensioni finali dei particolari degli scaffold sono state valutate tramite microscopia ottica, misurando pori e filamenti su diversi scaffold. È stato valutato anche il ritiro dopo sinterizzazione. I risultati sono riportati in **Tabella 1**.

Tabella 2 Dimensioni e ritiro degli elementi che compongono lo scaffold

Elementi	**Dimensioni (media, μm)**	**Deviazione standard (μm)**	**Ritiro**
Larghezza pori "grandi"	213	24	13.6%
Larghezza pori "piccoli"	119	15	20.4%
Altezza pori	248	17	25.2%
Diametro filamenti	280	11	-

La bassa deviazione standard conferma che il *robocasting* permette di ottenere buon controllo sulle dimensioni finali dell'oggetto. Come ci si aspettava, il ritiro verticale è maggiore rispetto a quelli rilevati in direzione orizzontale a causa del peso dello scaffold stesso. Il maggiore ritiro rilevato per i pori più piccoli è una possibile conseguenza della maggior densità di filamenti, che porta ad avere un maggior numero di punti di contatto che permettono un maggiore flusso di materia durante la sinterizzazione.

La struttura finale degli scaffold si mostra molto regolare e, nello scaffold a gradiente di porosità, il cambio di dimensione dei pori è molto evidente (**Fig. 5.18-19**)

Studi più approfonditi della struttura, eseguiti tramite microscopio ottico, hanno evidenziato la grande regolarità delle strutture ottenute, con filamenti diritti e pori di forma e dimensione simili. Osservazioni al microscopio elettronico hanno permesso di studiare la microstruttura degli scaffold, investigando il processo di sinterizzazione. È stato così osservato che sono stati prodotte due serie scaffold con microstrutture diverse, in tempi diversi, anche le condizioni nominali di processo sono rimaste invariate durante tutto l'arco temporale in cui è stato svolto il lavoro. Queste differenze possono essere attribuite a diversi fattori di errore (difetti nei materiali di partenza, errore nella preparazione dell'inchiostro, problemi con i forni) ma purtroppo non c'è stato il tempo di investigare a fondo la questione o di ripreparare gli scaffold appartenenti ad una delle due serie. Per poter comparare le proprietà degli scaffold tra le varie strutture, 47.5B-G e 47.5B-M, i diversi test sono stati effettuati su scaffold provenienti dalla stessa serie.

La prima serie presenta un basso livello di sinterizzazione, la superficie delle trabecole è irregolare e le singole particelle sono abbastanza distinguibili e si forma una rete di microporosità all'interno delle trabecole. Comunque si nota la presenza di colli di sinterizzazione e i filamenti sono ben saldati nei punti di intersezione tra strati diversi (**Fig. 5.23-24**). La scarsa densificazione ha un sicuro effetto negativo sulle proprietà meccaniche, ma può avere degli effetti positivi sull'aspetto biologico, fornendo punti di ancoraggio per le cellule, esponendo una superficie maggiore ai fluidi biologici e favorendo la diffusione di nutrienti e prodotti di scarto grazie alla rete di micropori.

Nella seconda serie è stato evidenziato un livello di sinterizzazione decisamente più alto, che porta ad avere trabecole lisce e molto dense. Le particelle non sono più distinguibili (**Fig. 5.27**). Questo secondo tipo di microstruttura migliora le proprietà meccaniche ma perde gli aspetti biologici positivi della prima serie.

La porosità risultante non è particolarmente alta, circa 50%, è diversa tra scaffold con lo stesso tipo di struttura, monoporosa o a gradiente, ma derivanti da serie diverse (**Tab. 5.7**), infatti la struttura più densa porta ad una diminuzione della porosità totale. Ciò nonostante, i livelli di porosità raggiunti in ogni scaffold sono accettabili per applicazioni di rigenerazione ossea.

Analisi chimiche condotte tramite EDS hanno dimostrato che non ci sono differenze composizionali tra le due serie di scaffold e che la loro composizione rispecchia quella ottenuta per le polveri.

Analisi grafica ottenuta tramite micro-CT ha confermato l'ottenimento di una struttura molto regolare e le dimensioni e le porosità calcolate con gli altri metodi.

Per valutare possibili applicazioni di sostituzione ossea in zone soggette a carico è stata effettuata una caratterizzazione preliminare delle proprietà meccaniche, effettuando un test di compressione lungo l'asse verticale degli scaffold. Inoltre è stato valutato il modulo di Weibull degli scaffold con gradiente di porosità della prima serie. Questo serve ad avere un'idea della riproducibilità del processo.

La resistenza a compressione degli scaffold della prima serie del tipo 47.5B-G è stata valutata testando 20 scaffold. La media dei valori di resistenza è pari a 6.05 MPa (deviazione standard= 2.85 MPa). La tipica curva sforzo-deformazione che è stata ottenuta (**Fig. 5.33**) presenta la forma tipica dei solidi ceramici cellulari. Infatti presenta numerosi picchi ad intensità diverse ed è una curva larga. Questo è riconducibile ad un meccanismo di frattura che prevede la rottura in diversi momenti e a diversi carichi delle trabecole più deboli, fino ad arrivare alla rottura di quelle più resistenti e al cedimento finale, che comunque non avviene mai di schianto.

Grazie all'alto numero di campioni testati è stato possibile valutare anche il modulo di Weibull, interpolando con il metodo dei minimi quadrati la curva ottenuta applicando l'equazione **4.11** (**Fig. 5.34**). Questi calcoli sono stati effettuati con lo scopo di valutare la repetibilità del processo produttivo, un processo altamente riproducibile dovrebbe portare ad una bassa distribuzione della resistenza meccanica. Il modulo risultante è pari a 3.139. Non è un valore elevato, frutto dell'alta dispersione di risultati ottenuti, anche se nessuno scaffold ha presentato resistenze inferiori rispetto a quelle riportate per l'osso trabecolare. Il basso modulo di Weibull è dovuto al basso livello di densificazione presentato dalle trabecole degli scaffold appartenenti alla prima serie, che lascia un gran numero di difetti, ma è anche legato al processo produttivo. Infatti se l'aria non è ben rimossa dall'inchiostro porta alla formazione di difetti di dimensione e distribuzione completamente casuale all'interno dei filamenti. Questi difetti non possono essere rimossi per sinterizzazione, date le loro dimensioni. Quindi la resistenza meccanica degli scaffold e la riproducibiltà del processo possono essere aumentati migliorando la rimozione dell'aria dall'inchiostro, magari con l'ausilio di strumentazione, come riportato in letteratura.

Per quanto riguarda gli scaffold monoporosi, a causa dei problemi relativi alla produzione, è stato possibile testare solo scaffold appartenenti alla seconda serie. La resistenza media ottenuta è pari a 9.94 MPa (deviazione standard= 4.65 MPa) e le curve sforzo deformazione sono simili a quelle ricavate dai test degli scaffold 47.5B-G della prima serie, suggerendo che il meccanismo di frattura non viene modificato. Non è possibile un confronto con gli scaffold testati precedentemente in quanto è possibile che la maggior resistenza sia frutto della maggior densificazione e non dovuta al diverso disegno della porosità. Scaffold a gradiente appartenenti alla seconda serie sono stati testati per valutare eventuali differenze di resistenza, ma la distribuzione dei valori è risultata troppo ampia per poter fare affermazioni in merito.

La bioattività degli scaffold è stata testata tramite immersione in SBF e valutazione della precipitazione dello strato di idrossiapatite sulle trabecole degli scaffold. Uno dei principali punti di interesse di questa tesi è la valutazione dell'influenza della porosità, monodistribuita o a gradiente, sulla bioattività del materiale. Per poter far confronti tra i due tipi di scaffold, 47.5B-G e 47.5B-M, i test sono stati eseguiti su campioni provenienti dalla prima serie.

La crescita dello strato di apatite è stata valutata tramite analisi XRD e osservazioni SEM e micro-CT dei campioni ottenuti immergendo gli scaffold in SBF per tempi diversi. Gli spettri di diffrazione di entrambe i tipi di scaffold, 47.5B-G e M, presentano un'evoluzione simile al crescere del tempo, che comporta la scomparsa dell'alone amorfo tipico dei vetri (intorno alla posizione $2\theta=30°$) e la comparsa

dei picchi tipici dell'idrossiapatite: il picco principale a 2θ=31.795°, per il piano cristallino (2 1 1), e quello a 2θ=25.689, riferito al piano (0 0 2)(**Fig. 5.36-37**).

Un'indagine più approfondita del meccanismo di bioattività degli scaffold è stata possibile congiungendo analisi SEM, micro-CT ed EDS. Per ogni tempo di immersione la superficie degli scaffold è stata analizzata morfologicamente e chimicamente (SEM+EDS) e su campioni immersi per due settimane è stata eseguita l'analisi micro-CT.

Il comportamento dei due diversi tipi di porosità è risultato essere molto simile, in termini di precipitazione (**Fig. 5.38-44**). Dopo sei ore si vede la formazione del gel di silice sulla superficie delle trabecole, l'EDS mostra una netta diminuzione della concentrazione di tutti gli elementi del vetro ad eccezione del silicio (**Fig. 5.43-48**). A 24 ore si assiste alla precipitazione di cristalli Ca-P amorfi, che poi si trasformano in idrossiapatite cristallina, e alla formazione dei primi cristalli aciculari di apatite. La superficie delle trabecole, a questo punto, è composta solo da silicio, calcio e fosforo. Da 72 ore ad una settimana si assiste alla crescita dei cristalli globulari di apatite che assumono la caratteristica forma a cavolfiore. Dopo una settimana le trabecole appaiono completamente rivestite da uno spesso strato di idrossiapatite che riduce la dimensione delle porosità. L'analisi composizionale rileva solo Ca e P. I campioni a due settimane, invece, presentano uno strato di apatite molto più sottile e discontinuo, le trabecole hanno dimensioni analoghe a quelle degli scaffold non trattati. Anche l'EDS conferma il poco spessore dello strato depositato, infatti è tornato ad essere presente il picco del silicio, che proviene dagli strati immediatamente sottostanti all'idrossiapatite. Questa riduzione dello spessore può essere dovuta ad una de coesione dello strato di apatite, che avviene tra la prima e la seconda settimana di immersione. Questo può essere dovuto a due fattori concomitanti: l'azione del flusso di SBF che può rimuovere lo strato depositato e il raggiungimento di uno spessore critico che rende fragile l'apatite cresciuta sui filamenti. L'analisi micro-CT mostra che le trabecole dello scaffold, dopo due settimane, non sono inspessite e presentano due fasi, una meno densa (parte strato esterno del filamento), composta da gel di silice e idrossiapatite che presenta una bassa densità apparente a causa della morfologia nanoporosa, e una più densa (parte interna del filamento), riconducibile al vetro. La densità apparente dell'idrossiapatite, comunque, tende ad aumentare con il procedere della cristallizzazione, come osservato in letteratura. I filamenti presentano tre diverse strutture ben localizzate all'interno dello scaffold. Sulla parte alta di entrambi i campioni sono presenti trabecole completamente composte da gel di silice e con un sottile rivestimento di apatite. Sui lati invece ci sono trabecole ben convertite in gel di silice ma con uno spesso strato di rivestimento. Le parti centrali e inferiori di entrambi i tipi di campione presentano invece strutture prevalentemente vetrose, con un basso grado di conversione in gel. Tutto questo suggerisce che la circolazione della soluzione all'interno degli scaffold è molto limitata, senza differenze tra le due strutture. Dove la SBF può fluire senza difficoltà, cioè negli strati superiori, si nota una grande conversione degli scaffold ma un sottile strato di apatite. Questo conferma la teoria di una rimozione dell'idrossiapatite depositata. Le zone laterali e inferiori dello scaffold, invece, sono state protette dal flusso violento di apatite dalle pareti e dal fondo del contenitore.

È stata valutata l'evoluzione del rapporto atomico Ca/P dello strato precipitato, per stabilire se l'apatite formatasi rispettasse o meno il rapporto stechiometrico. In entrambe le tipologie di campioni si è visto un incremento del rapporto ma che comunque non raggiunge il valore standard di 1.67 (**Tab. 5.11-12**).

La bioattività degli scaffold è stata valutata anche rispetto al rilascio di ioni in soluzione, durante il tempo di immersione. Per entrambe le tipologie di scaffold si sono misurate le concentrazioni di Si, Ca, P, K, Na e Mg a diversi tempi di immersione. Si è visto come, al netto di eventuali precipitazioni dovute all'instabilità del SBF, l'andamento della concentrazione di tutti gli ioni è coerente con studi precedenti che confermano la conversione del vetro in gel di silice e la precipitazione di apatite. Infatti, ioni di Si, Mg e K presentano un aumento della concentrazione, segno che vengono rilasciati dal vetro, mentre Ca e P diminuiscono col passare del tempo a causa della precipitazione di idrossiapatite (**Fig. 5.50**). Anche l'aumento del pH conferma la reattività della superficie delle trabecole, in quanto è dovuta al passaggio di ioni H^+ dalla soluzione al vetro. Così come durante le osservazioni morfologiche, anche queste analisi non hanno riscontrato differenze significative nel comportamento dei due diversi tipi di porosità. Ciò è legato alla scarsità di flusso di SBF all'interno degli scaffold, dove le due strutture sono diverse. La parte interessata dalle reazioni di scambio e precipitazione è principalmente quella esterna di entrambe i tipi di scaffold, che è molto simile in termini di dimensioni di porosità.

Infine sono stati testati a compressione scaffold dopo un lungo periodo di immersione, 2 e 4 settimane. Questo è necessario per valutare se l'impianto è in grado di fornire sostegno meccanico all'osso durante tutto il processo di rigenerazione. Anche queste prove sono state affette da una grande variabilità di risultati che non ha permesso di trarre nessuna valutazione quantitativa né in merito alla diminuzione della resistenza meccanica né in merito ad eventuali differenze tra gli scaffold 47.5B-G e i 47.5B-M. Ciò nonostante è stato rilevato un cambio nel comportamento dei materiali, infatti si è assistito ad un infragilimento degli scaffold. Le curve ottenute non presentavano più la forma allargata e con molti picchi, ma si sono ristrette e il loro andamento è diventato più regolare e lineare (**Fig. 5.52**). Questo è in accordo con la letteratura presente

1.3 4. Conclusioni e prospettive future

Gli obbiettivi di questa tesi erano di produrre scaffold per la rigenerazione ossea completamente amorfi e di valutare la possibilità di controllare la porosità al più piccolo livello richiesto per queste applicazioni (100 μm), oltre che l'ottenimento di strutture con diversa distribuzione dimensionale dei pori. Infine si è cercato di ottenere indicazioni dell'effetto della porosità sulle proprietà degli scaffold.

L'iniziale caratterizzazione del vetro utilizzato, il 47.5B, ha mostrato come questa particolare composizione sia ottimale per la produzione di oggetti amorfi, anche dopo sinterizzazione. Infatti è stato evidenziato come ci sia un buon range di temperature che possono essere utilizzate per consolidare gli scaffold senza che insorga cristallizzazione del vetro.

È stato dimostrato che è possibile ottenere porosità molto ridotte con un processo più semplice di quelli presenti in letteratura. Risultati simili sono stati ottenuti utilizzando polveri ultra fini (<1 μm), complessi set-up delle stampanti per *robocasting* e ugelli molto piccoli (100-200 μm). Le polveri sfruttate durante questo lavoro sono facilmente ottenibili tramite macinazione a palla, mentre l'utilizzo di ugelli grandi (410 μm) rende più continuo il processo, rendendone più difficile l'ostruzione. Queste semplificazioni sono importanti in vista di una futura industrializzazione del processo di produzione degli scaffold. Il metodo di produzione degli scaffold, utilizzato durante lo sviluppo di questa tesi, può comunque essere migliorato, in particolare durante la produzione dell'inchiostro, aumentando la rimozione dell'aria.

Le analisi morfologiche degli scaffold prodotti hanno mostrato come il processo di *robocasting* consente di ottenere una grande ripetibilità dimensionale ed un accurato controllo. Due tipi di scaffold sono stati prodotti, con porosità di dimensioni 100 e 200 μm. Una tipologia di scaffold presenta un'unica taglia di porosità, (≈200 μm), mentre l'altra presenta un gradiente, in quanto al centro è presente porosità più piccola (≈100 μm) e all'esterno più grande (≈200 μm). L'osservazione della microstruttra ha evidenziato come due serie di scaffold siano state prodotte. La prima serie, la più prodotta, mostra come le particelle siano poco sinterizzate, sono ancora distinguibili e unite solo da colli. Inoltre presentano una rete di vuoti interconnessi tra loro. La seconda serie, prodotta durante le ultime sessioni di stampa, mostra invece un elevato livello di sinterizzazione, dove le particelle sono completamente fuse tra loro. Questa seconda serie può essere il frutto di errori durante la produzione.

L'ottenimento di elevate proprietà meccaniche non era tra i principali obbiettivi del lavoro, ma sono comunque state valutate. La resistenza complessiva degli scaffold (6-9 MPa) si è rivelata paragonabile al quella dell'osso trabecolare. Il modulo di Weibull (m=3.139), collocato al limite inferiore del range di valori disponibili in letteratura, mostra come il processo non presenti un elevata riproducibilità dal punto di vista delle proprietà meccaniche. Pertanto, l'amplia distribuzione di risultati non ha permesso di poter stabilire eventuali differenze tra le varie tipologie di scaffold, legate alla differente porosità.

La bioattività degli scaffold è stata testata per valutare eventuali diversità causate dalla distribuzione della porosità. Le analisi morfologiche e chimiche della superficie degli scaffold, dopo immersione in SBF, non hanno evidenziato differenze tra i due tipi di campioni. Entrambi si sono mostrati altamente bioattivi, con buona conversione del vetro in gel di silice a tempi brevi e successiva precipitazione di uno strato di apatite sulla superficie. Queste osservazioni hanno però evidenziato come però si sia registrato flusso di SBF solo nella parte esterna degli scaffold, mentre nella zona centrale, dove è più marcata la differenza, le interazioni vetro-soluzione siano state molto limitate.

Le analisi della concentrazione di ioni rilasciati dagli scaffold (Ca, P, Si, K, Mg) e le misurazioni del pH sono in accordo con le osservazioni morfologiche. Infatti non ci sono evidenti differenze tra gli scaffold a gradiente e quelli monoporosi, ma in entrambi l'evoluzione delle quantità di ioni in soluzione

è coerente con i meccanismi di bioattività dei vetri silicati, il rilascio di ioni dovuti alla formazione del gel di silice e poi la precipitazione di calcio e fosforo. Il pH aumenta a causa del passaggio di ioni H^+ dalla soluzione al vetro. L'assenza di differenze tra scaffold 47.5B-G e 47.5B-M conferma la teoria di uno scarso flusso di SBF a cuore.

Infine è stata valutata la resistenza meccanica dopo immersione degli scaffold. A causa della grande variazione dei risultati, non è stato possibile quantificare la diminuzione della resistenza o constatare differenze tra le due diverse tipologie di scaffold. Comunque si è rilevato un infragilimento dei campioni, concorde con dati presenti in letteratura, e che, anche dopo 4 settimane, tutti i campioni testati hanno mantenuto proprietà adatte al supporto meccanico dell'osso.

Alcune linee guida per gli sviluppi futuri di questa ricerca possono essere:

- Ottimizzazione del processo: il processo di produzione può essere migliorato, per ottenere risultati più costanti. In particolare, si può aumentare la qualità del metodo migliorando la fase di preparazione dell'inchiostro, prestando attenzione alla rimozione dell'aria. Inoltre, è pensabile incrementare il livello di sinterizzazione, mantenendo comunque una struttura completamente amorfa degli scaffold.
- Studio degli effetti della porosità: in caso si riuscisse ad ottenere una migliore riproducibiltà del processo, sono necessari studi più approfonditi per stabilire il reale effetto della diversa porosità sulle proprietà degli scaffold. Questo serve per raggiungere un più alto livello di progettazione degli scaffold stessi.
- Sviluppo di un nuovo test per la bioattività: durante questa tesi è stato evidenziato come il metodo standard di test per la bioattività dei vetri, funzionale per polveri e oggetti massivi, non è in grado di valutare correttamente strutture porose, in quanto il flusso di SBF non è in grado di interessare correttamente le zone più chiuse. Appare quindi necessario lo sviluppo di un nuovo protocollo per strutture porose 3D, che sia in grado di esaltare le differenze causate dalle diverse porosità, per esempio forzando il flusso di SBF attraverso lo scaffold.

1 Introduction

Since the beginning of its existence, humankind had tried to repair and restore damages that may occur to the human body, caused by injuries or diseases. Humans started very early to experiment and use materials to build prostheses and even to implant them inside the body. The first known functional prosthesis is about 2600 years old, it is the reconstruction of a big toe founded attached to an Egyptian mummy. Bone fracture were treated with copper or bronze device since pre-Christian era, and advanced civilization, such as Romans, were reported to perform cranial and dental surgery with the implantation of gold plates and tooth. Nevertheless, the golden age of research in biomaterials began at the end of the 19th century, with the industrial revolution, when synthetic materials were produced and tested. At the beginning, the main request for new biomaterials, that are defined as "a non-living substance used in the fabrication of a medical device that somewhere has an interface with living tissue ", was to be non-reactive in the human body environment. Those were the first generation of biomaterials. With the evolution of the scientific knowledge and the development of more advanced materials, interactions body-material were possible. The new kind of biomaterials can react or stimulate a proper reaction in the body. In the second generation of biomaterials, bioactivity is the aim and it is defined as "the ability of a material to explicate its function by triggering an appropriate response from the living system that host it". Materials that show properties such as resorbability, bone bonding ability or drug delivery, belong to this class. Since 2000, researchers have developed materials that can interact with the body at a biochemical and biological level, by sending biomolecular signal that can activate determinate processes within the body. The third generation of biomaterials includes materials that have the properties of restore the function of the substitute tissue.

The earlier second-generation biomaterials that were developed, in the early '70s, are bioactive glasses for bone tissue regeneration and substitution. In orthopedic surgery, many different biomaterials are used, such as metals, polymers and ceramics, but bioceramics, hydroxyapatite and bioactive glasses and glass-ceramics are the only ones that belong to the second generation. A glass is considered bioactive if, when it is placed in contact with human fluid, it is able to stimulate the nucleation of hydroxyapatite on its surface. Hydroxyapatite is the mineral phase of the bone, and it can be used, along with bioactive glasses, as filler for bone defects or as coating for prostheses. Bioactive glasses are currently used in clinical application as fillers or blocks, especially during cranial and maxillofacial surgery. Since the last couple of decades, researchers have tried to reproduce the bone structure and properties, fabricating porous structures, known as scaffolds, using bioactive glasses. Scaffolds can act as templates in order to offer the best environment for the proliferation and the growth of bone cells. Large amount of studies and research have been carried on since, trying to obtain the perfect scaffolds. The first techniques used in the manufacturing of porous scaffolds were inspired by the ones applied in the field of porous ceramics, using the traditional approaches. Sol-gel foaming, polymer foam replication and freeze casting are some of the methods used. During the last decade, a whole new approach has gained attention and popularity in the fabrication of bioactive glass/glass-ceramic scaffolds: the additive manufacturing. This family of techniques, such as selective laser sintering, stereolithography or direct-ink writing, offers the unique and appealing possibility of a very precise control of the pore structure within the scaffolds, that is fundamental for bone regeneration.

The present work is about the fabrication and the characterization of totally amorphous bioactive glass scaffolds, manufactured by using robocasting 3D-printing technique. This method involves the extrusion of an ink, made by mixing bioactive glass powders and a polymeric binder, through a fine printing nozzle. It is a very appealing technique for the easiness of producing the ink and of the robocasting process and that allows obtaining very precise structures with dense and resistant trabeculae. Scaffolds with precise controlled porosity, at a scale of 100 µm, were achieved. Then, the influence of the presence of a porosity gradient, compared with monodispersed porosity, was studied. Graded and monoporous scaffolds were tested with respect to the mechanical and bioactive properties, then compared. Even if the robocasting method is well established and studied in the present literature, no evidence of such fine structure, achieved by using nozzle such big as 410 µm and particles just smaller than 32 µm, was found. To the best knowledge of the author, there are no studies on the effect of a change in the porosity structure in 3D-printed bioactive glass scaffolds.

This thesis, developed between the laboratories of the Department of Applied Science and Technology, at the Politecnico di Torino, and the ones of the Biomedical Science and Engineering, at the Tampere University of Technology, is composed by six chapters, containing a complete and exhaustive bibliographical research about bioactive glassed and scaffolds for bone tissue engineering and the description of the experimental work and results.

The first chapter is represented by this short introduction to the rest of the work.

The second chapter deals with a brief description of the bone structure and properties, and then it exhaustively explains the bioactivity mechanisms of glasses, their compositions and properties.

The third chapter describes all the aspects concerning the manufacturing of glass scaffolds: ideal properties, an excursus about all the materials used in bone regeneration and finally all the manufacturing processes that are used for fabricating scaffolds.

The fourth and the fifth are about the experimental work done during the developing of the present thesis. In the fourth chapter, materials, methods and protocols used for the production and the testing of the scaffolds are deeply described. In the fifth, the results and the discussion about them are presented.

In the last chapter, the conclusion and some future perspective are presented.

2 Bioactive glasses

2.1 Introduction

The history of bioactive glass began about fifty years ago, in 1967, when Larry Hench, the pioneer of bone substitute materials, met an US Army colonel on a bus ride to the US Army Materials Research Conference. The colonel, which had withstood many amputations serving with the Medical Corps in Vietnam, asked Hench why, if scientists were capable of making materials able to survive high energy radiation exposure, they were not able to produce materials that can survive the biological environment in the human body. In most of the cases, to amputate a limb was the only thing to do due to the lack of materials that can be used inside the body, which would reject plastic and metal components available to surgeons at the time. From that point, Hench started the work that led to the discovery of the first bioactive glass, the 45S5 Bioglass®, and to every following research [1].

Bioactive glasses were the first example of second-generation biomaterials and led way to a wholly new concept of materials in medicine. For the first time, materials were used that were not only inert and able to survive inside the human body without being toxic or degraded, but they were materials that could play an active role in the healing processes and bond in a proper way with the surrounding living tissues. It is very easy to understand how much such materials are appealing for medical purposes and why they have been so widely studied and investigated in the last fifty years. The easiness of modifying a glass composition and the possibility to insert almost any kinds of elements within the amorphous network leads to an almost infinite number of possibilities for researchers to experiment and tailor the properties of bioactive glasses. Thanks to that, countless types of glasses have been synthetized and studied, by changing the former oxides, the molar ratio or adding new elements in order to tune specific properties in the desired manner or improve them. All those efforts led to the development of three main type of bioactive glasses, sorted by their former oxides, silicate, phosphate and borate glasses, and to the creation of materials that exhibit properties such as anti-bacterial, angiogenesis (the ability to increase the formation of new blood vessels) or cancer treatment.

2.2 Bone: classification, structure and properties

Bioactive glasses, given their physical properties, stiffness and apatite-forming ability (see the section 2.3 for details), have been mainly used in contact with calcified hard tissues (bone and enamel). The human body contains more than two hundred bones, with very different shapes and dimensions, from the long femur to the little stapes (a very little bone in our middle ear, just 3-mm long). The bones altogether form the skeleton, which has may different roles: it supports the body, allows movement and protects the inner organs, blood cells are produced in the bone marrow, and bones are a storage for calcium, in the bone matrix, and iron, in the marrow.

A bone is a hard form of connective tissue, formed by an inorganic matrix which embeds cells and collagen organic fibers. The mineral phase, which represents the 60 wt.% of the bone, is made by a calcium phosphate called hydroxyapatite (HA, $Ca_{10}(PO_4)_6(OH)_2$). It is made by nanometric crystal well oriented in the same direction. The organic phase is formed by collagen fibers, 30 wt.% of the whole bone, along with bone cells [2].

There are five different types of bone in the human skeleton:

- Long bones: these are the ones where the length is bigger than the width. At each ends there is a large plate called epiphysis, while the long central part is called diaphysis, made by hard compact bone covered by cartilage for protection. This kind of bones have a spongy core, called cancellous (or spongy) bone and a hard external layer, called the compact (or cortical) one. Long bones are femur, humerus but also phalanges.
- Short bones: bones approximatively large as much as wide are called short bones. They have a small layer of compact bone and the inside is made of cancellous bone and marrow. These are the carpals and the tarsals, for example.

- Flat bones: the flat bones provide protection to the body and anchoring points for the muscles, they are strong and resistant. The core is made by spongy bone and marrow, while the surface is compact bone. Scapula, sternum and cranium are examples of flat bones.
- Irregular bones: if there is no other classification suitable for a certain bone, it is an irregular one, due to its very irregular shape. It is the case of the vertebras and the mandible.
- Sesamoid bones: the last kind of bones include the ones which are embedded in tendons, such as the patella, in the knee joint [3].

Bones have a layered and hierarchical structure (**Figure 2.1 Bone** hierarchical structure , from the bottom to the top, is characterized by: molecular sub-nanostructures, mineral and organic; nanostructures, collagen fibers and HA crystals; lamellae at the sub-micrometer level; Haversian canals and osteon as microstructures; and at the macroscale the cancellous and the compact bone [4].

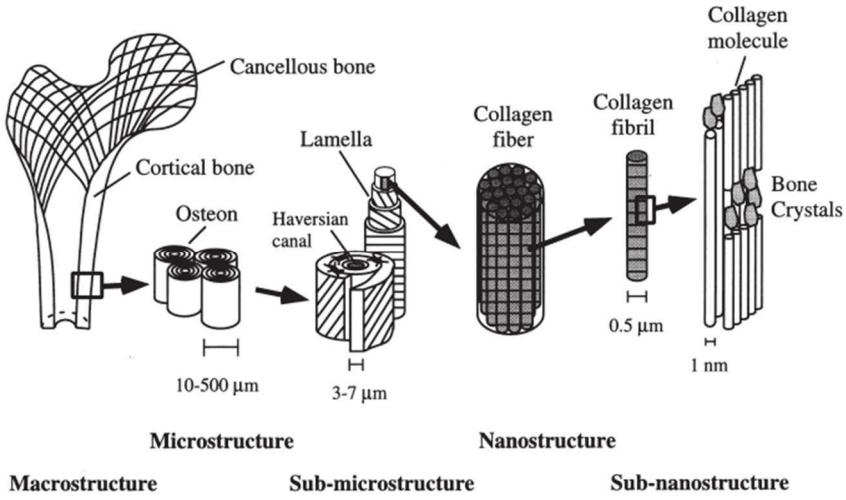

Figure 2.1 Bone hierarchical structure [4]

The outer layer is called periosteum and is composed by two different parts. It has a coat of fibrous connective tissue and, near the bone, it has a layer of bone progenitor cells, which has a big role in a fracture event. This layer also provides nutrition for the compact bone. The compact bone provides the mechanical strength and it has a layered structure [5]. The building block of this structure is a cylindrical unit called osteon, several millimeters long but only 0.2 mm large [6]. The osteon has a complex structure and it is composed by a central canal, called the Haversian canal, which host blood vessels and nerves. The Haversian canal is surrounded by bone lamellae. The lamellae are formed by HA crystals that grow within collagen fiber bundles, formed by collagen micro-fibrils. Osteons arranged in a dense and ordinate manner form the compact bone. Instead, in the spongy bone, there is plenty of void, between 50% and 90 vol.%, and the osteons are arranged to form rod- and plate-shaped trabeculae. Given the higher mechanical strength of the compact bone, it will grow more with respect to the cancellous one in the major loaded direction [2].

Human bones are alive and in constant change. This is possible thanks to the presence of different kinds of cells that live inside the cancellous and cortical bone. They are osteoblasts, osteocytes, osteoclasts and bone lining cells. Those cells live in the extracellular matrix (ECM), which is a mixture of water, collagen, 60-70% of minerals (such as HA) and proteins. There are two types of ECM: the first is called osteoid and is produced during the new bone formation process by osteoblasts and it is quickly mineralized and transformed in the second ECM type, the mineralized matrix [5]. Osteoclasts are the bigger of the bone cells and they have the task of destroying the bone, dissolving the mineral portion by mean of acids. They are always active, especially in case of a fracture or a prosthesis implantation. Due to the action of the osteoclasts, an environment with high concentration of phosphor and calcium is generated. In such conditions, the osteoblasts become active and start to produce new osteoid and to calcify it. Osteoblasts derive from pluripotential steam cells called mesenchymal marrow stromal cells, which are in the marrow bone or in the periosteum. When the ECM is fully mineralized, the osteoblasts get stuck into it, in little pockets called lacunae, and become the third type of bone cell, an osteocyte. Osteocytes keep the bone tissues alive, producing collagen, feeding the matrix, ruling the exchange of substances and the equilibrium between organic and mineral phases. If the osteoblasts line the bone,

they become bone lining cells. Those cells have no part in growing the bone, but they play a very important role in the resorption of it. In fact, where a layer of those cells is present osteoclasts cannot attack the underlying bone. During a fracture event, the layer of bone lining cells is removed, so the healing process can take place [2] [5].

The remodeling process of the bone, which occurs constantly and can follow a trauma or repeated mechanical stimuli, can be summarized in this way:

- Rest: the bone surface is covered by a protective layer of bone lining cells;
- Resorption: the protective layer is removed, the osteoclasts can cover the bone surface and attack it;
- Complete resorption: a small hole is formed on the bone;
- Repair: osteoblasts start filling the cavity with newly-formed bone till the hole is fully repaired.

If there is no equilibrium between the destruction and the formation of the bone, some diseases may occur such as osteoporosis, in case osteoclasts prevail [2].

Since the bone tissue is mechano-receptive, a good scaffold shall have mechanical properties as much similar as possible to the ones of the bone it is going to substitute. This will ensure a good and correct loading transfer, from the scaffold to the bone and vice versa. In order to design a proper scaffold, it is necessary to know the mechanical behavior of the different types of bones. This is not simple since the bone is a living tissue and for the characterization a dead bone is used. Bone is a composite material which merges a brittle phase, the HA, and a ductile one, the collagen. This enhances its fatigue resistance, because the collagen fibers, and the hierarchical structure with the Haversian canals, act as crack deflectors and stoppers. Furthermore, it has the ability to repair the micro-cracks that may occur and the organic phases have a viscoelastic behavior.

Even with all these difficulties it is necessary to have some data about the mechanical properties of the bones. Since there are two different types of bone, the cortical and the trabecular one, it is mandatory to distinguish them in the analysis of the mechanical behavior. In literature there are reported several data for the engineering properties of the bones, which have quite a large distribution, as reported in **Table 2.1**.

Table 2.1 Mechanical properties of cortical and trabecular bone, reproduced and modified from [7] [8]

Material property	**Cortical Bone**	**Trabecular Bone**
Compressive strength [MPa]	130-200	0.1-16
Tensile strength [MPa]	50-115	1-5
Compressive modulus [GPa]	11,5-17	0.12-1.1
Young's modulus [GPa]	7-30	0.05-0.5
Fracture toughness [MPa*$m^{1/2}$]	2-12	0.1-0.8
Porosity	5-10	50-90

Also, the bone is a highly anisotropic material, so it is important to know the direction in which the properties are calculated. For example, the cleavage resistance in the parallel direction of the bone is around 116 MPa while in the perpendicular direction it may varies between 40 and 92 MPa [2].

2.3 Bioactivity in glasses

A bioactive material is "one which has been designed to induce specific biological activity" (ESB consensus conference, 1987 [9]). This definition is prone to be declined according to the different application areas in medicine. In particular, focusing on bone regeneration and substitute materials, a bioactive material has the properties of bonding to living bone through the formation of bone-like apatite on its surface if implanted in living body [10].

Hydroxyapatite (HA), more specifically calcium hydroxyapatite, is the mineral phase of the bone, and it is a double salt, composed by tricalcium-phosphate and calcium hydroxide: $Ca_{10}(PO_4)_6(OH)_2$. HA has a hexagonal structure, both the biological and the synthetic one, with hydroxyls forming columns in the center of tetrahedron made by the phosphates (**Figure 2.2**).

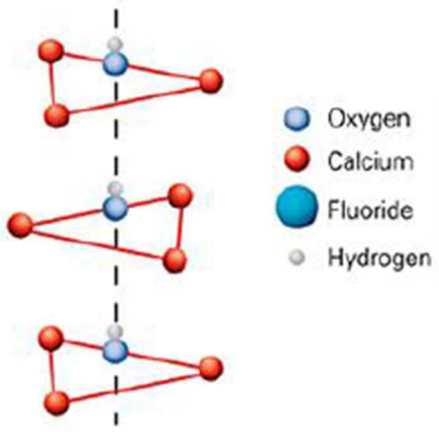

Figure 2.2 Columnar structure of hydroxyapatite [2]

Biological HA is almost totally nanocrystalline and it has piezoelectric properties. HA can be synthesized to be used as fillers or bulk materials in bone restoration [2]. Actually, biological HA differs from pure HA due to calcium-deficiency, the Ca/P atomic ratio is lower than 1.67, that is the stoichiometric one. This will lead to different crystallinity, composition, mechanical properties and dissolution rate. Moreover, biological HA is carbonate substituted. The easiness of substitution of ions in the HA lattice leads to the presence of several different ions within the biological HA lattice. Ca^{2+}, $(PO_4)^{3-}$ and OH^- are often substituted by CO_3^{2-}, Na^+, Mg^{2+}, K^+, Cl^-, HPO_4^{2-}, F^-. Also, there can be trace elements such as strontium and zinc. The formula for biological HA can be therefore expressed as: $(Ca,M)_{10}(PO_4,CO_3,Y)_6(OH,F,Cl)_2$. M represent elements that can substitute Ca^{2+} (Mg, Na, K, ions) and trace elements (Sr, Zn ions). Elements that can substitute for $(PO_4)^{3-}$ are represented by Y, such as acid phosphate [11].

The bioactivity of a glass is strictly correlated to the rate of growth of the HA layer on it, in vitro or in vivo environment. The HA formation process begins when the bioactive glass is implanted into the human body or it is soaked in solutions that mimic body fluids, such as the simulated body fluid (SBF) proposed by Kokubo et al. [12] The mechanism proposed for explaining the nucleation and the precipitation of crystalline apatite on the glass surface is a 5-stage process, and it is based on the dissolution of ions from the glass network:

1) Cation exchange: the first stage involves the exchange of mono- and bivalent cations, in particular Na^+ and Ca^{2+} within the glass, and H^+ ions from the solution. This will lead to the formation of silanol bonds (Si-OH) on the surface of the glass, according to the reaction: $Si\text{-}O^-Na^{2+} + H^+ + OH^- \rightarrow Si\text{-}OH^+ + Na^+_{(aq)} + OH^-$
   As a consequence, the solution pH will increase and a silica-rich layer will form. If present in the glass composition, also phosphate is lost. Since monovalent ions are less bonded to the glass network, they will be lost faster than bivalent ones;
2) With the ongoing of the exchanging reaction and the rising of the pH, Si-O-Si bonds are attacked by hydroxyl ions. When all the four Si-O bonds of a single Si atom are broken, soluble silica, $Si(OH)_4$, is lost in the solution. This increases the number of silanol at the interface;
3) Since HO- groups can react and condensate between each other, the third step involves the condensation and the polymerization of silanol groups. Doing so, a new silica-rich layer is formed and, since there is a high presence of water, it is a silica-gel and amorphous layer. It can absorb ions from the solution and be a good environment for the precipitation of HA;
4) Diffusion of calcium, Ca^{2+}, and phosphate, PO_4^{3-}, ions through the silica-gel and from the solution, forming an amorphous film on the silica-gel layer, which is rich in CaO and P_2O_5. When there is the right concentration of ions, in order to form HA, the amorphous film starts to crystallize;
5) Crystallization of the calcium and phosphate-rich layer and formation of HA. Due to the presence of carbonates, in the solution, and fluorides, released by the glass, the HA formed is not stoichiometric but it presents also carbonates and hydroxycarbonate apatite [13].

The evolution of this process can be studied by analyzing the concentration of ions in the solution at different time points (**Figure 2.3**).

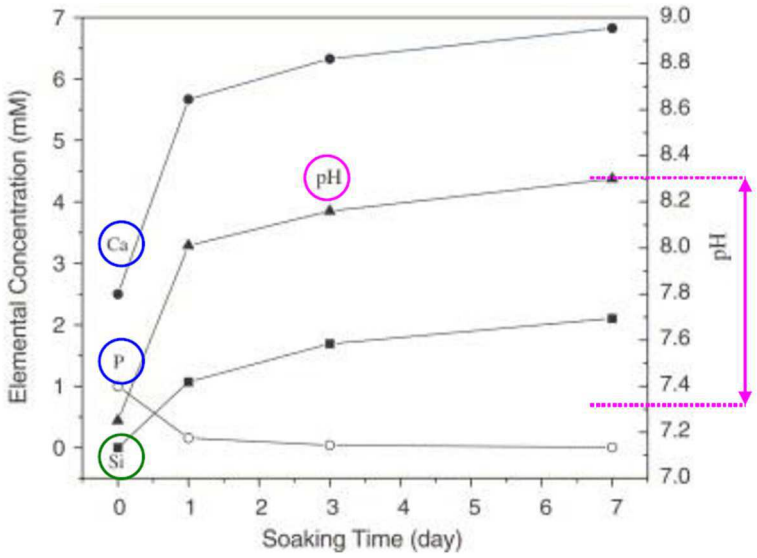

Figure 2.3 Variation of the concentration of Si, P, Ca and pH during immersion of a bioactive glass in SBF [2].

Silicon and calcium concentration increase due to the dissolution of soluble silica and the cationic exchange. On the other hand, phosphorus decreases after the precipitation of amorphous phosphate oxides on the silica-gel layer. Since ions H^+ bond to the Si-O groups to form silanols, the pH increases up to 8. A pH value of 8 is toxic for cellular life, but inside the body there is continuous flow of fluids that dilutes the solution around the glass [2]. Even if the dissolution of glasses and the precipitation and formation of crystalline HA layer extend for a quite long period of time, the nucleation of the first crystals of HA has been shown to be quite fast and depending on the molar percentage of Si in the glass. In fact, if the molar content is below the 53%, HA crystallizes in less than 2 hours and they can bond with bone and soft tissue either. When the presence of silicon oxide is increased up to 58%, the crystallization is slower and it takes two days before happening. Those types of glass bond only with bone tissue. If the silica content is greater than 60%, the glass is bioactive no more, and it does not bond with bone nor soft tissue. There is no sign of crystalline HA after four-week immersion, even if there is the formation of the amorphous calcium-phosphate layer [14].

The ability to react and dissolve within body fluids or equivalent solution and to precipitate HA on the surface is strictly related to the connectivity of the glass network. In order to form a glass, there is the need to have a former oxide that can give birth to the amorphous structure, without a long-range order. There are several forming oxides (P_2O_5, B_2O_3, V_2O_5…), but the more used and studied, especially for bioactive glasses, is silica (SiO_2). In silicate glasses, the network is formed by a series of silica tetrahedra, bonded together by Si-O-Si bonds, at the apex of the tetrahedra, as pictured in **Figure 2.4**.

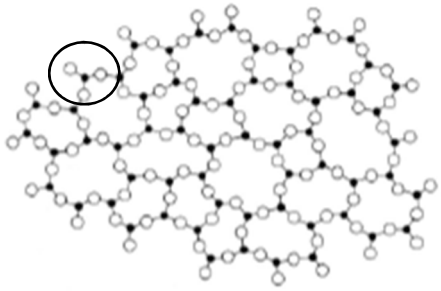

Figure 2.4 2-D representation of silicate-glass network, a tetrahedron is visible in the circle. Si atoms are pictured as black dots, oxygens as white ones [15].

Other kinds of oxides can act as network-modifiers. They disrupt the network by breaking, for instance, the Si-O-Si bond, and forming a non-bridging weak oxygen bond. Oxides such as Na_2O, CaO, MgO or K_2O are network-modifiers. For example, Na_2O will form an ionic bond, $Si\text{-}O^- Na^+$ [15]. In terms of dissolution kinetic, the less is connected the glass network, the fast is the dissolution of the glass. That is why glasses with high silica content (>60 mol%) are non-bioactive. The number of bridging-oxygen bonds of a silica tetrahedron can be expressed using the following notation: Q^n, where n is the number of bridging bonds. FitzGerald et al. demonstrated that the network of Bioglass is mainly composed by chain and ring of Q^2, almost the 70% of tetrahedra have just two bridging bonds, and for the remaining by Q^3 [16]. The composition of simple bioactive glass can be used to predict the network connectivity (which is the mean number of bridging-oxygen bonds each Si atom), N_c, and, further, the bioactivity of it. The formula is the following:

$$N_c = \frac{4[SiO_2] - 2[M_2^I O + M^{II} O] + 6[P_2O_5]}{[SiO_2]} \quad (2.1)$$

$M_2^I O$ and $M^{II} O$ represent the modifier oxides, mono- and divalent, that are present in the glass. In order for a glass to be bioactive, the network connectivity value must be within the range of 1.8 and about 2.6.

It is also interesting to notice that, despite P_2O_5 is a former-oxide, there is no sign of Si-O-P bonds in bioactive glass networks. Phosphates present in those glasses are in the form of orthophosphate ($[PO_4]^{3-}$) and can be considered as Q^0. So, they can form a separated nano-phase and are charge-compensated by modifier-oxides [17].

The five stages described before are those that happen in vitro, when the glass is implanted inside the body, the process is more complicated and longer and some of the new stages overlap with the previous ones. Still during the migration of phosphate and calcium ions, proteins are absorbed on the surface, then cells. The first ones that arrive are macrophages, which are the first response when a foreign body is detected. Then stem cells attach to the glass surface and start differentiating. It has been demonstrated that the presence of a bioactive glass can enhance and increase the differentiation and the growth of stem cells, called osteoblast progenitor cells, into active osteoblasts that quickly begin repair the bone by generating extracellular matrix (ECM) and mineralizing it. The control on cells genes activation is possible due to the dissolution of soluble silica and calcium ions from the glass. Thanks to those peculiar properties, bioactive glasses can be described as osteogenic materials. Within the classification of bioactivity and biomaterials, bioactive glasses are addressed as third-generation class A materials. While first-generation biomaterials are inert and second-generation can bond with the body's calcified tissues (primarily bone) and have an interaction with them, third-generation biomaterials are based on a whole new concept and are modified in order to send biochemical and biological signal to the body, so that they can stimulate a proper response. 45S5 Bioglass was the first material that belonged to the second generation, and later it was included in the third generation, too Regarding bone substitute materials, a further classification can be performed. In fact, there are two classes of them: class A and class B. Materials that lead to osteostimulation and osteopronduction are addressed as class A, whereas if their only effect is osteoconduction they are addressed as class B biomaterials [18]. When it comes to the restoration of large bone defects, the formation of new blood vessels, called angiogenesis, is fundamental for ensuring the delivery of enough nutrients, growth factors and oxygen and to allow stem cells to reach the injured site. Bioactive silicate glasses have proven also to increase angiogenesis, both in vitro and in vivo [19].

All the different stages of the bioactive process happened at different time points and it may happen that some in vitro and in vivo steps overlap. The time scale is summarized in **Table 2.2**.

Table 2.2 Timetable of the processes that follow the implantation of bioactive glasses inside the human body. In vitro processes happen also when the glass is soaked into SBF or similar solution, in vivo steps take place only within a living being.

Time scale (h)	In vitro	In vivo
0	Simple cation exchange and silanol formation	-
1	Release of complex ions	-
	Silica polycondensation	-
	Ca^{2+}, $(PO_4)^{3-}$ absorption, formation of the amorphous layer	-
2	HCA crystallization	Protein absorption and cell attachment
10	-	Macrophage adhesion
20	-	Osteoblast precursor cell arrival
100	-	Stem cell differentiation Extracellular matrix generation Onset of ECM mineralization

The bioactivity level of a material can be estimated through the bioactivity index, I_B, that is defined as the reciprocal of the number of days necessary for the 50% of the material surface, $t_{0,5bb,}$ to bond with living tissue multiplied by 100 [2]:

$$I_B = \frac{100}{t_{0,5bb}} \qquad (2.2)$$

2.3.1 Effect of devitrification on bioactive properties

As previously shown, the bioactive abilities of glasses rely on the dissolution of the amorphous network when it comes in contact with body, or similar, fluids. In order to increase the strength of the device, or due to processing temperature condition, it is possible that glasses undergo a process called devitrification. This process involves the modification of the amorphous network that turns into crystalline domains. Either if the devitrification is inducted or happens spontaneously, it is important to study the effect of crystallization on bioactivity of glasses. The effect of crystallization on different bioactive glasses was studied, in particular for silicate and wollastonite ($CaO.SiO_2$) forming glasses. During the devitrification, crystalline phases can form in dependence of the glass composition. Systems such as Bioglass form sodium calcium silicate (combeite, $Na_2O.2CaO.3SiO_2$) crystals, while glasses such as 1-98 (wt%: 6% Na_2O, 11% K_2O, 5% MgO, 22% CaO, 1% B_2O_3, 2% P_2O_5, 53% SiO_2) crystallize as wollastonite. It is also possible that some systems form diopside crystals ($MgO.CaO.2SiO_2$) [20]. Firstly Peitl Filho et al. then Arstila et al. showed that the presence of crystalline phases can significantly slower the formation of the HA layer on the glass surface, but that even with the 100% of crystallinity systems such as Bioglass are still bioactive. Even though, it is clear that the onset time of HA layer formation and the thickness of the same layer are affected by the amount of crystalline phase. If it is under the 60%, HA forms in less than 20 h on the glass surface. On the other hand, it takes about 25 h. The fully amorphous 45S5 has an onset time of less than 10 h [21]. The effect of devitrification on Bioglass, regarding the onset time of HA formation, is shown in **Figure 2.5**.

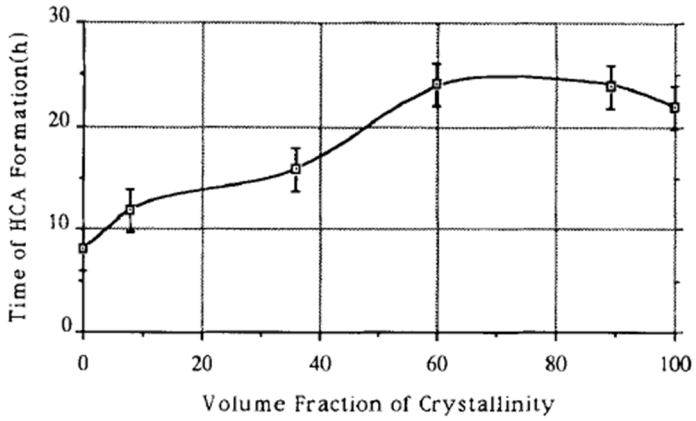

Figure 2.5 Effect of devitrification on the onset time for HA formation on Bioglass [21]

Both sodium calcium silicate and wollastonite crystal have been proved to dissolve in vitro, when immersed into SBF, but wollastonite is much slower compared to the former. Diopside crystals, instead, cannot be dissolved and are therefore not bioactive [20]. So, one of the aim of the studies performed over the last years was the development of bioactive glasses that can undergo thermal treatments without devitrification, to obtain, for example, good sinterability while maintaining high bioactive properties.

2.4 Bioactive glass compositions

Since the discover of 45S5 Bioglass about fifty years ago [1], there were a lot of efforts in the research and optimization of novel glass compositions in order to obtain highest level of bone-bonding activity, tailored dissolution properties, increased strength and better workability. The early researches were focused on silicate-based glasses, mainly by modifying the original 45S5 composition by changing the amount of oxides or adding some totally new ones (for instance MgO and K_2O). In the last twenty years, others former oxides than silica have been proven to have bioactive properties, in particular phosphate and borate-based systems. Even if it is the first bioactive glass ever developed, Hench's Bioglass is still one of the best compositions in terms of bioactivity among melt-derived biomedical glasses [13]. Some examples of compositions are shown in **Figure 2.6**

Composition (wt%)	45S5	13-93	6P53B	58S	70S30C	13-93B1	13-93B3	$P_{50}C_{35}N_{15}$
Na_2O	24.5	6.0	10.3	0	0	5.8	5.5	9.3
K_2O	0	12.0	2.8	0	0	11.7	11.1	0
MgO	0	5.0	10.2	0	0	4.9	4.6	0
CaO	24.5	20.0	18.0	32.6	28.6	19.5	18.5	19.7
SiO_2	45.0	53	52.7	58.2	71.4	34.4	0	0
P_2O_5	6.0	4.0	6.0	9.2	0	3.8	3.7	71.0
B_2O_3	0	0	0	0	0	19.9	56.6	0

Figure 2.6 Examples of bioactive glass compositions [22]

Bioactive glasses can be synthetized either by melting raw materials or via sol-gel method. The melting method involves the use of suitable precursors of the glass oxides, usually in form of granulates or powders. They are weighted and inserted into a crucible, usually made of platinum or graphite. Then it is heated inside a furnace, using a proper thermal cycle, and the molten glass can be poured into molds in order to obtain bulk pieces or into water to obtain a frit. A frit is composed by small chunks of glass, that are cracked due to residual stresses that are generated by thermal shock, and it is very useful in the production of glass powders, since it can be easily milled.

Sol-gel process is used to obtain high-purity materials and it was developed for bioactive glasses to overcome the problem of easy crystallization of the early 45S5 composition. It involves the hydrolysis and condensation of a metal-alkoxide solution in order to create a sol that then undergoes gelation. To obtain the glass material, the gel is dried and undergoes a thermal treatment to remove the organic phase [23].

2.4.1 Silicate-based bioactive glasses

When Hench started to think about a ceramic implant that can bond to bone, he decided to use a very simple system where all the atoms that form HA were present. So, 45S5 Bioglass is based on the ternary system SiO_2-Na_2O-CaO, with the adding of some phosphorus oxide. The composition was chosen near the eutectic in order to obtain a low melting, easily processable material. Thus, the first bioactive glass in history was born with the following molar composition: 45% SiO_2, 24,5% Na_2O, 24,5% CaO, 6% P_2O_5 [1]. Bioactive mechanism of silicate glasses is actuated following the steps described at paragraph 2.3.

By modifing the composition of 45S5 Bioglass within the ternary phase diagram SiO_2-Na_2O-CaO and adding others oxides, there can be found several bioactive glasses with different properties, such as the dissolution rate and percentage (**Figure 2.7**).

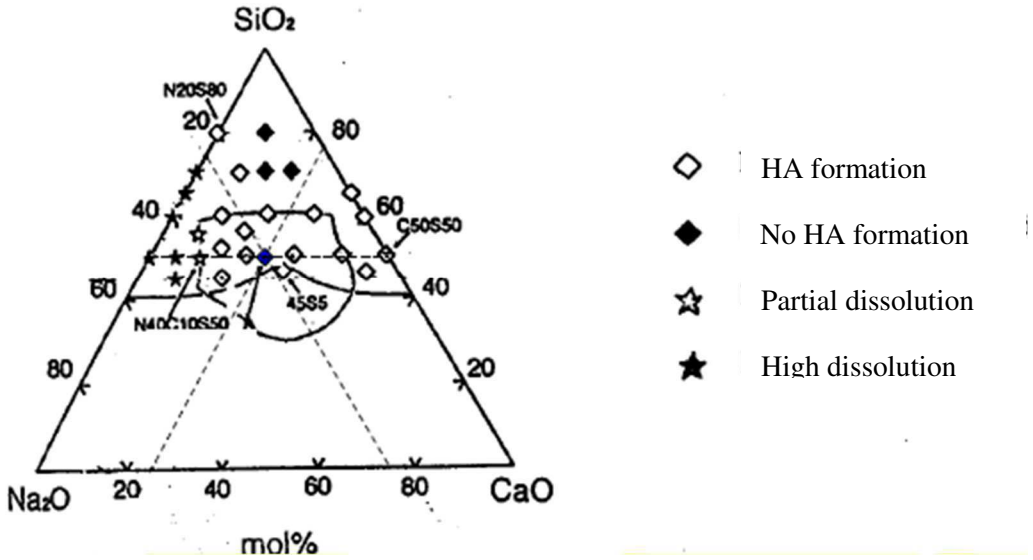

Figure 2.7 Ternary phase diagram of the SiO_2-Na_2O-CaO system showing the composition of different bioactive glasses. under the curved line there is the non-vitrification zone [2].

Even though more than 40 years have been passed since 45S5 Bioglass was discovered, it is still one of the most bioactive glasses ever produced. The main issue with the application of 45S5 glass is the poor workability of it. In fact, the glass transition temperature and the onset of crystallization are close, limiting the possibility of sintering by viscous flow. This leads to fragile devices, such as porous scaffolds, and to lower bioactivity due to the devitrification of the glass during the manufacturing process [22]. In order to overcome these problems, several alternative compositions have been designed and studied. One of the most famous is the so called 13-93. It was developed by Brink et al. in 1997, during the investigation of bioactive properties of several compositions belonging to the SiO_2-Na_2O-CaO-K_2O-MgO-B_2O_3-P_2O_5 system. 13-93 composition is the following (wt%): 53% SiO_2, 15% Na_2O, 11% CaO, 12% K_2O, 2% MgO, 3%B_2O_3, 4% P_2O_5. With respect to Bioglass, it is a much more complex system, and more oxides are introduced, such as K_2O, MgO and B_2O_3. 13-93 has been proved to be bioactive and to have a large working range, thanks to the higher presence of silica (>54%mol) and to the introduction of MgO, which is known to increase the working window of glasses [24] [25]. Using this glass type, Fu et al. managed to obtain a fully amorphous scaffold using the sponge replication (paragraph 3.5.3), with porosity and strength comparable with the trabecular bone [23].

2.4.2 Phosphate-based bioactive glasses

One of the aim of tissue engineering is the complete restoration of tissue and organs, as if the injuries never occur. This is not possible, regarding the field of tissue engineering, if the biomaterial used to support the healing process do not dissolve at the end of it. Within bone regeneration, if a bioactive glass is used as filler or scaffold, it shall dissolve at the same rate of the growing bone. Pursuing a material that can be resorbed by the body, since the '80s, researchers have tried to use phosphate-based glasses. In these glasses there is no more a silica network, but the former oxide is P_2O_5. The very appealing ability, for biomedical devices, of this kind of glasses is that they can dissolve completely in aqueous media, such as body fluids. Furthermore, the dissolution ratio can be varied of some order of magnitude by modifying the composition [26]. The low stability of such glasses is due to the asymmetry of the structural tetrahedron units, [PO_4], and to the easy hydration of P-O-P bond. Two steps are active during the dissolution of phosphate-based glasses, and are interdependent: one is the hydration, that involves Na-H ion exchange; the second is the rupture of the phosphate network due to break of P-O-P bonds in the hydrated layer. Metal oxides, such as TiO_2, CuO or Fe_2O_3, can be added to tailor and control the dissolution kinetics of the phosphate system [23]. The dissolution properties of phosphate glasses can be exploited also to achieve controlled release and in situ delivery of active ions. Antibacterial ions, such as copper, silver, gallium and zinc, can be incorporated in the glass network and, therefore, be released during the dissolution of the glass itself. Moreover, with respect to silicate-based glasses, the ion release from phosphate glasses is much more linear during application time [22]. Phosphate glasses, thanks to the fact that can be spun into fibers, can also be used in soft tissue engineering, and they are studied for nerve and muscular regeneration.

Regarding bone regeneration, phosphate glasses are appealing for the manufacturing of bioresorbable scaffolds that can dissolve, leaving bone to heal naturally. Vitale-Brovarone et al. modified the silicate-based glass CEL2 (45% SiO_2, 26% CaO, 15% Na_2O, 3% P_2O_5, 4% K_2O, 7% MgO, mol%) to obtain a phosphate glass named ICEL2 by inverting the molar percentage of silica and phosphate oxide. When slices made with ICEL2 are soaked into different aqueous media, such as water, SBF or TRIS, they show high dissolution, up to 75% of weight loss within four months [27]. Scaffolds manufactured using this glass also showed bioactive properties, since HA can form on glass trabeculae and human cells adhere and differentiate onto scaffold surface [23]. The dissolution rate of phosphate glasses can be modified by using metals that have also beneficial properties in bone regeneration such as strontium. Strontium ranelates (complex strontium salts) are used for treatment of osteoporosis. In fact, due to the similarities between strontium and calcium ions, the human body absorbs strontium in bones as if it is calcium. SrO is known to have anti-resorptive and bone forming effects. So, it can be interesting as doping element for bioactive glasses. Abou Neel et al. discovered that substituting sodium oxide with strontium oxide, up to 5 mol%, can significantly increase the dissolution rate, along with glass density and glass transition temperature. This is due to the fact that SrO generate modification in the phosphate network, increasing the number of Q^1 and Q^3 units and decreasing Q^2 ones. The increased degradation rate resolves also an increase in the ionic release. Na^+, Ca^{2+} and various anion phosphate (PO_4^{3-}, $P_2O_7^{4-}$ …) levels in the solution increase proportionally with the rate of dissolution. On the other hand, the strontium ionic concentration is proportional to the concentration of SrO in the glass and not to the dissolution rate. The control of the dissolution rate is useful also to limit the change within the pH of the solution. A too fast or too large variation in the pH might be toxic for cells [28].

2.4.3 Borate-based bioactive glasses

Among glass former oxides, boron oxide is appealing for bone tissue engineering and the manufacturing of scaffolds. In fact, borate glasses are less durable than silicate one, hence they can convert faster to HA than traditional bioactive glasses that use silica as network forming oxide. Borate glasses, made by pure boron, B_2O_3, have a much lower glass transition temperature than pure silicate one, about 260°C and 1100°C respectively. The glass transition can be tailored and increased by adding alkali atoms above a critical concentration. Borate and boro/silicate glasses are studied for biomedical application thanks to the faster and more complete conversion rate than silicate glasses, such as 45S5 Bioglass. In principle, the bioactivity mechanism is similar to that of silicate glasses and it involves the formation of a borate-rich gel layer, comparable to the silica gel. It is also possible to control the conversion rate by changing the glass composition, thus varying the conversion time from hours to months. Furthermore, regarding

scaffolds manufacturing, borate glasses can be sintered easier and in a more controlled way than silicate glasses thanks to their ability to readily undergo viscous flow [29].

The first bioactive glasses containing boron oxide were proposed by Brink and coworkers, in 1990, and they were borosilicate glasses. They analyzed several different compositions and found that glasses with different amount of B_2O_3 are bioactive [24]. A borate glass, known as 45S5B1, was obtained by Richard [ref], who substituted the whole silica content of 45S5 glass with boron oxide, maintaining the same amount of others elements. The new glass has proven to be more reactive than Bioglass and to promote faster bone growth in vivo. The possibility of controlling the conversion rate of borosilicate glasses into HA was investigated by Huang et al. They investigated the conversion rate of glasses based on 45S5 Bioglass composition, with different amount of boron oxide, as shown in **Figure 2.8**.

	Mole percent				
Glass	Na_2O	CaO	B_2O_3	SiO_2	P_2O_5
0B	24.4	26.9	0	46.1	2.6
1B	24.4	26.9	15.4	30.7	2.6
2B	24.4	26.9	30.7	15.4	2.6
3B	24.4	26.9	46.1	0	2.6

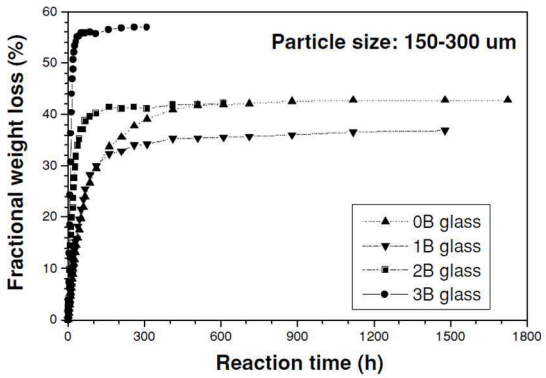

Figure 2.8 Molar composition of the four glasses investigated by Huang et al.(left) and the weight loss during soaking into phosphate solution (right) [30]

Particles of B3, a fully borate glass, were totally converted into HA in less than four days. Even for much longer time, B0 (which is 45S5 Bioglass), B1 and B2 maintain, instead, a silica-rich core [30].

An issue concerning the in vivo use of bioactive borate glasses is that high concentrations of $(BO_3)^{3-}$ are known to be toxic. Some in vitro tests have proven that borate glasses can be cytotoxic if the tests are carried out in static condition. When the tests are carried out in dynamic condition or even in vivo, the cytotoxic effect is no more present, thanks to the dilution of the ions. In fact, it has been proven that under a certain concentration (≈0.65 mM) there is no toxic effect. Healthier conditions for tissue culture can be achieved by inducing HA formation on the glass prior to cell seeding [29]. Borate glasses have also been proven to be suitable materials for the manufacturing of scaffolds. Fu et al. modified the composition of the silicate glass 13-93 in order to obtain the borosilicate glass addressed as 13-93B2. The final composition is the following, mol%: 22% CaO, 6% Na_2O, 8% MgO, 8% K_2O, 18% SiO_2, 36% B_2O_3, 2% P_2O_5. Through sponge replication, they were able to obtain a structure that mimics the trabecular human bone, with porosity of 72 vol.% and pore size ranging from 200 to 500 µm. Also, the mechanical properties are acceptable for bone-regenerative applications, in fact the compressive strength of the scaffolds "as-sintered" is about 6.4 MPa. One negative side of the fast conversion of borate glasses is the fast decrease of mechanical properties during soaking time. In fact, the strength drops down to about 1 MPa in 30 days. Borate scaffolds have been found to support cells growth and differentiation if the concentration of borate ions is kept under the toxic threshold [31].

2.4.4 Mesoporous glasses

Regarding bioactive glasses, it is worth to mention mesoporous glasses. This particular type of glasses belongs to the class of mesoporous or mesostructured materials. According to IUPAC nomenclature, a mesoporous material has a porosity with dimension ranging from 2 to 50 nm. These kinds of glasses are very appealing for tissue engineering proposes for the very high value of specific surface that can increase the ability to react with body fluid. Moreover, they can be used to host drugs inside the nanopores, for controlled drug delivery.

Ordered mesoporous structures can be obtained by coupling sol-gel method with supramolecular self-assembling processes. To do so, surfactants are used to build micelle, thanks to hydrophilic/hydrophobic

features of those molecules. In 1992, the first pure-silica mesostructured material was synthesized and applied as molecular sieve (**Figure 2.9**). Surprisingly, some studies found that pure-silica mesoporous glasses may have the ability to precipitate HA when soaked into SBF. This is in contrast to Hench's bioactivity mechanism, since there are no ions that can exit from the amorphous network [23]. A key role is indeed played by the textural features of the mesoporous silica, especially the ultra-high specific surface area (well above 100 m^2/g), but this issue is still controversial.

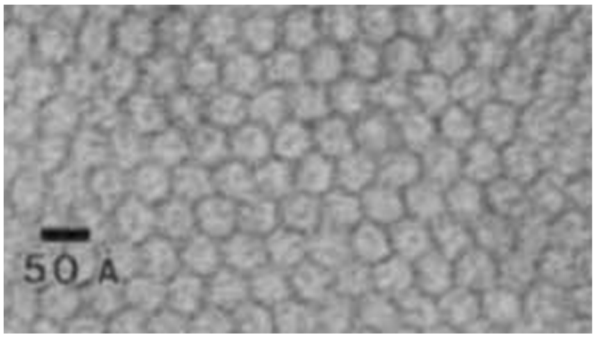

Figure 2.9 Transmission electron micrograph of pure mesostructured silica. It is possible to appreciate the highly ordered structure of mesopores [32]

As an evolution of mesoporous pure silica, proper mesoporous bioactive glasses (MBGs) have been prepared by incorporating additional oxides and they have shown high bioactivity. In 2004, Yang et al. synthetized the first MBG by using a block copolymer as a template for mesopores via the evaporation-induced self-assembly (EISA) process. The EISA process is based on the ability of surfactants to form an ordered mesostructure, based on the organization of micelle, above a critical micellar concentration (cmc) of surfactants. A water/ethanol solution of soluble silica and surfactants, below the cmc, is prepared. The ethanol evaporation leads to an increase of the surfactant concentration and to the formation of liquid-crystal mesophases formed by silica-surfactant self-assembled units. During this step it is important to avoid polymerization of the silica. Then it is possible to consolidate the structure and obtain a MBG by restarting the silica polymerization and through aging and thermal treatments [33] As a result, glasses are produced that are more bioactive than conventional melt-derived and sol-gel-derived ones by taking advantage of the high surface area exposed to biological fluids. In fact, the onset time for the in vitro HA precipitation was much shorter in MBGs than in sol-gel glasses with the same composition as ion-exchange mechanisms are emphasized and speeded up [34]..

2.5 Doping elements

It is possible to change and control over a very wide range the properties of bioactive glasses just by adjusting their composition using few oxides, such as SiO_2, MgO, B_2O_3, P_2O_5, CaO, Na_2O and K_2O. This offers an enormous number of possibilities for the optimization of bone substitutes. Bioactive glasses are even more appealing thanks to the fact that is very easy to add a lot more components in the network as trace dopants and to obtain wholly new properties or improve the already existing ones. In order to do so, doping elements such iron, copper, zinc, silver, titanium or aluminum can be added in form of oxides to the glasses recipes.

Iron is used for oncological treatment purposes. When iron is inside the amorphous network, it forms mainly micrometric magnetite crystals that grow into dendritical shapes. The glass is still bioactive, because HA forms on the amorphous portions of the surface. When a suitable cyclic magnetic field is applied to the glass, the hysteresis of the magnetic curve leads to the increase of the glass temperature. This unique property offers the possibility to treat bone cancer locally and in a very efficient way. Whenever a tumor mass is removed from the bone, the hole can be filled with Fe-doped glass powders or granulates. If there will be new tumor cells in the neighboring areas, the glass can be heated up to 50°C using a magnetic field, causing hyperthermia and death of the cancer cells [2].

Calcium, apart from playing an active part in the dissolution process of the glass, is a fundamental constituent of bones and it can activate bone remodeling. High calcium concentration activates special receptors that are present on both osteoblasts and osteoclasts, but while in the formers calcium ions

enhance the cell activity, in the latter they limit that. So, calcium promotes new bone formation. However, too high concentration can be toxic. Phosphate ions have the same behavior [2].

Zinc and magnesium have almost the same effects. They can prevent bone resorption by stimulating the proliferation and differentiation of osteoblasts and their bone mineralization ability. Zinc has also anti-inflammatory and antibacterial properties [35]. Magnesium is helpful during the manufacturing process of glasses since it can widen the workability windows and it increases bone cell adhesion [36].

Even though it is a bioinert ceramic, alumina can be used as a strengthener and it increases the wear resistance and the hardness of glasses containing it [29].

Copper, along with cobalt, has been studied for its angiogenetic properties. In fact, it is involved in the processes regarding the genesis and the replacement of the endothelium. Copper can be included into bioactive glasses also for its antibacterial properties [37].

Another very important element that can be used for antibacterial purposes is silver. Silver has a peculiar behavior since it has a narrow concentration window of application. In fact, if there is too less silver there are no effects, but if it is too much it is highly toxic. The use of silver is made easier thanks to the so called oligodynamic effect: the toxic effect of silver is worst for smaller cells, such as bacteria. So, it is important to carefully control the concentration of silver into the glass. There are two ways to insert silver ions in the glass network. It can be mixed and melted with the raw materials or it can be introduced by ionic exchange. If bioactive glasses are soaked into aqueous solutions, sodium ions exit from the glass and hydrogen ions enter. Whenever silver cations are also present in the aqueous solution, they can enter too. Bioactive glasses containing silver show an increase bioactivity, since silver is a very mobile cation, more than sodium, so it is more easily exchanged [2].

2.6 Bibliography

[1] L. Hench, "The story of Bioglass," *Journal of Materials Science: Materials in Medicine,* vol. 17, pp. 967-978, 2006.

[2] E. Vernè, *Biomateriali e Materiali Nanostrutturati,* Politecnico di Torino, a.y. 2016/2017.

[3] T. Pe, "Teach Pe," [Online]. Available: http://www.teachpe.com/anatomy-physiology/the-skeleton-bones/types-of-bones. [Accessed 18 settembre 2017].

[4] J. Henkel, M. A. Woodruff, D. R. Epari, R. Steck, V. Glatt, I. C. Dickinson, P. F. Choong, M. A. Schuetz and D. W. Hutmacher, "Bone Regeneration Basedo on Tissue Engeneering Concetpions - A 21st Century Perspective," vol. 3, pp. 216-248, 2013.

[5] [Online]. Available: http://emedicine.medscape.com/article/1948532-overview#showall. [Accessed 18 settembre 2017].

[6] [Online]. Available: https://www.britannica.com/science/osteon. [Accessed 18 settembre 2017].

[7] Q. Fu, E. Saiz, M. N. Rahaman and A. P. Tomsia, "Bioactive glass scaffold for bone tissue engineering: state of the art and future perspectives," pp. 1245-1256, 2011.

[8] F. Verland, J. Braux, J. Amedee and P. Laquerriere, "Inflammatory cell response to calcium phosphate biomaterial particles: an overview.," vol. 9, pp. 4956-4963, 2013.

[9] e. Williams D.F., Definition in Biomaterials, Elsevier, 1987.

[10] T. Kokubo and H. Takadama, "How usefull is SBF in predicting in vivo bone bioactivity?," *Biomaterials,* vol. 27, pp. 2907-2915, 2006.

[11] R. LeGeros and J. LeGeros, "Hydroxyapatites," in *An introduction to bioceramics*, 2nd ed., Imperial College Press, 2013.

[12] T. Kokubo, H. Kushitani, S. Sakka, T. Kitsugi and T. Yamamuro, "Soutions able to reproduce in vivo surface-structure changes in bioactive glass-ceramic A-W," *Journal of Biomedical Materials Research,* vol. 24, pp. 721-734, 1990.

[13] J. Jones, "Review of bioactive glass: from Hench to hybrids," *Acta Biomaterialia,* vol. 9, pp. 4457-486, 2013.

[14] L. Hench and O. Anderson, "Bioactive glasses," in *An introduction to bioactive ceramics*, 2nd ed., Imperial College Press, 2013.

[15] M. Salvo, *Ceramici avanzati,* Politecnico di Torino, a.y. 2015/2016.

[16] V. FitxGerald, D. Pickup, D. Greenspan, G. Sarak, J. Fitzgerald, K. Wetherall, R. J. J. Moss and R. Newport, "A neutron and X-ray diffraction study of bioglass with reverse Monte Carlo modelling," *Advanced Functional Materials,* vol. 17, pp. 3746-3753, 2007.

[17] R. Hill and D. Brauer, "Predicting the bioactivity of glasses using the network connectivity or split network models," *Journal of Non-Crystalline Solids,* vol. 357, pp. 3884-3887, 2011.

[18] L. Hench, "Bioactive glasses: gene activation," in *An introduction to bioceramics*, Imperial College Press, 2013.

[19] A. Gorustovich, L. Haro Duran, R. J.A. and B. A.R., "Angiogenic potential of bioactive glasses," in *An introduction to bioceramics*, Imperial College Press, 2013.

[20] H. Arstila, L. Huppa, K. Karlson and M. Huppa, "In vitro bioactivity of partially crystallised glasses," *Glass technology: European Journall of Glass Science and Technology A,* vol. 48, 2007.

[21] O. Peitl Filho, G. La Torre and L. Hench, "Effect of crystallisation on apatite-layer formation of bioactive glass 45S5," *Journal of Biomedical Materials Research,* vol. 30, pp. 509-514, 1996.

[22] A. Boccaccini and P. Ma, Tissue engineering using ceramics and polymers, Woodhead Publishing, 2014.

[23] F. Baino and C. Vitale-Brovarone, "Three-dimensional glass-derived scaffolds for bone tissue engineering: current trends and forecasts for the future," *Journal of biomedical materials research A,* vol. 97A, pp. 514-535, 2011.

[24] M. Brink, T. Turunen, R. Happponen and A. Yli-Urpo, "Compositional dependence of bioactivity of glasses in the system Na2O-K2O-MgO-CaO-B2O3-P2O5-SiO2," *Journal of Biomedical Materials Research,* vol. 37, pp. 114-121, 1997.

[25] M. Brink, "The influence of alkali and alkaline earths on the working range for bioactive glasses," *Journal of Biomedical Materials Research,* vol. 36, pp. 109-117, 1997.

[26] J. Knowles, "Phosphate based glasses for biomedical applications," *Journal of Materials Chemistry,* vol. 13, pp. 2395-2401, 2003.

[27] C. Vitale-Brovarone, E. Venré, F. Baino, G. Ciapetti, E. Leonardi and N. Baldini, "Bioresorbable phosphate scaffolds for bone regeneration," *Key Engineering Materials,* vol. 361, pp. 241-244, 2008.

[28] E. Abou Neel, W. Chrzanowski, D. Pickup, L. O'Dell, N. Mordan, R. Newport, M. Smith and J. Knowles, "Structure and properties of strontium-doped phosphate-based glasses," *Journal of the Royal Society Interface,* vol. 6, pp. 435-446, 2009.

[29] G. Kaur, Bioactive glasses. Potential biomaterials for future therapy, Springer, 2017.

[30] W. Huang, D. Day, K. Kittiratanaipiboon and M. Rahaman, "Kinetics and mechanisms of the conversion of silicate (45S5), borate, and borosilicate glasses to hydroxyapatite in dilute phosphate solutions," *Journal of Material Science: Materials in Medicine,* vol. 17, pp. 583-596, 2006.

[31] H. Fu, Q. Fu, N. Zhou, W. Huang, M. Rahaman, D. Wang and X. Liu, "In vitro evaluation of borate-based bioactive glass scaffolds prepared by a polymer foam replication method," *Materials Science and Engineering C,* vol. 29, pp. 2275-2281, 2009.

[32] C. Kresge, M. Leonowicz, W. Roth, J. Valrtuli and J. Beck, "Ordered mesoporous molecular sieves synthetized by a liquid-crystal template mechanism," *Nature,* vol. 359, pp. 710-712, 1992.

[33] C. Jeffrey Brinker, Y. Lu, A. Sellinger and F. Hongyou, "Evaboration-induced self-assembly: nanostructures made easy," *Advanced Materials,* vol. 11, p. 579, 1999.

[34] X. Yan, C. Yu, X. Zhou, J. Tang and D. Zhao, "Highly ordered mesoporous bioactive glasses with superior in vitro bone-forming bioactivities," *Angewandte Chemie International Edition,* vol. 43, pp. 5980-5984, 2004.

[35] M. Yamaguchi, "Role of zinc in bone formation and bone resorption," *THe Journal of Trace Elements in Experimental Medicine,* vol. 11, pp. 119-135, 1988.

[36] H. Zreiqat, C. Howlett, A. Zannettino, P. Evans, G. Schulze-Tanzil, C. Knabe and M. Shakibaei, "Mechanisms of magnesium-stimulated adhesion of osteoblastic cells to commonly ysed orthoapedic implants," *Journal of Biomedical Materials Research,* vol. 62, pp. 175-184, 2002.

[37] G. Hu, "Copper stimulates proliferation of human endothelial cells under culture," *Journal of Cellular Biocheistry,* vol. 69, pp. 326-335, 1998.

[38] E. Verné, O. Bretcanu, C. Balagna, C. Bianchi, M. Cannas, S. Gatti and Vi, "Early stage reactivity and in vitro behavior of silica-based bioactive glasses and glass-ceramics," *Journal of Material Science: Materials in Medicine,* vol. 20, pp. 75-87, 2008.

3 Bioactive glass-based scaffolds for bone repair

3.1 Introduction

In the United States, more than 6.2 million of bone fractures occur every year, 10 million people are affected by osteoporosis [1] and there are a lot of other disease or condition that may cause the need of bone regeneration or substitution, for example bone cancer, age-related disease, maxillofacial reconstruction or corrective surgery.

If the bone is not able to repair himself, there are many different ways that a surgeon can choose, depending on the type of bone involved, the entity of the damage and the age and health of the patient. In case of a fracture or trauma without the loss of bone materials, osteosinthesy means can be implanted, such as bone screws, intramedullary rod plaster (**Figure 3.1**) or an external mean is applied, the orthopedic.

Figure 3.1 Tibiae fracture treated with the implantation of an intramedullary nail [2]

When there are larger defects in the bone, due to tumor removal, big trauma or distraction osteogenesis (a surgical technique that allows to extend or modified the shape of the bone through an osteotomization and controlled distraction of the bone segments) [3], it may be not able to heal himself in a proper manner. In this case, it is necessary a kind of surgery called bone grafting. The surgeon transplants or implants new material, natural or man-made in the defect in order to help the natural healing process of the bone. A good material for bone grafts shall have the following properties: osteogenesis, osseointegration, osteoconductivity and osteoinductivity.

Osteogenesis is the ability to differentiate osteoblast from the osteoprogenitor cells present in the bone or in the new material, in order to produce new bone. Osseointegration is the ability of the graft to be incorporated by the surrounding bone without the formation of a fribrous layer. Osteoconductivity is the ability of the graft to act as a template, permanent or resorbable, supporting the growth of new bone and vessels. It is the ability to initiate and induce the bone formation. Osteoinductivity, in the end, is the ability of the material to induce the production of bone-forming cells via differentiation of multipotent mesenchymal stem cells. Those cells are in the surrounding tissue and produce osteoprogenitor cells [4].

There are three kind of bone grafts that can be employed:

Autografts: own patient's bone is used in this case. It is removed from a site where it is not strictly necessary, for example, the iliac crest, and transplanted. The main advantages of this kind of implant is that it is 100% compatible with the damaged bone and there is no risk of rejection and it is the only kind of bone graft that shows osteogenesis, osteoconductivity, osseointegration and osteoinductivity [4]. Unfortunately, allograft can only be used when the patient need little amount of new bone and it involved two different surgery [5], the removal of bone from an healthy site may cause death of the tissues nearby and the mechanical properties of the two different kind of bones often don't match [6].

Allograft, Xenograft: in order to solve some of the problems involved in the use of autograft, it is possible to transplant bone materials from another living being, humans (allograft) or not (xenograft). In this case, the availability of materials is much greater, there is a wider choice about the type of bone to be used and there is no need of a second surgery. In any case, to limit the risk of immunological reaction and the antigenicity of the allografts or xenografts, they are chipped and threated to remove antigenic structures. However, this type of bone grafts lack of osteogenic properties [4], due to the antigenic procedure that destroys growth factor and viable cells, and can cause the need of immunosuppressant drugs assumption or the transmission of viral and bacterial disease [6], such as HIV, tuberculosis or hepatitis C.

Synthetic materials: the alternative to the transplantation is the implantation of man-made biomaterials, in the form of granules or as scaffolds that have the task to simulate the bone structure and to stimulate the restoration processes of the healthy bone. These implants can be made of hydroxyapatite, bioactive glasses and ceramic-glasses.

A scaffold is a three-dimensional structure that is properly designed to act as a template for the regeneration or the remodeling of the bone. To do so, it has to mimic the structure of the bone, show the proper mechanical properties and interact in the right way with the biological environment of a damaged bone.

There are two main types of bone substitute scaffolds: permanent and bioresorable. The first one is made of non-biodegradable materials, and it is meant to stay in the fracture site, just being embedded in the new formation bone. The second type, instead, is composed by biodegradable component, in order to be resorbed leaving space at the new bone. In this manner, at the end of the healing processes, only human bone can be found. In this case is very important to tailor carefully the degradation kinetics and the loss of properties along the processes. In fact, especially in case of load bearing site, it is important that the scaffold maintains its mechanical properties over a minimum value, to support the growing bone. Many different materials have been tested and used to manufacture scaffolds for bone regenerations. Polymers were used to create bioresorbable scaffold, synthetic and naturally ones both, but they are too weak to have a good performance in load-bearing bone regeneration. Collagen, polyesters, polyglycolide, polylactide and polycaprolactone are some of the polymers that have been used in the manufacturing of scaffolds per bone tissue engineering. Due to the very low mechanical properties of polymer scaffolds, organic-inorganic composites were studied, to strengthening the polymer phase and to toughening the ceramic one. For this purpose, calcium-phosphate based ceramics and bioactive glass are used. Fully ceramic scaffolds are widely studied, such as calcium-phosphate and bioactive glass ones. They offer the best mechanical strength and they are very promising for the manufacturing of scaffolds and their biocompatibility and bioactivity is well documented. There are several kinds of calcium-phosphate scaffolds that can be found. One of the most used is hydroxyapatite (HA, $Ca_{10}(PO_4)_6(OH)_2$), which is the same mineral crystal that composes human bones. Different compositions can be used, as biphasic calcium-phosphate, gypsum ($CaSO_4$) and β-tricalcium phosphate (βTCP). They have the ability to grow HA on their surface when put in contact with biological fluid and some of them are also biodegradable. These elements can be mixed in order to tune their properties, such as bioactivity, mechanical ones and bioresorbabiliy [7]. Also, bioactive glass-based scaffold can be permanent or biodegradable both [1]. There are three main classes of glass that are used in the fabrication of scaffolds, sorted by their former oxide:

- Silicate based (SiO2): in this group there is the founder of all the bioactive glass, the 45S5 Bioglass by Hence, along a very large amount of other composition;
- Borate based (B2O3): some studies had shown that this kind of glasses may have a more enhanced bioactivity than the silicate-based family, but further investigations are needed;
- Phosphate based (P2O5): this glass family has been founded to have some peculiar properties of biodegradation, despite its bioactivity lower than the silicate-based glasses [6].

Beside the former oxides, a lot of other oxides can be used to tune the properties of the glasses, give them peculiar properties or modify the bioactivity processes.

3.2 Features and properties for a proper scaffold design

Since the aim of a bioactive glass scaffold is to substitute the damaged bone, guide and increase the healing process of the surrounding bone, it has to be as much similar as possible to the healthy bone. So, all the manufacturing process and the materials shall be carefully selected in order to obtain the suitable properties. Furthermore, the scaffold shall be obtainable in a very large variety of shape and dimension, maintaining a reasonable cost, to fit all the particular needs of the surgeons and the patients. Last but not least, it must sustain a sterilization process, as every biomedical device. The key features of a porous scaffold for tissue engineering are summarized in **Figure 3.2**.

1. **Ability to deliver cells**
   The material should not only be biocompatible (i.e. harmless), but also foster cell attachment, differentiation, and proliferation.
2. **Osteoconductivity**
   It would be best if the material encourages osteoconduction with host bone. Osteoconductivity does not only eliminate the formation of fibrous tissue encapsulation but it also brings about a strong bond between the scaffold and host bone.
3. **Biodegradability**
   The composition of the material, combined with the porous structure of the scaffold, should lead biodegradation *in vivo* at rates appropriate to tissue regeneration.
4. **Mechanical properties**
   The mechanical strength of the scaffold, which is determined by both the properties of the biomaterial and the porous structure, should be sufficient to provide mechanical stability to constructs in load bearing sites prior to synthesis of new extracellular matrix by cells.
5. **Porous structure**
   The scaffold should have an interconnected porous structure with porosity > 90% and diameters between 300-500 μm for cell penetration, tissue ingrowth and vascularisation, and nutrient delivery.
6. **Fabrication**
   The material should possess desired fabrication capability, e.g., being readily produced into irregular shapes of scaffolds that match the defects in bone of individual patients.
7. **Commercialisation potential**
   The synthesis of the material and fabrication of the scaffold should be suitable for commercialisation.

Figure 3.2 Overview of suitable properties for a scaffold aimed to bone regeneration [16]

3.2.1 Biocompatibility

Since the 3D scaffold will be placed inside the human body, it should have the ability to stimuli an appropriate response from the surrounding biological environment without modifying it or itself, unless that is the aim, for example a resorbable scaffold. In the medical field this mean that the scaffold has not to elicit a foreign body reaction, which is the way the human body respond to a corps that it does not recognize as its. When an external body is detected in the bone, the normal healing process does not occur. Instead an inflammatory event occurs and fibroblasts envelop the corps generating a fibrous tissue. When a material is implanted inside the human body, the first thing that happen is the adsorption of water molecules and proteins. Then, if there is not a proper biocompatibility, macrophages arrive on the surface of the device, trying to dismantle it. Since they do not succeed, they fuse together and form giant cells in order to eliminate the external body. The giant cells secrete cytokines (a protein signaling agent) that summon fibroblasts on site. They start to produce collagen to encase the biomaterial into an acellular-collagenous bag. This bag, which can be formed in 4-8 weeks, may lead to a prosthesis loosening, to the ejection of a subcutaneous implant or to the opacification of an ocular one [5].

The best biocompatible material for bone scaffold is the one that show properties of osteoconductivity, osteinductivity, osseointegration and osteogenesis. Unfortunately, the only type of bone substitutes that has all of these properties are the autografts, since they have a lot of disadvantages.

In case of scaffold that will undergo a degradation path, the disposal and removal of the degradation products shall be carefully studied. An accumulation of the by-products could trigger inflammatory response in the body. In the tissues surrounding the scaffold the metabolic activity and the vascularization are poor, so the elimination ability of the by-products is reduced [8]. For example, an inflammatory process can occur in response to the presence of calcium-phosphate particles. Despite the benefits that this kind of materials bring to the patient, in some case the low dissolution/precipitation process may lead to an inflammatory response and to a loosening of the implant [9].

3.2.2 Hierarchical structure and porosity

The human bone has a very complex structure on very different dimensional levels, from the nanoscale to the macroscale. In the cortical bone there are features, such as the smallest vascular channels and canaliculi, in the range of 1 to 5 µm, Volkman's canal and osteocytes' lacunae are in the range of 5 to 15µm and Haversian canal are up to 100 µm [10]. Since the scaffold shall act as a template for the correct growth of the bone, it should have peculiar features at many different dimensions. This mean that a correct design and manufacturing process lead to a highly porous scaffold, about 90% of voids, with interconnected pores and a dimension range that spread from 300 µm to less than 10. In fact, it has been showed that interconnected pores with size under 100 µm lead to a poor vascularization for the area and to hypoxic grown conditions. This mean that also cartilage will form, not only mineralized bone. Larger pores (>200/300 µm), on the other and, lead to a good vascularization and therefore to the formation of new mineralized bone, also at a higher ratio [11]. The disadvantage of larger pores is that they affect in a bad way the mechanical properties. However, pores between 500 and 1000 µm are useful in order to tune and decrease the Young's modulus of scaffolds. This is mean to avoid stress shielding of the bone by the implant. Even larger pores, with millimetric dimension, can be introduced, such as sutures' anchoring points for surgical fixation. Along macroporosity, also microporosity is needed. Pores between 2 and 10 micrometers enhance the specific area of the scaffold, increasing the protein adsorption, the cells adhesion and the diffusion of nutrients and the removal of waste. A porous structure, specifically on the surface, also increases the mechanical interlocking with the surrounding bone ensuring a better load transfer and avoiding the loosening of the implant.

3.2.3 Mechanical properties

Since the scaffold has to act as bone substitute during the period of new bone formation, it may have also to withstand mechanical loads, especially if the implant was made in a load bearing location. So, it is important that the scaffolds show adequate properties. They have to be strong enough not to break but they haven't to be to strong and stiff in order to achieve a correct load transfer to the bone. This task is not so easy to get, because each bone site in the human body is subjected to very different stimuli, so the mechanical properties of the scaffold shall be customizable with respect to the very specific application, implantation site, age and health of the patient, his/her lifestyle and so on. Despite the intrinsic fragility of the ceramic materials, due to the fabrication process that lead to the presence of defects, and the porosity that is generated in the scaffold, several research groups achieved to produce glass scaffolds that have the same properties of the human bone [1], as shown in **Figure 3.3**.

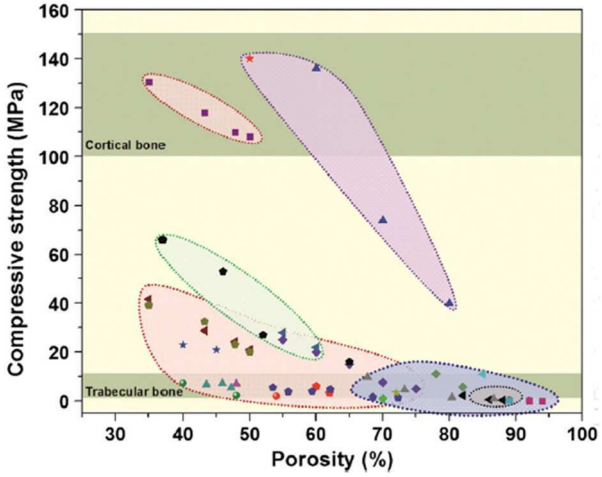

Figure 3.3 Porosity vs Compressive of different glass scaffold compared with the human bone. Gray: sol-gel; green: freeze casting; pink: thermally bonded particles; purple: solid free from fabrication; blue: polymer foam replication. Adapted from ref. [1].

For example, high mechanical properties are possible by producing anisotropic scaffold, through orientation of the pores. It has been found that in the direction parallel to the one of the pores the compressive strength is more than twice the one in the perpendicular direction. Such orientation is quite easily achievable by solid free form fabrication and unidirectional freezing of suspension. Also, flexural strength matching the one of the trabecular bone was achieved in some scaffold, but nothing comparable to the one of the cortical one. Another property that shall receive attention is the toughness of the scaffolds. Due to is fragile-ductile composite structure, human bones are very though materials, with the ability to increase the fracture work by means of crack deflection, organic bridging between mineral domains and microcracking. More, it has the unique ability to repair the crack, always restoring its properties. In order to use scaffolds as bone substitute in load bearing areas, their toughness must be adequate. Scaffolds have been toughened in different ways. For example, Peroglio M. et al. improved the mechanical properties of a biphasic hydroxyapatite/β-tricalcium phosphate scaffolds by infiltrating it with poly(ε-caprolactone), obtaining a coating of the internal structure of the scaffolds. In this way, polymeric fibrils crack-bridging was achieved as main toughening mechanism [12].

3.2.4 Surface properties

The surface of the scaffold is the main site where the first interaction between the biomaterial and the human body take place. Immediately after the implantation, the scaffold is kept in contact with the biological fluid, especially blood from the surgical procedure. In a few nanoseconds after that the biomaterial is placed into the body, a layer of adsorbed water forms on the surface. Water molecules may have different orientation, with respect to the interaction with the material. Right after, proteins interact with the water and they are adsorbed on the surface. The orientation of the water molecules determines if the proteins remain in its native state, so cells can recognize them and interact with them in the right way, or if the proteins are denatured, causing bad interactions with cells. Since the topography of the surface determines what kind, how many and the conformation of the proteins adsorbed, controlling the surface at a nano-metric level might be a very interesting method to tune the interaction between the biomaterials and the cells. This can be achieved by creating surfaces with topographical features that have the same dimensions of the proteins wanted to be adsorbed. Webster at al. demonstrated an enhanced osteoblasts adhesion on nano-patterned substrate. They produce nanophase titania and alumina, 32 and 23 nm grain size respectively, and notice that in fetal bovine serum there is a significant increase in osteoblast adhesion. They stated also that, since the adhesion increase was for the alumina and titania both, the interaction between the proteins, and later the cells, and the surface is independent from the chemistry of the surface but rely on the topography of the ceramic surfaces [13].

3.3 Materials for bone-tissue engineering

Even if this work is mainly focused upon the use of a silica-based bioactive glass for the production of scaffolds by direct ink writing, there has been a large use of different materials in order to manufacture bone substitute scaffolds, in the effort of mimicking the composite nature of the bones. Among them there are organic and inorganic ones, natural and synthetic. Furthermore, in recent years, researchers tried to couple them with bioactive molecules, proteins, drugs and even to seed and culture cells on them prior to the implantation [14].

3.3.1 Bioceramics and bioactive glasses

The first material used to obtain scaffolds, thanks to the fact that it is the mineral component of the bone, is hydroxyapatite (HA). Also, other calcium phosphate minerals have been used. Due to their similarity with the bone inorganic phases, these materials have great biocompatibility, but, since HA is stable in biological environment, they are not biodegradable and will stay unmodified in the bone. Calcium phosphates and their derivatives are classified as Class B bioactive materials according to the fact that they exhibit only osteoconductivity. Class A bioactive materials, instead, have also osteogenetic and osteoinductive properties. The huge family of the bioactive glasses belongs to this class. From the first 45S5 Bioglass developed by Hench, to the latest phosphate- and borate- based glasses, all of them are widely used in the manufacturing of bone substitution scaffolds.

3.3.2 Natural polymers

In nature it is possible to find some natural “reactors” for the synthesis of polymers, for example some microorganisms can produce long organic molecules as byproducts of their metabolism. Due to their natural source, this kind of polymers should not activate inflammatory or adverse responses when implanted into the body. Anyway, they lack of mechanical properties and to mass produce them is difficult, because it is hard to obtain high amount of materials, the extraction can be expensive and there can be some immunogenic troubles by introducing in the body a foreign kind of collagen. Some naturally occurring polymers have been tested as materials for bone tissue engineering. For example, polyhydroxyalkanoates (PHAs) derived from bacterial cultures have been used in blending with polyhidroxybutanoates and polyhidroxyhexanoates to tune their properties. Since they are thermo-processable, biodegradable and biocompatible polymers, PHAs are suitable for bone tissue scaffold manufacturing

3.3.3 Synthetic polymers

Man-made polymers offer a large number of advantages with respect to the naturally occurring ones, such as better processability, low cost, tailorable performances (mechanical properties, biodegradation rate, and biocompatibility), more constant products and properties. So great efforts were made to develop new and more performing biopolymers. For example, poly(D,L-lactic acid) (PDLLA) is one of the most promising. It is completely biodegradable and can be produced in combination with bioactive glasses and biomolecules can be added. Scaffolds loaded with growth factors, drugs and antibiotics are supposed to increase the speed of the regeneration process and to overcome the problems correlated to infection in the implant site and to foreign body response, which are the major drawbacks of the use of such polymers.

3.3.4 Polymer/bioceramic composites

In material engineering combining different kind of materials is common to obtain a new material with enhanced or properties, resulting from the characteristics of the starting raw materials. Thus, it is possible to control mechanical, physical and chemical properties. In the field of tissue engineering, especially for bone applications, merging polymers and bioactive glasses is very interesting and can lead to optimal results. One of the problems of using bioactive glasses is their intrinsic fragility, as they formally are ceramic materials and are often used in a porous structure, which is full of defects. Coupling them with polymers, for example by coating, is an effective way to increase toughness. Otherwise, polymers, despite being tough, are too weak for load-bearing bone substitution. Glass fillers have the effects of improve their mechanical properties. Also, biological and chemical advantages can be obtained. When they are degraded, polymers release acids that can provoke inflammatory responses. Glasses, instead, increase the pH of the fluids during their dissolution, so they can contrast and buffer

the effects of the polymer resorption. By the way, it is not so easy to obtain good composite materials, since the interaction between the two phases must be very well deigned to optimize all the properties.

3.4 Manufacturing Processes of bioactive glass-based scaffolds

3.4.1 Overview of the fabrication strategies

The first attempt to produce a bioactive glass-based scaffold was made in 2002 by Sepulveda et al. and the manufacturing method was based on a sol-gel process, with *in situ* foaming in order to obtain a porous structure [15]. Since there a lots of research groups had gone through a multitude of studies trying to find the perfect manufacturing process to obtain the perfect scaffold. This process should be the one that allows to obtain the optimal properties for a bone substitution, such as the correct mechanical strength, controlled and proper porosity, adequate surface morphology and the absence of toxic elements, which may remain from the use of poisonous solvents or production means. Furthermore, it has to be reliable and repeatable, in order to be quite a mass production process. But it shall be very customizable, aiming at a very high level of personalization for the unique patient. Last but not least, the manufacturing of the scaffold has to be economically convenient, fast and as safer as possible regarding the workers and the environment both. As inspiration for the development of new manufacturing techniques, bioceramic researchers looked at the process already used in the field of porous ceramics, trying to do almost the same things with bioceramics and bioactive glasses.

The processes and the technologies that have been developed till now can be grouped in two different main groups: conventional and Rapid Prototyping (RP), or Solid Freeform Fabrication (SFF) [16]. The first group of methods follows the top-down manufacturing approach, which involves the removal of pieces from a bulk material in order to create the wanted shape. They are also called subtractive manufacturing technologies, since material that compose the scaffold is removed after the initial fabrication. In the second group are included the technologies that involve a bottom-up approach, the artefact is built piece by piece, exactly in the final shape. Those are the additive manufacturing technologies.

A short overview of the techniques used in the manufacturing of scaffolds for bone tissue engineering, listed in **Table 3.1**, will be provided. They will be divided into conventional and SFF. RP technologies, with particular emphasis on Direct Ink Writing (DIW), will be discussed in a deep manner, since they are the basis of the present work.

Table 3.1 Overview of the manufacturing techniques for the production of scaffold for bone tissue engineering

Conventional		
	Foaming techniques	Gel-casting foaming, sol-gel foaming, H_2O_2 foaming
	Thermal consolidation of particles	Organic-phases burning out: polymeric porogens, starch consolidation, rice husk method
	Porous polymer replication	Coating methods, foam replication
	Freeze-drying	Freeze casting of suspension, Ice-segregation-induce self-assembly (ISISA)
	Thermally induced phase separation (TIPS)	
	Solvent-casting and particulate leaching (SCPL)	
Rapid Prototyping		
	Selective laser sintering (SLS)	
	Stereolithography (SLA)	
	Direct ink writing	3D printing Ink-Jet printing Robocasting

It is important to notice that almost every method for the production of bone scaffolds, but in the case of composite with polymers, involves a consolidation step, the sintering of the glass powders. In the field of bioactive glass this is a crucial passage, since a devitrification of the material leads to a loss in the bioactive properties. On the other hand, sintering at to low temperature means a bad densification that leads to low mechanical properties. So, it is very important that the thermal behavior of the material is well known and that the sintering process is carefully programed.

3.4.2 Sintering of crystalline ceramics and glasses

Sintering is the consolidation process of an already shaped body, called green, which may be formed out of ceramic powders only, by means of pressure, or a mixture of powders and a binder, such as water or a polymeric one. It is a thermal process, achieved by heating the green at a temperature that is about 0,5-0,75 the melting temperature and keeping it at that temperature for a certain amount of time. In this way, powders densify, generating chemical bonds between them and reducing the green's volume.

The sintering process can be sorted by mean of different parameters. The first one might be whether or not pressure is applied as aid to the process. In case of absence of pressure, the process is called "natural sintering", if it is applied, "sintering under pressure". Pressure can be used in many ways, for example as uniaxial pressure or isostatic pressure (hot isostatic pressure, HIP, sintering). Another classification can be made on the different phases that are developed during the process. Four different kind of sintering can be found:

- Solid state sintering: the only phase that is present during the process is the solid one, without formation of liquid. The main mechanism for the densification is diffusion in the solid state;
- Liquid-phase sintering: it occurs when a small amount of liquid appears during the process, 5-10%. It enhances the sintering by rearranging the particles and forming liquid bridges between them. This increase the surface area in contact between two particles but the liquid phase is not enough to fill the porosity. The properties of the liquid condition the densification. This process is widely used in the fabrication of ceramics, but it may lower the maximum application

temperature, especially for structural application, due to the softening point of the solidified liquid phase.

- Vitrification: when the liquid phase is high enough to fill the pores. This typically required more than 25% in volume of liquid phase that can be formed by a reaction between solid state precursors or by melting of one of them. During cooling, the liquid phase can either crystallize or vitrify.
- Viscous sintering: this process involves the heating of a glass mass above or near its softening temperature and the densification of it by viscous flow under the effect of surface tension forces.

Two more kind of sintering can be, reactive or non-reactive, depending if the precursor powders can react one with another during the heating or not. [17]

Before it is possible to gain the actual densification of the powders, during the heating, it is necessary a step-in order to remove the binder, if it is present. It is mandatory to have a good control over this stage and to achieve the best removal as possible, in order to avoid contamination that can change the properties (mechanical, physical, chemical…) and the aspect of the resulting product.

3.4.2.1 Thermodynamical Driving Force: Reduction of the free energy

The driving force of the sintering is the reduction of the total surface free energy of the compound. The total surface energy of the compact is expressed as γA, where γ is the specific surface energy, of the solid-gas interface, and A is the total surface are. Thus, the reduction can be expressed as following:

$$\Delta(\gamma A) = A\Delta\gamma + \gamma\Delta A \qquad (3.1)$$

$\Delta\gamma$ is the variation in the surface energy due to the reducing of the solid-gas interface, which leads towards densification of the compact. On the other hand, a reducing of the superficial area, ΔA, leads to coarsening without densification. The firs path results in a correct sintering, the second leads only to a gain growth, without the removal of the pores, as **Figure 3.4** shows. The two path that lead to a decrease of total energy surface may occur together, but usually the surface area reduction happens at lower temperature than the densification.

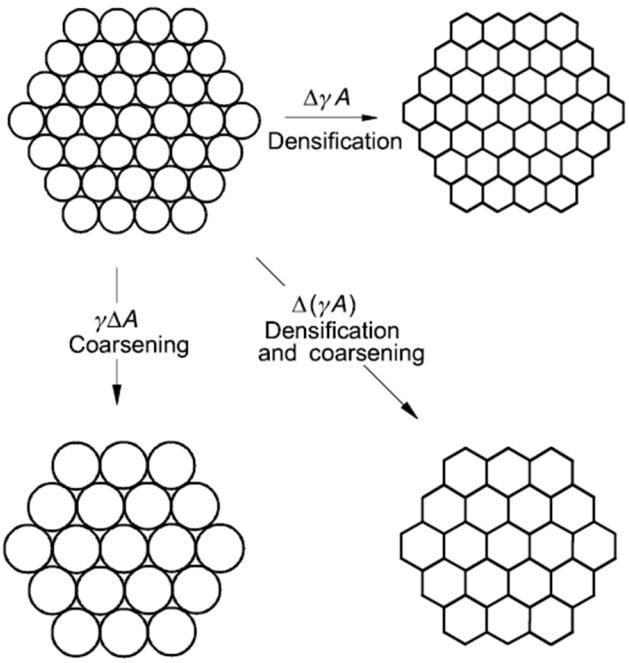

Figure 3.4 Driving force effects: coarsening without pores removal and densification [18]

After the densification of the powders a stage of grain growth may occurs, this growth in the grain size is called Ostwald ripening. This is due to the fact that grain boundaries are high energy areas, so, according to thermodynamic laws, they tend to be minimized to reduce the total energy. During this phenomenon small grains disappear, they are incorporated into the bigger ones, and the average grain

size increase. This effect appears in solid-state sintering and liquid-phase sintering both. Since the densification rate lowers as the grain size increases, it is little probable that the compact densifies after coarsening, so it is important to support the densification during the process [19].

3.4.2.2 Kinetic aspect: necks formation and diffusion

Referring to a solid state sintering, it is possible to describe the sintering process dividing it into different steps. The first one, the *initial stage,* involves the creation of necks between two different grains. This leads to a little shrinkage, about 5% if coarsening does not occur. During the *intermediate* stage, there is the diffusion of material from the grains to the voids, in order to reduce the total surface energy. At the end of the latter stage, the compact has been turned into a 3D structure with a network of interconnected channel-like pores. This stage ends when only 5-10% of porosity is left. The *final stage* starts when the pores network starts to break into isolated porosity and coarsening takes place more substantially. This is why it is hard to remove the last pores. To describe the basic theory for sintering, the particles are approximated to a spherical shape.

Since powders are not an infinite flat surface, the equilibrium pressure between the solid and the gas phases is different from the vapor pressure, P_∞. According to the La Place law, the internal pressure, P_i, for a spherical shape, with radius r, is:

$$P_i = P_\infty + \left(\frac{2\gamma}{r}\right) \qquad (3.2)$$

γ is the surface tension between the gas and the solid.

For a pore, the same formula is applied but the radius is considered negative.

So, the inner pressure in a spherical grain is greater than the one on as infinite plan surface and on the spherical surface there are compressive forces acting. In case of two grains connected by a neck, a toroidal shape with concave sides, **Figure 3.5**, the external surface is in compression the neck surface is in traction. This results into a different pressure in the bulk that leads to a material flow from the grain to the neck region. For the same reason, there is also a difference in the vapor pressure between the grain surface and the neck area, provoking also a process of evaporation and condensation and a gas-phase diffusion. In this case, however, the limiting factor is the condensation rate, that control the kinetic of the process.

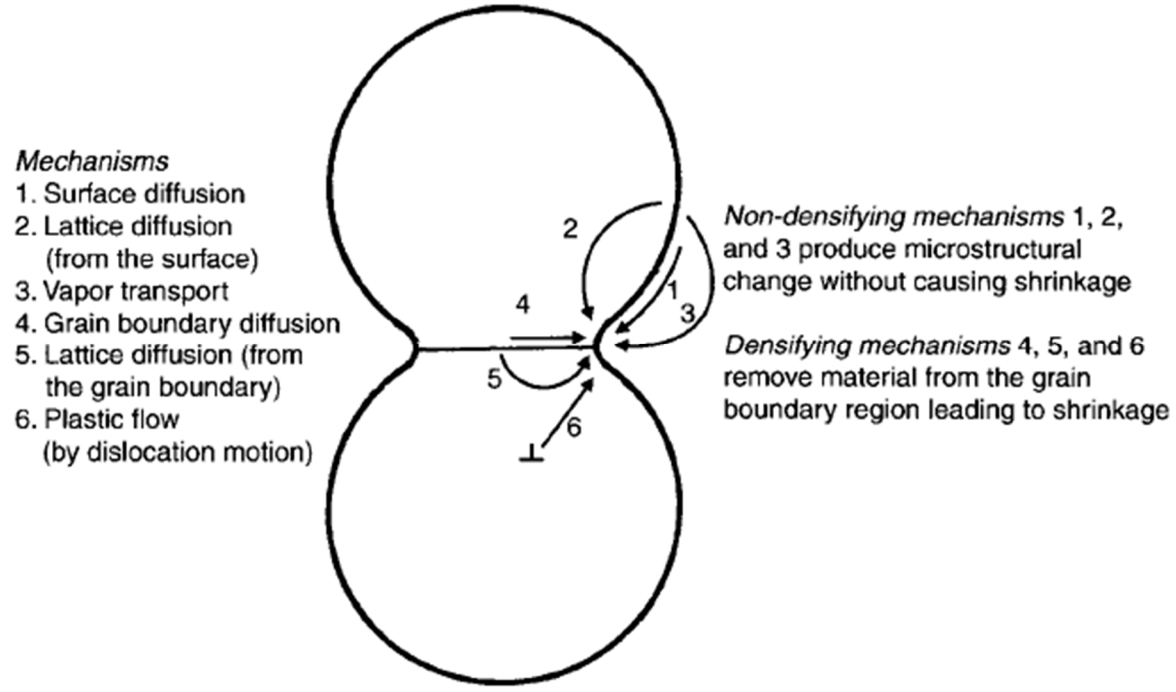

Figure 3.5 Scheme of spherical grains bounded by neck with description and effects of the different mechanisms of diffusion [20]

Depending on the site where the atoms that are diffusing came from, there are different mechanisms of diffusion that leads to a different result, in densification and in microstructure both. Bulk, grain surface and grain boundary can be sources of material. Atoms can diffuse through different means, this also imply that different diffusion coefficient controls the rate of their flows. During sintering several kinds of diffusion can occur: on the surface, inside the grain lattice, between grain boundary and on gas phase.

If the material source for diffusing atoms is the grain surface, so there will be no appreciable densification, the distance between the centers of the grains does not change. There is only a consolidation. On the other hand, if atoms came from the bulk or the grain boundaries, there will be densification. In order to stay in contact, the centers of the gain will come closer. Depending on the mechanism, different parameters may control the process. An overview of the different mechanisms, their effect and parameters are listed in the table above, **Table 3.2**.

Table 3.2 overview of material flow mechanisms, the material sources, their effects and the parameters involved

Diffusion Mechanism	**Material source**	**Effect**	**Parameters**
1) Surface diffusion	Grain surface	Consolidation	Surface diffusivity
2) Lattice diffusion	Grain surface	Consolidation	Lattice diffusivity
3) Vapor transport: a. Evaporation/ condensation b. Gas diffusion	Grain surface	Consolidation	Difference in vapor pressure Gas diffusivity
4) Grain boundary diffusion	Grain boundary	Densification	Grain boundary diffusivity
5) Lattice diffusion	Grain boundary	Densification	Lattice diffusivity
6) Plastic flow	Bulk	Densification	Viscosity

In practice, every one of these mechanisms can occur at the same time and they merge their effects. The neck creation and growth rate depend on the different parameters (**Figure 3.6**), proper of each mechanism, on the radius of the particles, the smaller it is, the faster the neck grows, and on the temperature, by an Arrhenius-kind equation.

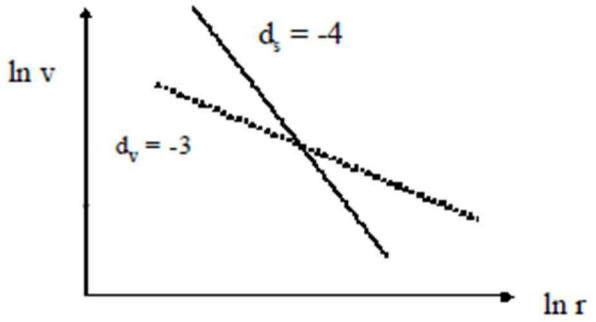

Figure 3.6 Dependence of the neck growth rate on the grain radius. Temperature and time are fixed [19]

3.4.2.3 Microstructure

To obtain a performing ceramic artefact, the control on the final microstructure is essential. Stated the brittle nature of the ceramic, if at the end of the sintering process too big pores remain, the mechanical properties will be much affected. Since is important to understand how the different parameters, such as grain size distribution, atmosphere, temperature increase rate, influence the final result.

Due to the grain size distribution, surface with different curvature will appear at the contact point of different sized grains. According to the Laplace law, on the smaller grain side, which has a positive curvature, there will be a compressive force toward the bigger one, which has a negative curvature. This means that, due to the pressure gradient, there will be a flow of material from the small grain to the big

one, till the disappearance of the former. The only case of stable grain boundary is when they are perfect flat. It is the case of a six-sided grain [18], as pictured in **Figure 3.7**.

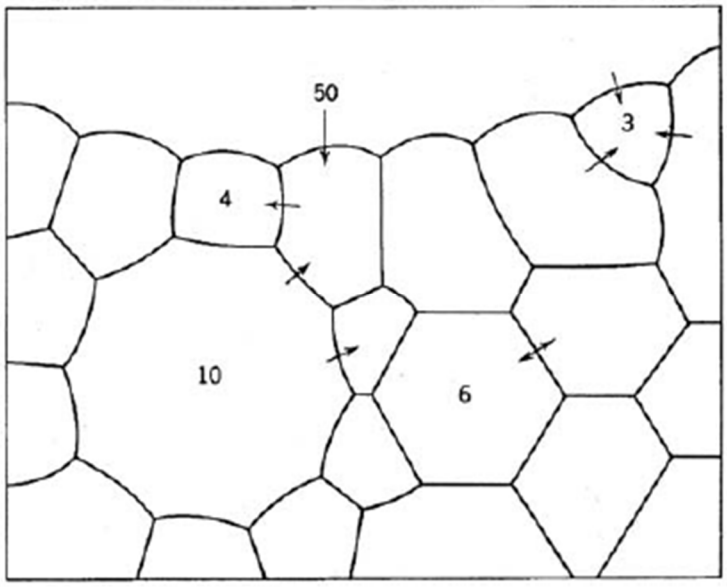

Figure 3.7 Scheme of the grain boundary migration. Sign of the curvature change when the number of sides change from less than size to more than six (numbers in the picture refer the number of sides of the grain). Arrows show the directions of the motion of the boundaries [17]

The shift of the grain boundaries can be limited by the presence of second-phase precipitates, with effect proportional to their diameter, and by pores. Such as grain boundaries, also pores can move, due to the effect of their curvature. Their mobility depends on their size and the diffusion mechanism that is involved. Depending on the velocity of the pores with respect to the one of the grain boundaries, different microstructures may occur:

- Pores with the same velocity as the grain boundary: they move together and different pores can catch up with other pores, forming a bigger one. The result is an intergranular pore.
- Pores much slower than the grain boundary: the pore and the grain boundary separate and the growth rate of the grain increase. The pore will be incorporate, there can be several big grains with many intragranular pores.

3.4.2.4 Liquid-phase sintering

All that was previously discussed, mainly applies at the case of solid state sintering, which is the easiest to model and discuss. Different mechanisms are involved when a liquid phase appears during the sintering. This liquid might come from some of the components of the materials or might be originate by mean of sintering aids, which can be introduced in the compact for very different reasons, one of them is to give birth to a liquid phase during the sintering.

When a liquid appears during the sintering, different phenomena take place:

- Increasing in the adhesion between grains;
- The migration of the liquid can close some of the porosity, with a certain amount of shrinkage. Since the liquid fraction is low, less than 10% of the volume, it is not capable of eliminate all the porosity only by itself;
- Diffusion in liquid phase can speed up certain processes.

The presence of a liquid makes achieving the sintering easier.

The liquid formation is more controllable if it comes from a sintering aid rather than from an incongruent melting of one of the compounds. A sintering aid can be a low melting point element or a compound that can easily react with the densifying material, producing a liquid. This liquid can be either permanent

and be present through all the sintering, solidifying at the end of the process, most likely into an amorphous phase, or it can disappear during the sintering.

The liquid-phase sintering can be divided into different processes:

1. Formation of the liquid phases (form melting or reaction), the liquid redistributes in the compact;
2. Due to the formation of capillary stress, the particles of the green are rearranged;
3. Solution-precipitation processes lead to the densification of the material;
4. A further densification is achieved through the removal of pores trapped in the liquid phase.

According to the three-stage model theory, developed by Cannon and Lenel, these points can be grouped in three stages (**Figure 3.8**):

- Initial stage (1)
- Intermediate stage (2,3)
- Final stage (4)

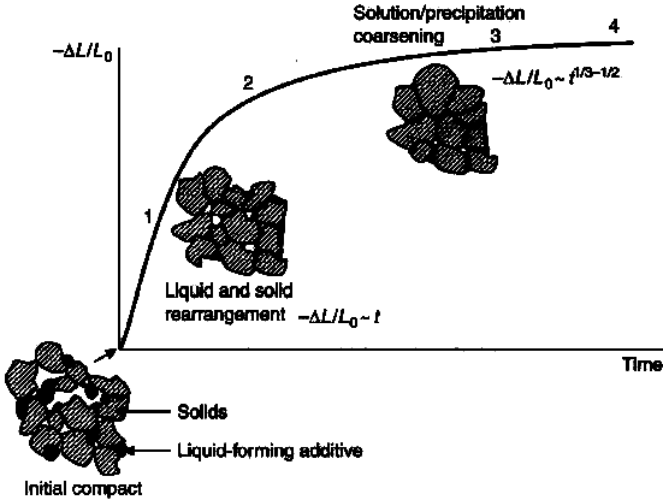

Figure 3.8 Stages of liquid-phase sintering: 1) liquid formation and rearrangement; 2) solid rearrangement due to capillary forces; 3) solution-precipitation densification; 4) pores removal from the liquid phase [20]

During the initial stage, the wetting angle, θ, plays a crucial role in the flows of the liquid. If it is greater than 90°, the liquid won't wet the particles and there will be no flow. If lower, there will be a dispersion of the liquid within the compact, with the formation of menisci between the particles. When θ is less than 90°, a liquid flow is started and the capillary force can be quite high at the micrometric scale, like several MPa for a curvature of 0.5 µm and a surface energy of 1 J/m^2. The pressure gradient causes rapid flow of the liquid, the rearrangement of the solid particles and to a pore filling. More, due to Laplace law, there is less pressure inside the liquid meniscus that in the pore, so it creates capillary forces that keep together the grains. The first stage is over when all the solid particles are coated by a thin liquid film and the fluid is dispersed homogeneously within the compact, reducing gas-solid interfaces [20].

Now the intermediate stage takes places. The grains partially dissolve in the liquid, preferentially in the contact area with the liquid, and the material diffuse towards the surface of the liquid, where precipitation takes place. The consequences of this process are a flattening of the contact area, a modification of the grain shape and a reduction of the pore that leads to the densification of the compact.

The final stage, that involve solid-solid state sintering, occurs when the contribution to the densification of the dissolution/precipitation process is negligible. In this stage all the mechanisms of the solid-state sintering are active and lead to the final density of the artefact.

A later model, proposed by Kwon and Yoon, suggest that the controlling and essential process of the liquid-phase sintering is the pores filling by the liquid.

3.4.2.5 Sintering of an amorphous material

Since an amorphous material, such a glass, does not have a crystalline structure and, therefore, grains that can coarsen do not exist, the predominant sintering mechanism is the viscous flow of the material. In this case, the fundamental parameters involved in the sintering are the heating rate and the viscosity of the material, more precisely, the viscosity as function of the temperature. The latter parameter influences the models that can be used to represent the kinetic of the sintering process, the former one can change the densification curve of the glass. In fact, the higher is the temperature increase rate, the higher will be the temperature to obtain a certain densification. This is a kinetic effect, the glass does not have enough time to flow and densify. For glassy materials it is fundamental, in order to obtain a high density, that the sintering temperature is lower than the onset of crystallization. If crystals form inside the materials, in fact, they will stop the viscous flow and the sintering process itself.

3.5 Conventional technologies

The conventional technologies include all the manufacturing methods but the ones that involve the replication of a computed model, those are the SSF techniques. Among the conventional methods for the manufacturing of glass-ceramic and polymer/glass composite scaffolds both there are the foaming methods, the thermal consolidation of particles, the porous polymer replication techniques, the freeze-drying processes, the thermally induced phase separation and the solvent-casting and particulate leaching.

3.5.1 Foaming Methods

This group of method involve the use of a foaming agent and melt-derived glasses or sol-gel based glasses can be used both. Usually a slurry or a suspension is prepared and the foaming agent is added. Methods for producing the pores and the bubbles in the scaffold can include: direct injection of gasses; vigorous agitation; gas generation through chemical reaction; thermal decomposition of peroxides.

The method that involve the use of a foaming process are:

- Gel-cast foaming
- Sol-gel foaming
- H2O2 foaming

Some of the drawbacks of the foaming techniques might be the presence of some close porosity, not interconnected with other pore, non-porous skin layer and mechanical properties just acceptable.

3.5.1.1 Gel-cast foaming

The gel-casting is a process that allows to obtain bulk object in many different shapes and involves the use of meld-derived glass powders that are mixed into a solution of organic monomers, forming a slurry. The slurry is then poured into a mold and the initiator and the catalyst are added. The polymerization takes place *in situ*, inside the mold, and the polymeric gel allows to maintain the desired shape. After the unmolding, it is necessary to remove the solvent and the polymeric phase. If the solvent used is water, it can be removed drying the part, if not, or to remove the polymer, the green undergoes pyrolysis in order to burn out the organic components. In the end, it is sintered to obtain a dense material. In the early age of gel-casting process, it was developed by using multifunctional acrylate monomers in organic solvents, but the use of non-aqueous solvents involves environmental problems and major costs, efforts were made to use water as solvent. For example, it was possible by using acrylamide gel system [21].

In order to use this manufacturing method to obtain porous scaffold for bone regenerative applications, it is fundamental to insert a foaming step during the gelation process. The foam can be achieved either by injection of gases or by mechanical frothing, but in most of the case a surfactant is required to be added at the powder solution, in order to stabilize bubbles. Tailoring the desired structure of the porosity of the scaffold, a major concern parameter is the so-called *induction period* or *idle time*, which is the time that occurs between the addiction of the initiator and the catalyst to the suspension and the beginning of the polymerization and the setting of the final structure. The whole process is shown in **Figure 3.9**. During that time, it is possible to mold the foam in the desired shape and changes in the bubble structure take place. Two opposed processes come about: a thinning process of the lamella that. surround bubbles and thinning resist mechanisms. The former is due to drainage due to gravity or capillary forces, Van der Waals attractions that occur between thin films that causes local

depression. The latter involve the high viscosity of the liquid, surfactant chains cohesion, elasticity of the surfactant walls and electrostatic repulsion between the two sides of a very thin film. All these mechanisms can result in the shrinkage and disappearing of some bubbles and in the coalescence of some others. A high control of the chemistry and kinetic of these processes allows to obtain a suitable structure for bone substitute scaffold, for example, with open porosity but maintaining enough walls to have certain mechanical properties. The consideration discussed in this paragraph are common to all the methods that involve the foaming of a solution or a slurry [22].

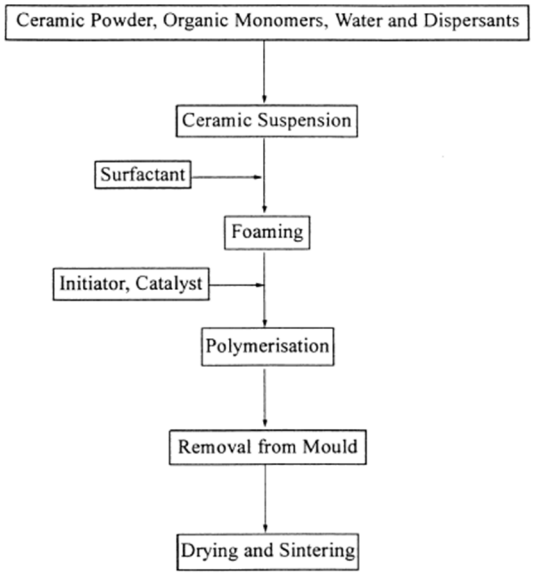

Figure 3.9 Flowchart of the gel-casting foaming method, with *in situ* polymerization. Foam can be obtained by vigorous agitation or by injection of gasses both [22]

Scaffolds for bone tissue engineering have been produced by gel-casting foaming. For example, Z.Y. Wu et al., produced a bioactive glass foam scaffold using ICIE 16 melt-derived glass (49.46% SiO_2, 36.27% CaO, 6.6% Na_2O, 1.07% P_2O_5 and 6.6% K_2O, molar percentages). By careful optimization of all the processing parameters, such as particle size, catalyst, surfactant, monomer, sintering, they achieved a scaffold with modal pore size of 379 µm and modal interconnect size of 141µm, which are suitable for bone regeneration. The compressive strength is at the lower limit of the trabecular bone one, 1.9 MPa and Ha precipitates after 3 days of immersion in SBF [23]. The internal structure of scaffolds is usually assessed with micro-computed tomography (µCT), as in **Figure 3.10**.

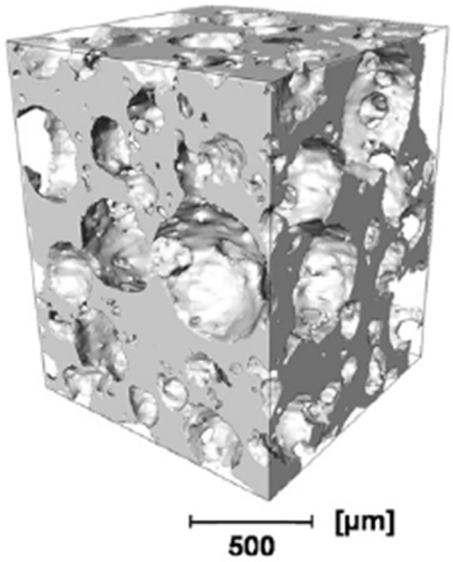

Figure 3.10 Melt-derived bioactive glass scaffold by gel-cast foaming process [23]

3.5.1.2 Sol-gel foaming

Porous scaffold made with sol-gel derived glasses were the first kind of bone substitutes crafted, by Sepulveda et al, (2002). This fact was due to the lack of melt-derived glass that can undergo a sintering process without crystallize. To obtain a porous structure it is necessary to introduce a foaming step during the sol-gel synthesis of the glass, such as in the gel-cast foaming. Unlike the gel-casting foaming, where the glass has been already prepared, in the sol-gel foaming, the foam structure is obtained at the same time of the glass synthesis. Since the gelation time for conventional sol-gel is a few days, it is necessary to add also an accelerator, alongside to the surfactant. For example, in the first work of Sepulveda et al (2002) hydrofluoric acid (HF) was used to decrease the gelation time in the production of a sol-gel derived glass scaffold. In their work, the surfactants (i.e. polyethylene glycol) and the catalyst were added after the completion of the hydrolysis of the alkoxide precursors, under vigorous agitation. When the right viscosity was reached, the sol-gel was poured into a mold and left aging. After, the evaporation of the solvent was carried and the structure was sintered. A double level porosity is achievable with this process: an interconnected macroporosity, due to the surfactant action; a nanoporous structure, due to the intrinsic sol-gel texture [15]. The major drawback is the high brittleness of the scaffolds produces so far. Compressive strength achieved are no higher than 2. 5 MPa, just at the lowest value for the cortical bone strength. But, with respect to bulk sol-gel glass object, it is possible to obtain greater dimension, several centimeters, without the crack typical of monoliths. This is due to the thin walls of the structure, which reduce the path for the evaporation of the water through the nanopores. By a careful tailoring of the process parameters, such as type of glass, surfactant, catalyst, temperature, is possible to obtain a certain amount of control onto the final pore structure.

It is also possible to obtain a sol-gel glass based scaffold by *in situ* foaming. Rainer et al. produced a scaffold mixing silica sol-gel glass with diisocyanate ad a polyol, which are precursors of polyurethane (PU) foam. The polymerization was conducted in the presence of a catalyst and a surfactant, water was used as foaming agent (it reacts with isocyanate groups producing carbon dioxide). With this method, a glass-loaded PU foam was obtained and, after undergoing a thermal treatment, the final scaffold presented a porosity of 48% and a median pore diameter of 50 µm, but it had also pore larger than 200 µm (**Figure 3.11**) [24].

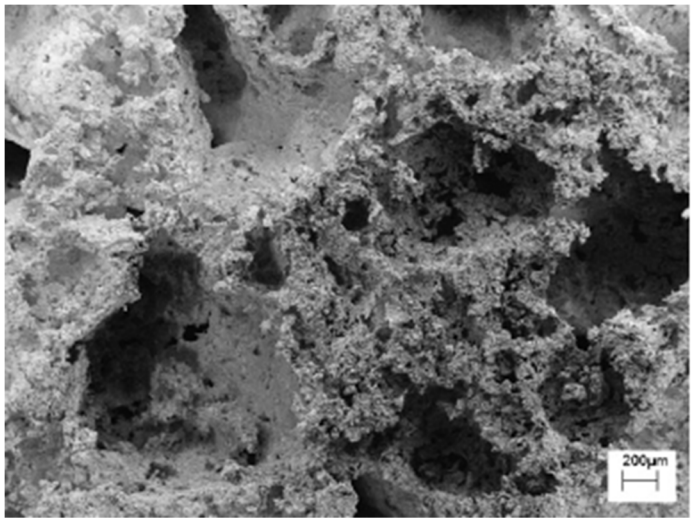

Figure 3.11 FE-SEM image of the inner structure of a scaffold produced by in situ foaming [24]

3.5.1.3 H_2O_2 foaming

Another way to obtain porous structure by means of foaming agent is to use peroxide solution. If the peroxide solution is heated at temperature around 60°C, it will release gasses that can be used as foaming agent to produce bubbles and pores in the scaffold. Using this manufacturing process, a phosphate glass based scaffold was obtained by Navarro et al. They mixed a glass powders (molar composition: 44.5% P_2O_5, 44.5% CaO, 6% Na_2O, 5% TiO_2), sieved under 30µm, with different amount of peroxide solution, in order to prove the effects of different amount of H_2O_2 on the final structure. The slurry was cast into a mold and then foamed for 2.5 h at 60°C. Then the dried compact was sintered. Varying the amount of peroxide, time and temperature of thermal treatment, they were able to obtain different levels of interconnection, different pore geometry, a maximum total porosity of 55% and pore sizes ranging from 20 µm up to 500 µm [6] [25]. The pores network is visible in **Figure 3.12**

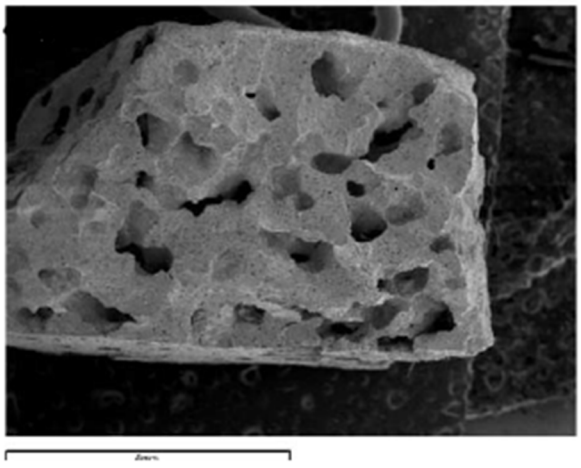

Figure 3.12 macrostructure of foamed H_2O_2 scaffold [25]

3.5.2 Thermal consolidation of particles

The common thing in this group of manufacturing techniques is the use of ceramic powders and of traditional ceramic formic method to shape the scaffolds. The last step, for everyone of this method, is the sintering step. In order to obtain the needed porosity, in some studies, researchers mixed sacrificial template particles into the glass slurry. These particles can be synthetic, polyethylene (PE) for example, or can have a natural origin, starch and rice husk are used as porogen particles as well. The main advantages of these methods are that they are inexpensive and obtaining complex shape is quite easy, thanks to the advanced forming technologies of ceramic artefact. Controlling the advancement of the densification is possible to adjust the level of porosity. More, using sacrificial particles of different size

is possible to obtain gradient porous structure. On the other hand, it is difficult to obtain high levels of porosity and a good interconnection between them.

3.5.2.1 Scaffold manufacturing without the use of porogen particles

In this kind of process, no sacrificial phases are added to the slurry used to create the green. The porosity is controlled only by varying the size of the particles and the sintering process. In fact, in order to obtain a porous scaffold at the end of the process, the sintering shall be stopped as soon as necks are formed between the particles and they are enough to confer the proper mechanical properties at the final object. This technique is very simple and is easy to obtain complex shapes, without the need of checking the dispersion of porogen particles. On the other hand, it allows to obtain only low porosity, under 50%, and a strict control on the particle shapes and sizes is necessary, since these parameters affect strongly the final result. In literature some groups achieved to manufacture melt-derived bioactive glass scaffold using this method.

Fu et al. (2007) obtained a scaffold shaped in the form of the articulating surface of a proximal tibia using a silica glass (**Figure 3.13**), the so called 13-93 (weight percentage: 53% SiO_2, 6 % Na_2O, 12% K_2O, 5% MgO, 20 % CaO and 4 % P_2O_5). The particles were sieved in the size range between 255 and 325 µm. As binder, they used an aqueous solution of poly-(vinyl alcohol) and slip-casting as forming method. Optimizing the sintering protocol, they managed to obtain a scaffold, which was not crystallized, that showed a 40% of porosity and the diameter of the interconnections between pores in the range of 100 to 300 µm. The compressive strength is low compared to the cortical bone, around 22 MPa. This is due to the low level of densification that is needed to obtain a porous structure, higher compressive strength is achievable only by reducing the porosity [26]. Also borate-glass based scaffold has been obtained using the same technique, by Liang et al. They prepared different scaffolds using a sodium calcium borate glass, investigating the effects of different dimensional distributions and shapes. Scaffolds were manufactured using spheroidized and irregular particles, with dimension varying between 90 and 425 µm. They obtained a maximum porosity of 40% using bigger and irregular particles, due to the less efficient packaging with respect to the spherical ones and to the low sintering process compared to the smaller ones. No dimension of pore size and interconnections or mechanical properties were reported, but the morphology is similar to the one obtained by Fu et al. [27]

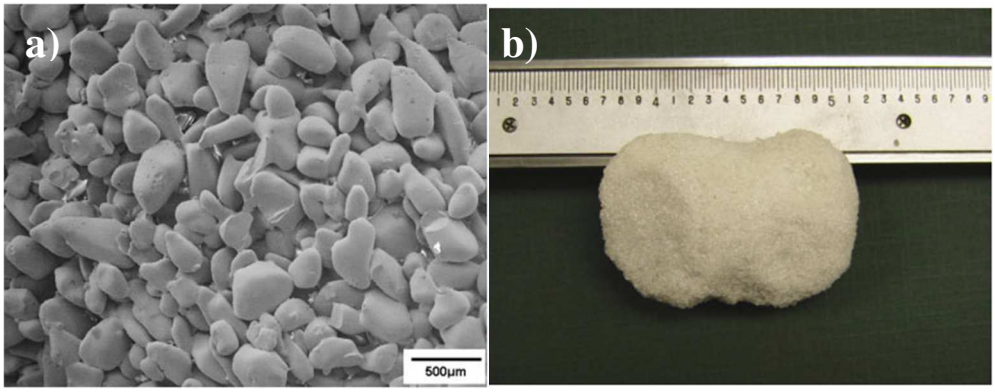

Figure 3.13 a) surface morphology of the scaffold after sintering. The different particles are clearly distinguishable and sintering necks are bridging them; b) scaffold shaped as an articulating surface of a proximal tibia. Adapted from ref. [26]

With this method is also possible to obtain polymer-glass composite scaffolds. Lu et al. used microsphere made by an acid lactic-glycolid acid copolymer and Bioglass to obtain a porous structure. As with full ceramic particles, the porosity is around 40% and the mechanical properties at the lowest level of the cancellous bone ones [28]

3.5.2.2 Polymeric fillers used as porogen particles

In order to increase the porosity of the scaffolds and to have a better control on the shape and dimension of the pores, an organic filler can be introduced in the slurry, before molding. These sacrificial particles must be removed previously the sintering process and they must not leave any kind of residual in the

scaffold. In fact, if the removal step is not well controlled, black char (organic combustion residual) may form on the surface of the compact, avoiding good sintering and limiting the bioactivity of the glass. Many different polymeric particles can be used as fillers. In literature, researchers manufactured bioceramic porous scaffolds, glass-based and not, using polyethylene, wax, camphor and others.

In 2001, Livingston et al. obtained a porous scaffold using 45S5 Bioglass particles mixed with camphor ($C_{10}H_{16}O$). They mixed powders, size range of 38-75 µm, with sacrificial particles having dimensions between 210 and 350 µm. Then the compact, obtained by dry pressuring, underwent a heat treatment at 640°C for 30 minutes in order to remove the camphor and sinter the glass particles. The resulting scaffolds presented a 40% crystallization degree, 21% of porosity and pore size in a range of 200-300 µm [29].

Polyethylene powders, in different size range (100-300 µm and 300-600 µm), were used by Vitale Brovarone et al. as organic filler. Different porous scaffolds have been prepared mixing different volume fraction of PE powders and melt-derived glass. The glass used had a molar composition of 50% SiO_2, 44% CaO, 6% K_2O and was crushed and sieved under 106µm. Disk-shaped scaffolds were obtained by thermal treatment at 950°C for 2 hours. The aim of this work was to find a compromise between total amount of porosity and mechanical properties. Changing the size of PE particles pore with size greater 100 µm or above 200 µm can be obtained, with a total porosity from 50% to 70% and good interconnections between the pores. Micropores, above 10-10 µm, presence was also assessed by mercury intrusion porosimetry for every glass-PE volume ratio and PE particle size. A maxim compressive strength of 6 MPa, comparable to the trabecular bone, was obtained for small particles and low vol% of PE. In this kind of glass, a good bioactivity during *in vitro* tests is due to the presence of β-wollastonite crystals on the surface of the pores [30].

More recently, paraffin wax was used as porosifier to create scaffold based on apatite/wollastonite glass system, by Zhang et al. Powders of paraffin wax (250-650 µm) were mixed with glass particles (weight composition: 44.7% CaO, 16.3% P_2O_5, 34.0% SiO_2, 4.6% MgO, 0.5% CaF_2) in different ratios, then the compact was sintered around 1100°C for 6h, obtaining a glass-ceramic scaffold. In this way, interconnected porosity of 70% was obtained and pores, due to the thermal decomposition of the plastic filler, had dimensions in the range of 250-350 µm. Mechanical properties showed a strong dependence upon the total porosity, but the minimum value was assessed at 5MPa, still acceptable for non-loading site bone substitution (**Figure 3.14**a). The good bioactivity of this kind of glass was proved by SFB immersion tests and it also demonstrated to be a good substrate for mesenchymal stem cells (MSC), as shown in **Figure 3.14**b [31].

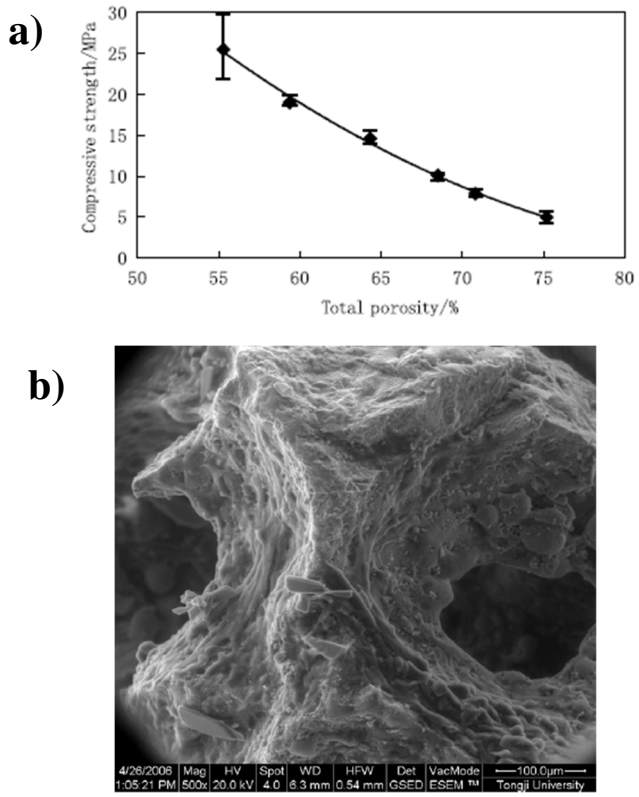

Figure 3.14 a) variation of compressive strength with the total porosity; b) ESEM image of the inner porosity of the scaffold after 48h culture of MSCs. Adapted from ref. [31]

3.5.2.3 Starch consolidation method

Among the sacrificial filler used to obtain porous structures, there are also some that have natural origins. Starches of different plants (corn, rice and potatoes) are used to generate a gelled system with the glass powders and they act as a porogen particles during the thermal treatment, when they are burned-out leaving voids and pores. This technique was developed by Lyckfeldt at al. in 1998, initially for alumina porous scaffold.

The consolidation process is possible due to the ability of starches of absorbing water if heated. Starch grains are insoluble in water under 50°C, so it is easy to mix them with glass particles and handling them. During the water absorption around 70-80°C, the starch particles swell irreversibly and lead to the gelation of the system, with great increase in the viscosity. Since starches remove water from the suspension by swelling, ceramic particles are forced to stack together, increasing the strength of the green body. More, starch particles themselves act as binders [32]. Some of the great advantages of this method are the very low costs of the starches and the non-toxicity of the reactants.

Different groups used the starch consolidation method to manufacture bioactive glass scaffolds. Vitale Brovarone et al. tried different kind of starches, tailoring the changes in properties of porous scaffold made from a SiO_2-Cao-Na_2O-MgO system glass (respective molar percentage: 50%, 25%, 16%, 9%). They prepared different samples using corn, rice and potatoes starches by mixing, under magnetic stirring, them with glass particles and heating up to 80°C. Previously, starch grains were sieved above 63 µm and glass powders under 106 µm. When the gelation point was reached, the solution was poured into a mold and the residual water removed. Two steps heat treatment was necessary to the burn-out of the organic phases, firstly, and to the sintering of the glass, in second place. After different specimen sets, at different wt% of starches and glass powder, researchers managed to optimize the parameters in order to obtain a suitable scaffold. The organic content needs to be in the range between 20-26%, as to gain a compromise between porosity, pore size and sintering. In fact, to low starch content leads to a low porosity and to high amount of it limits the sintering capability, resulting in low mechanical properties. To achieve a good shape maintenance and avoid crack and uneven shrinkage, 40% of solid particles is needed. The starch type seems to not affect this much the process, if not that corn starch grains have lower dimension, resulting in a too small pore size. With this method, pores in dimensional

range 50-100 µm and highly interconnected (**Figure 3.15**) were obtained and scaffolds produced in this way showed compressive strength similar to the cancellous bone one, around 6 MPa. More, a very good bioactivity was observed, along with a certain resorption degree [33] [34].

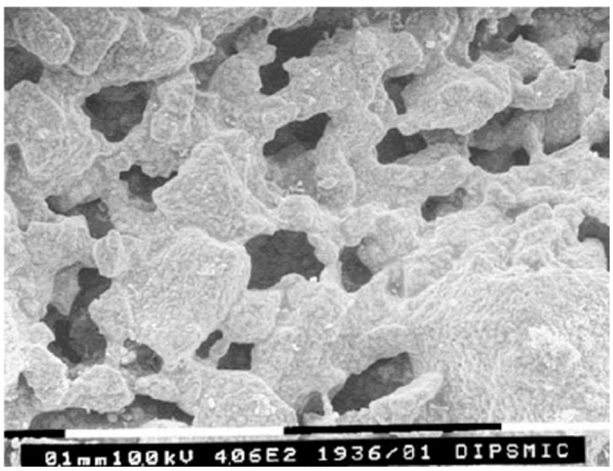

Figure 3.15 Micrograph of glass scaffold obtained using potatoes starch as a pore generating agent. Adapted from ref. [34]

3.5.2.4 Rice husk method

In the last decades there were huge efforts to reduce waste generation in every kind of industry or, at least, to find another way to reuse and recycle them. One example of waste material with high availability is rice husk, especially in those countries that produce it. It is obtained during the refinement of rice, after the harvesting. It is a valuable material, which contains organic materials for the most part (≈75%) but also silica in the amorphous phase (≈15%) and water. For example, rice husk is used during the synthesis of silicon carbide whiskers, used as strengthener in ceramic and metal matrix composites.

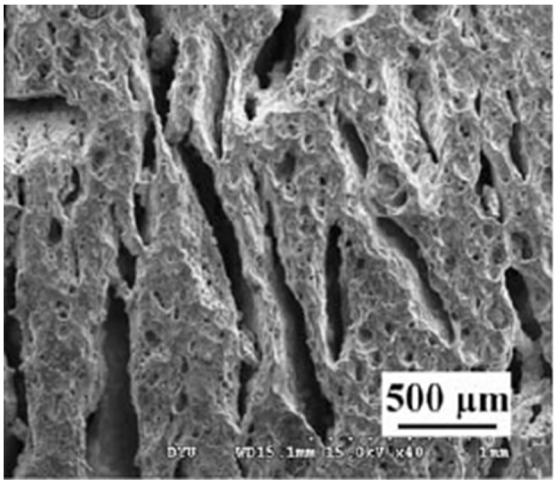

Figure 3.16 Elongated pores in a scaffold obtained by rice husk burning-out [35]

In order to confer more value to this kind of waste, rice husk was also used as a porogen agent in the fabrication of a Bioglass based scaffold, by Wu et al. They used the original 45S5 Bioglass sieved into two different size range, under 25 µm and from 25 to 75 µm, and studied the effects of different wt% of rice husk in the morphology and the mechanical strength. The fabrication of the scaffold involved the mixing of Bioglass powders and rice husk grains, with different dimensions (under 355 µm and 355-600 µm range), in different weight ratios, 20/80, 25/75, 30/70. A poly(vinyl alcohol)(PVA) aqueous solution was used as a binder. After uniaxial pressing, the compacts underwent a burn-out stage at 450°C and a subsequent sintering step at 1050°C. In this way, partially crystallized scaffolds were obtained. Morphological analysis showed elongated pores of different sizes, as in **Figure 3.16**, this fact is due to the shape of the rice husk. Pores were find in macro- and meso- size range both, varying from more than 420 µm to between 25 and 80 µm. But the smaller ones are usually isolated. As usual with scaffolds

obtained via organic phases burn-out, the porosity was quite low, less than 50% and the mechanical strength matched the one of the cancellous bone. Some data are collected in **Figure 3.17** [35].

Material code	45S5 Bioglasss® (wt%)	Rice husk (wt%)	45S5 Bioglasss® particle size (μm)	Rice husk particle size (μm)
20GL80RS	20	80	25–75	≤355
30GL70RL	30	70	25–75	355–600
25GS75RL	25	75	≤25	355–600

Material code	Apparent density (g/cm^3)	Porosity (%)	Compressive strength (MPa)
20GL80RS	1.5 ± 0.3	45.9 ± 2.2	7.2 ± 3.5
30GL70RL	1.6 ± 0.6	43.5 ± 1.7	6.8 ± 2.7
25GS75RL	1.4 ± 0.5	47.2 ± 2.7	5.4 ± 2.3

Figure 3.17 Composition and physical properties of different samples obtained by using the rice husk method. Adapted from ref. [35]

3.5.3 Porous polymer replication

In order to achieve a higher level of porosity and a more defined and interconnected structure, researchers stared to use polymeric foam as template for their scaffolds. The ability to obtain very controlled structure in the field of polymeric foam is well demonstrated and structure with open porosity and more than 90% of pores volume are easily achievable. The basic idea was to replicate the foam structure by coating the walls using a ceramic slurry and then consolidate it. Composite scaffolds and glass-ceramic were obtained both, depending whether or not a burning-out treatment was carried on.

3.5.3.1 Coating method

With this method is possible to obtain polymer-bioceramic composite scaffolds. Different kinds of polymeric substrates, foams, meshes, fibrous bodies, can be coated using different methods, such as electrophoretic deposition (EPD) and slurry dipping. In these techniques no sintering stages or burning-out are carried, in order to maintain the organic phase. The final result is a composite with a polymeric core and a bioceramic surface coating. The polymeric core shall increase the toughness of the scaffolds and resorbability can be achieved [28].

One example of this kind of scaffolds can be found in the work of Roether et al. They used a poly(DL-lactide), a biodegradable polymer, foam obtained by induced phase separation followed by termed freeze-drying and covered it by means of slurry dipping technique and EPD using a slurry made by 42%wt of Bioglass in water. The latter coating method was possible thanks to the presence of charged particles in the suspension. The polymeric foam showed a highly oriented porous structure, with tubular pores, more than 100μm in diameter, interconnected with micropores, 20-30 μm in diameter. Slurry dipping proved to offer more control on the coat thickness and a better replication of the foam, while EPD was prone to occlude some of the pores [36]

3.5.3.2 Polymer foam replication

Contrary to the previous method, in the polymer foam replication the organic phase is fully removed and its only aim is to act as a template for the glass-ceramic phase. So, after the coating of the foam by a slurry, all the structure is subjected to a double-stage thermal treatment, as to achieve the complete burning-out of the polymeric foam and to densify the ceramic phase. An overview of the process is displayed in **Figure 3.18**. With this process silicate, borate and borosilicate bioactive glass-derived scaffolds were obtained. The foam replication has several advantages, such as highly porosity level, up to 90%, and allows to obtain structures very close to the cancellous bone. On the other hand, the scaffolds show very low mechanical properties [1].

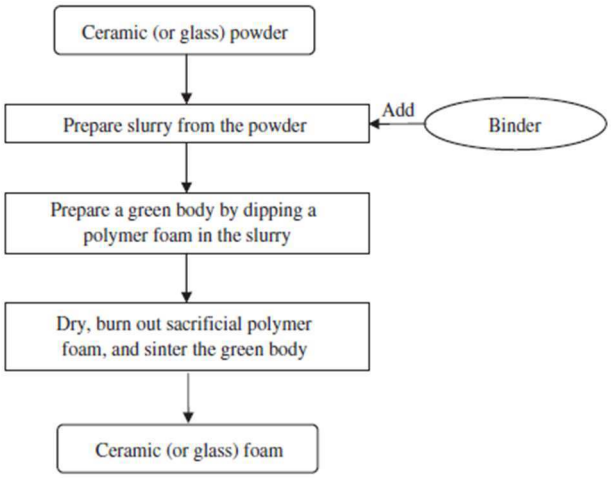

Figure 3.18 Flowchart of the polymer foam replication [37]

The first use of this technique in the field of bone tissue engineering was made by Chen et al. in 2006. They used a PU foam as template, covering it with a slurry made with Bioglass powders and PVA solution as a binder. Coating was obtained, as usual with this technique, by immersion of the foam in the slurry and following removal of the excess slurry by squeezing. The coat thickness is adjustable by multiple immersions. Then the PU was removed by heat treatment and the glass sintered. The porosity obtained in this way was incredibly high, more than 90%, open and interconnected, with pore in the range of 510-720 µm. The structure is very similar to the one of the cortical bone, but the high level of porosity and the typical hollow structure of the glass-ceramic trabeculae, due to the removal of the PU template, affect severally the mechanical properties (**Figure 3.19**). In fact, the compressive strength is in a range of 0,1-0,4 MPa, anyway still comparable to the lower values recorded for the trabecular bone [37].

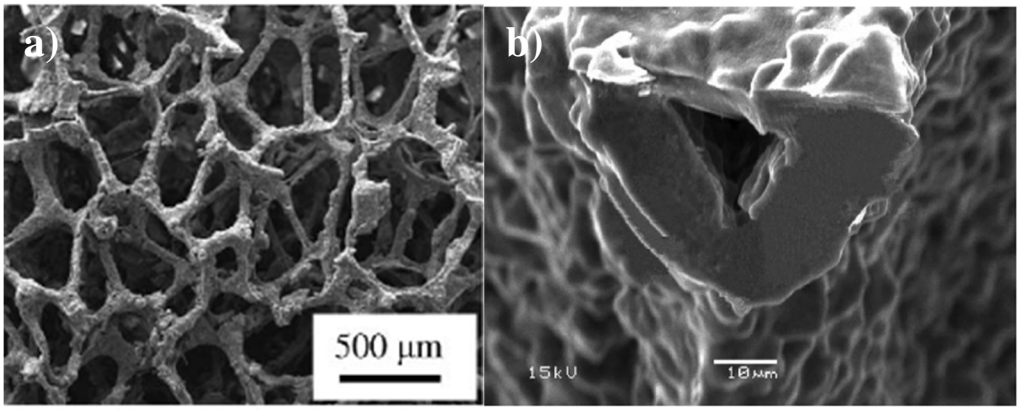

Figure 3.19 a) trabecular structure of a scaffold obtained by polymer foam replication; b) hollow structure of a trabecula. Adapted from ref. [37]

The polymer foam replication was also used to obtain graded porous scaffolds, by modelling the polymeric foam before the infiltration with the slurry. Bretcanu et al. obtained such a scaffold just by preforming the PU foam. In this way, they were able to produce continuous and stepwise (double layer structure) porosity gradient. The foams were pre-formed by forcing them into 2D and 3D aluminium molds. The change in the porous structure is directly related to the grade of compression of the foam in the mold. Then, the pre-formed foams were infiltrated as usual with a Bioglass slurry, the PU was burned-out and the ceramic phase sintered [38]. **Figure 3.20** shows a scaffold obtained by pre-forming of a PU foam.

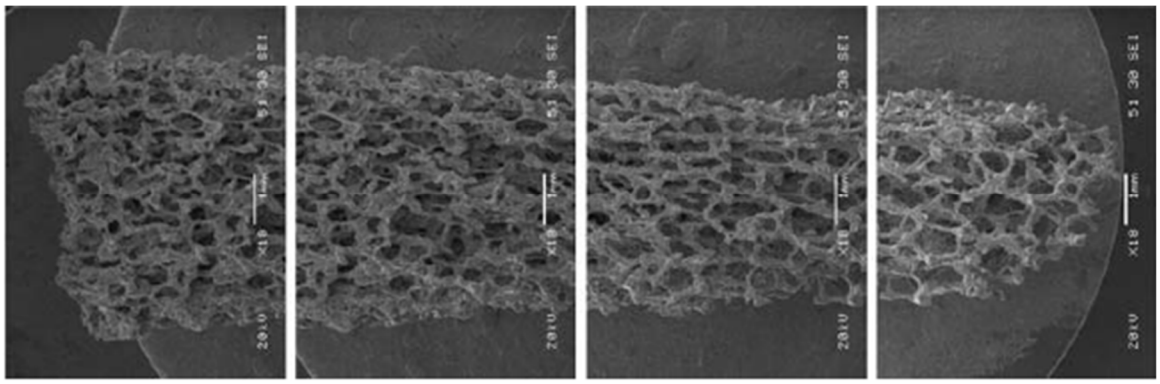

Figure 3.20 3D porosity graded Bioglass scaffold obtained by pre-forming a PU foam [38]

3.5.4 Freeze-drying

Instead of using an organic template as porogen agent, it is possible to use ice crystals in order to generate the porous structure. The liquid solution is subjected to a fast and directional freezing, resulting into the formation of elongated ice crystals of the solvents. Once the solvents have been removed, it is possible to consolidate the scaffold. The flexibility of this method is great, porous scaffolds were obtained using polymers, ceramics and glasses, melt-derived and sol-gel-derived both.

3.5.4.1 Freeze-casting of suspension

In this approach, a colloidal suspension of glass particles is poured into a mold, then it is rapidly frozen. Since the cooling rate is not usually homogeneous in all direction, this leads to the formation of oriented and elongated ice crystals. The frozen solvent is removed by sublimation under vacuum at cold temperature. This step is crucial, since a not controlled removal of the solvent can destroy the porous structure of the scaffold. When the solvent is completely removed, the scaffold is thermally treated in order to sinter the particles. The main advantages of the freeze-casting is in the oriented microstructure of the pores, that confers to the scaffolds much higher compressive strength with respect to the method discussed till now. On the other hand, obtaining suitable pore dimensions only use water as solvent is not possible, since pore size-range for this kind of suspension is 10-40 µm, which is too low for bone substitute application. In order to obtain a bigger width in necessary to include organic solvents in the solution, such as 1,4-dioxane, or completely change the solvent, for example camphene [1].

Fu et al. manufactured a glass scaffold by using an aqueous solution of 60%wt dioxin as solvent. They mixed 5-20% of very fine particles, under 5µm, of 13-93 glass (weight: 53% SiO_2, 6%Na_2O, 12% K_2O, 5% MgO, 20% CaO, 4% P_2O_5) with a disperser and 1% of PVA ad a binder. After the directional freezing, performed using a cold steel plate, and the removal of the solvent, a burn-out and a sintering steps were performed. The resulting microstructure showed ordinate columnar pores (**Figure 3.21**) with diameters between 90 and 110 µm. Varying the concentration of the glass particles affected the total porosity and the size of the single pores. The compressive strength assessed where higher than the values related to the cancellous bone, ranging from 50 to 10 MPa as the porosity increases from 35 to 70% [39].

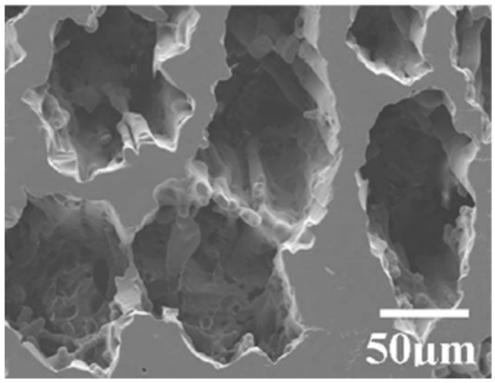

Figure 3.21 Columnar microstructure of a scaffold obtained by freeze casting of suspension. Adapted from ref. [39]

3.5.4.2 Ice-segregation-induced self-assembly (ISISA) of a sol-gel

Similar to freeze-casting method, the ISISA of a sol-gel involve the rapid freezing of a sol-gel by immersion in liquid nitrogen at a controlled rate and then the sublimation of the frozen solvent. Tailoring the physiochemical parameters of the process is possible to achieve a sophisticated control upon the resulting microstructure. These parameters include the solvent composition, the concentration and nature of the solute, the temperature gradient and the cooling rate. Modifying the chemical composition of the sol-gel is possible to achieve control on the size of the pores and by changing the immersion rate is possible to achieve porous graded scaffolds.

Minaberry et al. demonstrated the feasibility of this process by making a porous scaffold using a bioactive sol-gel-derived glass belonging to the SiO_2-CaO system. After the gelation of the sol-gel, it was poured into a mold and then dipped at defined rates into liquid nitrogen, -196°C. After the solvent removal, the green body was subjected to annealing, in order to completely eliminate process residuals, such as salts, acid, organic molecules, and to achieve a certain degree of consolidation. They managed to obtain a well-defined structure, with highly oriented pores. They also assessed the influence of cooling rate on the porous structure, in fact, higher rate favor supercooling and the formation of a lot and small ice crystals, preventing the formation of big pores. Nevertheless, pores no larger than 20 µm were achieved and, due to the very thin walls and struts, low compressive strength resulted, less than 0.2 MPa [40]

3.5.5 Thermally induced phase separation (TIPS)

This technique is mainly used to obtain polymeric scaffolds but also resorbable polymer/glass composite can be achieved. The process is based on the change of the solubility between two different polymers as function of the temperature. In fact, two polymers can be totally soluble one into the other at a certain temperature but be almost totally insoluble at lower temperature. If a solution of these polymers is prepared and then cooled under the upper critical solution temperature, they will separate, forming two distinguishable phases. With an adequate chemistry of the polymers is possible to control the amount of the two phases and their morphologies. One of the two phases will be rich in polymer, the other will be polymer-poor. The latter phase is the one that will be removed in order to obtain the porous structure. With this technique is possible to obtain highly porous structure, up to 97% of porosity. Along with scaffold for bone tissue engineering, also soft-tissue engineering scaffolds can be made, incorporating also nanoparticles for enhanced bioactivity [16] [28].

Maquet et al, developed a composite scaffold based on Bioglass and bioresorbable polymers, poly(D,L-lactide)(PDLLA) and poly(lactice-co-glyco.lide)(PLGA). They made two series of samples, one for each polymer, varying the amount of Bioglass powders (mean particle size <5 µm). The solution was obtained by mixing the polymer and the glass with a solvent, in this case dimethyl carbonate was used. The TIPS was achieved by immersion for 2 h in liquid nitrogen and then the solvent was removed by freeze drying under vacuum. Despite the polymer used and the volume charge of glass particles, 10/25/50%vol with respect to the polymer, the porosity obtained was always very high, >90%. The effects of the different amount of glass were a decrease in the porosity and increase in the apparent density whenever the glass to polymer ration increased, a change in the shape of the pores and the dispersion of the particles, more uniform with more glass. At lower content, Bioglass particles did not interfere with the crystallization of the solvent, so the morphology was similar to the pure polymer foam, with preferential orientation of them. At higher content the pore shapes were more irregular. Good mechanical strengths were achieved, since both composite scaffolds, with 50%vol of glass, had shown compressive modulus around 25MPa [41]

3.5.6 Solvent-casting and particulate leaching (SCPL)

As the TIPS, also this process allows to create polymer and polymer/glass composite scaffolds. The base of this process is the solvent-casting technique, where a solution of a polymer is poured into a mold and consolidated removing the solvent by means of evaporation or lyophilization, obtaining a nanoporous structure. In order to obtain macropores, a water-soluble salt must be added to the solution, as porogen particles. After the removal of the solvent, the structure is immersed in water and the salt particles are leached away so pores are formed. All the required steps are pictured in **Figure 3.22**. This technique allows to obtain high porosity level, greater than 90%, with dimension of the pores up to 500 µm and a good control on the size and shape of them. This fact is due to the simple operation, changing

porogen morphology, dimension and total amount confer a certain control on the final structure. More, this technique does not require advanced equipment. Nevertheless, several cons are present: final shapes are limited, often as flat sheet and tubes; retention of toxic solvents is possible; in case of biological molecules and proteins incorporated in the scaffolds, they can be denatured by the solvent, decreasing their activity; shapes of porogen are limited, usually salt-particles are cubic-like, spherical or equiaxed; a good interconnected pore network is difficult to achieve. Polymer/ceramic composite can be achieved by mixing the desired particles within the solution. So, for example, HA and bioactive glass scaffolds were obtained [42] [28].

Figure 3.22 Processing steps of a porous scaffold by SCPL. In this scheme is not reported the addition of ceramic particles, that shall occur before step A [42]

Recently, Niu et al. produced a scaffold via SCPL with hierarchical structure, incorporating particles of mesoporous silica-based bioactive glass (m-BG) derived from sol-gel process. The particles synthetized with this method show highly ordered channel structure, with average dimension of 5nm. They mixed the m-BG powders with poly(L-lactide)(PLLA) in different weight ratio (15/30%) and use NaCl particles as leaching porogen. The salt particles had a size around 400µm. After removing the solvent and leaching away the salt, they assessed that the different amount of m-BG did not affect the porosity obtained, which was around 70%, but had a huge effect on the morphology of the surface. With lower volume ratio, the surface is smoother, more similar to the pure polymer scaffold, while with higher ratio it become coarse. The presence of the glass also increased the mechanical strength, reaching compressive strength of 4.2 MPa [43].

3.6 Rapid Prototyping

In recent years, a whole new kind of manufacturing technologies has come out: the additive manufacturing technologies (AMTs). The first one was developed in 1986 by Chuck Hull and it was based on Stereolithography [44]. The AMTs, also known as rapid prototyping (RP) or solid freeform fabrication (SFF), revolutionized the concept of fabrication in a lot of industrial sectors. They allow precisely controlling the construction of an object piece by piece, offering the opportunity to create shapes and details that cannot be achieved by conventional technologies. In addition, the level of flexibility and customization provided by SFF techniques is enormous.

There are a lot of different AM processes that can be used, but the starting point for everyone is a computer aided design (CAD) model or even a CT of the object that is intended to be reproduced. Then it is slashed into layers along one of its axes and the AMT builds the object making each layer, one at time. Ideally, all kinds of materials can be processed, ranging from metals to polymers, from ceramics to cells. AMTs related to ceramic materials can be divided into two big groups: direct and indirect fabrication techniques. With direct AMT, it is possible to obtain a complete artefact, without the need

of a post-process treatment. In fact, direct AMTs melt and consolidate the ceramic particles during the shaping of the object, either by means of a laser beam, in the case of selective laser sintering (SLS), or by using an electronic one, and this process is called electron beam melting (EBM). If post-treatments are needed, such as debinding and sintering, the AMTs are referred as indirect methods. Four categories of indirect AMTs exist, based upon the basic techniques:

- Laminated object manufacturing (LOM): the binders are included in the feedstock and sheets of materials are glued together and then cut in the suitable shapes;
- Extrusion-based techniques: a filament of material is extruded by a robot-controlled nozzle; methods such as robocasting, fused modelling deposition (FMD) and dispense plotting belong to this group;
- Stereolithography: these methods rely on light beam, such as digital light processing (DLP) and laser-based systems (SLA)
- Fusing of bed powders: ceramic particles are kept together by a binder that is deposited on the bed, as in the 3D printing, or melted, as in SLS method, if it is already in the feedstock.

In the biomedical field, AMTs are very appealing due to their ability to produce patient-specific devices without increasing in costs or the need of expensive tools. Moreover, with respect to the conventional fabrication techniques, most of the time they do not involve the use of toxic solvents that can remain entrapped in the structure. They are currently used in maxillo-facial surgery, as drill guides, and in dentistry. Furthermore, the range of materials that can be use is very wide, from ceramics, as bioactive glasses and calcium phosphates, to bio-polymers and even to living cells and drugs [45]. In **Figure 3.23** it is possible to see the main characteristics of the different RP techniques and the wide variety of biomaterials that can be used.

RP techniques for bone scaffold fabrication.

Technique	Process details	Processed materials for bone tissue engineering	Advantages (+) and disadvantages (−)
3D Plotting/direct ink writing	→ Strands of paste/viscous material (in solution form) extrusion based on the predesigned structure → Layer by layer deposition of strands at constant rate, under specific pressure → Disruption of strands according to the tear of speed	→ PCL → Hydroxyapatite (HA) → Bioactive glasses → Mesoporous bioactive glass/alginate composite → Polylactic acid (PLA)/polyethylene glycol (PEG) → PLA/(PEG)/G5 glass → Poly(hydroxymethylglycolide-co-ε-caprolactone) (PHMGCL) → Bioactive 6P53B glass	+: → Mild condition of process allows drug and biomolecules (proteins and living cells) plotting −: → Heating/post-processing needed for some materials restricts the biomolecule incorporation
Laser-assisted bioprinting (LAB)	→ Coating the desired material on transparent quartz disk (ribbon) → Deposition control by laser pulse energy → Resolution control by distance between ribbon/substrate, spot size and stage movement	→ HA → Zirconia → HA/MG63 osteoblast-like cell → Nano HA → Human osteoprogenitor cell → Human umbilical vein endothelial cell	+: → Ambient condition → Applicable for organic, inorganic materials and cells → Quantitatively controlled → 3D stage movement −: → Homogeneous ribbons needed
SLS	→ Preparing the powder bed → Layer by layer addition of powder → Sintering each layer according to the CAD file, using laser source	→ PCL → Nano HA → Calcium phosphate (CaP)/poly (hydroxybutyrate–co-hydroxyvalerate) (PHBV) → Carbonated hydroxyapatite (CHAp)/poly(L-lactic acid) (PLLA) → PLLA → β-Tricalcium phosphate (β-TCP) → PHBV	+: → No need for support → No post processing is needed −: → Feature resolution depends on laser beam diameter
SLA	→ Immersion of platform in a photopolymer liquid → Exposure to focused light according to desired design → Polymer solidifying at focal point, non-exposed polymer remains liquid, → Layer by layer fabrication by platform moving downward	→ Poly(propylene fumarate) (PPF)/diethyl fumarate (DEF) → PPF/DEF-HA → PDLLA/HA → β-TCP	+: → Complex internal features can be obtained → Growth factors, proteins and cell patterning is possible −: → Only applicable for photopolymers
FDM	→ Strands of heated polymer/ceramics extrusion through nozzle	→ Tricalcium phosphate (TCP) → TCP/polypropylene (PP) → Alumina (Al_2O_3) → PCL → TCP/PCL	+: No need for platform/support −: → Material restriction due to need for molten phase
Robotic assisted deposition/ robocasting	→ Direct writing of liquid using a nozzle → Consolidation through liquid-to-gel transition	→ HA/PLA → HA/PCL → 6P53B glass/PCL	+: → Independent 3D nozzle movement → Precise control on thickness → No need for platform/support −: → Material restriction

Figure 3.23 Overview of AMTs employed for bone tissue engineering, along with materials used, advantages and disadvantages of the single techniques. Adapted from ref. [44]

3.6.1 Selective laser sintering

As a direct AMT, the SLS involves just one step, inside the machine, to create a full object. A CO_2 or a Nd:YAG laser is used to perform a scan over a bed of powders, the path is controlled by a computer and follows the sliced CAD model of the object. As pictured in **Figure 3.24**, the setup is composed by two different chambers, the laser and a scanning system. The powder feedstock is prepared in one of the chambers, then a roller transfers the materials into the other chamber, building the power bed layer-by-layer. As soon as the roller has finished to prepare the layer, the laser scans the surface, consolidating the powders. After that, the roller builds another layer and so on [45]. In order to obtain the desired properties for the scaffolds, it is necessary to tune very carefully a lot of parameters.

SlS can involve three different method of binding particles together:

- Solid-state sintering
- Liquid-state sintering
- Full melting.

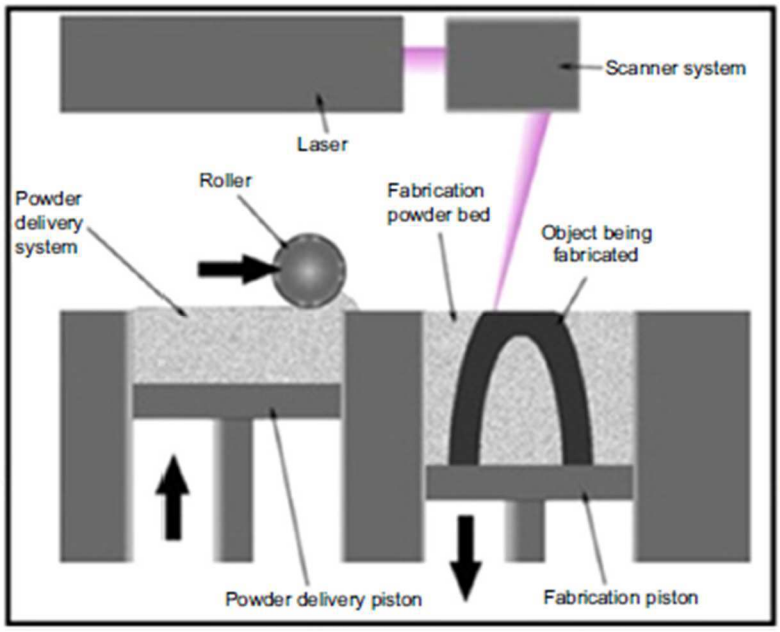

Figure 3.24 Working scheme of a SLS machine [46]

The second one is mainly used for materials that present a difficult sintering, the last, which is called selective laser melting (SLM), is used for low-melting point materials, such as metals, and allows obtaining very high levels of density. In order to be used with this method, the materials must absorb light in the wavelength range of the laser and their powers must be flowable, in order to ensure a correct formation of the bed. Their ideal particle dimension range is between 10 and 150 µm. More fundamental parameters are the ones involving the laser. Laser energy density, scanning speed and the hatching distance (the distance between two lines scanned by the laser) have a great influence on the resulting pore structure, shown in **Figure 3.25**. Increasing the laser energy, or decreasing the scanning speed, mean higher amount of energy transferred to the materials, so higher temperature reached. The final temperature depends also upon the temperature of the bed that can be set, for example, at 140°C. In most of the cases, using higher energy means increasing the total amount of liquid phase formed; eventually it leads to the melting of the materials, which results into achieving more dense objects. The cons are a loss in dimensional accuracy. If the hatch distance is too narrow, the two laser paths can overlap, affecting dramatically the pore structure, decreasing the porosity. The thickness of the layer plays a crucial role, in fact it controls the morphology of the porosity. An optimized layer can lead to interconnected porosity and pore size suitable for bone regeneration. The thickness can influence the fusion degree of the particles, decreasing it means less densification of the particles and more pores. But a too thick layer may result in low adhesions between subsequent layers and into delamination. On the other hand, if the layer is too small, the roller might remove and displace previously bonded particles. For biomedical applications polymers, ceramics and metals are reported to be used in SLS AMT [46]

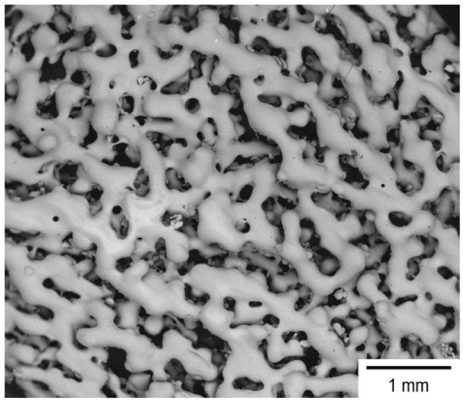

Figure 3.25 Typical morphology of a glass scaffold manufactured by SLS. A network-like structure and the sintering necks are visible [45]

For their structure and properties, bioactive glasses are suitable to be used in SLS process, for obtaining glass- and glass-ceramic-based scaffolds. Since the heating and cooling processes are very fast with respect to a conventional process, SLS can be appealing for bone tissue engineering applications. Despite the very brief time of the heating process, crystallization of glasses has been reported during fabrication. To the best of the author's knowledge, the first glass scaffold based on a 45S5 system, fabricated via SLS, was prepared by Liu et al. in 2012 [50]. Other bioactive glasses were also used with this AMT. Liu and co-workers optimized the laser power in order to achieve the best sintering and densification. They found that if the laser power is increased too much, holes and big voids started to appear in the glass layer. This is due to the fact that at high energy of the laser, in this case 20-30 W, the material melts and can flow through the layers below. An optimized laser power results also in optimized mechanical properties, such as fracture toughness and hardness. Both of them reach their maximum value when the glass is well sintered but it stays below its melting point. The improvements of mechanical properties are due to a partial crystallization of the glass, despite the very fast heating. In fact, XRD and FTIR analysis assessed the presence of a crystalline phase composed by $Na_2Ca_2Si_3O_9$. This phase is formed among the others because of the rapid thermal process [47]. SLS technique has been proved suitable also for the manufacturing of composite scaffolds. In a recent work, Gao et al. [51] manage to produce a scaffold with admirable mechanical properties by reinforcing the glass with graphene. Moreover, they used also a sol-gel derived glass, the so called nano-58S (58%SiO_2, 33%CaO and 9%P_2O_5, molar percentage). They prepared the feedstock by mixing glass powder, with size around 48nm, with a solution of dispersed graphene in N-methyl-2-pyrrolidone and drying (**Figure 3.26**). Graphene was added in different ratio, from 0,1 to 1,5 wt%. The scaffolds were made by SLS in nitrogen atmosphere for preventing oxidation. By means of several analyses, such as Raman spectroscopy, FT-IR, and TEM imaging, the researchers evaluated a good dispersion of the graphene in the glass matrix, as well as the presence of a nanotexture that can promote protein adhesions; interestingly, the nanostructure typical of sol-gel glass survived the SLS process. High mechanical properties were observed for samples with 0.5 wt% of graphene, while they decreased in more charged samples, probably due to an agglomeration of the graphene. Compressive strength of 48 MPa was observed, well above that of the cancellous bone, thanks to the reinforcement provided by the carbonaceous filler. A toughening of the scaffolds occurred, too. Graphene can reinforce the matrix in different ways, common to composite materials:

- Crack bridging: it is possible that the crack manages to propagate through a graphene flock, but without breaking it. In this case the flock holds together the two side of the crack;
- Pull-out: as in fiber-reinforced composites, graphene particles can dissipate energy by being extracted from the matrix, through the breaking of the interface with the glass;
- Crack deflection: since the graphene is tougher than the glass, usually the crack cannot proceed through it and it is obliged to deviate from its path. A longer crack means more energy required, hence more dissipation;
- Crack tip shielding: due to the interface debonding, a lot of energy is required and in the vicinity of graphene the crack tip is reduced;

HA layers were found after 7 days of immersion in SBF [48].

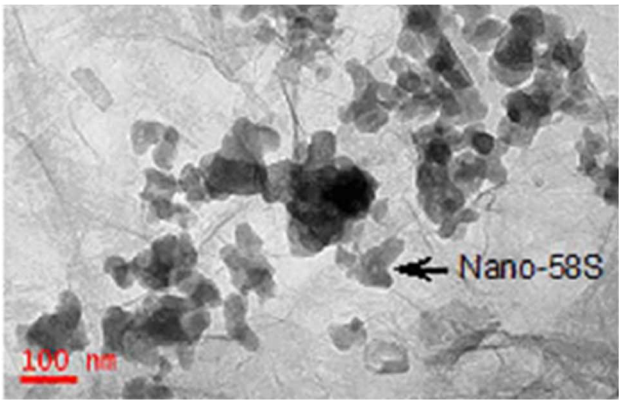

Figure 3.26 Nano-S58 particles mixed with graphene. Adapted from ref. [48]

Even if the SLS method can be used as a direct technique, in order to achieve better dimensional accuracy and to reduce the laser power needed, it is possible to use the SLS as an indirect process. To introduce a post-processing process can be appealing, with respect to the advantages. In this case, a binder is incorporated into the feedstock and mixed with the powders. Often it is an organic one. Then the laser is used to melt the binder, which can hold together the glass particles. The wettability of the materials by the binder and the dimension of the glass particles are very important parameters. Smaller particles might result in better mechanical properties, but more binder is needed and a good and homogeneous dispersion is difficult to obtain. The total amount of the binder influences the strength of the green, which must be enough to withstand handling and the removal of non-sintered powders, and the shrinkage and the final density of the scaffold. Indirect SLS can be used to obtain glass and glass-ceramic composite scaffolds [45]. Kolan et al. [52] fabricated a glass scaffold, based on 13-93 glass, via indirect SLS. They used stearic acid as binder, because it leaves almost none carbon residue and it is a low melting polymer. They optimized the process by starting from the energy density. It is very important because it is related to the other parameters, scan speed, laser power and scan spacing (**equation 3.3**), and because it is the key to a correct melting of the binder

$$E_d = \frac{P_l}{v * d} \qquad (3.3)$$

E_d: energy density
P_l: lasere power
v: scan speed
d: scan spacing

The optimal energy density was assessed by visual inspection at 1 cal*cm^{-2}. They adjust the other parameter without changing the energy density. With this work, this group was able to underline both the advantages and the disadvantages of the SLS in terms of obtainable porosity. In fact, due to the unbounded particles that sustain the structure, it is possible to create large features that are hard to obtain with other methods. The researchers manage to obtain pore size of some millimeters. On the other hand, it is difficult to obtain features below some hundreds of micrometers. The ability to decrease the dimension of the pores relies on the dimension of the laser spot and on the possibility to remove the loose particles that is harder the smaller are the pores. The smaller feature achieved was around 300 µm. However, a certain surface roughness and the presence of micropores are intrinsic with this technique and this can help increasing the specific area of the scaffold, offering more anchoring points for cells. It was also obtained a compressive strength up to 11 MPa, perfectly in the range of the cancellous bone [49].

3.6.2 Stereolithography (SLA)

Stereolithography is a light-assisted AMT and it was the first RP technique, developed by Hull in 1986 [47]. Even if it is the first one, SLA is one of the most powerful techniques between the ATMs. It has the best resolution - commercial available machines can print features at 20 µm while making big objects - and can use a lot of different materials, from polymers and ceramics even to hydrogels and cells. This method involves the use of a liquid UV-light curable polymer stored in a tank, a UV-laser, a dynamic

mirror system and a movable platform. The laser beam is patterned on the surface of the bath in order to cure the polymer on the surface and build the first layer of the object. Then the platform moves downwards, allowing more viscous polymer to cover the material previously cured. Now the laser scans again the surface, building the next layer, and so on. Even if most of the SLA use the same mechanism as the first from Hull, and are known as bottom-up systems, another type of machine has come out, following a top down approach. In the second generation, the polymer is illuminated from the bottom of the vessels, which has to be transparent, and the platform moves upward. With respect to the other kind it has several advantages, such as no recoating of the surface needed, protection from the oxidation, since the object is immersed, and a smaller amount of feedstock is needed [50]. A novel kind of illumination method has been recently developed and it is very promising in order to greatly reduce the processing time. In the digital light projection (DLP) systems, a digital mirror device (DMD) is used to illuminate, usually with visible blue light, and reproduce each single layer at once, without the need of a beam scanning the surface. The DMD is composed by millions of mirrors that can be switched on/off in order to recreate a 2D array of pixels. In this way, the only time needed to build a layer is the one related to the exposure of the materials. Moreover, it has great lateral resolution, about 40 µm, and allows the use of high loaded inks with ceramics (40-60%). The main problem that occurs with ceramic-filled inks is the high viscosity that reduces the capability of the ink itself to recoat the surface of the bath in the top down approach. **Figure 3.27** Two different kind of SLA: Right: top-down approach; Left: DLP bottom-up approach shows two different SLA set-ups.

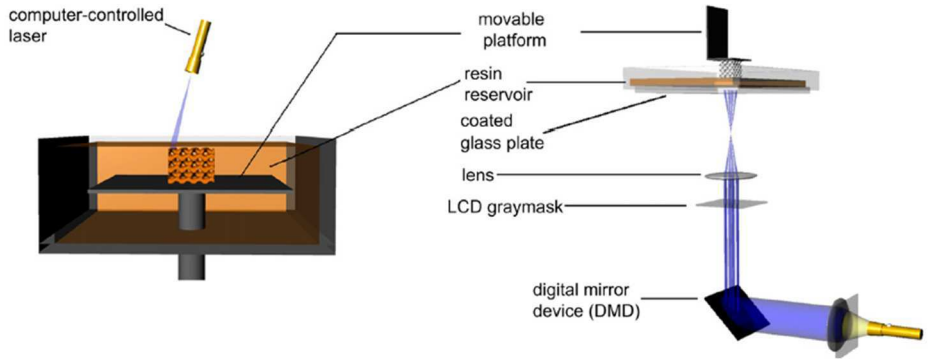

Figure 3.27 Two different kind of SLA: Right: top-down approach; Left: DLP bottom-up approach [50]

More types of advanced SLA have been developed. The micro-SLA (µSLA) uses a single photon beam, in order to increase the resolution and decrease the layer thickness, under 10 µm. With this method a HA scaffold with interconnected pores showing a dimension around 300 µm had been made [51]. The other type of advanced SLA is the so-called two photon polymerization (TPP). By using a near-infrared ultra-short-pulsed laser and a radical quenching system, features at the nano-level have been reached. The method is based on the almost simultaneous absorption of two photons by the photoinitiator. Even if the photons have low intensity, this mechanism allows enough energy to be transferred to start the polymerization. Moreover, this technique is ultra-rapid.

One of the main limitations of SLA is the quite low availability of photo-curable resins. In order to obtain a sufficient low viscosity and the ability of solidify, in time shorter as possible, when irradiated with light, the most used composition include monomers or low-weight oligomers with several functional groups. These types of resins usually turned out in brittle, glassy and rigid materials. Elastomeric and biodegradable resins have been reported and under constant development. Polymer-ceramic composite can be made by mixing the resin with ceramics particles. In order to obtain a good result, the total amount of ceramic fillers cannot be more than about 50 wt.% and the particles must be smaller than the layer thickness. Also, full ceramic artefacts can be created provided that the polymeric phase burns-out. In order to overcome the disadvantages of a low percentage of ceramic powders in the resins, an indirect method have been developed by merging SLA with gel-casting. Previously an epoxy model is manufactured using SLA, then it is filled by a ceramic slurry and removed by thermal treatment. Li et al. [55] produced a Bioglass scaffold using this technique. They made the negative of the scaffold by SLA, using a commercial photo-resin, then they filled it with a slurry made by 45S5 particles, water and polyacrylamide and performed the removal of the binder and the sintering of the glass. By µ-CT

analysis, they found that the resulting glass-ceramic scaffold was almost an exact negative replica of the polymeric template (**Figure 3.28**), they just assessed some normal shrinkage. The mechanical strength was found to be improved with respect to other scaffolds obtained by direct photo-curing of a ceramic-filled resin. The evaluated compressive strength was about 12MPa. Since the scaffolds were made out of Bioglass, also the bioactivity assessed was good, with formation of HA layers [52].

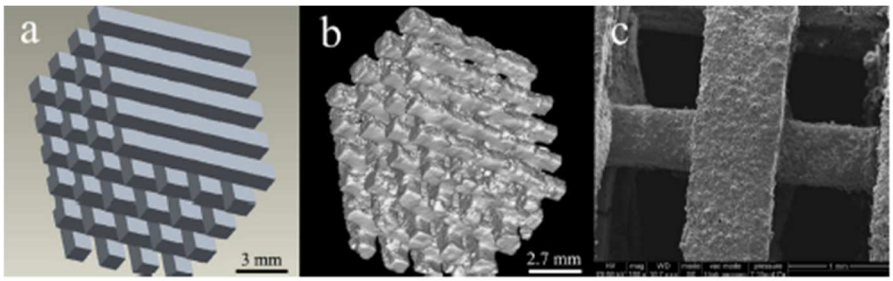

Figure 3.28 a) CAD model of the polymeric template; b) µ-CT image of the glass-ceramic scaffold; c) SEM micrography of the porosity [52]

3.6.3 Direct ink writing

Many different AMTs can be stored under the family of the direct ink writing (DIW) techniques and with many different names, such as direct ink assembly. They all have in common the use of a computer-controlled translation stage, which is used to move a patter-generating device, for example a print-head or a nozzle, to generate an object with predetermined structure and features. Two different approaches can be used: 1) droplet-based; 2) continuous (filamentary). The former involves the use of an ink-jet print head to deposit the materials on the chosen path. Methods such as 3D printing (3DP) and ink-jet printing (IJP) are droplet-based. The filamentary techniques are based on the use of a nozzle to extrude a continuous filament of ink. These techniques are known under several names such as robocasting, dispense plotting, extrusion free forming and direct-write assembly.

3.6.3.1 3D printing (3DP)

The 3D printing technique has a very similar setup with respect to the SLS. In fact, it is necessary to create a powder bed that can be moved downward. A set of blades or rollers is used to do so. Then, in order to create the layer of the object in printing, a binder is patterned by a print head following a CAD model. The print head works in the same way as a common ink-jet printer one does, it can be a continuous inkjet printing (CIJ) or a drop-on-demand (DOD) one. In the first case the head produces a continuous flow of ink through a nozzle, drops are generated by acoustic waves and they are deviated by means of an electric field; in the second one the drop is generated, only when needed, by a piezoelectric or a thermal system [53]. The type of printer has a great influence on choosing and designing the ink. Usually the binder is water-based, but it can be also organic-based. When the layer is completed, the powders are subjected to heating in order to dry it out and consolidate it. Then it is moved downward and another powder layer is spread in place. This cycle is repeated until the object is fully built (**Figure 3.29**). Then a process called depowdering needs to be done, in order to remove the loosen powders. It is a crucial step for the production of porous scaffolds, since it is very easy to produce cracks in the green body. If necessary, the last processes are the burning-out of the binder and the sintering of the powders. There are several parameters to control in order to obtain a good final scaffold. Before starting the actual printing, parameters of the powder bed and ink delivery system must be optimized. Since powders are transferred from a feed bed to the printing one, they must have good flowability and good packing ability. These aspects are mainly controlled by particle shape, roughness, size and size distribution. Rounder particles are better than irregular ones. Greater dimensions mean more flowability but low resolution. Powder features also influence the layer thickness. Thicker layers need more binder, while thinner ones may result in bad resolution due to flow of the binder [44]. Usually particles between 20 and 40 µm are used, larger particles lead to formation of voids, while smaller ones decrease the resolution, since the binder is spread across the powder bed by capillary forces [45]. Other important parameters are the ones related to the ink drops. The drop volume and saturation of the binder are related to the packing density. The saturation is given by merging data on the packing density and the drop volume and it controls the strength of the green body. Wettability of the powders has a crucial effect, too. High values of it result in low resolution, while poor wettability can lead to poor binding [44].

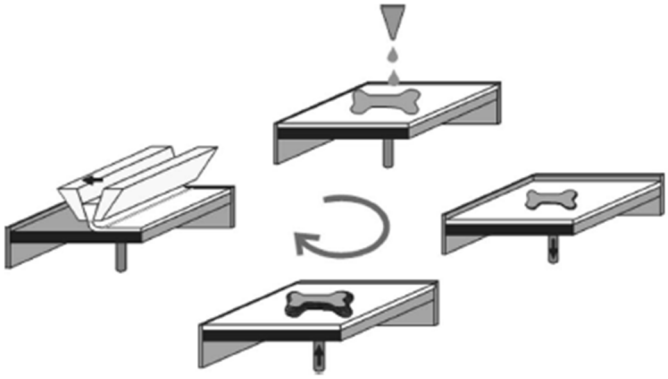

Figure 3.29 Steps of a 3DP process, from left, clockwise: formation of the new layer on the powder bed; jetting of the binder; lowering of the building bed; extraction of the green body. The first three steps are repeated as many time as needed [45]

In the field of bone tissue engineering, this technique is very promising for the manufacturing of strong glass-derived scaffolds with a porosity around 50%. Various kinds of glasses/glass-ceramics have been tested, using composite powder or glass (then added with a binder) as starting feedstock. In the latter case, the crystalline phase is obtained during the sintering. Different scaffolds were reported in literature. The most common bioceramics used are HA, calcium phosphates (CP), 45S5 Bioglass and 13-93 glass. They all proved to be suitable for load-bearing application, with compressive strength up to about 70 MPa, but the porosity is usually low, under 50% [45]. Very recently, Mancuso et al. demonstrated the possibility to manufacture a porous glass-ceramic scaffold, based on silicate-based glass, with mechanical properties matching the cortical bone ones and with dimensions of several centimeters. They used two different type of glass, called NCL2 and NCL7, with very complex composition. As former oxide they used mainly SiO_2, but they also introduced P, B, Na, Ca, K, Mg, Mn, Al, Fe, Li, Mo, Se, Cr oxides as modifiers. A so large amount of oxides was introduced to obtain the wanted thermal properties and crystallization behavior. Glass powders in the range of 20 to 53 µm were used and mixed with maltodextrin as solid binder. The liquid binder, jetted by the printer, was a commercial one. By hot-stage microscope analysis and X-ray diffractometry, they were able to adjust the sintering process in order to obtain high mechanical properties. In fact, they obtained flexural strength around 36 MPa, demonstrating that these scaffolds are suitable for load-bearing application. The drawback is that the porosity was quite low, ranging from 15 to 33%, even if it had features in the right size range for bone substitution, 150-400 µm, and interconnected pores, as shown in **Figure 3.30** [54].

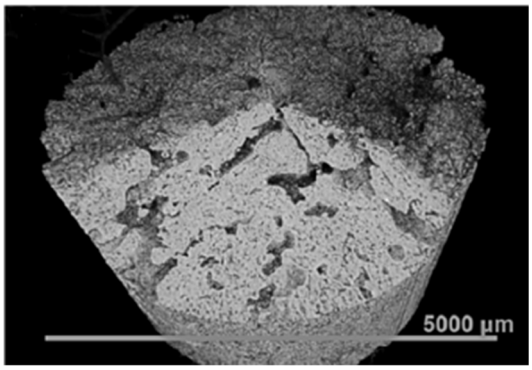

Figure 3.30µCT of a glass-ceramic scaffold obtained by 3DP. Adapted from ref. [54]

3.6.3.2 Ink-jet printing (IJP)

The ink-jet printing (IJP) is a technique based on the disposing of ink droplets to create an object layer-by-layer and it is similar to the 3DP. The main difference is in the ink. In 3DP, it is composed only by the binder and the ceramic particles are contained in the building bed, while in IJP all the components are included in the ink. The mechanisms of the print head are the same as the ones used in 3DP, CIJ or DOD. The DOD method is more common in tissue engineering, allowing the deposition of drops with a diameter in the range of 25 to 50 µm. The key advantage of this technique is the spatial accuracy on

the x-y plane, up to 10 µm. Anyway, the precision of the process is affected by the physical and chemical properties of the ink. Viscosity and surface tension rule the way the droplets are formed and their shape, either at the exit of the nozzle and on the substrate. The wettability of the substrate by the ink, its surface tension and the interaction between droplets are the main concerns for the precision of the system. For 3D objects, the solidification and consolidation stage of the ink is fundamental. Either it happens due to solvent evaporation, temperature change, gelling or photocuring, that step will determine the final shape of the object. IJP is a very powerful technique in the field of tissue engineering, since it allows a wide range of materials to be printed. Biocompatible polymers are widely used, for example poly(lactic acid) or poly(caprolactone), due to their good biocompatibility, low cost and easy processability. Hydrogels are also very promising materials for this application. Mainly based on natural polymers, such as agar, alginate and cellulose, they can provide an optimal replica of the extracellular matrix and can be printed altogether with living cells. Scaffolds for bone regeneration can also be printed with this process. Also, hard ceramic scaffolds for bone regeneration can be manufactured by IJP. HA and TCP have been used for this purpose. Since ceramics cannot be processed at molten state due to their high melting temperature, they are mixed with a binder to obtain a suitable ink. The production of ceramic scaffolds, as usual, involves one more step, a thermal treatment to remove the binder and sinter the ceramic particles. With IJP it is possible to use several nozzles at the same time, to reduce the time of printing a single layer and to obtain composites by using different inks [55]. No reports on glass-based scaffolds produced by IJP have been found in literature.

3.6.3.3 Robocasting

Robocasting is one of the different names and kinds of the direct ink writing technique based on the continuous extrusion of a filament. Some other names of robocasting can be direct-ink assembly, extrusion free-forming or dispense plotting [45]. Other similar approaches are the fusion deposition modelling, where a melt paste is extruded, or the micro-pen writing, that is not suitable to print ceramics [56]. All these techniques are based on the ink being extruded by a nozzle, using pressurized air, in order to produce a rod that is deposited by a computer-controlled head, which usually follows a CAD file. A scheme of the set-up is represented in **Figure 3.31**.

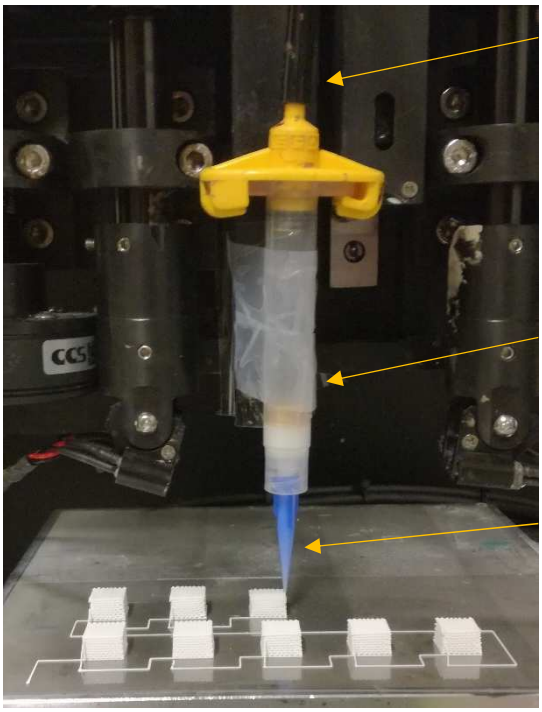

Figure 3.31 Experimental set-up used for robocasting during this thesis. The arrows highlight, from bottom to top, the nozzle, the syringe and the pressured air injector

Robocasting is dependent on the availability of inks with very specific properties. The ink is a slurry, composed by glass or ceramic particles and a polymeric binder, to form a colloidal slurry. The requirements that the ink must provide were discussed in first place by Cesarano et al. in 1999 and are still completely valid. In order to be used as robocasting ink, a colloidal slurry shall:

- Be pseudo-plastic. In fact, the ink has to flow through a small nozzle, but without applying too much pressure;
- Set-up into a non-flowable mass. It has to maintain the rod-like structure even after the dispensing on the building surface;
- It has to be strong enough to bear the weight of the overlying layers without deformation [57].

A colloidal ink is prepared by mixing colloidal particles in an aqueous mean, then polyelectrolytes are usually added as dispersant to provide stability. Those are linear polymers with ionizable groups, for example poly(acrylic acid). Change in pH or other conditions provoke changes in the surface charge that influence the stability of the suspension and lead to the fluid-gel transition [58].

In rheology science, a pseudoplastic fluid is a liquid that has a shear-dependent viscous behavior. When a fluid is subjected to a shear stress, τ, the shear rate, $\dot{\gamma}$, is related to the shear stress through the viscosity, η, and a coefficient, n (**Figure 3.32**):

$$\tau = \tau_y + \eta * \dot{\gamma}^n \qquad (3.4)$$

τ_y is the yielding stress, which may also be equal to zero, and is the minimum stress value necessary to observe flow of the fluid. A material that follows equation 3.4 is known as Herschel-Bulkley material [58]

There are three classes of fluids, sorted on their viscous behavior, determined by the value of the coefficient n:

- Newtonian, n=1: they have a constant deformation, independent on the shear applied;
- Pseudoplastic or shear thinning, n<1: the shear stress increase with decreasing slope when the shear rate rises;
- Dilatant or shear thickening, n>1: the shear stress slope increase with increment on the shear rate [59].

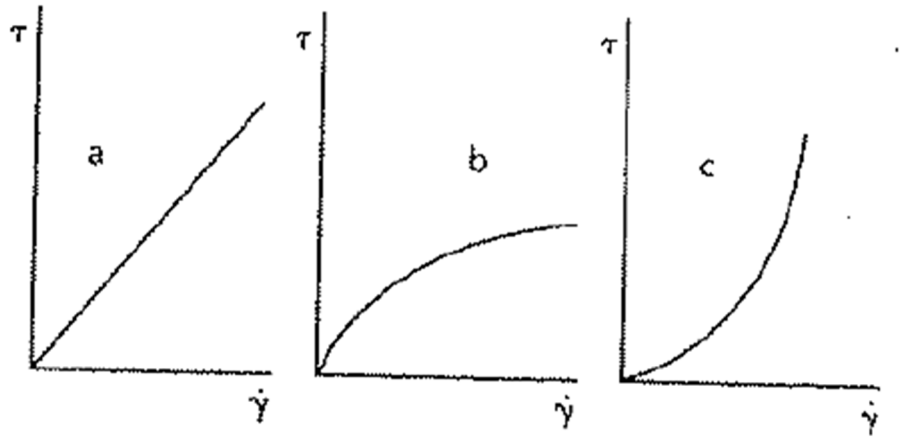

Figure 3.32 Viscous behavior of fluids: a) newtonian; b) pseudoplastic; c) dilatant [59]

Despite the huge development during the last two decades, the three main characteristics described by Cesarano are still valid. The robocasting building principle relies on the ability of the ink to change its viscosity, through physical and chemical process, in order to become strong enough to support the on-building structure. For example, Cesarano et al. achieved the transition between a pseudoplastic fluid and a dilatant one, and so the strength needed, by drying of the rods. Thus, the particles volume fraction increases and the ink changed behavior [57]. One of the drawbacks of extruding directly in air is the possibility of uneven shrinkage, due to different air flows in the structure. In order to avoid that and print finer features, thanks to the avoided clogging of the nozzle, some groups used a non-wetting oil bath as printing environment. So, the drying is avoided and shape retention is obtained by recovery of the gel elasticity. Then the oil is removed and the structure is dried in a controlled environment. In air, it is also necessary to coordinate the feed rate with the drying kinetics, in order to allow previous layers to get enough strength. This issue is avoided by extruding in oil. Otherwise, it is mandatory to control the viscoelastic behavior of the ink and also its ability to fuse with the underlying rods. The first aim in

ink preparation is to achieve a stable dispersion and a loading as highest as possible, to reduce the drying shrinkage, then the fluid-to-gel transition is promoted by a physical or chemical change in the system.

The rheology of the ink at the gel state is important during the extrusion process and the actual printing phase. There are two main delivery systems for ink in robocasting:

- Constant-displacement: the ink is injected at a constant flow rate by mechanically displacing the plunger of the cartridge, varying the pressure as needed;
- Constant-pressure: the plunger is moved by pressurized air that it is maintained at a constant pressure [56].

The latter method has a simpler set up, but the material feed might not be constant if the rheology of the ink changes during the process. The shear stress applied to the ink varies with the distance from the axis of the nozzle, according to the following equation:

$$\tau_r = \frac{r\Delta P}{2l} \qquad (3.5)$$

τ_r: shear stress at the position r

r: distance from the center of the nozzle

ΔP: pressure gradient applied

l: nozzle length

A Herschel-Bulkley material that flows through a nozzle may generate a three-velocity zones profile due to the stress gradient:

- A central core of unyielded materials, which is in gel state and flows a constant velocity;
- A mid layer of yielded materials, which is in fluid state and exhibits a laminar flow;
- An external slip fluid layer, attached to the nozzle walls, that is depleted of colloidal particles.

This situation leads to an overall plug flow of the ink, as shown in **Figure 3.33**. The larger is the nozzle, the smaller is the effect of the laminar zone.

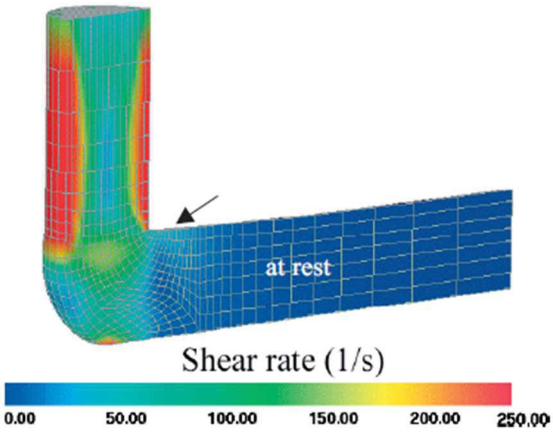

Figure 3.33 Computed-model of the flow of an ink through a 250 µm nozzle with a speed of 5 mm/s. Adapted from ref. [58]

Once the rod is deposited on the layer lying underneath, it is important that the ink exhibits enough mechanical strength in order to support the new to-build layer without large deformation and to maintain the shape of the as-deposited structure. In fact, if the ink is too weak, it might happen that it bends between two lines of the underlying layer, as shown in **Figure 3.34**

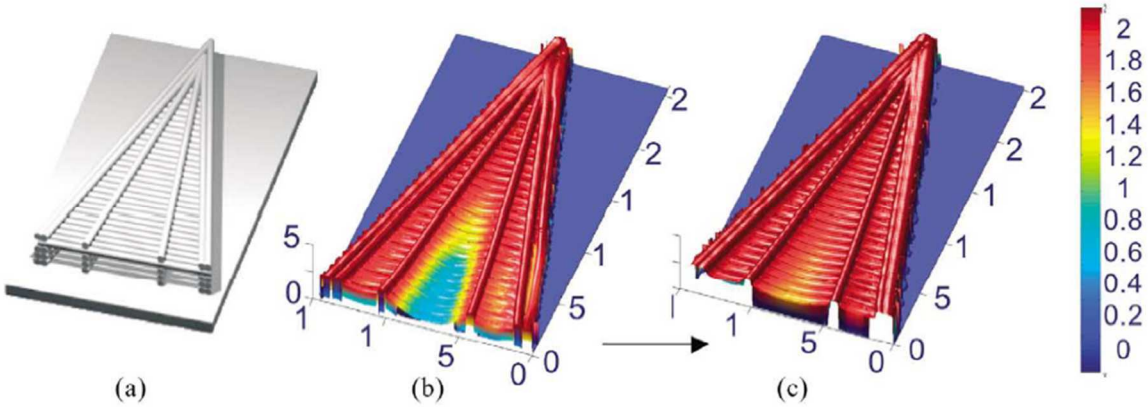

Figure 3.34 Example of test for evaluation of the ink strength: a) CAD model of the structure; b,c) evaluation of the height of the extruded rods from the buidling plane for different inks. The strength of the ink increases in the direction of the harrow. All distances are expressed in mm [60]

The elastic properties of the ink can be controlled by tuning the attractive forces between the particles that form the colloidal suspension. A colloidal gel is capable to transfer loads if a critical volume fraction of colloidal particles is reached. This fraction, φ_{gel}, is known as gel point and it is inversely proportional to the attraction forces between particles. For a certain colloidal gel of constant volume fraction, φ, above the gel point, an elastic property, y, can be obtained by the following equation:

$$y = k\left(\frac{\varphi}{\varphi_{gel}} - 1\right)^{x} \qquad (3.6)$$

where k is a constant and x a scaling exponent, usually of value around 2.5. This relationship allows obtaining elastic properties of the material, such as elastic modulus G or shear yield stress τ_y. For an ink of given φ, increasing the attraction forces between particles means a reduction of the gel point and thus an increment of the mechanical properties of the ink [58].

Along with the intrinsic properties of the ink, there are several other factors that influence the final outcome of the printing process. The final diameter of the extruded rod is determined not only by the diameter of the nozzle, but also by the pressure of the air and by the printing velocity. These two parameters have to be contemporaneously adjusted to obtain a constant shape. If the pressure is too low or the speed too high, the elastic recovery of the ink will cause breakdowns of the lines due to a lack of materials. On the other hand, if there is too much pressure and too slow movement, the rods will be large and deformed, provoking a total loss of the structural features. The spacing along the z axis is fundamental to achieve a good adhesion between the layers and avoid delamination or loss in mechanical properties. It shall be not too great, to let the rods adhere to the underlying layers, but not too little, to avoid deformation of the extruding rod and the lines underneath. The printing substrate plays also a crucial role. In fact, it has to be perfectly plane and shall allow attachment during printing, in order to block the structure and avoid any movements, but also, when the object is completed and dry, its detachment from the substrate must be easy to avoid damages. Since with this technique features in the range of few dozens of micrometers are printed, even micrometrical deviation from the planarity in the printing substrate may lead to defects.

The robocasting technique was first used for producing bioceramic scaffolds for bone regeneration by Franco et al. in 2010. They developed a hydrogel-based ink containing calcium phosphates, such as HA and β-TCP, and print it using nozzle diameters ranging from 100 to 250 μm. In their work they highlighted the effect of the grain size distribution and proposed Pluronic, a surfactant block co-polymer (polyethylene oxide (PEO)–propylene oxide (PPO)–polyethylene oxide (PEO)), as dispersant to form the colloidal ink. The use of a large distribution of powder size allows increasing the particles volume loaded within the ink, because the smaller particles promote the rearrangement of the bigger ones, facilitating the slip of the ink. This leads to a lower pressure needed for the extrusion and to the possibility of using smaller nozzle diameters. Moreover, the use of a conical tip prevents the formation of dead zones inside the nozzle, avoiding the clogging of it [61].

Pluronic was used also by Fu et al. for the first bioactive glass-based scaffold for bone application [62]. Plurionic, also known as F-127, is one of the three binders used for robocasting in bone application, alongside ethyl cellulose/polyethylene glycol and carboxymethyl cellulose. The last two are processed in ethanol instead of water, which is used for F-127. Thus, early ionic dissolution of the glass is prevented, but the control of the whole process is much more difficult. For example, the robocasting must be performed in a controlled chamber, within an ethanol-rich environment to prevent evaporation [63]. F-127 has a thermally reversible fluid-gel transition due to water adsorption/desorption on the -OH groups of the PPO block. At temperature around 0°C Pluronic forms liquid solution in water because it adsorbs on the polymer, extending the chains and making them to slide across each other. When the temperature rises up to 40°C the adsorption of water is energetically unfavorable and the polymeric chains form micelles and the solution changes from a fluid state to the gel one [64]. If glass particles are dispersed in the solution, Pluronic stabilizes them sterically, by generating Van der Waals or hydrogen bonding with the surface of the particles using the -OH groups in the polymeric chains [62]. It was observed that the presence of glass particles inside the Pluronic suspension lowers the temperature at which the state transition takes place. This is due to a preferential bonding of water to glass than to the Pluronic. In this way water is subtracted from the F-127 much earlier than what would happen in a pure Pluronic-water solution. F-127-based inks offer the advantages to be printed directly in air, making much easier the whole process.

In order to print in a non-wetting oil bath, the printer set-up is more complicated, because it needs a tank to contain the oil and often also the possibility of heating it. Moreover, the printing substrate is a multilayered structure, composed by a basic layer and two soluble ones. Franco et al. used an alumina sheet coated by an oil-soluble layer and a top one made of corn syrup, which is oleophobic. When the structure is printed on the corn syrup layer, the water inside the ink starts to dissolve the top layer, exposing the oil-soluble one to the oil. When also the mid layer is dissolved, the printed structure detaches easily from the alumina plate [61]. A similar method was also used by Fu et al. [62]. Substrates for printing in air can be composed of only one layers. Nommeots-Nomm et al. [64] used commercial OHP acetate sheets. They are perfectly flat, after drying the structures detach very easily and they are cheap.

Robocasting has been proved as a very valuable method for the fabrication of glass scaffolds for bone application, even for load-bearing sites. Using particle size ranging from 30 µm down to 1 µm and extrusion nozzle with diameters between 100 and 580 µm, it is possible to obtain glass structures smaller as 100 µm with porosity dimensions varying from few hundreds of micrometers up to half a millimeter. The total porosity is not so high, mostly around 50-60%, but 70% pore volume was achieved. With this technique considerable compressive strength are obtainable, in most of the case higher than the cancellous bone one, ranging from 13 MPa up to value that hare higher even than the cortical bone resistance, such as 142 MPa [64]. The use of sol-gel derived glasses has also been reported [45]. The deposition modelling offers a very easy control on the structure of the scaffolds, giving the opportunity to create graded porous devices. Also, the whole method can be carried out without the use of chemicals and products that can be toxic for the human body.

3.7 Bibliography

[1] Q. Fu, E. Saiz, M. N. Rahaman and A. P. Tomsia, "Bioactive glass scaffold for bone tissue engineering: state of the art and future perspectives," pp. 1245-1256, 2011.

[2] "Fisioterapia Rubiera," [Online]. Available: http://www.fisioterapiarubiera.com/dolore-osso/intervento-chirurgico-per-la-frattura-della-tibia/.

[3] P. K. Patel, "Distraction Osteogenesis," 2015.

[4] A. Oryan, S. Alidadi, A. Moshiri and N. Maffulli, "Bone regenerative medicine: classic option, novel strategies and future directions," 2014.

[5] E. Vernè, *Biomateriali e Materiali Nanostrutturati,* Politecnico di Torino, a.y. 2016/2017.

[6] F. Baino and C. Vitale-Brovarone, "Three-dimensional glass-derived scaffolds for bone tissue engineering: Current trends and forecast for the future," vol. 97A, 2011.

[7] V. A. Marco, C. A. Narvaez-Tovar and D. A. Garzon-Alvarado, "Design, Materials, and Mechanobiology of Biodegradable Scaffolds for Bone Tissue Engineering," 2015.

[8] J. Henkel, M. A. Woodruff, D. R. Epari, R. Steck, V. Glatt, I. C. Dickinson, P. F. Choong, M. A. Schuetz and D. W. Hutmacher, "Bone Regeneration Basedo on Tissue Engeneering Concetpions - A 21st Century Perspective," vol. 3, pp. 216-248, 2013.

[9] F. Verland, J. Braux, J. Amedee and P. Laquerriere, "Inflammatory cell response to calcium phosphate biomaterial particles: an overview.," vol. 9, pp. 4956-4963, 2013.

[10] S. J. Smiske, R. A. Ayers and T. A. Bateman, "Porous Materials for Bone Engineering," 1997.

[11] L.-C. Gerhard and A. R. Boccaccini, "Bioactive Glass and Glass-Ceramic Scaffolds for Bone Tissue Engineering," vol. 3, pp. 3867-3910, 2010.

[12] M. Peroglio, L. Gremillard, C. Gauthier, L. Chazeau, S. Verrier, M. Alini and J. Chevalier, "Mechanical properties and cytocompatibility of poly(ε-caprolactone)-infiltraded biphasic calcium phosphate scaffolds with bimodal pore distribution," *Acta Biomaterialia,* vol. 6, pp. 4369-4379, 2010.

[13] T. J. Webster, R. W. Siegel and R. Bizios, "Osteoblast adhesion on nanophase ceramics," *Biomaterials,* vol. 20, pp. 1221-1227, 1999.

[14] Q. Chen, J. Roether and A. Boccaccini, "Tissue engineering scaffolds from bioactive glass and composite materials," in *Tissue Engineering*, vol. 4, R. R. &. F. C. N Ashammakhi, Ed., 2008.

[15] P. Sepulveda, J. R. Jones and L. L. Hence, "Bioactive sol-gel foams for tissue repairs," vol. 49, pp. 340-348, 2002.

[16] L. Roseti, V. Parisi, M. Petretta, C. Cavallo, G. Desando, I. Bartolotti and B. Grigolo, "Scaffold for Bone Tissue Engineering: State of the art and new perspective," *Materials Science and Engineering C,* vol. 78, pp. 1246-1262, 2017.

[17] M. N. Rahaman, Ceramic processing and sintering, II ed., CRC Press, 2003.

[18] S.-J. L. Kang, Sintering: densification, grain growth and microstrucutre, Elsevier Butterworth-Heinemann, 2005.

[19] P. Fino, *Scienze e tecnologie dei materiali ceramici,* Politecnico di Torino, a.y. 2014/2015.

[20] L. C. De Jonghe and M. N. Rahaman, "Sintering of Ceramics," in *Handbook of Advanced Ceramics*, Elsevier, 2003.

[21] O. O. Omatete, M. A. Janney and S. D. Nunn, "Gelcasting: From Laboratory Development Toward Industrial Production," *Journal of the European Cereamic Society,* vol. 17, pp. 407-413, 1997.

[22] P. Sepulveda and J. G. P. Binner, "Processing of Cellular Ceramics by Foaming and in situ Polymeristion of Organic Monomers," *Journal of the European Ceramic Society,* vol. 19, pp. 2059-2066, 1999.

[23] Z. Y. Wu, R. g. Hill, S. Yue, D. Nightingale, P. D. Lee and J. R. Jones, "Melt-derived bioactive glass scaffolds produced by a gel-cst foaming technique," *Acta Biomaterialia,* vol. 7, pp. 1807-1816, 2011.

[24] A. Rainer, S. M. Giannitelli, F. Abbruzzese, E. Travenrsa, S. Licoccia and M. Trombetta, "Fabrication of bioactive glass-ceramic foams miomicking human bone portions for regenerative medicine," *Acta Biomaterialia ,* vol. 4, pp. 362-369, 2008.

[25] M. Navarro, S. del Valle, S. Martinez, S. Zeppetelli, L. Ambrosio, H. A. Planell and P. M. Ginebra, "New macroporous calcium phosphate glass ceramic for guided bone regeneration," *Biomaterials,* vol. 25, pp. 4233-4241, 2004.

[26] Q. Fu, M. N. Rahaman, B. S. Bal, W. Huang and D. E. Day, "Preparation and bioactive characteristics of a porous 13–93 glass, and fabrication into the articulating surface of a proximal tibia," *Journal of Biomedical Material Research Part A,* vol. 28A, pp. 222-229, 2007.

[27] W. Liang, M. N. Rahaman, D. E. Day, N. W. Marion, G. C. Raley and J. J. Mao, "Bioactive borate glass scaffold for bone tissue engineering," *Journal of Non-Crystalline Solid,* vol. 354, pp. 1690-1696, 2008.

[28] K. Rezwan, Q. Chen, J. Blaker and A. R. Boccaccini, "Biodegradble adn bioactive porous polymer/inorganic composite scaffolds for bone tissue engineering," *Biomaterials,* vol. 27, pp. 3413-3431, 2006.

[29] T. Livingston, P. Ducheyene and J. Garino, "In vivo evaluation of a bioactive scaffold for bone tissue engineering," *Journal of Biomedica Materials Research,* vol. 62, pp. 1-13, 2002.

[30] C. Vitale Brovarone, E. Verné and P. Appendino, "Macroporous bioactive glass-ceramic scaffolds for tissue engineering," *Journal of Material Science: Materials in Medicine,* vol. 17, pp. 1069-1078, 2006.

[31] H. Zhang, X.-J. Ye and J.-S. Li, "Preparation and biocompatibility evaluation of apatite/wollastonite-derived porous bioactive glass ceramic scaffolds," *Biomedical Materials,* vol. 4, p. 045007, 2009.

[32] O. Lyckfeldt and J. M. F. Ferreira, "Processingo fo porous ceramics by "Starch consolidation"," *Journal of the european ceramic society,* vol. 18, pp. 131-140, 1998.

[33] C. Vitale Brovarone, S. Di Nunzion, O. Bretcanu and E. verné, "Macroporous glass-ceramic materials with pioactive properties," *Journal of Materials Science: Materials in Medicine,* vol. 15, pp. 209-217, 2004.

[34] C. Vitale Brovarone, E. Verné, M. Bosetti, P. Appendino and M. Cannas, "Microstructural and in vitro characterization of SiO2-Na2O-CaO-MgO glass-ceramic bioactive scaffolds for bone substitutes," *Journal of Materials Science: Materials in Medicine,* vol. 16, pp. 900-917, 2005.

[35] S.-C. Wu, H.-C. Hsu, S. Hsiao and W.-F. Ho, "Preparation of porous 45S5 Bioglass-derived glass-ceramic scafofld by using rice husk as a porogen additive," *Journal of Materials Science: Materials in Medicine,* vol. 20, pp. 1229-1236, 2009.

[36] J. Roether, A. Boccaccini, L. Hench, V. Maquetc, S. Gautier and R. Jérome, "Development and in vitro characterisation of a novel bioresorbable and bioactive composite materials based on

polylactide foams and Bioglass for tissue engineering applications," *Biomaterials,* vol. 23, pp. 3871-3378, 2002.

[37] Q. Z. Chen, I. D. Thompson and A. R. Boccaccini, "45S5 bioglass-derived glass-ceramic scaffolds for bone titissue engineering," *Biomaterials,* pp. 2414-2425, 2006.

[38] O. Bretcanu, C. Camaille and A. R. Boccaccini, "Simple methods to fabricate Bioglass-derived glass-ceramic scafoflds exhibiting porosity gradient," *Journal of Material Science,* vol. 43, pp. 4127-4134, 2008.

[39] Q. Fu, M. N. Rahaman, S. B. Bal and R. F. Brown, "Preparation and in vivo evaluation of bioactive glass (13-93) scaffolds with oriented microstructures for reparir and regeneration of load-bearing bones," *Journal of Biomedical Materials Research A,* vol. 95A, pp. 235-244, 2009.

[40] Y. Miniaberry and M. Jobbágy, "Macroporous Bioglass scaffolds prepared by coupling sol-gel with freeze drying," *Chemistry of Materials,* vol. 23, pp. 2327-2332, 2011.

[41] V. Maquet, A. Boccaccini, L. Pravata, I. Notingher and R. Jérome, "Porous poly(α-hydroxyacrid)/Bioglass composite scaffolds for bone tissue engineering. I: preparation and in vitro characterization," *Biomaterials,* vol. 25, pp. 4185-4194, 2004.

[42] Y. Ding, M. T. Souza, W. Li, D. W. Shubert, A. R. Boccaccini and J. A. Roether, "Bioactive glass-biopolymer composites for applications in tissue engineering," in *Handbook of Bioceramics and Biocomposite*, Springer International Publishing, 2015, pp. 1-26.

[43] Y. Niu, L. Guo, J. Liu, H. Shen, J. Su, X. An, B. Yu, J. Wei, J.-W. Shin, H. Guo, F. ji and D. He, "Bioactive and degradable scaffolds of teh mesoporous bioglass and poly(L-lactide) composite for bone tissue regeneration," *Journal of Material Chemistry B,* vol. 3, pp. 2962-2970, 2015.

[44] S. Bose, S. Vahabzadeh and A. Bandyopadhyay, "Bone tissue engineering using 3D printing," *Materials Today,* vol. 12, 2013.

[45] R. Gmeiner, U. Deisinger, J. Schönherr, B. Lechner, R. Detsch, A. Boccaccini and J. Stampfl, "Additive manufacturing of bioactive glasses and silicate bioceramics," *Journal of Ceramic Science and Technologies,* vol. 6, pp. 75-86, 2015.

[46] S. F. S. Shizari, S. Gharehkhani, M. Mehrali, H. Yarmand and H. S. C. Metselaar, "A review on powder-based additive manufacturing for tissue engineering: selective laser sintering ad inkjet 3D printing," *Science and Technology of Advanced Materials,* vol. 16, 2015.

[47] J. Liu, H. Hu, P. Li, C. Shuai and S. Peng, "Fabrication and characterization of porous 45S5 glass scaffolds via direct selective laser sintering," *Materials and Manufacturing Processes,* vol. 28, pp. 610-615, 2013.

[48] C. Gao, T. Liu, C. Shuai and S. Peng, "Enhanced mechanisms of graphene in nano-58S biactive glass scaffold: mechanical and biological performance," *Scientific Reports,* vol. 4, p. 4712, 2014.

[49] K. C. Kolan, M. C. Leu, G. E. Hilmas, R. F. Brown and M. Velez, "Fabrication of 13-93 bioactive glass scaffolds for bone tissue enginnering using indirect selective laser sintering," *Biofabrication,* vol. 3, p. 025004, 2011.

[50] F. P. Melchels, J. Feijen and D. W. Grijpma, "A review on stereolithography and its applications in biomedical engineering," *Biomaterials,* vol. 31, pp. 6121-6130, 2010.

[51] B. Thavornyutikarn, N. Chantarpanich, K. Stthiseripratip and G. Thouas, "Bone tissue engineering scaffolding: computer-aided scaffolding techniques," *Prog Biomater,* vol. 3, pp. 61-102, 2014.

[52] Z. Li, X. Chen, N. Zhao, H. Dong, Y. Li and C. Lin, "Stiff macro-porous bioactive glass-ceramic scaffold: Fabircation by rapid prototyping template, characteriaion and in vitri bioactivity," *Materials Chemistry and Physics,* vol. 141, pp. 76-80, 2013.

[53] S. Porro, *Materials for MEMS and characterization of technological processes,* Politecnico di Torino, a.y. 2016/2017.

[54] E. Mancuso, N. Alharbi, O. A. Bretcanu, M. Marchal, M. A. Brich, A. W. McCaskie and K. W. Dalgarno, "Three-dimoensional printing of porous load-bearing bioceramic scaffolds," *Journal of Enigineering in Medicine,* vol. 213, pp. 575-585, 2011.

[55] M. Guvendiren, J. Molde, R. M. Soares and J. Kohn, "Designing biomaterials for 3D printing," *ACS Biomaterials Science&Engineering,* vol. 2, pp. 1679-1693, 2016.

[56] J. A. Lewis, J. E. Smay, J. Stuecker and J. Cesarano, "Direct ink writing of three-dimensional ceramic structure," *Journal of the American Ceramic Society,* vol. 89, pp. 3599-3609, 2006.

[57] J. Cesarano, *Robocasting of ceramics and composites using fine particle suspensions,* Albuquerque: Sandia National Laboratory, 1999.

[58] J. A. Lewis and J. E. Smay, "Three-dimensional periodic strucutre," in *Cellular ceramics: structure, manufacturing, properties and applications*, Wiley-VCH, 2005, pp. 87-100.

[59] M. Sangermano, *Scienza e tecnologia dei materiali polimerici,* Politecnico di Torino, a.y. 2014/2015.

[60] J. A. Lewis, "Direct-write assembly of ceramics from colloidal inks," *Current Opinion in Solid State and Material Science,* vol. 6, pp. 245-250, 2002.

[61] J. Franco, P. Hunger, M. Launey, A. Tomsia and E. Saiz, "Direct write assembly of calcium phosphate scaffolds using a water-based hydrogel," *Acta Biomaterialia,* vol. 6, pp. 218-228, 2010.

[62] Q. Fu, E. Saiz and A. Tomsia, "Direct ink writing of highly porous and strong glass scaffolds for load-bearing," *Acta Biomaterial,* vol. 7, pp. 3547-3554, 2011.

[63] A. Deliormanli and M. Rahaman, "Direct-write assembly of silicate and borate bioactive glass scaffolds for bone repair," *Journal of the European Ceramic Society,* vol. 32, pp. 3637-3656, 2012.

[64] A. Nommeots-Nomm, P. Leeb and J. Jones, "Direct ink writing of highly bioactive glasses," *Journal of the European Ceramic Society,* p. http://dx.doi.org/10.1016/j.jeurceramsoc.2017.08.006, 2017.

[65] T. Pe, "Teach Pe," [Online]. Available: http://www.teachpe.com/anatomy-physiology/the-skeleton-bones/types-of-bones. [Accessed 18 settembre 2017].

[66] [Online]. Available: https://www.britannica.com/science/osteon. [Accessed 18 settembre 2017].

[67] [Online]. Available: http://emedicine.medscape.com/article/1948532-overview#showall. [Accessed 18 settembre 2017].

4 Materials and methods

4.1 Introduction

This chapter contains the description of the process that was used to fabricate the glass scaffolds, from the production of the glass starting from raw materials to the robocasting of the scaffolds. It also describes the analyses that were performed on the glass and on the scaffolds, in order to obtain a complete characterization of the materials used.

The production of the glass and part of the analyses (part of the thermal characterization, mechanical test, SEM observation and XRD) where made at Politecnico di Torino, in the laboratories of the department of Applied Science and Technology. The robocasting process, the left thermal analysis and the bioactivity test were performed at the Tampere University of Technology, at the faculty of Biomedical Sciences and Engineering. The micro-CT analyses were performed at Innovation Center Iceland (ICI) in Iceland.

4.2 47.5B: a bioactive glass for robocasting

The bioactive glass used during the development of the present thesis was chosen among a set of six glasses, created by Verné et al, [1]. The different melt-derived glass compositions belonging to the SiO_2-P_2O_5-CaO-MgO-K_2O-Na_2O system were studied to understand the roles of modifier oxide ratio and MgO upon the bioactivity kinetics.

The compositions of the six different glasses are listed in **Table 4.1**

Table 4.1 Composition (mol%) of the six glasses produced by Verné et al, [1]

Glass	SiO_2	P_2O_5	CaO	MgO	K_2O	Na_2O
47.4A	47.5	2.5	30	0	10	10
47.5B	47.5	2.5	20	10	10	10
45A	45	5	25	10	10	5
45B	45	5	25	10	5	10
42.5A	42.5	2.5	30	15	0	10
42.5B	42.5	2.5	30	15	10	0

One of the main effect of the different amount of modifier oxides is a change in thermal behavior, in terms of characteristic temperatures and crystallization. 45A and 42.5B present fast devitrification during cooling down, so they were expected to be not very suitable for bone applications since crystallinity limits bioactivity. All the remaining compositions showed similar thermal behavior and characteristic temperatures, listed in **Table 4.2**, with the exception of the 47.5B.

Table 4.2 Characteristic temperature of the glasses

Glass	T_g (°C)	T_{x1} (°C)	T_{x2} (°C)	T_{m1} (°C)	T_{m2} (°C)
47.4A	580	800	850	1000	1050
47.5B	540	800	-	1010	-
45B	580	780	880	1000	1250
42.5A	600	830	930	1090	1250

Three out of four compositions present the crystallization of two different phases, at temperatures ranging between 800 and 900°C, with the corresponding two melting temperature. Only the 47.5B has just one crystalline phase. This can be explained by the presence of magnesium oxide combined with the lower content of CaO, compared with all the other glasses. In fact, the peaks revealed by X-rays diffraction performed on devitrified 47.5B are correlated with the presence of one silicate phase ($Na_2CaSi_3O_8$), while is absent the other one ($K_4Ca(SiO_3)_3$), which is formed in the other compositions and is less stable than the former. The other effect of MgO presence is the lowering of the glass transition

temperature and the broadening of the working windows of the glass, represented by the difference between the glass transition temperature and the crystallization temperature.

In vitro bioactivity tests, performed by SBF soaking of glass and glass-ceramic samples, showed an increase in the pH of the solution, meaning that the process of ionic exchange occurred and suggesting the formation of HA layer. The presence of apatites, in particular hydroxycarbonate apatite, on the surface was confirmed by X-ray diffraction and scanning electron microscope imaging, as shown in **Figure 4.1** HCA globular agglomerates on 47.5B glass surface.

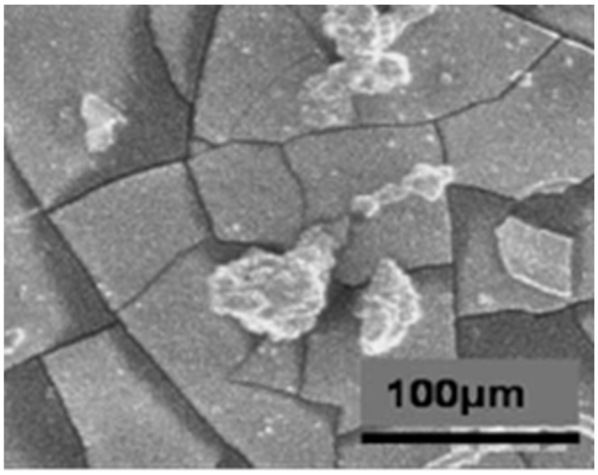

Figure 4.1 HCA globular agglomerates on 47.5B glass surface [1]

The work of Verné et al. showed, interestingly, how changes in composition within the SiO_2-P_2O_5-CaO-MgO-K_2O-Na_2O system, even if they affect the thermal stability and properties of the glasses, seem to have very low influence on the bioactivity mechanism of the glasses. Also, a partial devitrification does not decrease the ionic exchange in a drastic manner, as revealed by tests in SBF.

Since the aim of this thesis is to obtain fully amorphous scaffolds using robocasting technique, the 47.5B composition was chosen thanks to its bioactivity and the higher difference between T_g and T_x, that ensure a good workability.

4.3 Scaffolds manufacturing process: from glass precursors to 3D printing

4.3.1 47.5B Glass powders preparation

The glass used in this thesis was developed at Politecnico di Torino by Verné et al, [1], and it was chosen among the other compositions proposed in the same paper due to the presence of the magnesium oxide that increases the crystallization temperature, thus widening the processing window (glass sinterability). Since the aim of this work is to obtain bioactive glass-based scaffolds that are totally amorphous, so it is necessary a large difference between the glass transition temperature and the onset of devitrification of the materials. This glass is silica-based and belongs to the SiO_2-CaO-MgO-P_2O_5-Na_2O-K_2O group. In particular its composition is reported in **Table 4.3**

Table 4.3 Composition of the 47.5B glass, expressed in molar percentages

SiO_2	**P_2O_5**	**CaO**	**MgO**	**Na_2O**	**K_2O**
47,5	2,5	20	10	10	10

4.3.1.1 Melting and quenching process

To obtain the glass a melting-quenching process was used. First of all, as precursors, the following raw materials were used:

- Silicon oxide (SiO_2)
- Calcium phosphate ($Ca_3(PO_4)$)

- Calcium carbonate ($CaCO_3$)
- Hydrated magnesium carbonate ($(MgCO_3)Mg(OH)_2*5H_2O$)
- Sodium carbonate (Na_2CO_3)
- Potassium carbonate (K_2CO_3)

All the reactants were manufactured by Sigma-Aldrich.

The precursors undergo decomposition reactions during the melting, in order to provide the oxides present in the glass. The reactions happen as it follows:

- $Ca_3(PO_4) \rightarrow 3CaO+P_2O_5$
- $CaCO_3 \rightarrow CaO+CO_2$
- $(MgCO_3)Mg(OH)_2*5H_2O \rightarrow 5MgO+4CO_2+6H_2O$
- $Na_2CO_3 \rightarrow Na_2O+CO_2$
- $K_2CO_3 \rightarrow K_2O+CO_2$

Based on this set of reactions, calculations were made in order to obtain the weight needed per every reactant. The equation used is represented as:

$$g_{reac} = \frac{g_{glass}}{100} * \%weight\ ox * \frac{PM_{reac}}{PM_{ox}} \quad (4.1)$$

To obtain 100g of 47.5B glass the reactants needed are listed in **Table 4.4**

Table 4.4 Molecular weight and grams of reactants needed to prepare 100g of glass

Reactants	**Molecular weight**	**g**
SiO_2	60.0843	45.33585
$Ca_3(PO_4)$	310.1828	12.31813
$CaCO_3$	100.0892	19.87396
$(MgCO_3)Mg(OH)_2*5H_2O$	485.6524	15.42918
Na_2CO_3	105.9888	16.83632
K_2CO_3	138.2058	21.95399

All the chemicals were available in form of powders and, after being, were inserted into a polyethylene bottle and manually mixed, by shaking the bottle, until an homogeneous blend was obtained.

Figure 4.2 Glass casting in water to obtain a frit

The melting process was carried out in a Carbolite 1800 furnace. The mixed precursors were inserted into a platinum crucible, filling it around three quarter of its volume. The powders were poured little at time and were compressed, in order to remove gasses and compact them to insert as much powders as possible in the crucible. Then the crucible was covered with a lid, to avoid splashes in the furnace due to CO_2 developing during carbonate decomposition, and it was putted into the furnace. The melting protocol was the following:

- Heating ramp at a velocity of 10K/min until 1000°C;
- At 1000°C the lid is removed. All carbonates are decomposed and it might get stuck in the crucible;
- Heating ramp at velocity of 15K/min up to 1500°C;
- Temperature hold for 30 minutes in order to homogenize the melt;
- Casting in distilled cold water to avoid devitrification (**Figure 4.2**).

It was chosen to pour the melt glass in water, instead of using a mold, to obtain a glass frit, pictured in **Figure 4.3**. It is formed by glass particles in the dimension range of few millimeters that are badly cracked due to residual stresses generated by the thermal shock of the quenching process. In this way any further milling process is easier. The frit was dried using paper sheets.

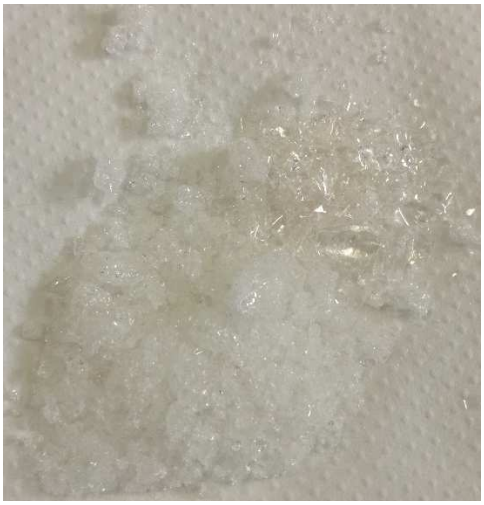

Figure 4.3 47.5B glass frit obtained by quenching molten glass in water

4.3.1.2 Milling and sieving

Since particles with dimension lower than 32 µm were needed for the ink preparation, the glass frit was milled using a zirconia single ball mill (Pulverisette 0, Fritsch, Germany). The mill was used with a vibrating platform and the process was controlled by adjusting the amplitude of the vibration. On the vibrating platform there is no indication of the amplitude, so the adjustments were made manually and the suitable point was found to be the amplitude that made the ball jumping a little inside the jar. The process optimization lead to the following protocol for glass milling:

- 10g of frit were introduced inside the jar;
- They were milled for 20 minutes at the amplitude discussed before;
- The powders were manually sieved using a mesh number 450 (stainless steel sieves, Giuliani, Italy).

The milling process was optimized by tuning cycle time, glass quantity and vibration (**Figure 4.4**).

The particles bigger than 32 µm that were blocked by the mesh underwent another milling cycle. The efficiency of the first and the second milling both was around 50%. Then it decreased and a third milling cycle was convenient no more. So, the remaining particles were melted again, following the melting protocol, and crushed another time.

Figure 4.4 left: Ball mill with powders inside; right: the sieve used in the process

4.3.2 Ink fabrication and cartridge loading

Making the ink, which is a colloidal suspension of 47.5B particles in an aqueous solution of Pluronic F-127, is rather simple, but it has to be carried out very carefully to obtain good results, in terms of processability and scaffold properties. In fact, every defect in the ink, such as inhomogeneous dispersion of the powders or air bubbles trapped, would affect the successive steps.

4.3.2.1 Pluronic aqueous solution

The first step in the preparation of the ink is to make the binder solution. Pluronic is sold by Sigma-Aldrich in the form of powder and it was mixed with water using a magnetic stirrer. F-127 solution was prepared in different weight percentages, in order to evaluate the effect of the binder concentration upon the ink processability and strength. 25%, 27.5% and 30wt% solutions were made for preliminary trials and the concentration of 27.5wt% was eventually chosen as the best one for the fabrication of the scaffolds. 50ml of solution was made at once, by inserting Pluronic powders, and weighted with a precision of 1mg, into a 100ml plastic bottle (AB265-S/FACT scale, Meter Toledo). Distilled water, weighted in the same way as the Pluronic, is then added and the bottle is placed into a water bath with ice to keep the temperature low. The solution is stirred at least for a night time but, if flocs were still present inside the solution, it would be stirred till an optically clear liquid was obtained.

4.3.2.2 Glass mixing

The crucial phase for obtaining a good ink and a repeatable and stable process is mixing glass powders with binder. This step is fundamental to achieve a homogenous ink and a low content of air inside it. During this work, it was optimized and a suitable process was found, but since it is a manual and very low automatized process, the ability of the operator to assess the correct dispersion and air content is crucial. During the optimization tests for the ink recipe, two different glass volume loads were tested, 30 and 35vol% of glass. The glass loading influences the viscosity of the ink and the capability of the lines to maintain themselves straight while crossing a gape in the layer underneath, as well as the shrinkage during sintering. Based on the ability of the ink to maintain the shape after extrusion, 35vol% loading of glass particles had been chosen to carry the printing of the scaffolds manufactured during this research.

The ink was made in small plastic pot and the amount of glass and binder was tuned to fully fill the cartridge. To do so, 3,806g of glass were necessary. Calculation based on the density of the glass and the 27.5wt% Pluronic solution were carried out to obtain the Pluronic grams needed for 35% glass loading:

$$\begin{aligned} g_{F127} &= V_{F127} * \rho_{F127} \\ V_{F127} &= \frac{V_{47.5B}}{0{,}35} * 0.65 \\ V_{47.5B} &= \frac{g_{47.5B}}{\rho_{47.5B}} \end{aligned} \qquad (4.2)$$

g_{F127}: F-127 solution grams

V_{F127}: F-127 solution volume

ρ_{F127}: F-127 solution density

$g_{47.5B}$: glass grams

$V_{47.5B}$: glass volume

$\rho_{47.5B}$: glass density

The density of the binder is 1.067g/cm^3 and was calculated from commercial information, while the glass one was calculated using the Archimedes' principle and it is 2.640g/cm^3. In order to obtain a fully loaded cartridge, along with 3.806g of glass, 2.857g of Pluronic were used.

To obtain the highest repeatability possible for the whole process, a protocol for the ink mixing was developed, but variations may occur in dependence of factors that were un-controllable, such as temperature and humidity. It consists in alternating mixing phases with cooling and air removal ones. A typical ink preparation was carried on following the next steps:

- Weighting glass powders, ±1 mg, in a small plastic pot (AG245 scale, Oy G.W.Berg&Co);
- Flatting the surface of the powders by tapping the pot on the table;
- Weighting the Pluronic solution, ±5mg (high precision is difficult to achieve due to the viscosity of the solution that generate quite large drops) using a Pasteur pipette dropwise. Due to the thermal behavior of the binder, it was kept in ice bath during the process;
- The ink is mixed for 1 min using a vortex mixer (Vibrofix VF1 electronic, Ika-Werk) at 2500rpm;
- Then it is cooled for 1 min into an ice bath while being gently tapped to remove air bubbles trapped inside;
- At least 5 cycle mixing-cooling are made, to be sure to achieve a good dispersion of the glass.

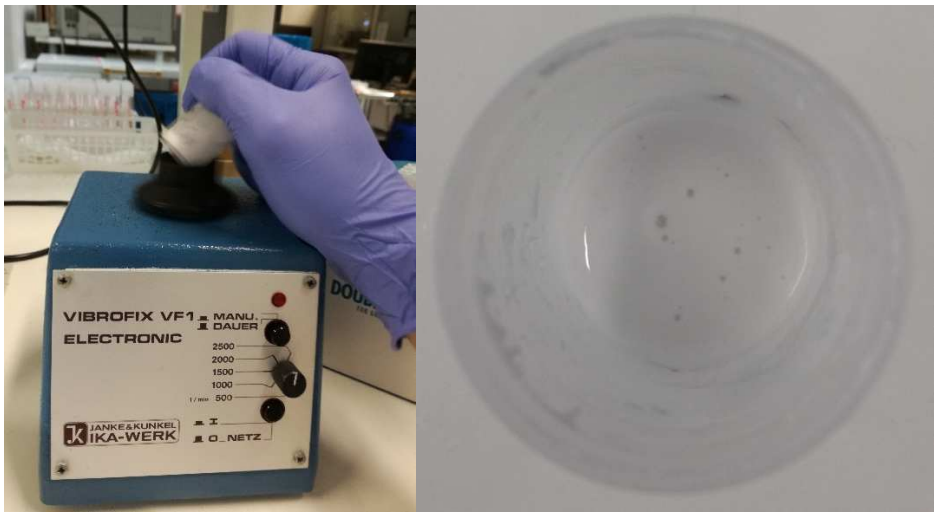

Figure 4.5 Mixing of glass with Pluronic solution (left); air bubbles on the surface of the ink (right).

If during the process the ink heated too much, becoming too viscous to be well mixed, the pot is placed in freezer for about 1 minute to obtain a larger temperature drop as compared to the ice bath. When no more air bubbles appear on the surface, the ink is ready to be loaded in the printing cartridge. To have a suitable viscosity, before filling the cartridge, the ink is kept 2 minutes in freezer.

4.3.2.3 Cartridge loading

The printing cartridge is composed by a plastic barrel and a small plunger (**Figure 4.6**). The plunger needs to be inserted completely in the barrel and it will be pushed by air during the printing. It also acted as a valve, the air can flow through the plunger in order to apply an isostatic pressure against the ink, but it cannot pass the plunger in the other way.

Figure 4.6 Cartridge and plunger

It is not possible to fill directly the cartridge from the pot, since it would trap too much air in the ink. So, a common 10 ml injection syringe is used in an intermediate step. The filling process can be divided in three passages, shown in **Figure 4.7**:

- Filling of the injection syringe: the ink is poured from the pot into the syringe, then the plunger is inserted and pushed until the ink starts to exit from the tip of the syringe;
- Preparation of the cartridge: the plunger is pushed all the way down to the bottom of the cartridge, so there is no air in it. Then the tips of the syringe and the cartridge are joined by a connector, which can be screwed into the cartridge and where the syringe tip can fit;
- Filling of the cartridge: by pushing slowly the plunger of the syringe the ink is transferred to the cartridge.

Figure 4.7 Cartridge loading process (from top to bottom): loading of the injection syrigne; preparation of the cartridge: the plunger is fully pushed and the two tips are matched by the connector; cartridge fully filled

During the process, special care has to be paid avoiding the formation of air bubbles trapped between the walls of the barrels and the ink. To reduce this, both the injection syringe and the cartridge are kept in freezer before filling them. The cold walls reduce the ink viscosity and the formation of air bubbles is less likely. Then the plunger must be moved very slowly and it can be tapped on the table to move the air towards the surface of the ink, to be eliminated. It is also important that the cartridge is not completely full, but the plunger must stay at least a centimeters and half below the top of the barrel. In fact, the nozzle of the printer air pump must enter the barrel to ensure a perfect sealing and the plunger shall have some space to move. Since pressurized air flows through it during the printing process, in case of an interruption of it, the air will push upward the plunger to release the pressure. If the piston cannot move

freely because it is too close to the printer nozzle, there will be some pressure on the ink and it will flow in unwanted moments.

Prior printing, the ink is left to rest for one hour, in order to stabilize itself.

4.3.3 Robocasting

Once the ink rested for one hour, it is ready to be printed. The 3D printer used during this thesis is a Tabletop-3Dn (nScrypt Inc., Orlando, Florida, USA), with base set-up (**Figure 4.8**). The printer has two main parts, the printing tower and the printing base. The printing tower presents two printing heads that can be used simultaneously to use two different materials. The only movement that is allowed to the printing tower is along the Z axis, and its position determines the height of the printing. The printing base is a metal plate that is used as a support during the printing. It has to be as flat as possible to avoid errors during the process. The plate is moved on the X-Y plane, with respect to the printing tower, to extrude the ink in the correct pattern. This machine is capable of high precision and repeatability, for instance about 10µm accuracy along the X and Y axis and about 5 µm along the Z axes, and it is suitable for printing all kind of different materials, from electronics on textile to ceramics and bioprinting [2].

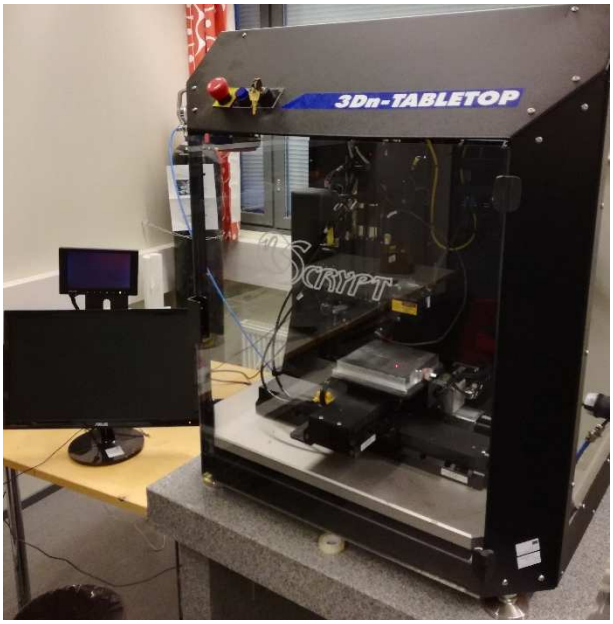

Figure 4.8 Tabletop-3Dn printer

Usually ceramic tips are used, but the ones provided by the manufacturer have a too small diameter for bone scaffold applications, just up to 100 µm. Plastic tips were used, with an inner diameter of 410 µm (Nordson EDF Optimum® SmoothFlow™), they can be screwed to the tip of the cartridge. Since the new tips do not fit in the standard structure, a modification was required. The cartridge is manually attached to one of the two printing heads using adhesive tape. This does not affect the accuracy of the printing because the forces applied on the cartridge during the process are low and the tape provides enough stability to it. Before attaching the syringe to the printer is necessary to couple it with the air line. The printer uses a “pressure control” system instead of a “displacement control”. The whole set-up is shown in **Figure 4.9**

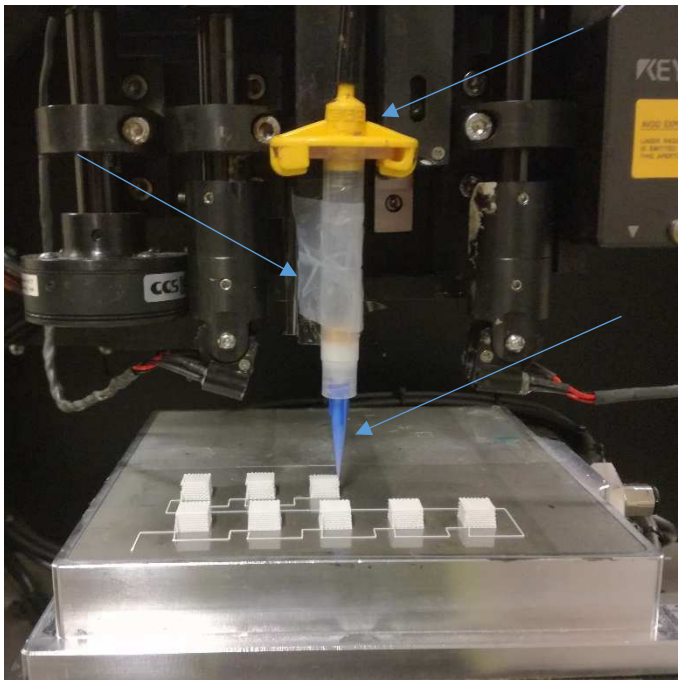

Figure 4.9 3D printer at work. The arrows indicate, from top to bottom: the air line; the cartridge; the tip. On the metal printing plate there are several scaffolds already printed.

Acetate sheets, Colour Laser Printer & Copier OHP Film (Folex AG, Seewn, Switzerland) are used as printing substrate, due to their flatness, the good adhesions that they have with the ink and the easiness to detach the scaffolds from them once they are dry [3].

Once the cartridge is loaded and fitted in position and the OHP sheet is placed on the platform, the processing parameters can be adjusted form the computer program, Machine Tools 3.0 provided by nScrypt. The interface is very simple and easy to use. The three main things that need to be provided as input to the program are:

- The design script: this printer is not based on 3D CAD models but on script files that can be written as text file. In order to obtain the desired structure, it is necessary to program every single movent that the print head shall do, along the X, Y and Z axes. This can be done as a simple program, where each line is related to a single movement, following a spatial vector (**Figure 4.10**). It is also possible to determine the relative velocity between the print head and the building platform. This programming methodology allows building porous structure with controlled dimension and in different shapes, cubic and cylindrical for instance, but also more complex ones. However, during the design process, the z spacing between layers are pre-determined by the diameter of the nozzle and it cannot be changed.

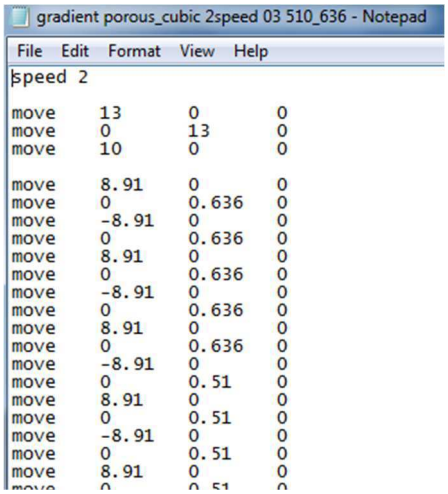

Figure 4.10 First lines of the script used to manufacture gradient porous scaffolds.

- Starting Z value, zero level: due to the modification of the printing system, it is necessary to manually insert the value along the Z axis that the printer shall use as starting point for the printing. To do so it is necessary to lower the print head, by the console in the program interface, until the tip of the nozzle touches consistently the acetate sheet. This is intended to happen when strong resistance is felt trying to move the OHP film.
- Air pressure: the extrusion pressure affects strongly the thickness of the extruded rods, the adhesion between layers and the stability of the process. If it is too low not enough material will be extruded, the lines are likely be thin and prone to break. If it is too high, lines will thicken and the smaller features will be lost. Pressure shall be adjusted also according to the print head speed, since their effects overlap.

Prior to start the actual printing, it is necessary to find the right pressure. Due to the uncontrolled printing environment, temperature and humidity can change the condition and the pressure needed to print can change of few psi. They also have effect during the preparation of the ink. So, usually, some trials are made, tuning the pressure till the suitable condition is reached. Then it is possible to begin the actual print, producing several scaffolds at time.

If the printing is interrupted for any reason, for example it happens that some defects are produced and lead to bad printing, hence, it is necessary to change the nozzle since it is possible that it is clogged. Every time the nozzle is changed, a new zero level must be measured.

The design and the processing parameters were optimized to obtain two different kinds of squared scaffolds. The first one has graded porosity, and it was designed to have a central core of smaller pore, about 120µm spacing between neighboring lines, and an outer layer of bigger pore, with size about 220µm. The inner core has a width of 2mm and the overall dimension is about 6.5 mm. From hereafter the graded scaffold will be addressed as 47.5B-G. The other kind of scaffold is derived from this one and it presents monopores with the same size of the bigger ones in the graded scaffolds. Due to the bigger pores and the manufacturing process, the second kind of scaffold is slightly bigger than the 47.5B-G, with width about 7.5mm. This scaffold will be addressed as 47.5B-M hereafter. The height is the same for both, since they are made of 20 glass layers, and it is about 4.5mm. The design of the pattern followed by the printing head for building one layer of the two scaffold types is shown in

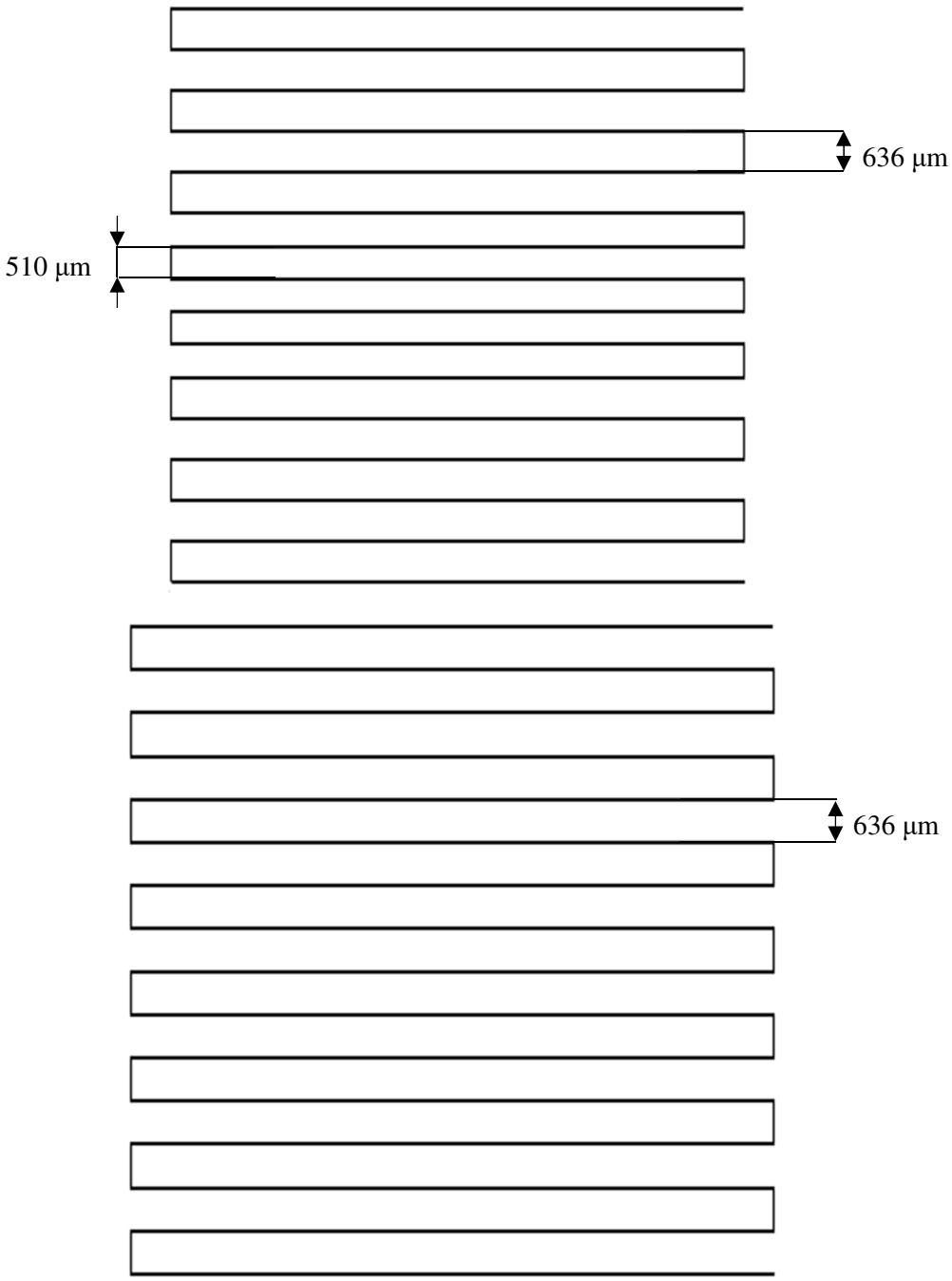

Figure 4.11 Printing head pattern for the printing of one layer for the 47.5B-G scaffold (top) and for the 47.5B-M one (bottom)

Once the printing is completed, the PHO sheet with the scaffolds is carefully moved on to a table and the scaffolds are left to dry for 48h. When the substrate is moved, in order avoid the introduction of deformations and tensions in the still wet and soft scaffolds, a rigid support is used. The foil is shifted form the printing plate on the support and from it on the table. When the scaffolds are dried they are detached from the acetate sheet just bending it a little, they came off very easily. If not sintered immediately, they are stored in the dryer.

4.3.4 Sintering

As in every manufacturing process of a ceramic component, formed using a slurry paste, sintering is a fundamental step for the fabrication of glass scaffolds. Its aim is to give mechanical resistance to the structure by consolidating and bonding each other the glass particles. The thermal treatment used in this

work is a two steps process. In fact, besides the proper sintering of the glass, burning out the polymeric binder is necessary. If the binder is not removed properly, a carbon residue will remain on the scaffolds and it will prevent glass form sintering in the right way. The most noticeable difference between a complete burning out of the polymer and an incomplete one is the color, it will turn from glassy with to different gradation of black.

The furnace used is a small furnace (Nabertherm) with alumina walls. The scaffolds are placed on an alumina plate, turned upside down with respect to the printing direction. This is necessary to compensate the residual stresses due to uneven shrinkage during drying. The base, which has some residual tractions, needs to be free to shrink in order to avoid crack formation during sintering. The scaffolds are placed in symmetrically starting from the center of the plate, so the heat and air flow is as similar as possible for every one of them. To ensure enough air flow between the scaffolds, they are about 2 cm distant from each other, as shown in **Figure 4.12**.

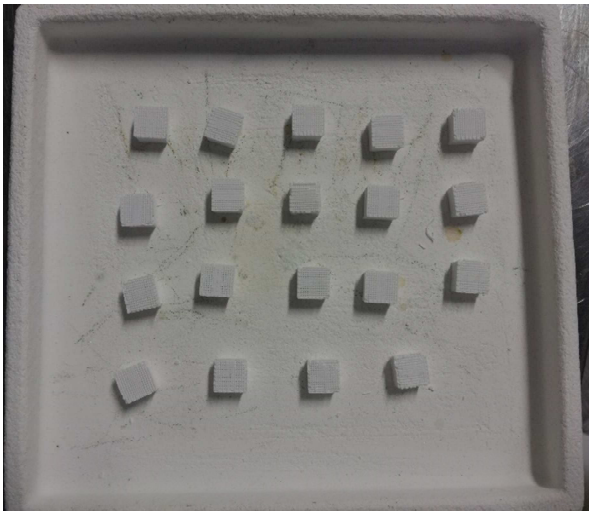

Figure 4.12 Scaffolds displaced on the alumina plate before sintering

The thermal treatment was optimized in order to achieve a good removal of the Pluronic from the scaffolds. To be sure of that, the heating rate was kept very low and several steps were made. These also helped releasing the residual stresses, avoid the formation of cracks. The actual temperature in the furnace was measured using a thermocouple, in order to be as much precise as possible. The sintering process is carried out in air at a heating rate of 1°C/min and it follows the sequent scheme:

- Heating from room temperature to 200°C;
- Holding at 200°C for 30min;
- Heating up to 400°C and holding again for 30min;
- Rising the temperature at 500°C and holding for 30min;
- Final heating up to 600°C and sintering for 1h;
- Slow cooling at room temperature in the close and turned off furnace.

Just the last step leads to actual sintering, the others are part of the debinding process. All those steps and the very slow heating rate are applied because the binder removal has to be complete and with faster process it was not possible to achieve it. Even with this program, some scaffolds remain black or cracks appear after sintering.

After the sintering, the scaffolds are collected and stored into a drier, to avoid reaction with the air humidity.

4.4 Characterization

To have a better understanding and control on the printing process and to study the properties of the printed scaffolds, from the chemical, mechanical and bioactive points of view, several kinds of analyses were performed on raw materials and final object both. All the analyses performed on the different type of samples are show in **Table 4.5**

Table 4.5 Analyses performed on different samples

	Thermal properties		**Chemistry, structure, morphology**				**Mechanical properties (compression)**			**In vitro bioactivity**	
	DSC	HSM	EDS	SEM	XRD	Optical	Compressive strength	Weibull modulus	After SBF.	Ionic release	XRD/EDS after SBF immersion
Glass powders	X	X	X	X	X						
Graded scaffold				X	X	X	X	X	X	X	X
Monoporous scaffold				X	X	X	X		X	X	X

4.4.1 47.5B glass and powder characterization

The first step to plan the whole process is to gain a good knowledge of the raw materials. In this case, due to the manufacturing process and the final aim of the devices, it was necessary to evaluate the shapes and dimension of the powders, the chemical composition and the thermal properties of the glass, in terms of crystallization and sintering behavior. So, the following analyses were performed: density evaluation; scanning electron microscopy (SEM) observation; energy dispersion spectroscopy (EDS); differential thermal analysis (DTA); hot stage microscope (HSM); X-ray diffraction (XRD)

4.4.1.1 Density evaluation

The density of the glass was experimentally evaluated using the Archimedes' principle. When a body is immersed into a liquid, a buoyancy force is applied to the solid, and this force is proportional to the volume of the body and to the density of the liquid. If the object is fully immersed, the following relationship is true:

$$W_{o,a} = W_o - W_d$$

$Wo_{,a}$: apparent immersed weight of the object

W_o: weight of the object

W_d: weight of displaced fluid

So, there is a correlation between the density of the fluid, $\rho_{w,}$ and the one of the object, $\rho_{o,}$ which is possible to evaluate by weighting the object in air and in a fluid of known density

$$\frac{\rho_o}{\rho_w} = \frac{W_o}{W_d} = \frac{W_o}{W_o - W_{o,a}} \qquad (4.3)$$

A piece of glass was casted by remetling some powders and pouring it on a metal plate. Then it was placed on the sample holder, which is handmade (**Figure 4.13**). The instrument is composed by a support plate where the becker containing distilled water (ρ=1g/cm^3) is placed, lifted with respect to the scale, and the measuring unit that has to be placed on the scale (AB265-S/FACT scale, Meter Toledo). The glass was then measured three times in air and three more when fully immersed in distilled water and the density was calculated using equation 4.3.

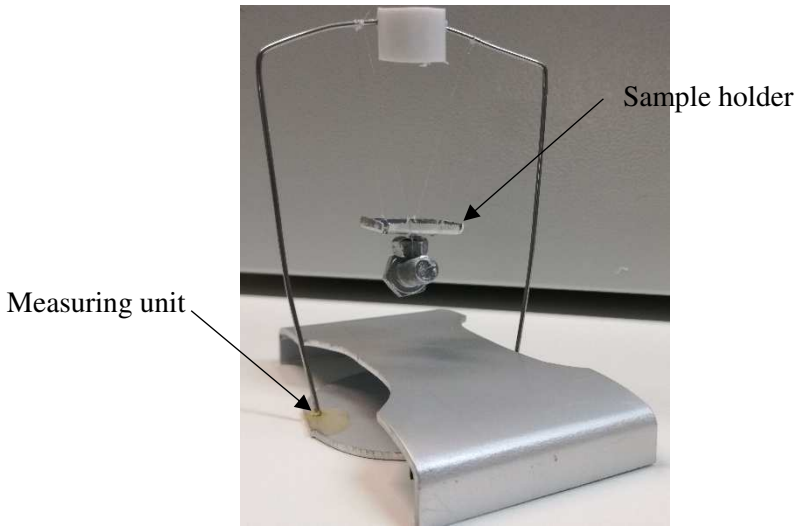

Figure 4.13 Experimental set-up for the evaluation of bulk object density using the Archimedes' principle

4.4.1.2 Particles shape and dimensions

Parameters such as the size distribution and the shape of the particles are fundamental in the robocasting manufacturing process. Chen et al. [4] demonstrated how a larger particle size distribution lowers the extrusion pressure due to a better packing with respect to a narrow size distribution. Furthermore, the density of the extrudates is increased. In order to evaluate those aspects and to gain knowledge of the outcome of the milling process, the powders were analyzed by mean of a scanning electron microscope (SEM)(Supra™ 40, Zeiss, Oberkochen, Germany). The shape and the dimension of the particles were assessed.

A scanning electron microscope is a very powerful investigating tool, which allows magnification up to 10^6 times, with a nanometric resolution. It is 1000 times the maximum magnification achievable with a conventional optical microscope(1000x). Instead of light as probe, as in optical microscopes, electrons are used in the SEM apparatus. Electrons can have a much shorter wavelength than photons, thus interacting with much smaller features. A SEM is based on the interaction between high energy electrons with matter. When a high energy electron, accelerated by a voltage of 1-20 kV, impacts on the surface of a material, it can produce several kinds of different electrons, with different energies and coming from different depth, according to the "ionization pear" model. The ones with the higher energy are the backscattered electrons. Those are generated through elastic scattering of the impinging electrons and have the same energy. They belong to the primary beam. Secondary electrons, instead, belong to the materials and are emitted due to the impact with an electron of the beam. Backscattered and secondary electrons can be used to obtain images of the samples. Auger electrons and X rays, also produced during the interaction between electrons and matter, can be used to perform compositional analysis.

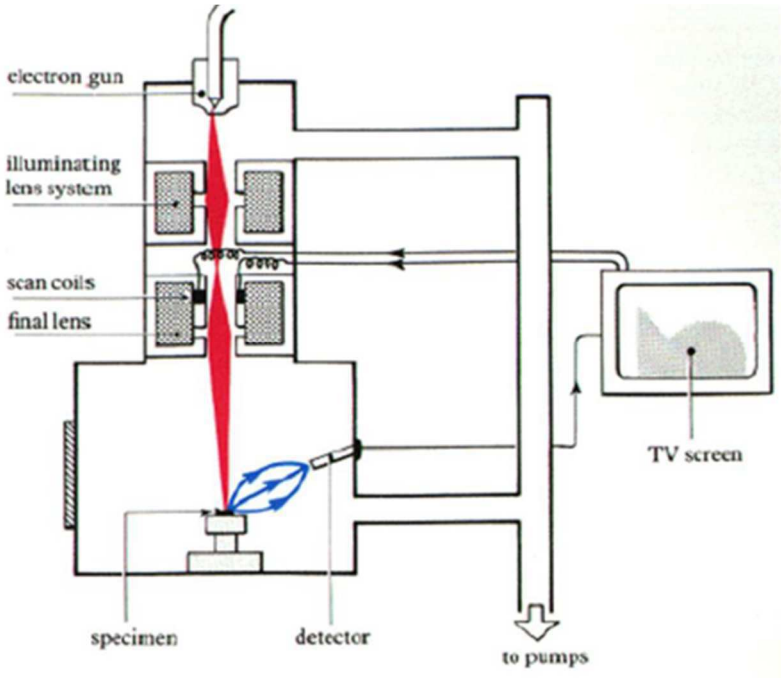

Figure 4.14 Working scheme of a scanning electron microscope [5].

A SEM apparatus can be divided in three different sections (**Figure 4.14**): the electron gun; the lens system; the sample chamber. In every section vacuum is held by pumps, with pressure ranging from 10^{-4} to 10^{-8} bars in dependence of the emitting filament used. Vacuum is needed in order to prevent damage to the electron gun and to avoid interaction between electrons and particles in the chamber, which would make impossible any kind of analysis. The electron beam is produced using mainly two effects, the thermoionic emission and the field effect:

- Thermoionic emission: the atoms are heated in order to provide their electrons with enough energy to overcome the work function and escape from the materials. Then a couple of electrodes is used to accelerate them and guide them towards the lens system. Tungsten and lanthanum exaboride are used as materials to build the tips.
- Field emission: in this case electrons are extracted from the materials using a strong electric field. The only material suitable for building tips for field emission is tungsten, because it is the only one that can withstand the strong mechanical stress. With this type of electron guns, much higher current densities are achievable, with respect to the thermoionic ones. This is an advantage when analyzing insulating materials.

The electronic beam passes through a series of electro-magnetic lenses that focus the electrons on a very small spot, down to 10 nm. Two sets of scanning coils are used to deflect the electron beam across the specimen. Thus, a raster scansion of the surface is performed and data from each point of the sample can be collected and analyzed. The sample chamber contains the sample holder with the specimen and all the detectors. For sample imaging, the most used are the backscattered electrons and the secondary ones. The formers are collected by a solid-state detector that is situated over the sample, at the end of the lens system. The latter are revealed by an Everhart-Thornley detector, which can amplify the signal. Images are build counting the number of electrons detected form each point of the specimen surface [5] [6].

4.4.1.3 Chemical composition and structure

To ensure that the process of glass preparation was carried out in the proper manner, the glass powders were analyzed to check the chemical composition and the absence of any kind of crystalline structure. Both of the analyses were performed on powders milled and sieved under 32 µm, the same used in the 3D-printing process. To do so, energy dispersive X-ray spectroscopy (EDS) was performed at the same time of the microscopy observations, since the EDS detector is embedded into the SEM. The presence of chemical elements such as silicon, potassium, magnesium, sodium, calcium and phosphorus, according to the recipe of the glass, was investigated and their concentrations were compared to the

theoretical composition of the 47.5B glass. Since oxygen was also detected, but it was overestimated due to environmental contamination, calculations were carried out to find the relative concentration without considering the oxygen.

Energy dispersive X-ray spectroscopy is a technique used for semi-quantitative chemical analysis by measuring the energy of X-ray photons. When a highly energetic electron strikes the surface of the sample, different particles are emitted. Those can be electrons, and they are used for example in SEM imaging, or it can be an X-ray photon. When a secondary electron is expelled due to a collision with an impinging one, a vacation is generated in the orbital level of the secondary electron. If there are electrons in orbitals with higher energy, one of them may jump in the less energetic orbital and release the additional energy by emitting an X-ray photon. The energy of the photons is typical of the particular atom and it can be used to univocally identify the element. During EDS analysis, a semiconductor detector measures the energy of the X-rays emitted by the sample and it counts them. The results are shown in spectra where the energy is plotted against the intensity of the signal. The energy of the photons is used to perform qualitative analysis and to detect the composition of the sample. Usually the resolution of the spectrum is about 130-155eV, lower compared to other methods of X-ray analysis (such as wavelength dispersive spectroscopy), but enough to distingue K levels of neighboring elements. Quantitative analysis can be done by counting the number of photons emitted. In this case, though, it is necessary to use corrective factors, the ZAF correction. The number of X-rays emitted from the sample is related to the number of electrons impinging on the surface, but it is affected by the nature of the element itself. The three parameters that influence the emission are:

- Z, the atomic weight: if more electrons are backscattered, less electrons can produce X-rays. The higher is Z, the more electrons are backscattered due to coulombic repulsion so less X-rays can be emitted;
- A, absorbance: X-rays mostly came from beneath the surface of the sample, so they can be absorbed by it. The absorbance of the sample can reduce the number of photons exiting the samples and it is related to the position of the detector with respect to the surface, the take-off angle;
- F, fluorescence: X-rays emitted form one elements can be absorbed by another one if they have enough energy, exciting it. That might cause the emission of X-rays from the excited elements, affecting the measurement [6].

The EDS analysis was performed during the SEM morphological investigation, since the detector for X-rays is embedded in the SEM apparatus.

The absence of crystalline domains inside the glass was assessed by means of X-ray diffraction. When X-ray photons collide on the surface of a materials, they are diffracted in every direction by the electrons belonging to each atom. If the diffracted radiation constructively interferes between each other, it is possible to detect that signal. In the field of atomic structure, this can happen if the Bragg's law conditions are satisfied. Supposing having some parallel crystalline planes, with a fixed distance, d, between each other, and an X-ray beam, wavelength λ, colliding on the surface with a certain angle θ. Some of the photons will be diffracted by the first layer, some by the second and so on (**Figure 4.15**). So, the diffracted waves have different path lengths.

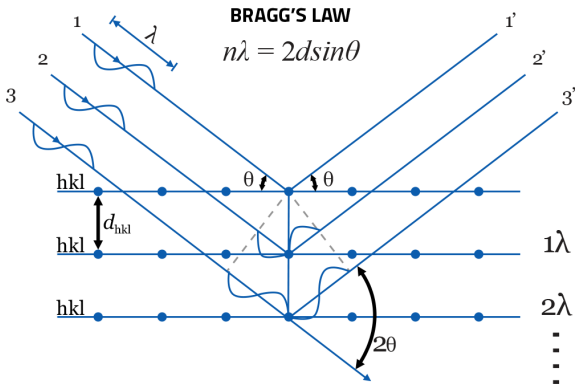

Figure 4.15 Bragg's law and diffraction of X-rays by crystalline planes [7]

Constructive interference may occur only if the difference in the length of the path between two different X-rays is a multiple of the wavelength, nλ. This condition is satisfied only for fixed value of interplanar distance and for some angle of diffraction. The mathematical correlation can be expressed by the Bragg's law:

$$n\lambda = 2dsin\theta \qquad (4.4)$$

When the law is satisfied, a strong wave is diffracted by the sample and can be detected, producing a peak in the spectrum [8]. The analysis can be performed using a diffractometer. It is composed by two moving parts, i.e. the X-ray tube, for the generation of the beam, and the detector. A scheme of the experimental set-up is shown in **Figure 4.16**. Samples are usually in form of powders, to have a random distribution of the orientation of the crystals, and are placed into a sample holder. The surface of the powders must be as flat as possible to reduce errors in the measurement. The photon beam is focused by collimators and a filter is used to obtain almost monochromatic light.

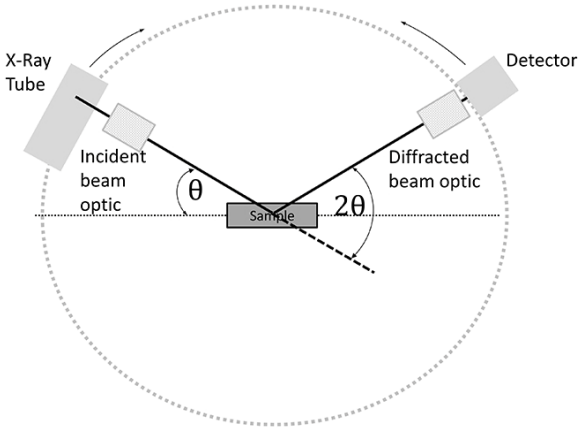

Figure 4.16 Scheme of a diffractometer [9]

The x-ray tube and the detector are moved simultaneously in order to keep the same relation between the angles. Especially the incident and the reflection angle must be equal. When the θ angle satisfies the Bragg's law, a very intense flux is detected and spectrum can be shown plotting the diffraction angle, 2θ, versus the intensity of the diffracted beam. Each series of peaks can be related to a particular chemical structure [8].

47.5B powders were analyzed by means of X-ray diffraction (X'Pert Pro PW3040/60 diffractometer PANalytical, Eindhoven, The Netherlands) varying the diffraction angle between 10 and 70 degrees.

4.4.1.4 Thermal characterization of powders

One aim of the present work is to obtain a fully amorphous porous scaffold for bone regeneration, as partial crystallization might lead to a decrease of bioactivity. Thus, having a proper knowledge of the

thermal behavior and thermal properties of the glass is fundamental, with special care to sintering and crystallization during thermal treatment.

Differential scanning calorimetry (DSC) is an analysis based on heat exchange during endothermal or exothermal transformations. The instrument is composed by two identical sample holders that can be heated separately. One holder hosts the crucible, that can be made of Pt or Al_2O_3 and contains the sample, whereas the other one supports the reference that usually is an empty crucible. The two samples are heated while the temperature is measured. If a change in temperature is detected, energy is accordingly provided to one of the two furnaces in order to maintain the thermal equilibrium between them. Whenever an endo- or exothermal phenomenon occurs, more energy is given to the sample or to the reference to keep the equilibrium. The difference of energy is plotted versus the time or the temperature in order to obtain the graph. The evaluations of glass transition, crystallization and melting processes are possible using this technique [10].

The characteristic temperatures of the glass, glass transition temperature (T_g), crystallization temperature (T_x) and melting temperature (T_m), were determined by DSC analysis performed between 40 and 1400°C (STA 449 F1 Jupiter®, Netzsch, Germany). 30±0,5 mg of glass powders, with particle dimension below 32 µm, were placed into a Pt crucible, paying attention to achieve a complete coverage of the bottom of the crucible. An empty Pt crucible was used as a reference. Both the crucibles were weighted while empty, along with the lids. Then they were covered and placed on the DSC sample holder, using a sapphire disc as spacer, in order to protect the holder. The measurement was performed using a heating rate of 10K/min and using nitrogen as protective gas. The results were analyzed using the Proteus® software provided by the instrument manufacturer.

Using the same instrument and the same processing parameters, it is also possible to evaluate the nucleation rate curve by appling the Marotta method [11]. The crystallization temperature was evaluated on samples that undergo thermal treatment at different temperature. The thermal program followed for each sample was the following:

- Heating from 40°C to the wanted temperature;
- Isothermal treatment for one hour, in order to simulate the sintering process;
- Cooling down to 200°C;
- Heating up to 1000°C while performing DSC analysis.

Measurements were performed each 10°C from 560°C, just above the glass transition, to 640°C, where high crystallization was detected.

The behavior of the glass during heat treatment, in terms of maximum shrinkage, softening and melting, was assessed by hot stage microscopy (HSM) analysis. This method involves the heating of a cylindrical sample and the acquisition of images during the thermal process. The instrument (Expert System Solution, Modena, Italy) is composed by a sample holder, where to place the sample, a furnace and a webcam that can acquire the image during the treatment. A proper software is capable of calculating the shrinkage of the materials and identifying the characteristic temperature of the materials.

For this measurement, a cylinder (approximately diameters of 2-3 mm and height about 5mm) was prepared shaping a slurry, made of 47.5B powders and ethyl alcohol, into an appropriate mold. The sample underwent heating from room temperature to 300°C at a rate of 10°C/min, acquiring one image each 10°C. Then the heating rate was lowered to 1°C /min and one picture was taken each minute, until 1400°C were reached.

4.4.2 Porous scaffolds characterization

Once the manufacturing process of the scaffolds is completed, it is necessary to perform several analyses to study the final characteristics of the structure. Those studies involve structural and morphological characterization, also at a molecular level, and the characterization of the mechanical properties, in particular the evaluation of the compressive strength.

4.4.2.1 Structure and morphological characterization

The aim of the manufacturing of scaffolds is to produce structures that can mimic the trabecular bone, in order to provide the most suitable environment for the growth of healthy bone tissue. To do so, it is important to have a complete analysis of the scaffold morphology, of the whole structure and of the

single features (e.g. line spacing, strut surface, pore characteristics). To do so it is necessary to use different techniques, also in different times of the process optimization. The evaluation of the structural features and the morphological characteristics, such as horizontal and vertical spacing between neighboring lines and their diameters, was performed by optical microscopy. Pictures of cross sections of the scaffolds along the Z axis and the X-Y plane were taken at a magnification of 50x, and then features of interest were measured using the free software ImageJ. Four different features were evaluated: the spacing between lines in regions of smaller porosity and larger porosity; the distance between two rods on the vertical direction; the diameter of the rod. All those characteristics were assessed by measuring them in several different scaffolds and in different areas of the same scaffold. Then the average dimensions were calculated. This analysis was performed also during the design optimization of the scaffolds, in order to modify the 3D-printer script to obtain the desired features.

By performing the same analysis on dried green body scaffold, it was possible to calculate the shrinkage during the sintering process. It was evaluated in different directions and regions: vertical shrinkage; horizontal shrinkage in region of smaller porosity; horizontal shrinkage in region of larger porosity.

Once the design was optimized to obtain pores of about 100 and 200µm and the printing process was consolidated, it was necessary to obtain the most complete structural characterization as possible, in order to understand the final structure of the trabeculae, the shape and the interconnection of pores and the total porosity. X-ray micro-computed tomography (micro-CT) is a powerful method that allows obtaining all those information in once. Biomaterials researches began using micro-CT recently, since 2004, and it rapidly became a well-established technique for 3D imaging of scaffolds thanks to the completeness of information provided and the advantages that a non-destructive analysis method provides [12]. Micro-CT is similar to computed tomography applied in medical uses, but it has a much lower spatial resolution, down to 1 μm^3. Basically, 3D models of the samples are reconstructed by stacking 2D cross section images. The technique consists on taking several x-ray projections of the object, while the sample is rotated by 180° or 360°. Each projection is a representation of the absorption density distribution of the object, along the X-ray beam direction. Due to the different phases and materials inside the scaffolds, the absorption of X-rays varies in the samples, generating beams of different intensity that hit the scintillator screen. Since the distance between the X-rays source, the rotational center of the sample and the screen is fixed (**Figure 4.17**), it is possible to reconstruct the exact position of each points in the specimen using the planar projection by means of an algorithm. This process is known as "tomographic image reconstruction". 2D maps are created by calculating the attenuation coefficient in spatial point and using a threshold value to denote each pixel [13]. Then a 3D modelling program can reconstruct the 3D image by stacking the pixels maps. The reconstruction shall be manually optimized by adjusting different parameters such as post-alignment, beam-hardening correction and ring artifacts correction level. Also, it is important to choose carefully the region to be analyzed, the so called "region of interest".

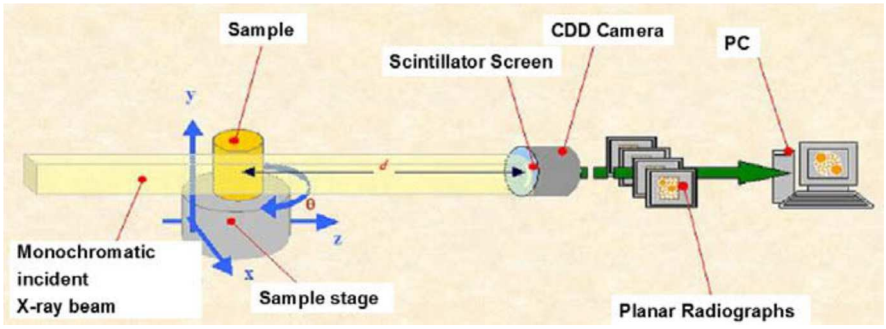

Figure 4.17 Apparatus scheme of micro-CT set-up [13]

The porosity of the scaffolds was also evaluated, for graded and monoporous types both, by the "density method". The scaffolds, thanks to their regular shape, can be approximated by a parallelepiped and their volume can be calculated as height*length*width. The dimensions of the scaffolds were measured using a caliper and then they were weighted. The porosity percentage, P% was calculated accordingly to the following equation:

$$P\% = \left(1 - \frac{M_s}{M_t}\right) * 100 \quad (4.5)$$

M_s is the actual mass of the scaffold;

M_t is the theoretical one, evaluated by multiplying the volume by the density of the glass.

Porosity was evaluated by this method for every scaffold used for mechanical properties tests.

4.4.2.2 Mechanical properties: Compression strength and Weibull modulus

Mechanical strength is important in bone substitute application, especially in load bearing sites. Scaffolds shall have strength close to the bone in order to support it during the restoration process and to allows a correct stress transfer. In this work, compressive strengths of the 47.5B-G and 47.5B-M scaffolds were calculated in order to evaluate how the different porous structure influences the mechanical properties and if the scaffolds produced by robocasting are suitable for load-bearing application. Compression test (MST Criterion, Model 43, MST, Minnesota, USA) was performed on the two different types of scaffold, with the aim to measure the compressive strength of the structures. 20 graded scaffolds and 5 monoporous ones were tested. It was chosen to test 20 graded samples in order to evaluate also the Weibull modulus.

The fracture of a fragile material is strongly affected by probability, in particular, by the probability of finding a defect of a certain dimension in a region where the stress applied is enough to provoke the catastrophic propagation of that defect, according to the Griffith theory. Due to this fact, the mechanical behavior of fragile materials, such as the glass that is used to produce bone scaffolds, cannot be described precisely, but it is necessary to use a statistical theory, known as Weibull statistic. The Weibull statistic, developed by Weibull in 1939, consists in the calculation of the survival probability of a certain number of samples that are subjected to a certain stress, for example tension, flexion or compression. The main concept is the weakest link theory: the sample is divided in little volume units that act as rings in a chain. The strength of the chain is equal to the strength of the weakest link and the failure of the link is completely independent of what happen to the others. The reliability of the whole structure is determined by the reliability of the single volume units.

Considering N samples, all made in the same way of a fragile material, and subjected to a certain stress, compression for instance, it is possible to determine the average strength, $\overline{\sigma}$:

$$\overline{\sigma} = \frac{1}{N}\sum_{i=1}^{N} \sigma_i \quad (4.6)$$

It is also possible to generate a probability distribution function of fracture, $p(\sigma)$:

$$p(\sigma) = \frac{number\ of\ fracture\ at\ \sigma}{N} \quad (4.7)$$

So, the average strength can be expressed in function of the probability distribution, combining the 4.5 and the 4.6 equation and obtaining:

$$\overline{\sigma} = \sum_{i=1}^{N} \sigma_i p(\sigma_i) \quad (4.8)$$

The typical distribution of the strength value for brittle materials is narrow and asymmetrical, very different from the curve associated with a ductile material (**Figure 4.18**).

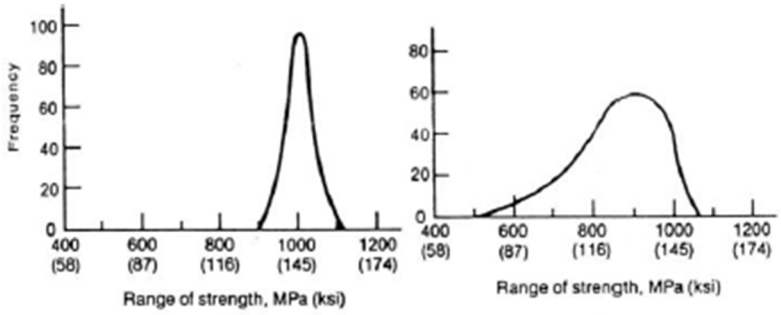

Figure 4.18 Strength distribution of a ductile material, metal, (left) and of a fragile material, ceramic, (right) [111]

It is possible to express the survival probability, P_s, as the product of the survival probabilities of the N volume units. Considering an infinite number of units, with an infinitesimal volume, the Weibull distribution function can also be expressed as:

$$P_s = e^{-\int_V \varphi(\sigma) dV} \qquad (4.9)$$

The function φ(σ) is dependent on the value of the applied stress:

$$\varphi(\sigma) = \begin{cases} \frac{1}{V_0}\left(\frac{\sigma - \sigma_u}{\sigma_0}\right)^m & \sigma > \sigma_u \\ 0 & \sigma \leq \sigma_u \end{cases} \qquad (4.10)$$

where m, σ_u, σ_0 are the Weibull parameters. σ_u is the minimum stress under which the probability of failure is nil. Usually for ceramic materials its value is considered 0. σ_0 is the tension at which the survival probability is equal to 36,8%. m is the Weibull modulus, it indicates how much the experimental fracture stress values are close to the average one. The higher m is, the narrower the distribution is, as shown in **Figure 4.19** [111].

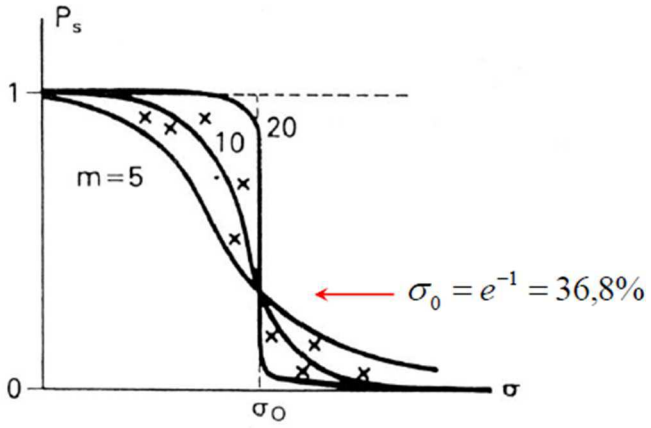

Figure 4.19 Effects of the Weibull modulus on the survival probability [111]

The Weibull modulus can be used as an index of the repeatability and reliability of a manufacturing process, since it is strictly dependent on the defects size and distribution. A well-established process shall produce devices with the same defects presence and distribution, so a high value of m. In order to estimate the repeatability of the printing process, in particular of the ink making phase, the Weibull modulus was calculated testing, 20 graded scaffolds subjected to compressive loads. Only one type of scaffolds was tested because the design of the scaffold has no influence on the defect distribution, which is mainly caused by the presence of air bubbles inside the ink.

The Weibull modulus was calculated by fitting the experimental data using the following equation [15]:

$$\ln\left(\ln\left(\frac{1}{1-P_f}\right)\right) = m\ln\left(\frac{\sigma}{\sigma_0}\right) = m\ln(\sigma) - m\ln(\sigma_0) \quad (4.11)$$

where $P_f(\sigma)$ is the probability of failure, calculated as $(1\text{-}j)/n$. n is the total number of the sample and j is the specimen rank in ascending order of failure. m is the Weibull modulus and σ_0 is the scale factor.

4.4.3 *In vitro* bioactivity evaluation

The preliminary evaluation of the bioactivity of the 47.5B glass scaffolds, in terms of hydroxyapatite (HA) formation and ionic release in vitro, was carried on using the testing procedure proposed by Macont et al. [16]. The experimental procedure involves the immersion of the samples in simulated body fluid (SBF) [17] for a certain amount of time. The mass of the sample and the volume of the solutions are kept at a constant ratio of 150mg/100ml (1.5 mg/ml) and the specimen were placed into an orbital shaker incubator (Multitron AJ 118 g, Infors, Bottmingen, Switzerland), at 37°C and at a speed of 100rpm. After a defined immersion time, the solution is analyzed by means of inductively coupled plasma optical emission spectroscopy (ICP-OES) (5110 ICP-OES, Agilent Technologies) in order to evaluate the concentration of ions in solution and the possible precipitation of HA.

ICP-OES relies on the emission of photons by excited atoms to perform quantitative and qualitative analysis. The instrument is composed by two different parts: the ICP torch, where plasma is produced and elements ionized, and the optical spectrometer, where the light emission is analyzed. The plasma is produced by using a radio frequency (RF) signal, with high power and high frequency, that can ionize argon gas that is used to sustain the torch. Usually the torch is made of three concentric silica tubes and a copper coil, connected with the RF generator. In this condition an annular plasma is generated, with temperature ranging from 10000 to 5800 K. The samples, usually in the liquid state, are withdrawn and nebulized, in order to create an aerosol. A stripper gas, for example Ar, is used to make the aerosol flow through the inner tube of the torch, so the sample have to pass in the center of the plasma. Here the droplets are immediately separated from the solvent, vaporized and atomized. Then atoms and ions are excited and photons are emitted. In order to detect different kinds of atoms with the ICP-OES, it is necessary to obtain a high level of optical resolution to separate the different emissions, a bandpass of 0,01 nm at least. This can be achieved by using a plane grating monochromator, for example. It consists of a series of ruled lines on a reflecting surface. When a polychromatic light beam impinges on the surface, a spatial dispersion of the different wavelengths is accomplished, as shown in **Figure 4.20**.

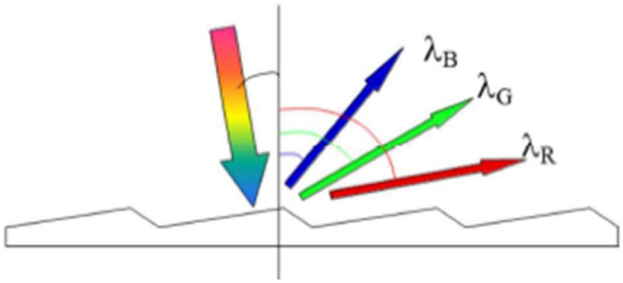

Figure 4.20 Spatial dispersion of a polychromatic beam using a plane grating monochromator [5]

Photomultipliers or charge coupled device (CCD) are used to detect the monochromatic beam, obtained from the grating, and to calculate the intensity of the beam itself. The use of an ICP offer several advantages with respect to others analytical technique. For example, the extremely high temperature allows to ionize a wide range of elements, it is possible to detect over 70 elements at time and it has a low detection limits (0,1-100ng/mL) [18].

In order to evaluate the dissolution of the 47.5B glass scaffolds and if the different porosity design affects in some ways the precipitation of HA, immersion tests were carried on using 47.5B-G and 47.5B-M scaffolds both. For the experiment, three samples of each type were prepared by reducing their masses to approximately 150 mg. The scaffolds were machined using a scalpel and manually polished, using ethyl alcohol to wet the polishing paper. It was not possible to use a polishing machine, since the surface

of the bioactive glass would have reacted with the water used to wet the polishing paper. The same amount of glass was removed from each side of every scaffolds, trying to obtain a final structure as square and symmetric as possible. Then they were placed in a 150ml polyethylene bottle with flat bottom and around 100 ml of SBF solution were added (**Figure 4.21**). The amount of SBF was calculated in order to maintain the ratio between glass mass and SBF volume equal to 150mg/100ml. The bottles were then placed into an orbital shaker incubator. At each time point, 1ml of solution was withdrawn from each bottle and put into a 10ml tube, previously filled with 9ml of ultra-pure 1M nitric acid. The tubes were collected and stored in fridge at 4°C until the analysis. The time points chosen for the analysis are: 6 h, 24 h, 48 h, 72 h, 1 w and 2 w. The volume of SBF was restored again using 1 ml of pure SBF, prepared at the beginning of the immersion test and stored into a volumetric flask at 37°C. A bottle of 100 ml of pure SBF was prepared and analyzed in the same way of the scaffold specimens in order to control the stability of the SBF. The pH of each sample was also measured at each time points (Orion Star A111 pHmeter, Thermo scientific).

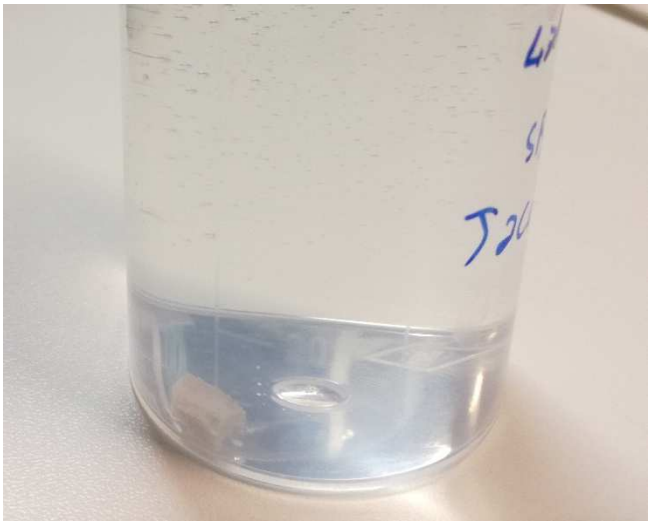

Figure 4.21 47.5B-G scaffold in SBF solution for immersion test

The SBF solution was prepared following the protocol indicated by Kokubo et al, [17]. In order to have enough SBF for filling the plastic bottles and to have solution for restore the volume during the immersion test, 2 L of solution were prepared. A volumetric flask (2000 ml) was prepared by washing it three times with distilled and ion-exchanged water, then once with nitric acid and three times again with distilled and ion-exchanged water. Then it was filled by three quarters with distilled and ion-exchanged water and put in incubator at 37°C.

Table 4.6 Reactants used in the preparation of SBF solution, with the mass necessary for 2L and the manufacturers of the chemicals products

Reactant	**Mass (g)**	**Manufacturers**
NaCl	15.992	VWR chemicals
$NaHCO_3$	0.700	VWR chemicals
KCl	0.448	VWR chemicals
$K_2HPO_4*3H_2O$	0.456	VWR chemicals
$MgCl_2*6\ H_2O$	0.610	VWR chemicals
HCl 1M (*aq*)	80	VWR chemicals
$CaCl_2*2\ H_2O$	0.736	VWR chemicals
Na_2SO_4	0.142	Riedel-de Haen
Tris(hydroxymethyl)aminomethane (Tris base)	12.144	Sigma Haldrich

All the reactants were weighted (AB265-S/FACT scale, Meter Toledo) and inserted one at time in the volumetric flask, in the exact order as in **Table 4.6**. The volumetric flask was heated and mixed vigorously using a magnetic stirrer during the whole process. Only about 90% of HCl was added, the

remaining was used after to adjust the pH. The chemicals were added very carefully, leaving the solution mixing for some minutes after pouring one reactant in order to accomplish complete dissolution before adding the next one. All the grains and powders that stitched on the walls of the flask were cleaned by spraying distilled and ion-exchanged water. It is necessary to be extremely cautious when adding the reactants after the hydrochloric acid to avoid precipitation. When all the reactants were dissolved, the solution was left stirring for 20 minutes. The temperature of the solution was raised to 37°C and the pH was adjusted to 7.40 by adding the remaining HCl very carefully with a Pasteur pipette, drop by drop. Once the pH was at the right value, the total volume of the solution was raised to 2L by adding distilled and ion-exchanged water. The solution was stored in the volumetric flask, sealed with parafilm, at 37°C, in incubator.

The growth of HA on the scaffold surface and its stoichiometry were also assessed by XRD (**Figure 4.22**), performed on the whole scaffold, and by SEM+EDS analysis. One more sample for each time points and for each scaffold type was prepared and treated in the same way of the ones used for the immersion tests. At the chosen time point the scaffold was removed from the SBF, washed with ethanol and dried. Then XRD and SEM+EDS analysis were performed.

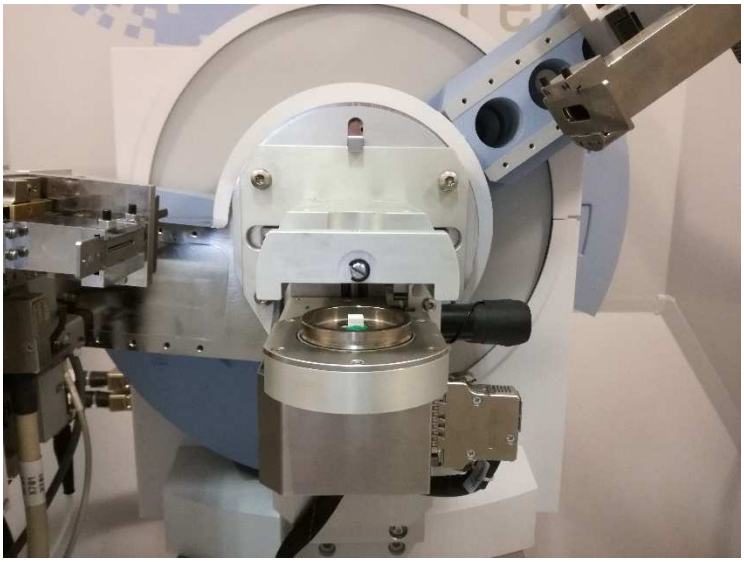

Figure 4.22 Diffractometer used for the XRD analysis

The variation of mechanical properties during the application time was also evaluated. In fact, it is important to know if the scaffold can sustain and support in a proper manner the bone during all the healing processes. 5 scaffolds for each porosity design were soaked into SBF, using the same previous protocol, for 2 and 4 weeks. Then their compressive strength was tested. For this test the scaffolds were not machined to lower their weight to 150 mg in order to not introduce defects that can affect the mechanical properties. Anyway, the mass (mg) -to-SBF volume (ml) ratio was maintained of 1.5.

4.5 Bibliography

[1] E. Verné, O. Bretcanu, C. Balagna, C. Bianchi, M. Cannas, S. Gatti and Vi, "Early stage reactivity and in vitro behavior of silica-based bioactive glasses and glass-ceramics," *Journal of Material Science: Materials in Medicine,* vol. 20, pp. 75-87, 2008.

[2] "nScrypt," [Online]. Available: https://www.nscrypt.com/3d-series-equipment/tabletop/. [Accessed 03 12 2017].

[3] A. Nommeots-Nomm, P. Lee and J. Jones, "Direct ink writing of highly bioactive glasses," *Journal of the European Ceramic Society,* 2017.

[4] Z. Chen, K. Ikeda, T. Murakami and T. Takeda, "Effect of particle packing on extrusion behavior of pastes," *Journal of Material Science,* vol. 35, pp. 5301-5307, 2000.

[5] F. Giorgis, *Materials for MEMS and charcterization of technological processes,* Politecnico di Torino, a.y. 2016/2017.

[6] M. Pavese, *Scienza e tecnologia dei materiali funzionali,* Politecnico di Torino, a.y. 2014/2015.

[7] Veqter, "X-ray diffraction," [Online]. Available: http://www.veqter.co.uk/residual-stress-measurement/x-ray-diffraction.

[8] W. Callister, Materials science and enginnering- an introduction, 5th ed., Wiley, 2000.

[9] A. L. Library, "X-ray powder diffracatometry," [Online]. Available: http://lipidlibrary.aocs.org/Biochemistry/content.cfm?ItemNumber=40299.

[10] M. Sangermano, *Scienza e teconologia dei materiali polimerici,* Politecnico di Torino, a.y. 2014/2015.

[11] M. Davis and I. Mitra, "Crystallization measurements using DTA methods: applications to Zerodur," *Journal of the American Ceramic Society,* vol. 86, pp. 1540-1546, 2003.

[12] S. Bertoldi, S. Farè and M. Tanzi, "Assessment of scaffold porosity: the new route fo micro-CT," *Journal of applied Biomaterials and Biomechanics,* vol. 9, pp. 165-175, 2011.

[13] C. Renghini, V. Komlev, F. V. E. Fiori, F. Baino and C. Vitale-Brovarone, "Micro.-CT studies on 3-D bioactive glass-ceramic scaffolds for bone regeneration," *Acta Biomaterialia,* vol. 5, pp. 1328-1337, 2009.

[14] P. Fino, *Scienze e tecnologie dei materiali ceramici,* Politecnico di Torino, 2014/2015.

[15] F. Baino and C. Vitale-Brovarone, "Mechanical properties and reliability of glass-ceramic foam scaffolds for bone repair," *Materials Letters,* vol. 118, pp. 27-30, 2014.

[16] A. Macon, T. Kim, E. Valliant, K. Goetschius, R. Brow, D. Day, A. Hoppe, A. Boccaccini, I. Kim, C. Ohtsuki, T. Kokubo, A. Osaka, M. Vallet-Regì, D. Arcos, L. Fraile, A. Salinas, A. Teixeira, Y. Vueva, R. Almeida, M. Miola, C. Vitale-Brovarone, E. Verné, W. Holand and J. Jones, "A unified in vitro evaluation for apatite-forming ability of bioactive glasses and their variants," *Journal of Materials Science: Materials in Medicine,* vol. 26, p. 115, 2015.

[17] T. Kokubo, H. Kushitani, S. Sakk, T. Kitsugi and T. Yamamuro, "Solutions able to reproduce in vivo surface-structure changes in bioactive glass-ceramic A-W," *Journal of Biomedical Materials Research,* vol. 24, pp. 721-734, 1990.

[18] X. Hou and B. Jones, "Inductively coupled plasma/optical emission spectrometry," in *Encyclopedia of analytical chemistry*, R.A. Meyers, 2000, pp. 9468-9485.

5 Results and discussion

5.1 Introduction

In this chapter, all the results collected during the development of the present thesis are reported and discussed. These include the characterization of the 47.5B glass powders, the presentation of the optimized manufacturing process and all the analyses performed on the scaffolds obtained thereof.

5.2 Glass powder characterization

In order to evaluate the outcome of the fabrication process of 47.5B glass powders, described in section 4.3.1, SEM micrograph and EDS compositional analysis were carried out. For the correct optimization of the sintering process, also the thermal properties and behavior of the powders were investigated.

5.2.1 Morphological evaluation

For obtaining a good ink to be used in robocasting, it is suitable to have a wide particle size distribution of the powders. This will ensure a better particle packing within the nozzle during the extrusion, thus ensuring a better flowability and homogeneity of the ink [1]. A qualitative investigation of the particle shape and size distribution was performed through SEM imaging.

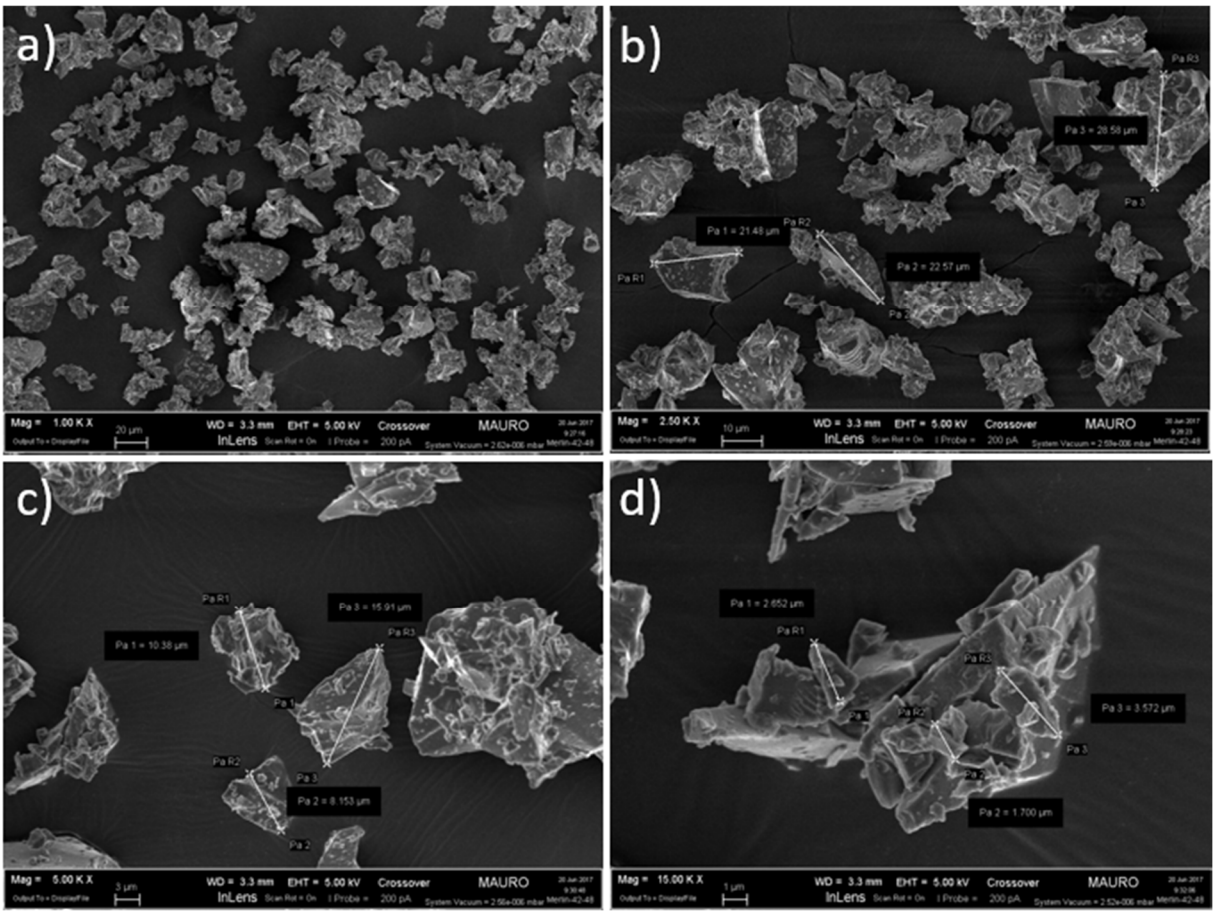

Figure 5.1 SEM micrographs of 47.5B powders sieved under 32 µm at different magnification: a) 1000x; b) 2500x; c) 5000x; d) 15000x

In **Figure 5.1 a**, it is possible to appreciate that there is a large distribution size, with particle that are roughly equiaxial with quite sharp edges. An evaluation of particle size was performed and it was noticed that glass particles have sizes ranging from about 30 to less than 10 µm (**Figure 5.1 b, c**). At higher magnification (**Figure 5.1 d**), very small particulate (size below 1 µm) was seen adhered on the surface of bigger particles.

SEM imaging has proven that to produce glass powders by milling a glass frit is a suitable method to obtain raw materials for the making of ink that can be applied for robocasting manufacturing.

5.2.2 Compositional assessment

In order to assess the final composition of the powders, EDS analysis was performed along with SEM observation. To have valid statistical data, three different areas of the powder sample were analyzed and the presence, measured by weight percentage, of O, Na, Mg, Si, P, K and Ca was investigated. The measurement of the oxygen concentration usually is affected by errors, so it was not reported. The results, average wt% and standard deviation, compared to the theoretical values are shown in **Table 5.1Errore. L'origine riferimento non è stata trovata.**.

Table 5.1 Glass powder composition (wt%) compared with theoretical values

Element	**Measured Wt%**	**Standard deviation**	**Theoretical Wt%**
Na	10.08111	0.621782	12.1789
Mg	6.188725	0.651389	6.4378
Si	34.32914	0.949408	35.3362
P	4.071565	0.237615	4.1021
K	24.1952	0.607706	20.7124
Ca	21.13427	1.701514	21.2325

Experimental average values are in good agreement with the nominal ones. Low standard deviations confirm the compositional homogeneity of the melt-derived material.

Thanks to the elaboration of the data, EDS compositional analysis showed how melting raw materials is a good technique to obtain precise glass compositions.

Structural assessment of these powders was performed by XRD. As expected, no peaks appeared within the diffraction spectrum but the amorphous halo, centered about 30°, can be see and it is typical of silicate glasses (**Figure 5.2**).

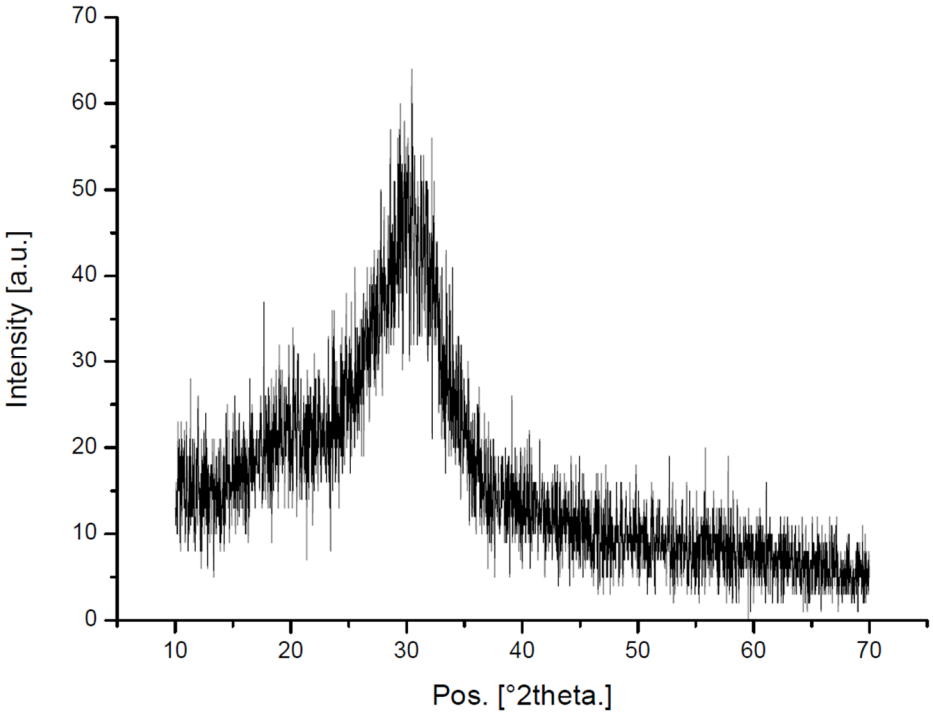

Figure 5.2 XRD spectrum of 47.5B glass powders (φ<32μm)

5.2.3 Glass density

The evaluation of the density of the 47.5B glass is important to achieve a complete characterization of the material, and it is mandatory for the preparation of the ink used during the 3D-printing process. In fact, the ink is based on a precise volume ratio between glass powder and polymeric binder. As described in paragraph 4.4.1.1, Archimedes' principle was used.

The glass chuck was weighted in water and air both, then the density was evaluated by using the equation 4.3 reported in section 4.4.1.1. The density value measured is: ρ_g=2.640±0.002 g/cm^3.

5.2.4 Thermal characterization

To manufacture a fully amorphous glass scaffolds, it is necessary to have a complete knowledge of the thermal behavior of the bioactive glass. A good fabrication method shall be able to treat thermally the green scaffolds achieving enough sintering of the glass particles but avoiding crystallization of them. In fact, devitrification shall be eliminated since crystalline phases are less bioactive than amorphous ones, and the HA form slower on their surfaces [2]. Different thermal analyses were used and merged in order to obtain a characterization as much complete as possible. DSC, HSM and XRD were used for this purpose.

5.2.4.1 Differential scanning calorimetry

The first step that is necessary to understand the thermal behavior of any kind of glass is to determine its characteristic temperatures. These are the glass transition temperature, the crystallization onset and the crystallization peak temperature. They are very important because their difference, that is known as workability window, is the key for obtaining a well sintered product while maintaining low the crystalline phase or, even better, for avoiding it to form at all. It is also interesting to evaluate the melting temperature of the glass.

The measure was performed by heating the powders at a rate of 10 K/min, between 40 and 1400°C, using nitrogen as protective gas, in order to avoid oxidization reactions during the measure. Analyzing the so obtained curve, shown in **Figure 5.3**, it was possible to evaluate the characteristic temperatures of the 47.5B glass:

- Glass transition temperature, T_g: during the glass transition, there is a change in the specific heat of the material. This will result into a step that can be seen in the DSC graph. The glass transition temperature can be defined as the inflection point of the step. The T_g of 47.5B glass is equal to 547°C;
- Crystallization onset temperature, T_x: it is the starting point of the devitrification process. T_x can be find by drawing the tangential liens to the first part of the crystallization peak and to the curve baseline. The temperature corresponding to the intersection of the two lines is the onset of crystallization. T_x was assessed to be 760°C.
- Crystallization peak temperature, T_c: devitrification is an exothermal process, which is represented as a well-defined peak in the DSC analysis. The T_c is the temperature corresponding to the maximum of the crystallization peak, which is also the point of highest crystallization speed. For this glass, T_c is at 806°C;
- Melting temperature, T_m: in reverse with respect to the crystallization, melting is an endothermal process, so it is represented as a valley within the curve. The melting temperature is the temperature corresponding to the minimum of this valley. In this case, T_m is assessed as 1004°C.

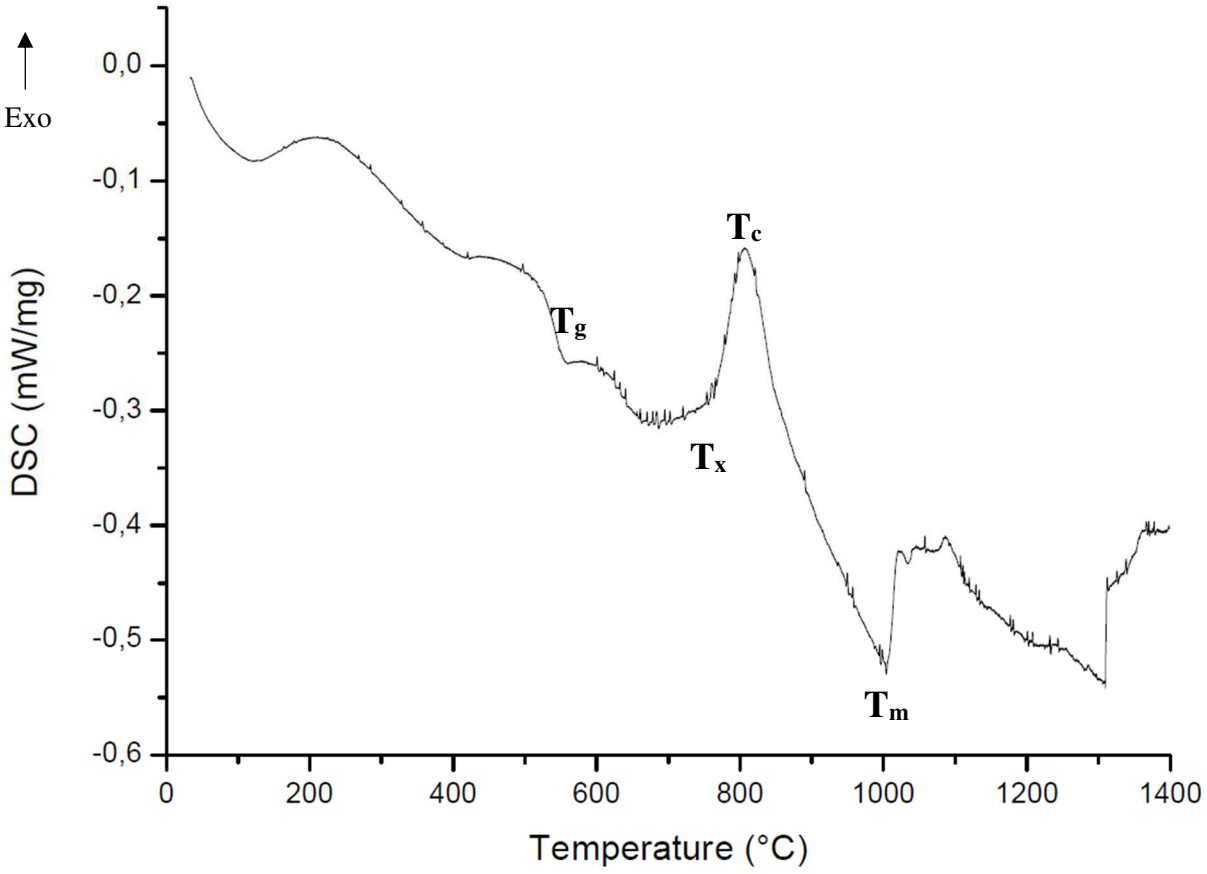

Figure 5.3 DSC analysis of 47.5B glass powders (φ<32 µm) with characteristic temperatures

The glass presents a good workability window, since the difference between the glass transition temperature and the crystallization peak temperature is more than 250°C. Thus, it shall be possible to obtain a good sintering while, at the same time, avoiding the devitrification. The characteristic temperatures are collected in **Table 5.2**

Table 5.2 Characteristic temperature of 47.5B bioactive glass

Glass transition (T_g)	**Crystallization onset (T_x)**	**Crystallization peak (T_c)**	**Melting (T_m)**
547°C	760°C	806°C	1004°C

The results obtained are comparable to those shown by Verné et al, [3]. Verné et collaborators characterized also the crystalline phases formed during heating that is a complex crystal formed by silicon, calcium and sodium ($Na_2CaSi_3O_8$)

5.2.4.2 Hot stage microscope

More information about the shrinkage behavior of the material and its viscous flow transformation during heating can be achieved through hot stage microscope. In particular, it is possible to correlate temperature of the glass to points with fixed viscosity: first shrinkage (T_{FS}); maximum shrinkage (T_{MS}); softening (T_S); ball (T_B); half ball (T_{HB}); flow point, and melting (T_F) [4]. HSM is a complementary technique to the DSC,

During the measurement, the instrument dedicated software builds the shrinkage curve and recognizes the fixed viscosity points from imaging analyses (**Figure 5.4**).

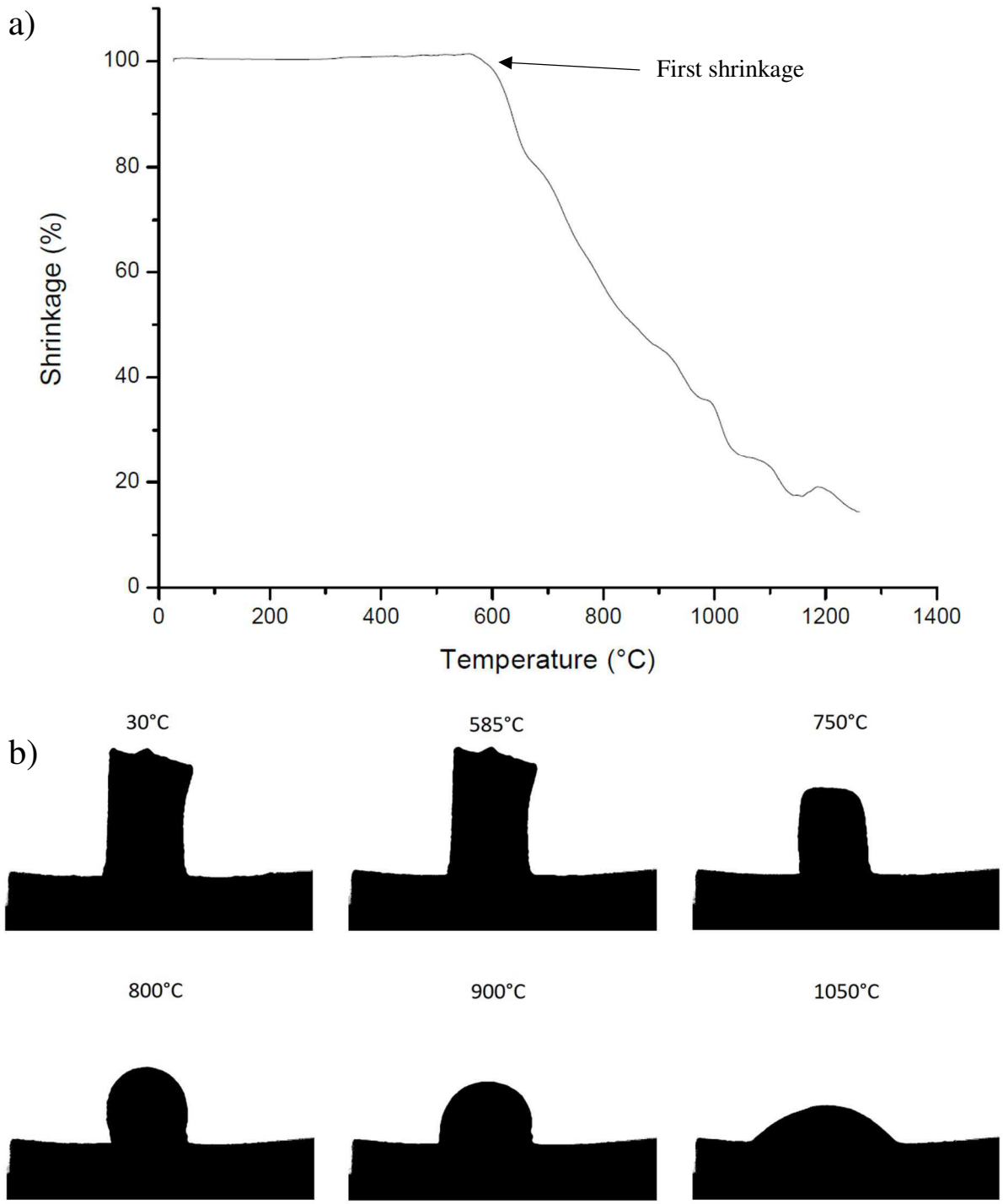

Figure 5.4 a) HSM curve; b) pictures of the glass cylinder at characteristics points, from lower to higher temperature: room temperature; first shrinkage; softening; ball; half-ball; flow point, melting.

From the curve analysis (**Figure 5.4 a**), it is possible to identify the first shrinkage, corresponding to the end of the steady linear stretch, but there is no plateau that indicates the maximum shrinkage and that precedes the melting of the sample. This peculiar behavior can be related to a slow crystallization kinetic with respect to the heating ramp used for the measure (1°C/min), even if it is quite low. The maximum shrinkage is reached when the crystallization level is high enough to stop the viscous flow [5]. If the devitrification kinetic is very slow, it is possible that the crystals formed into the amorphous matrix are to less to stop the viscous flow of the glass, that increases with the temperature. Therefore, the point of maximum shrinkage is not visible. A second hypothesis may be that the elimination of the maximum shrinkage plateau is due to the large dimensional distribution. Much smaller particles have a different

behavior during the heating and they flow at lower temperature than the bigger ones, causing continuous shrinkage of the material.

However, it is still possible to identify the fixed-viscosity points of the glass by imaging analysis through a dedicate software. The software analyzes the shape of the cylinder during the heating and recognizes the characteristic temperature, as shown in **Figure 5.4 b**. The fixed-viscosity points and characteristic temperatures are listed in **Table 5.3**.

Table 5.3 Fixed-viscosity points and characteristic temperatures of 47.5B glass

Fixed viscous points	Temperature
First shrinkage	585°C
Softening	750°C
Ball	800°C
Half ball	900°C
Flow point	1050°C

Since DSC and HSM are complementary technique, it is useful to compare and discuss together the results obtained by these analyses (**Figure 5.5**).

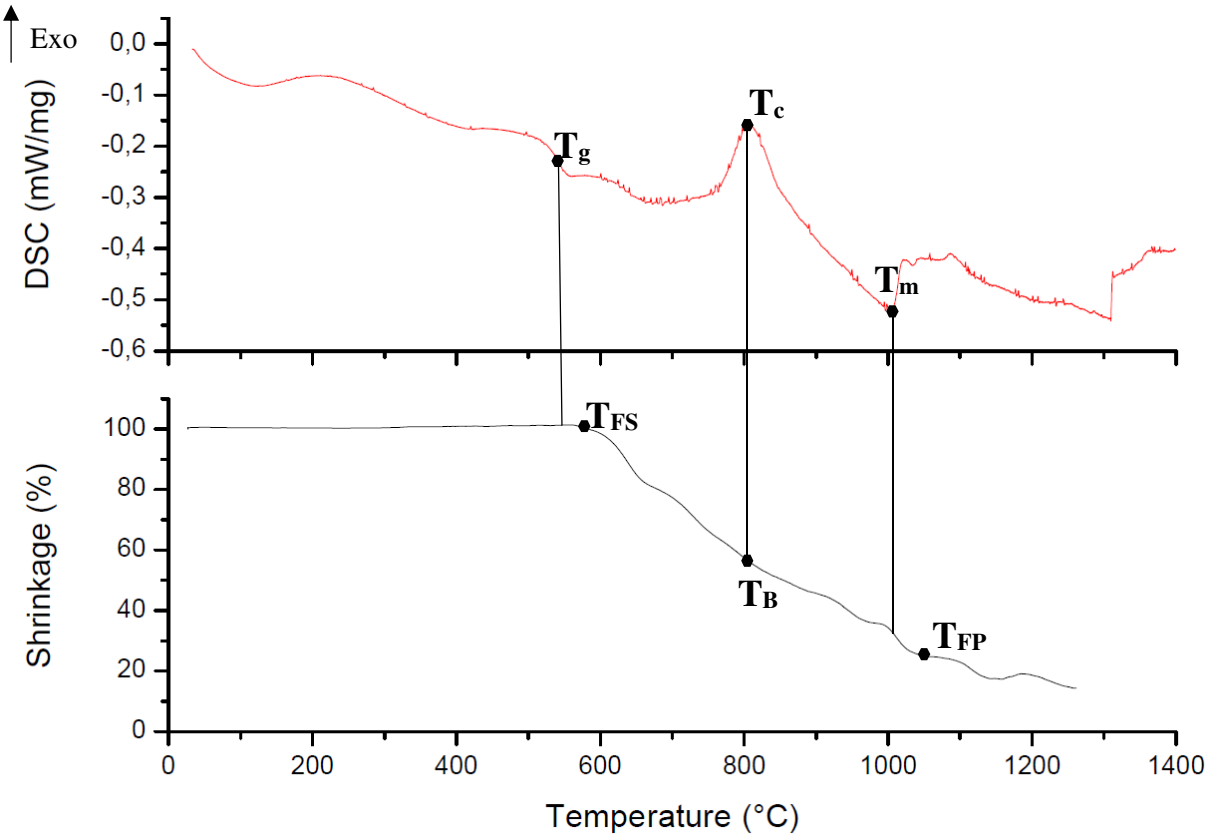

Figure 5.5 Comparison between DSC (up) and HSM (bottom) curves. The characteristic temperatures are highlighted

As expected, the first shrinkage is a slightly higher temperature than the glass transition, since it is necessary that viscous flow processes are activated for the shrinkage to happen. The ball temperature happens at the same point of the crystallization peak. Usually the T_c corresponds to the maximum shrinkage, but, as explained before, when the devitrification rate is too slow viscous flows might continue during all the measurement, hiding the plateau. Anyway, it is possible to speculate that the maximum shrinkage is reached somewhere between T_{FS} and T_B. T_{FP} matches the melting temperature measured by DSC, the difference is due to the method that the HSM uses to identify the flow point, related with the contact angle.

All that information is very useful for designing the sintering treatment to be used within the scaffold manufacturing process. During the sintering it is necessary that the glass powders undergo enough viscous flow to consolidate the structure, but the temperature shall be low enough to avoid the destruction of the object shape. So, a possible sintering temperature might be in the range between T_g (547°C) and T_S (750°C). Temperature under T_{FS} are included because sintering involves holding high temperature for long amount of time, i.e. 1 hour, and viscous flows have more time to take place than during the HSM measurement.

5.2.4.3 Crystallization evaluation

One of the main aim of the present work was the achievement of a complete amorphous scaffolds, in order to maintain intact the bioactive properties of the 47.5B bioactive glass. Therefore, it was necessary to study the crystallization behavior of the glass, simulating the sintering process. In order to decrease the number of variable parameters, the holding time at the sintering temperature was fixed to 1 hour. Then, using the DSC instrument, powders were treated at the following temperatures: 560°C, 570°C, 580°C, 590°C, 600°C, 610°C, 620°C, 630°C, 640°C. The lower temperature, 560°C, was chosen above the T_g, as the minimum temperature to have sintering, then the temperature was increased until strong crystallization was detected.

From the DSC curves obtained analyzing the treated powders, shown in **Figure 5.6**, it was possible to notice that, in this range of temperature, there is no effect on the glass transition temperature, which remains constant at 547°C.

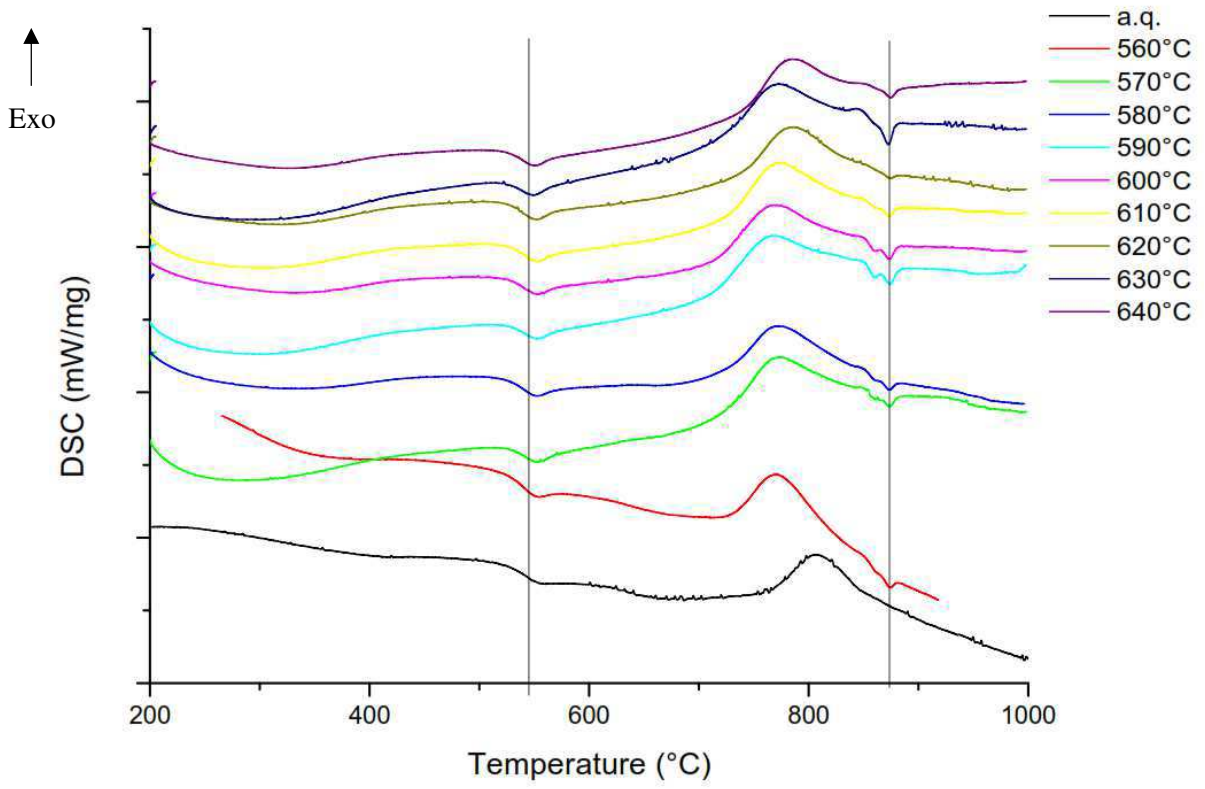

Figure 5.6 DSC analysis of 47.5B glass powders after 1-hour temperature hold at increasing temperatures, from 560°C to 640°C. DSC of powders as quenched (a.q.) is shown for comparison. Black lines highlight the T_g (547°C) and the T_m (875°C) of the new formed phase.

Even after the treatment at the lowest temperature, 560°C, it is possible to notice the formation of an endothermic peak at 875°C. This is proof of the formation of a new low-melting phase that separates into the glass during the heat treatment, which has a melting temperature of 875°C. The peak becomes more pronounced at higher temperature, signifying that higher amount of material crystallized with increased temperature.

The extent of crystallization can be assessed by measuring the areas underneath the crystallization peak. Littler areas indicate that during the previously-applied thermal treatment a bigger portion of the glass underwent devitrification. The analysis was performed using the Proteus software and the results are listed in **Table 5.4**.

Table 5.4 Crystallization peak areas evaluated after 1-hour thermal treatment at different temperatures

Treatment temperature (°C)	**T_c (°C)**	**Peak area (J/g)**
560	771.4	65.25
570	773.6	68.65
580	773.3	65.17
590	769.2	63.45
600	767.4	65.36
610	776	67.49
620	784.8	68.86
630	77.28	62
640	784.8	50.66

The area underneath the crystallization peak is constant for most of the temperatures investigated. A strong decrease is shown only at the higher temperature, at 640°C. This fact indicates that a certain extent of crystallization is happening.

The sequential DSC analyses on thermally treated glasses is also useful to gain qualitative information about the nucleation rate of crystals within the glass network. Davis et al. [117], demonstrated how the Marotta method can be applied to obtain a curve that is proportional to the nucleation rate. If during a thermal treatment some nucleation takes place inside the glass, the crystallization peak, evaluated by a DSC scan, shall be shifted leftward with respect to the peak of untreated material. This shift becomes greater while approaching the temperature corresponding to the maximum nucleation speed and, once it is reached and overtaken, the peak starts to return back. So, it is possible to create a nucleation rate-like curve by plotting $[(1/T_c-1/T_c^0)]$ vs holding temperatures, where T_c is the peak temperature after hold and T_c^0 is the peak temperature of the untreated glass. The crystallization peak temperatures are shown in **Table 5.4**.

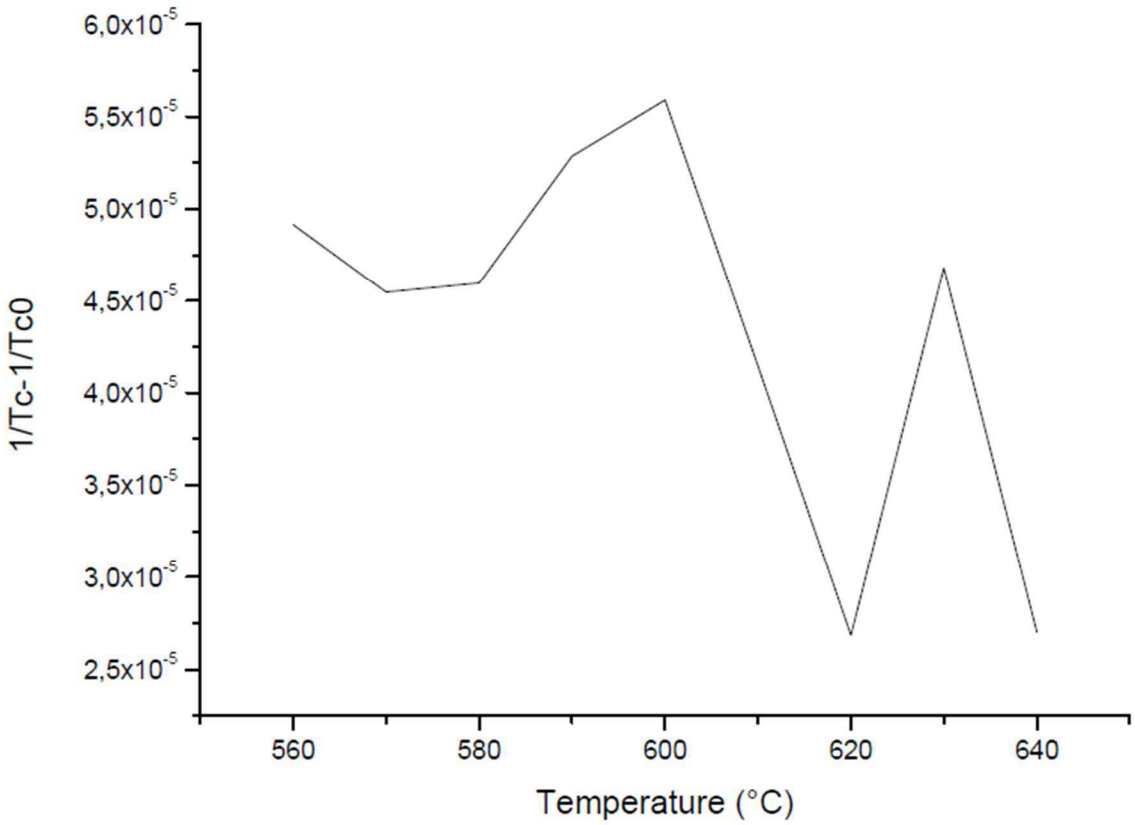

Figure 5.7 Nucleation rate-like curve obtained applying the Marotta method to 47.5B glass powders

Figure 5.7 shows the curve obtained by application of the Marotta method. The maximum speed of nucleation, which correspond to the highest point of the curve, can be assessed at 600°C. The irregularity in the curve, corresponding to the thermal treatments performed at 620°C and 630°C, is due to experimental error during the measure. Anyways, it is clear the descending trend of the curve after the treatment at 600°C.

At the same time, while DSC sequential analyses were performed, some sintering trials were carried out using 3D-printed scaffolds for investigating the debinding process. The sintering temperatures used were 560, 580, 600, 620, 630 °C. To evaluate if some crystallization tokes place, XRD analyses were performed on powders obtained by manually grinding the scaffolds. The diffraction spectra are shown in **Figure 5.8**.

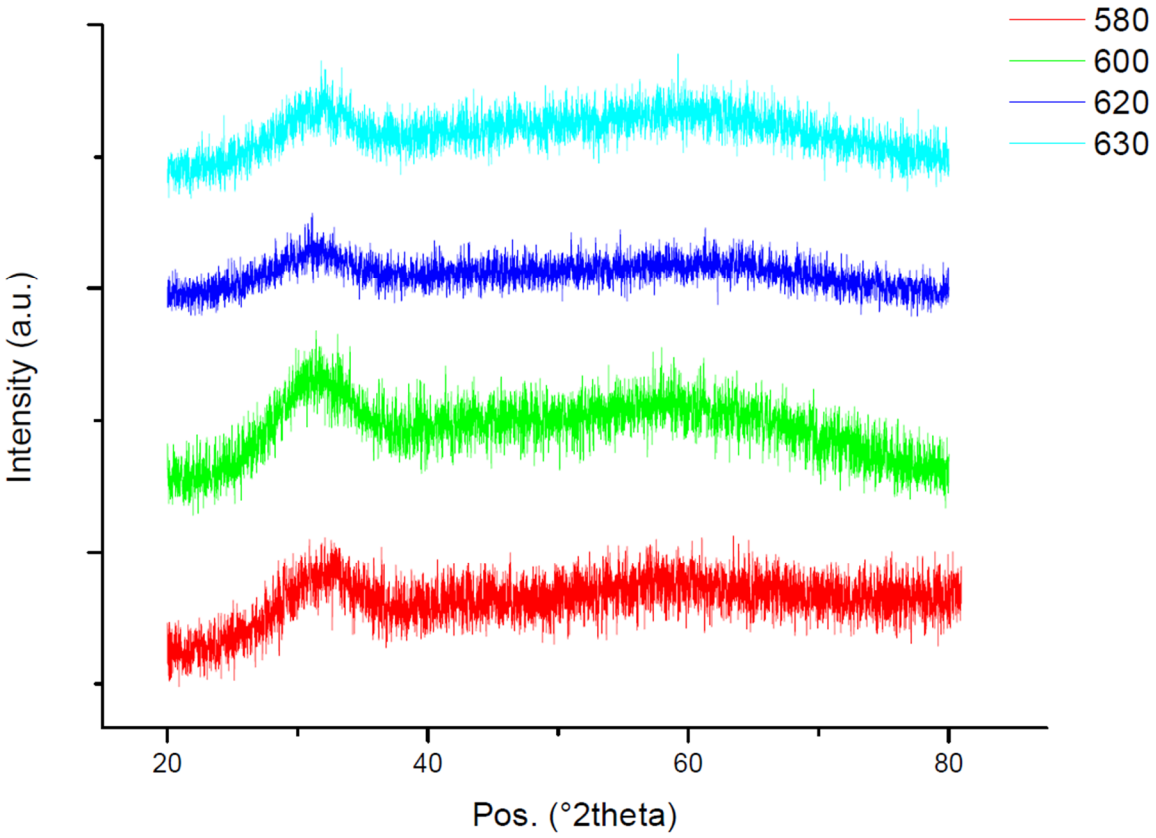

Figure 5.8 XRD performed on 47.5B glass powders obtained by grinding scaffolds sintered at different temperatures

As it is possible to see, there is no sign of crystallization peaks in anyone of the spectra while the amorphous halo is clearly visible. Anyway, it is possible that some crystallization happened on the surface of the scaffolds, especially at 630°C or even at 620°C, but the signal might be lost because of the grinding. If there is a very small amount of crystalline phase formed on the surface, when the scaffolds were grinded, the high amount of amorphous powders coming from the inside of the struts can hide the crystal-related signals during the measurement.

All the information obtained through the thermal characterization of glass powders can be merged and are very useful to determine the optimal temperature for the sintering process. Considering the following facts:

- First shrinkage at 585°C;
- Highest nucleation rate at 600°C;
- Detection of no crystalline phases up to 630°C by XRD

It was decided to sinter the scaffolds through a 1-hour temperature hold at 600°C. This is a conservative value, since one of the main aim of this project is to obtain a fully amorphous structure. It is known that to sinter at such quite low temperature can affect other properties such as densification of the scaffold structures and the mechanical properties.

5.3 Scaffold manufacturing process

Robocasting is a technique that allows easy control on the fabrication of grid-like structures, giving the possibility of creating porosities with well-defined shape and dimension. The possibility of building scaffolds with the minimal porosity dimension required for bone repair application (≈100 μm) was investigated, along with the construction of a graded porosity.

This was possible only by careful optimization of the raw materials, the ink used for the extrusion, and of the printing process itself. This section describes how the manufacturing process was tailored and carried on.

5.3.1 Ink optimization

The first step for the fabrication of glass scaffolds through direct ink writing was the optimization of the ink recipe. This means that the right glass powders-to-Pluronic F-127 solution volume ratio needs to be find and, moreover, it is necessary also to tailor the concentration of Pluronic in the aqueous solution. The two main parameters that were considered during the optimization were the processability and the strength of the ink. The latter property is operatively defined as the ability of maintaining straight the extruded rod while crossing a gap over two underlining lines.

- Processability: it can be qualitatively evaluated considering the mixing phase of the glass powders with the binder, the removal of trapped air from the ink and the filling of the cartridge. A good level of processability implies that the viscosity of the processed ink can be easily kept low, without too frequent cooling of it. This depend on the F-127 concentration in the aqueous solution and on the volume ratio of between binder and glass. Since Pluronic has a thermally reversible viscous behavior, it is liquid at low temperature (≈4°C) and it gels at high temperature (≈40°C) [7], the higher its content is in the binder solution, the faster it gels at room temperature during the ink preparation, making harder to obtain a homogenous distribution of powders. The amount of glass has a similar effect on the viscosity of the ink. More glass powders mean higher viscosity of the ink and more material to mix. Furthermore, as second effect, glasses can lower the gelation point of the Pluronic solution. In order to obtain a good processability, Pluronic and glass contents shall be kept low both.
- Ink strength: in order to achieve a very regular and controlled structure, the extruded ink shall stay undeformed, maintaining the shape of a perfect cylindrical rod, from extrusion to sintering. Doing so, it is possible to obtain very regular pores, even using large spacing between lines, and a high strength means also that the rods can withstand the weight of the overlaying layers without collapsing. Again, Pluronic concentration and powder volume have a crucial role. Increasing the amount of F-127 leads to a stronger gel network, which also forms at lower temperature. Higher volume of powders increases the strength of the ink by increasing the viscosity. Regarding the strength, it seems desirable to have high concentration of Pluronic in the binder and great amount of glass in the final ink.

It is easy to see that these two parameters require opposite conditions, so it is necessary to carefully tailor them. A poor processability will lead to a very difficult mixing process and to an ink with inhomogeneities and a lot of air trapped inside, while an ink with low strength will turned into irregular and collapsed structures.

The optimization of the ink was conducted considering three different concentration of Pluronic in the binder, 25, 27.5, 30 wt%, and two different volume ratios of the glass, 30, 35 vol%. Thus, several different inks were tested with a preliminary structure composed by eight layers of six lines, long 5 mm, spaced by 1 mm. Thereafter the inks will be addressed with a code: XX-YY, where XX is the volume ratio of glass powders in the ink and YY the Pluronic weight percentage in the binder. The ink composition that have been tried were: 30-25, 35-25, 30-30, 35-30, 35-27.5. All the structures were printed using a conic nozzle with a tip diameter of 410 µm and the printing pressure was changed according to each ink. In fact, the viscosity of the ink has a great influence on the printing pressure.

- 30-25: along with the 35-25 this ink was the first ink tried during the present work. This ink is characterized by a low concentration of Pluronic in the aqueous solution and a small amount of glass. Thanks to that, the processability of this ink is very high, the viscosity remains low at room temperature, requesting just a few cooling steps. On the other hand, the strength of the ink was very low, resulting into a collapsing of the bottom layers and into a curvature of the rods over the gaps. A pressure ranging from 9 to 10 psi was necessary;
- 35-25: due to higher content of glass in the ink, with respect to the 30-25, the processability was a little decreased but the strength of the ink was increased. Thus, the structures obtained are much more regular, without evident curvatures of the rods, as shown in **Figure 5.9**. The printing pressure was raised to 14-15 psi;

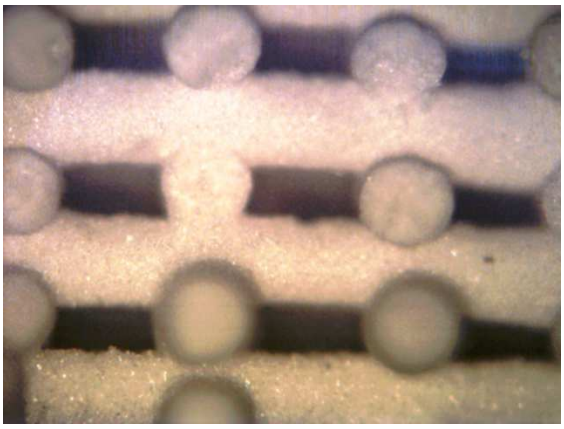

Figure 5.9 Robocast structure obtained by using the 35-25 ink (optical microscopy, 50X, nominal diameter of the rod: 400 μm)

– 30-30: this composition was testedin order to increase the strength of the 30-25 while keeping a good processability. In fact, from the previous trial, it seemed that the processability is mainly affected by the glass content instead of the Pluronic concentration. Even though, while the processability remained very good, the strength of the ink resulted insufficient. **Figure 5.10** shows how much the rods are curved while crossing the space between two underlying lines. The pressure used was increased up to 24-25 psi;

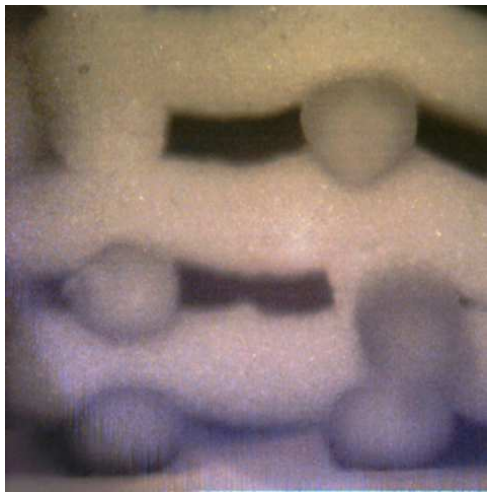

Figure 5.10 3D-printed scaffold using 30-30 ink (optical microscopy, 50X, nominal diameter of the rod: 400 μm)

– 35-30: 30-25 and 30-30 inks proved that just the 30 vol% of glass powders inside the ink was not enough to provide enough strength to the ink itself. So, the glass fraction was increased and the 35-30 ink was made. The processability of this ink was extremely low, the ink gelled very fast and a lot of air was trapped inside. But, as expected, the strength of the ink was excellent, leading to a very good structure (**Figure 5.11**). The pressure needed for printing was 25-26 psi;

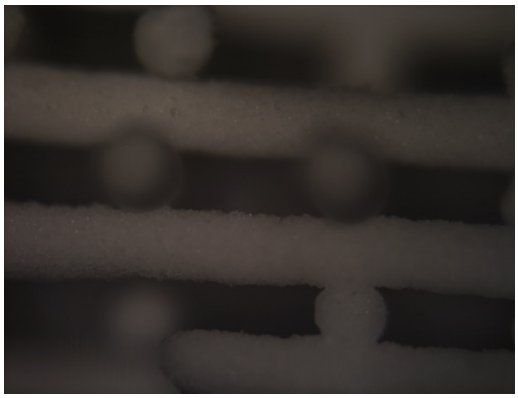

Figure 5.11 Structure printed with 35-30 ink (optical microscopy, 50X, nominal diameter of the rod: 400 μm)

– 35-27.5: this composition was obtained by trying to maintain the strength of the 35-30 while getting close the processability of the 35-25. The reduction of the Pluronic concentration leaded to a high increase in the processability of the ink, the lower viscosity made easier mixing powders and binder together and the gelation point was high enough to allow regular cooling after a couple of mixing cycles. Moreover, the air removal was quite easy. The structure obtained by printing the 35-27.5 ink presented straight rods and just a little deformation of the bottom layers (**Figure 5.12**). The pressure used during printing ranged from 18 to 21 psi.

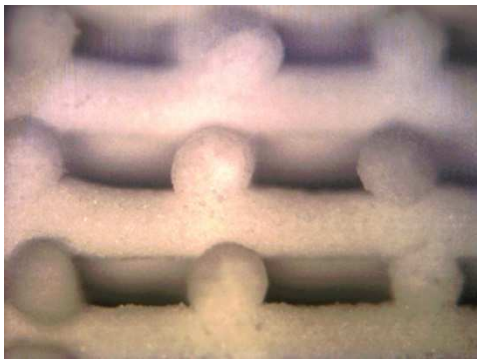

Figure 5.12 Porous structure obtained by printing 35-27.5 ink (optical microscopy, 50X, nominal diameter of the rod: 400 μm)

In the end, after all the different ink were tested, it was chosen to fabricate the scaffolds by using the ink prepared mixing 35 vol% of powders with a 27.5 wt% aqueous solution of Pluronic (**Figure 5.12**). In **Table 5.5** the different ink composition are listed and a mark is given to each parameter considered for the ink choice; the composition selected for further processing is, indeed, the result of a compromise.

Table 5.5 Ink compositions with a mark given for the two parameters, processability and ink strength. The marks are comparative and range from poor to excellent. The ink chosen for the robocasting process is written in bold.

Ink composition	Processability	Strength
30-25	Excellent	Poor
35-25	Very good	Acceptable
30-30	Very good	Poor
35-30	Poor	Very good
35-27.5	**Good**	**Good**

5.3.2 Printing and sintering process of 47.5B glass scaffolds

Once the ink recipe was defined, it was possible to optimize the robocasting process. In order to have a good outcome of the printing process, it is necessary to adjust several parameters that will affect the results:

−Air pressure: the Tabletop-3Dn printer used during the development of this thesis works in "pressure control", which means that there is no control on the displacement of the plunger in the cartridge but just the force applied to it can be modulated. In terms of material feed, "displacement control" printer might be able to provide more stable feed, since the resistance to flow of the ink shall decrease during the unloading of the cartridge. However, Fu et al. [7] demonstrated that also with "pressure control" the feed is stable enough for robocasting purposes. The material feed is proportional to the pressure, i.e. the more pressure is applied the more material is extruded. A correct material feed is important to obtain rods of constant diameter, without any interruption, and a good adhesion to the previously-deposited layer. If too less ink is extruded, the rods will have a small diameter and will be prone to break. With low feed, the rods have a small diameter, they are subjected to traction by the moving tips and eventually they will break, as shown in **Figure 5.13**. Moreover, if the rods have a small diameter, they are not pressed enough against the underlying layer, leading to bad adhesion between layers. This can cause delamination during drying and sintering. If the ink feed is too high, material will accumulate at the end of the tip, resulting into very large rods that may close the smallest pores.

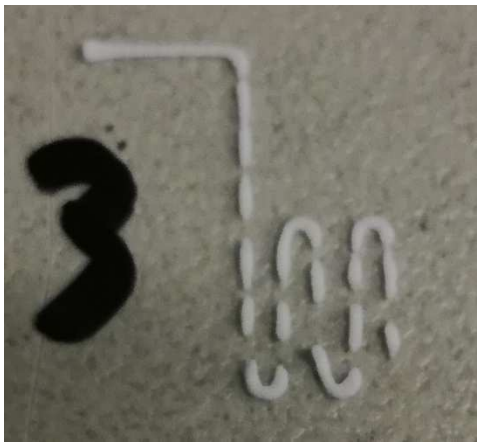

Figure 5.13 Rod brakeage during the printing of the first layer due to insufficient pressure/material feed

- Scanning speed: the speed at which the printing head moves, on the horizontal plate with respect to the base-plate, even if in this particular case it is the plate that moves, has an analogous effect to the air pressure. High speed leads to the same result of low material feed, i.e. the rods are stretched and eventually breaks. Low speed turns into ink accumulation, enlarged rods and loss of the smallest features, as shown in **Figure 5.14**. So, air pressure and scanning speed are parameters that must be adjusted accordingly one another. During actual printing processes, it is used to maintain fixed the scanning speed at a value that it is known to work, then the air pressure is adjusted in a range of some psi at the beginning of the process. This is made this way because the scanning speed is included into the design script and is harder to modify;

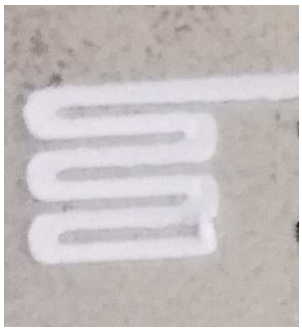

Figure 5.14 Deformed rods due to low scanning speed/high material feed

– Z spacing: it is the space that the nozzle moves upward once a layer is completely printed. This parameter is mainly determined by the tip diameter. Since the rod diameter is proportional to the nozzle dimension, if the Z spacing is too little, the extruding lines will be pushed onto the underneath layer, losing the cylindrical shape and deforming the already printed rods. On the other hand, if the movement is too wide, the two layers will not touch themselves, achieving no adhesion at all. It is very important to have high control also on the distance between the acetate films and the tips during the extrusion of the first layer. Every change in height will create a defect that might have influences on the other layers.

Considering all of that, the robocasting of both types of scaffolds, 47.5B-G (graded) and 47.5B-M (monoporous), was performed using a scanning speed of 2 mm/s, a Z spacing of 300 μm and air pressure ranging from 18 to 22 psi. All the parameters but the pressure were maintained fixed, and the pressure was adjusted a bit every printing session. Once the right parameters were found, a very constant and stable printing process can be achieved, and all the ink could be extruded from the syringe without any interruption, sequentially printing several scaffolds (**Figure 5.15**)

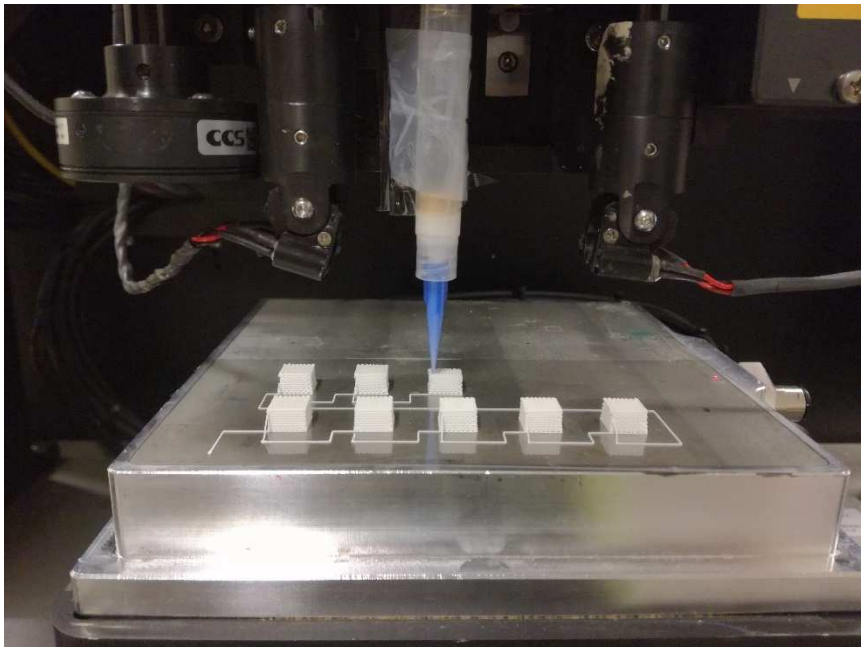

Figure 5.15 Sequential robocasting of several 47.5B scaffolds

The design of the scaffolds was optimized through several trials. Once the sintering temperature, 600°C was defined as explained in section 5.2.4, scaffolds with different spacing between neighboring lines were printed and sintered; then, the porosity width was assessed by measuring several pores onto different scaffolds. In order to build large porosity (≈200 μm), the spacing between the center of two following lines shall be of 636 μm, while for building small porosity (≈100 μm), it was necessary to decrease the space down to 510 μm. Those spacing took also into account the diameter of the rod. The scaffolds obtained are shown in **Figure 5.16**.

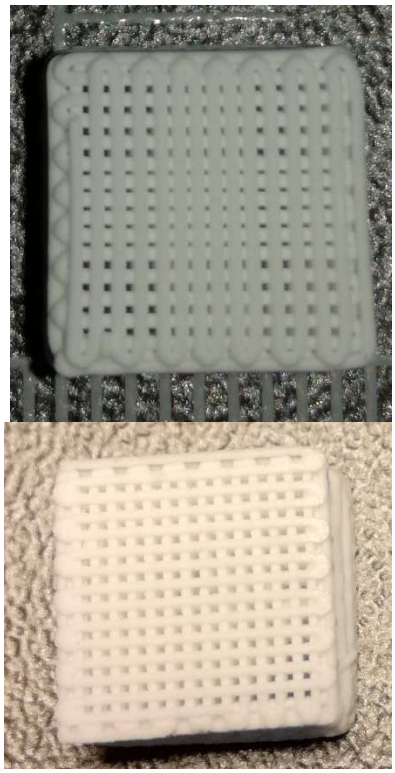

Figure 5.16 Graded (up) and monoporous (bottom) green scaffolds obtained after robocasting and drying

Once the scaffolds were printed and sintered, the final feature dimensions and the shrinkage during thermal treatment was assessed measuring a large number of pores (more than 20 each type), both large and small. The results are reported in **Table 5.6** and shown in **Figure 5.17**

Table 5.6 Dimensions and shrinkage of the different features of the 3D-printed scaffolds

Features	Dimension (average, µm)	Standard deviation (µm)	Shrinkage
Large pores width	213	24	13.6%
Small pores width	119	15	20.4%
Pores height	248	17	25.2%
Rod diameter	280	11	-

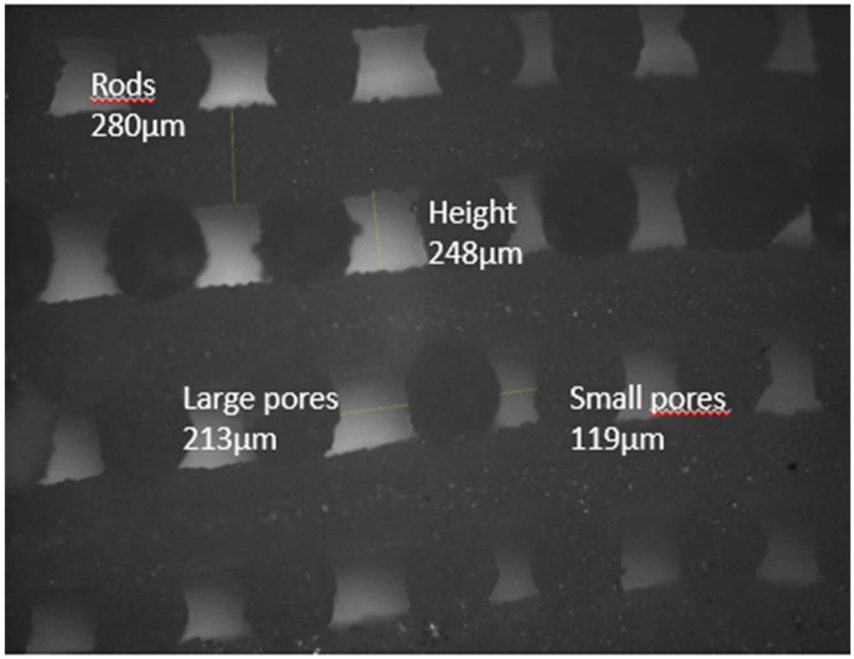

Figure 5.17 Graded scaffold and change in porosity (optical microscope, 50X): larger porosity on the left and smaller porosity on the right. Dimensions of the main features are indicated.

The low standard deviation confirmed the high dimensional control achievable with this kind of manufacturing process, even if sometimes features with very different dimensions can be found (such as large pores as large as 264 µm or as narrow as 164 µm). The effect of the thermal treatment was also an overall shrinkage of the scaffolds (**Figure 5.18**).

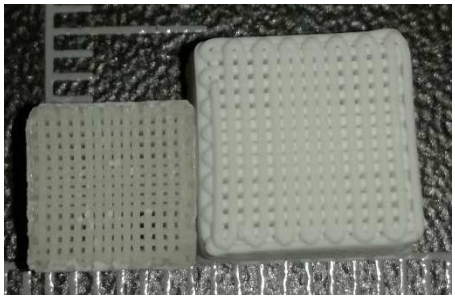

Figure 5.18 Graded scaffolds, pre- (right) and post-sintering (left)

As expected, the shrinkage along the Z axis was greater than the one on the horizontal plane, due to the compression applied by the weight of the scaffold itself. Instead, more interesting is the fact that the shrinkage is higher where there is the smaller porosity with respect to the larger one. This can be an effect of the greater number of intersection points between lines of two different layers in the small porosity than in the areas where the pores are bigger. More contact points allow more mass flow during the sintering process, leading to higher shrinkage.

In the end, very regular and well-defined structures were obtained, both for the graded design (**Figure 5.18**) and the monoporous scaffold (**Figure 5.19**).

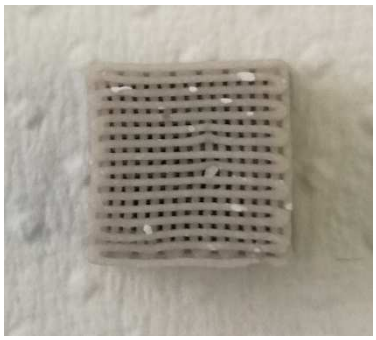

Figure 5.19 Monoporous scaffold after sintering

5.4 Scaffold characterization

Once the scaffolds were produced, it was necessary to characterize them in order to have knowledge of the properties that may affect the application as bone substitute materials. These include morphology of the scaffolds, at macro- and micro-scale level, structure of the trabeculae and mechanical properties. All of them were investigated and the results are shown here.

5.4.1 Morphology: structure and porosity

In order to have a good evaluation of the outcome of the fabrication process of the scaffolds, in terms of macro- and microstructure, morphological and structural analysis were performed through SEM observation and micro-ct imaging. This was also necessary to have a better understanding of other properties of the scaffolds, such as mechanical properties or in vitro bioactivity.

The structures obtained are highly regular, the rods remained straight during the sintering process and present a regular section. The porosity is made of regular channels, both vertical and horizontal, generated by the separation between glass lines and the tilting of the layers with respect to the underlying one. Within the graded scaffolds, the change in porosity is easily appreciable (**Figure 5.20**).

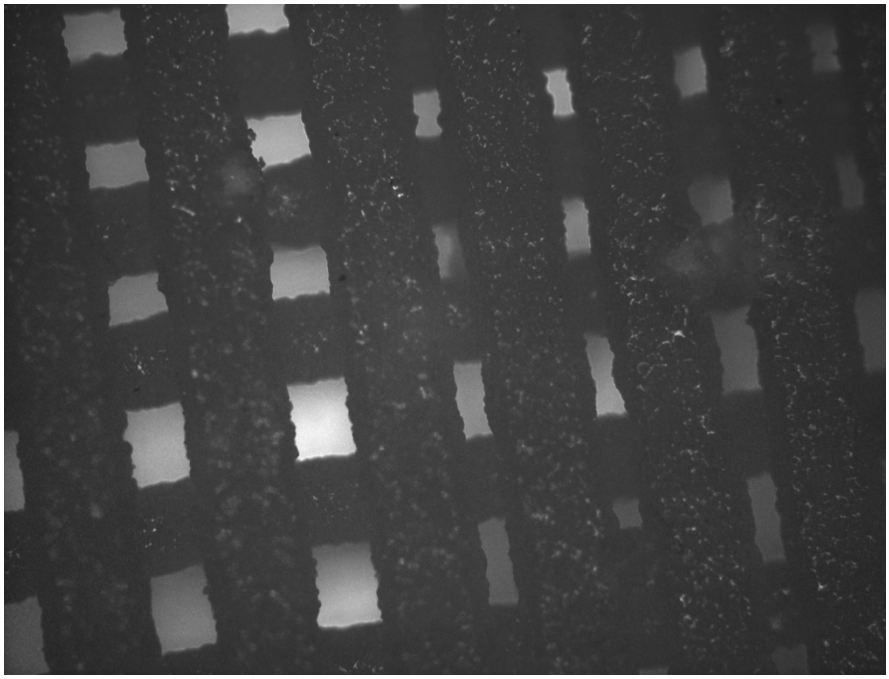

Figure 5.20 Top view of graded scaffold, with the different porosity: large (left bottom), small (top right) and intermediate (top left and bottom right) (Optical microscope, 50X)

It is also interesting to notice how, due to the narrowing of the distance between rods to form the small porosity, areas with a third different kind of porosity were formed. There the pores have a rectangular shape (see also **Figure 5.16**).

The same regularity has been found by observing the top of a monoporous scaffold (**Figure 5.21**).

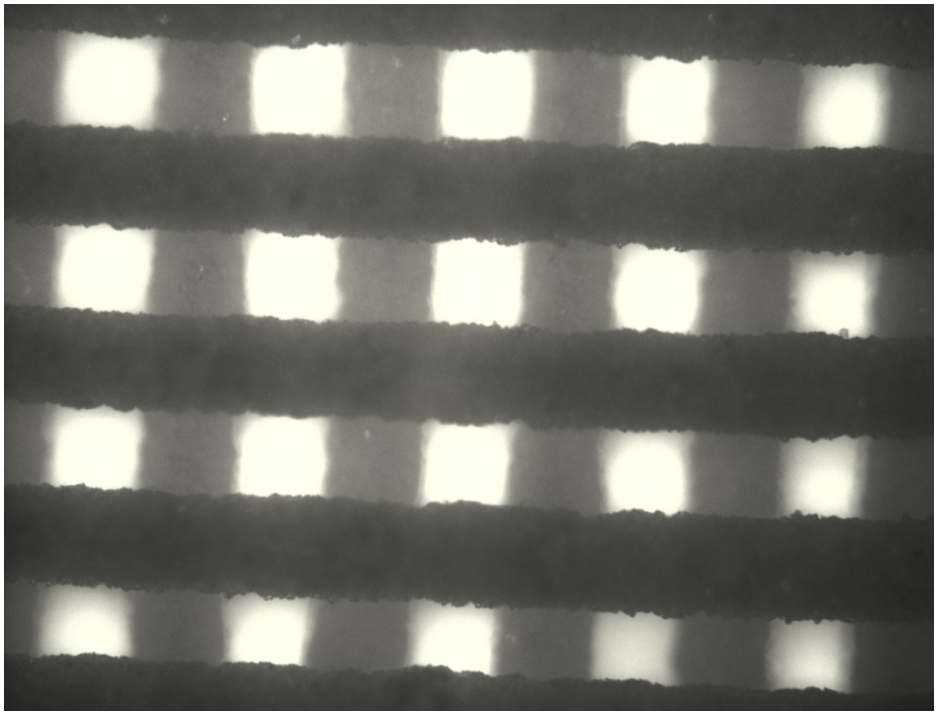

Figure 5.21 Top view of the grid-like structure of a 47.5B-M scaffold (Optical microscope, 50X)

The regularity of the pores obtained can be appreciated also observing a cross section image of the scaffold (**Figure 5.22**). it is possible to notice how the rods do not bend over the gaps and that they maintained a circular shape.

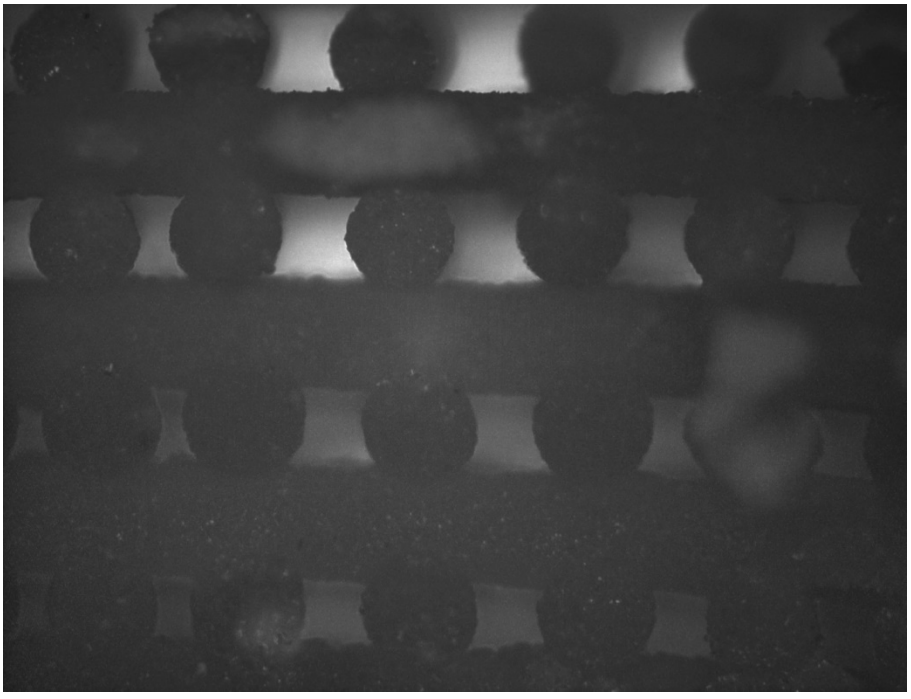

Figure 5.22 Cross-section of graded scaffold in the area of larger porosity (Optical microscope, 50X)

More accurate morphological investigations were carried on using a SEM, especially to understand the level of sintering reached during the thermal treatment. It was noticed that two different microstructures were obtained in scaffolds printed on different times but sintered under the same conditions. So, two different series of scaffolds, both graded and monoporous, were printed. The reason of this different sintering behavior is unknown, but it could be due to errors in the ink preparation, defect in the raw

materials, furnace issues or uncontrollable environmental conditions. Unfortunately, during the development of this thesis, there was no time to investigate the problem, thus further studies are needed. For comparing the effect of the scaffold design on the different properties, mechanical and in vitro bioactivity, scaffolds from the same series were chosen.

The first series of scaffolds produced presented a quite low level of sintering, the single glass particles are still distinguishable and the trabecular surfaces are rough and irregular (**Figure 5.23**).

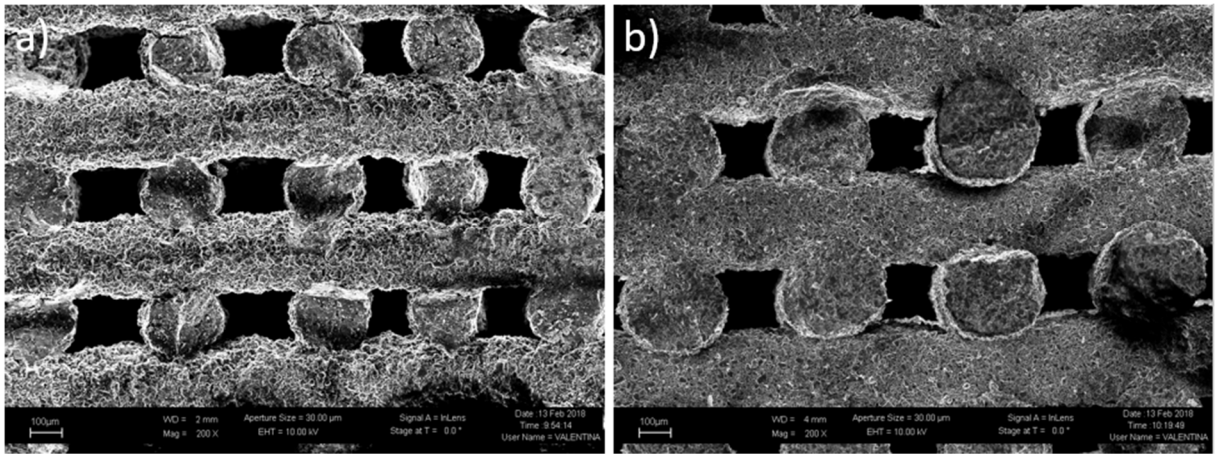

Figure 5.23 Cross-section of 47.5B-G (a), large pores on the left and small ones on the right, and 47.5B-M (b). The regular pore structure is appreciable, along with the irregularity on the surface (SEM, 200X).

At higher magnification is clear how the sintering is not at an advanced state, inter-particle pores are clearly visible, but also the sintering neck that formed between glass powders (**Figure 5.24**a). Even though, rods are well joined together, so good that in some points crack get through two different layers as they were a unique piece (**Figure 5.24**b).

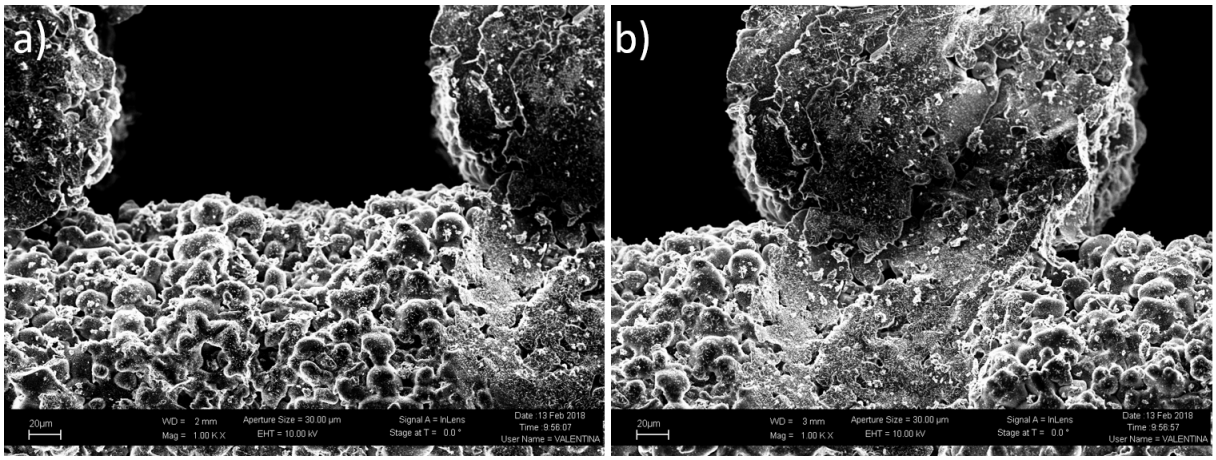

Figure 5.24 SEM image (1000X): a) bottom part of a pore, the particles are distinguishable and sintering necks are visible; b) crack propagating across the junction of two rods (one perpendicular and one parallel to the image plane) that appear well welded together

Analyzing closer the microstructure of the trabeculae, it is evident the diffused network of inter-particle porosity, which is due to the low level of sintering, and the junction points between glass powders (**Figure 5.25**).

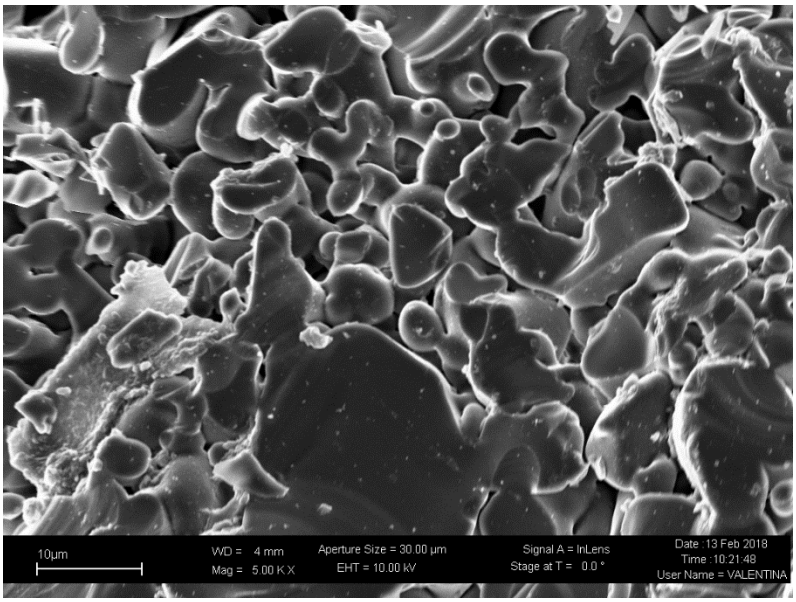

Figure 5.25 Surface microstructure of a trabecula (5000X).

It was also possible to assess the presence of defects due to air bubbles trapped into the ink during its preparation. That leads to the presence of big voids that can not be filled during the sintering process (**Figure 5.26**).

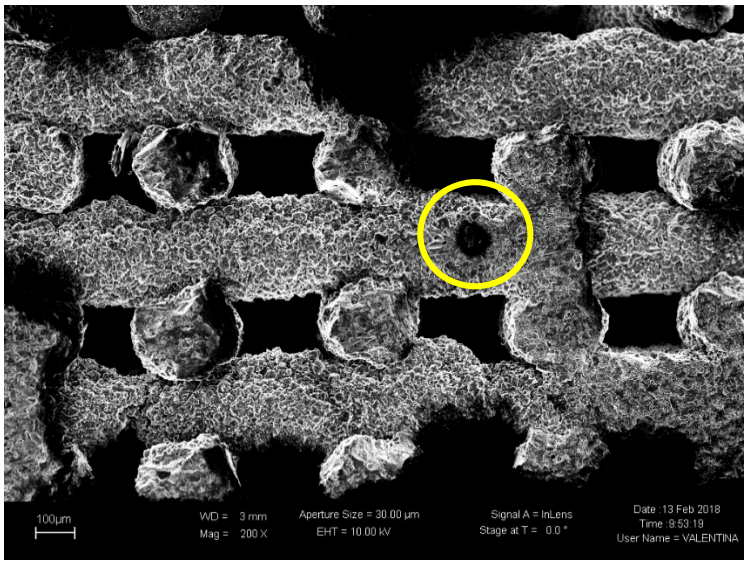

Figure 5.26 Cross-section of 47.5B-G scaffold with a defect caused by air trapped inside the ink (yellow circle)

This kind of microstructure has effect on different properties. The low densification of particles and the presence of diffused micropores lower the mechanical resistance, since every defect can act as crack starting point. But, on the other hand, the surface roughness and the micropores themselves might enhance the bioactivity. Micro-asperities on the surface can increase the area exposed to biological fluids and hence the scaffold reactivity, promote cell adhesion, and the micro-pores can make easier diffusion of nutrients and waste products, towards and away from proliferating cells [8].

The second series of scaffolds produced present a very well densified microstructure, the glass particles are no more distinguishable, and the trabecular surface is smooth and plain (**Figure 5.27**a). At higher magnification it is possible to see how the inter-particles porosity is almost completely disappeared and the particles are fused together, also in the areas of contacts between different rods. Still, pores derived from air trapped in the ink are present (**Figure 5.27**b).

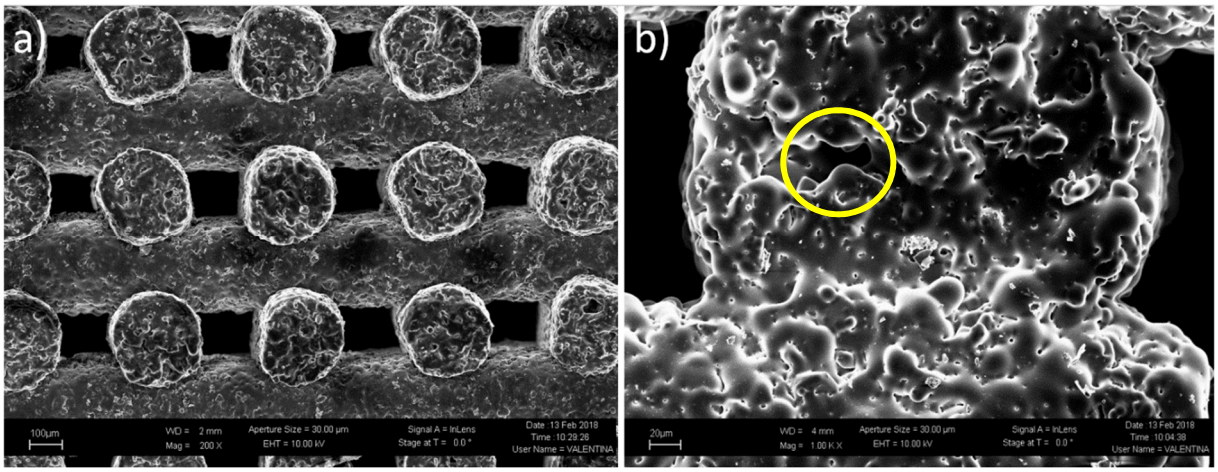

Figure 5.27 Second series 47.5B-M scaffold, cross section: a) channel porous structure (200X); b) trabeculae section with air-bubble derived pore (yellow circle) (1000X)

This second kind of microstructure might offer enhanced mechanical properties, thanks to the better densification of the struts with respect to the first series, but more plain surfaces can result in worst cell adhesion and diffusion of body fluids through the micro-pores is no more possible.

Despite the different microstructure, the two different scaffold designs, in both the series, have a porosity suitable for potentially supporting new bone formation. In fact, pores between 100 and 200 μm are suitable to allow the correct vascularization and to avoid hypoxic growth conditions of the bone [8].

The total porosity of the different scaffolds was evaluated as described in section 4.4.2.1. Different values were obtained for the different design and the different series, **Table 5.7**. The resulting porosity is not extremely high, but still acceptable for bone repair application (minimum recommended porosity around 50% [9]).

Table 5.7 Total porosity of the different scaffold types and series

Series	Scaffold type	Porosity (%)	Standard deviation (%)
First	47.5B-G	49.1	5.5
	47.5B-M	58.4	2.8
Second	47.5B-M	42.5	4.55

In order to assess the final composition of the bioactive glass scaffolds, EDS was performed onto scaffolds belonging to both series. An example of spectrum obtained is shown in **Figure 5.28**. Three different areas of scaffolds belonging to each series were analyzed. Results are reported in **Table 5.8**.

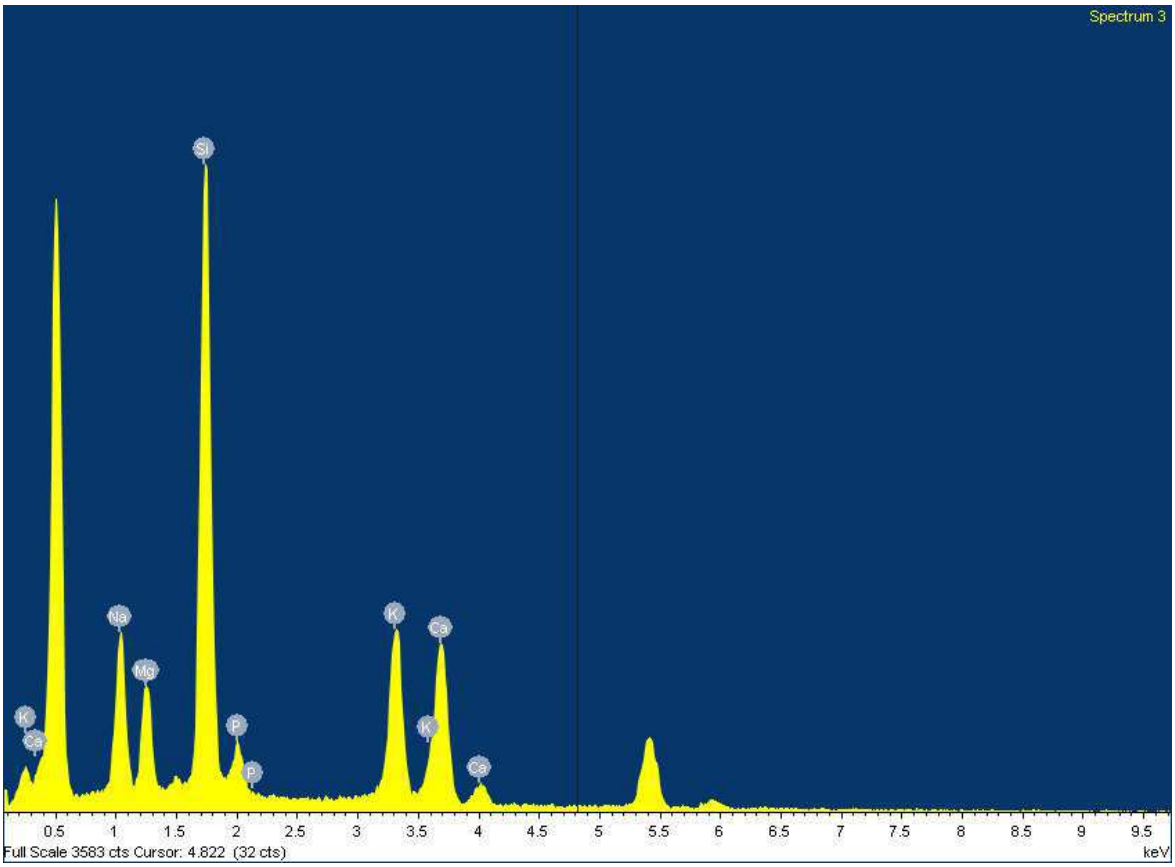

Figure 5.28 EDS spectrum of a 47.5B glass scaffold (the unlabeled peaks are the ones related to the chromium used for the metallization of the sample)

Table 5.8 Composition, expressed as wt%, of scaffolds belonging to the two different series fabricated, compared to the theoretical composition

	Elements	Weight %	Standard deviation	Theoretical
First series	Na	8.906667	0.748755	12.1789
	Mg	5.86	0.389744	6.4378
	Si	38.88333	1.083159	35.3362
	P	4.436667	0.3139	4.1021
	K	19.53	1.220205	20.7124
	Ca	21.99	1.54	21.2325
Second series	Na	11.01	0.932899	12.1789
	Mg	6.453333	0.181751	6.4378
	Si	38.60667	0.710587	35.3362
	P	4.36	0.269629	4.1021
	K	19.03333	0.699452	20.7124
	Ca	20.53667	1.158203	21.2325

No relevant differences between the two series were assessed, nor with the theoretical composition. It is necessary to state that, in the analysis of one single area on the scaffold of the first series, sulfur was detected, in very low percentage (1.19 wt%). The contamination can be due to environmental contamination of the sample or to some disturb during the measurement.

A better and more complete characterization was possible thanks to the micro-CT analyses performed by Dr. Gissur Örlyngson at the Innovation Center Iceland (ICI). When the samples were sent to Iceland, there was no clue on the fact that two different microstructures were obtained during the production of

the scaffold. So, the analyses were performed on graded scaffold belonging to the first series and on monoporous ones coming from the second series.

Micro-CT images highlighted the rather regular structure obtained in both the series and for both the scaffold design, but also the differences in the densification of the trabeculae.

The analyses of the 47.5B-G showed that the differences in the pore size between the central zone of the scaffold and the peripheral one is clear and well defined (**Figure 5.29a**).

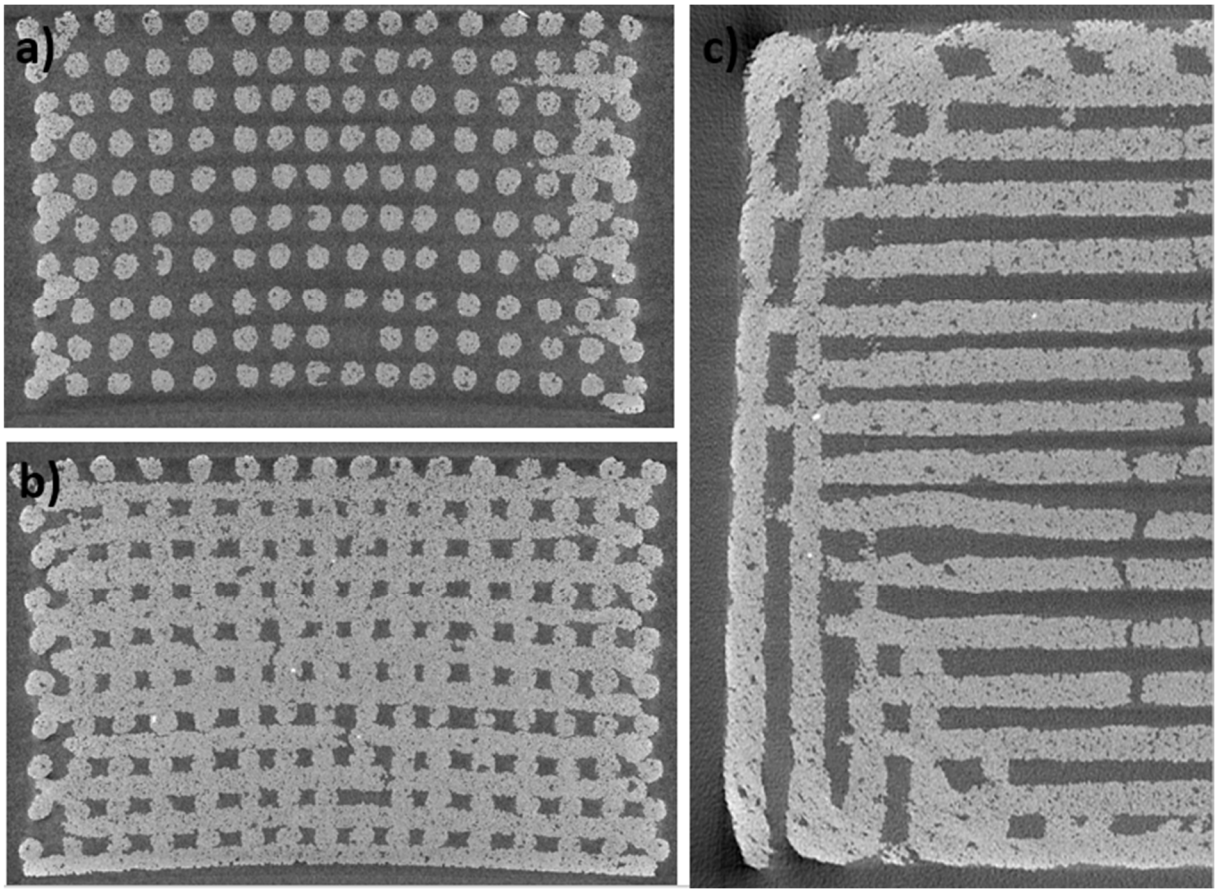

Figure 5.29 Micro-CT images of 47.5B-G scaffold: a) vertical section on a plane that passes through the gap between 2 central rods; b) vertical section on a plane that cuts through the rods parallel to the image plane; c) horizontal section on the mid-height of the scaffold, showing also the border of the scaffold (nominal strut diameter: 275 μm).

In **Figure 5.29a-b**, it is possible to notice that the porosity is all connected and formed by vertical and horizontal channels, that intersect each other and form a grid-like structure. The porosity gradient is also appreciable in **Figure 5.29c**, by the top view. The rods showed a constant diameter even if some irregularities or some cracks are present. These defects are mainly due to uneven shrinkage during the drying and sintering processes and to consequent residual stresses. 3D reconstruction of the scaffolds allows better understanding of all the features described so far (**Figure 5.30**). The low densification of the particles, noticed during SEM observations, is here confirmed. In fact, in all the images it is possible to observe a grainy microstructure with residual inter-particle voids.

The features and dimensional characteristics were measure again during the micro-CT analyses (**Table 5.9**) and they are in agreement with those obtained by optical observation (**Table 5.6**). The rod diameter assessed by micro-CT is in perfect agreement with the nominal value.

Table 5.9 Dimensions of the 47.5B-G (first series) features measured by micro-CT

Features	Dimension (average, µm)	Standard deviation (µm)
Large pores width	139	32
Small pores width	174	18
Pores height	190	30
Rod diameter	275	32

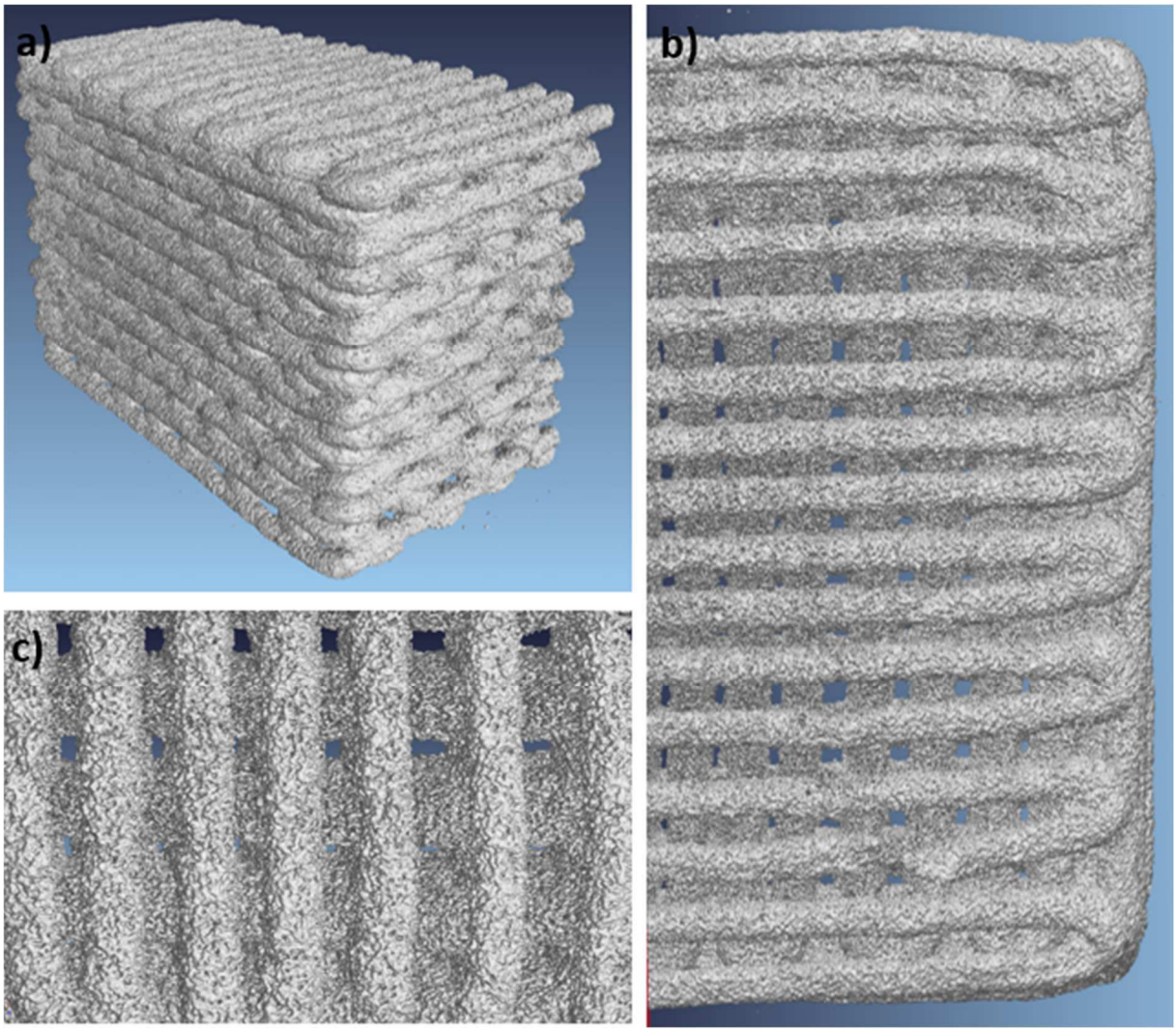

Figure 5.30 3D images obtained by micro-CT of a 47.5B-G scaffold: a) lateral view; b) top view; c) magnification of the areas of porosity change (nominal strut diameter: 275 µm).

The total porosity is in accordance to the one calculated by the density method, because it results equal to 47.1% (standard deviation=3.1%).

Micro-CT was also used for the analyses of second-series monoporous scaffolds. As for the previous case, the images showed a good regularity in the structure and in rod diameter, which is mostly constant. The porosity structure is equal to the one of the 47.5B-G design, but the distance between rods is the same in every part of the scaffold (**Figure 5.30**). With respect to the first-series microstructure of the 47.5B-G scaffolds shown in **Figure 5.29**, here the rods appear much denser and more uniform, not grainy. The voids that are visible in the filaments are derived from air bubbles that remained trapped inside the ink. The dimensions of the structural features, measured as it was done for the 47.5B-G, are slightly smaller than those of the first-series, reported in **Table 5.6**, due to the higher densification of the second-series scaffolds.

Table 5.10 Dimensions of the 47.5B-M (second series) features measured by micro-CT

Features	Dimension (average, μm)	Standard deviation (μm)
Pores width	180	25
Pores height	147	19
Rod diameter	300	10

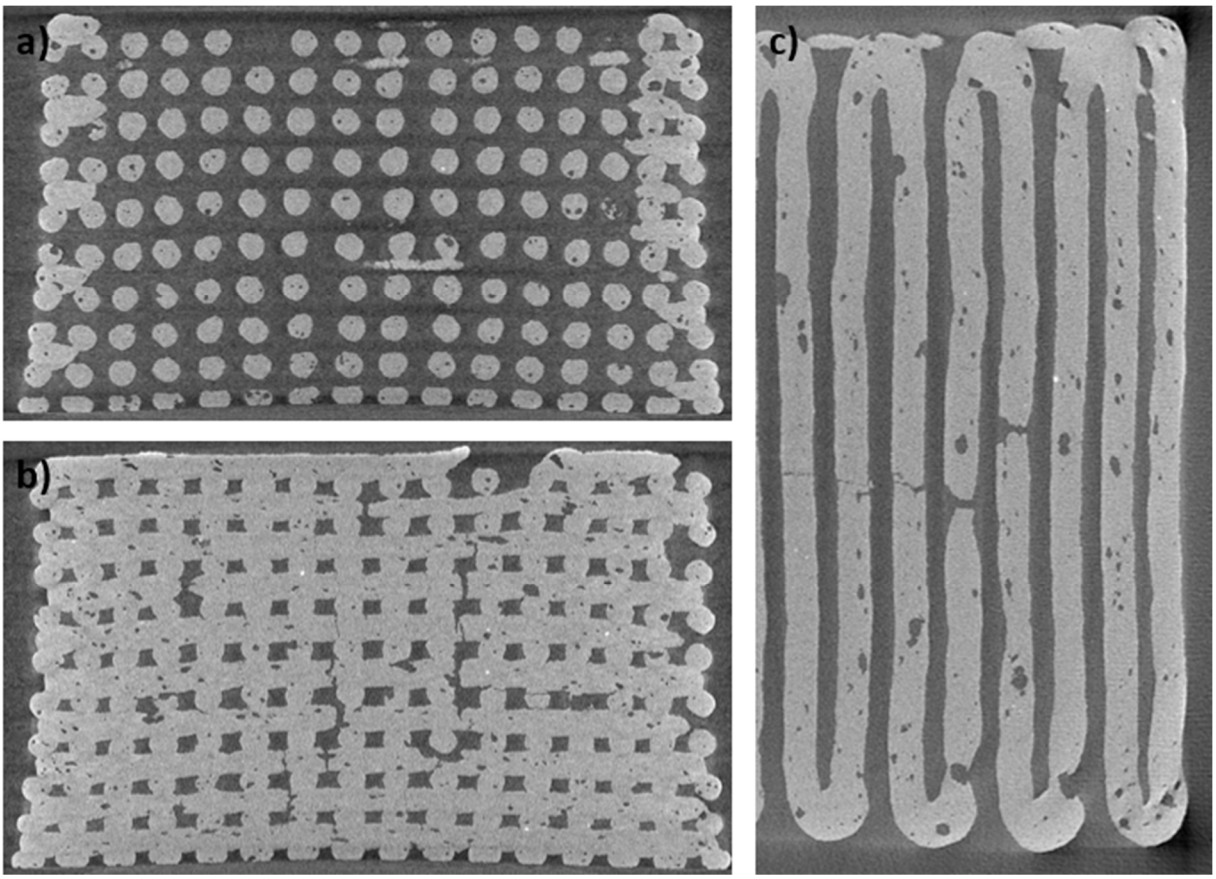

Figure 5.31 Micro-CT images of 47.5B-M scaffold: a) vertical section on a plane that passes through the gap between 2 central rods; b) vertical section on a plane that cuts through the rods parallel to the image plane; c) horizontal section on the mid-height of the scaffold, showing also the border of the scaffold (nominal strut diameter: 300 μm).

The total porosity calculated with the micro-CT analysis was, again, in accordance with the value calculated for the monoporous second-series scaffold by the density method (**Table 5.7**). In fact, it resulted equal to 40.5% (standard deviation=4.2%).

The whole structure of the monoporous scaffold is appreciable also in the 3D reconstruction (**Figure 5.32**). Also in this pictures, the difference in densification of the structure is appreciable if compared to the first-series graded scaffold represented in **Figure 5.30**.

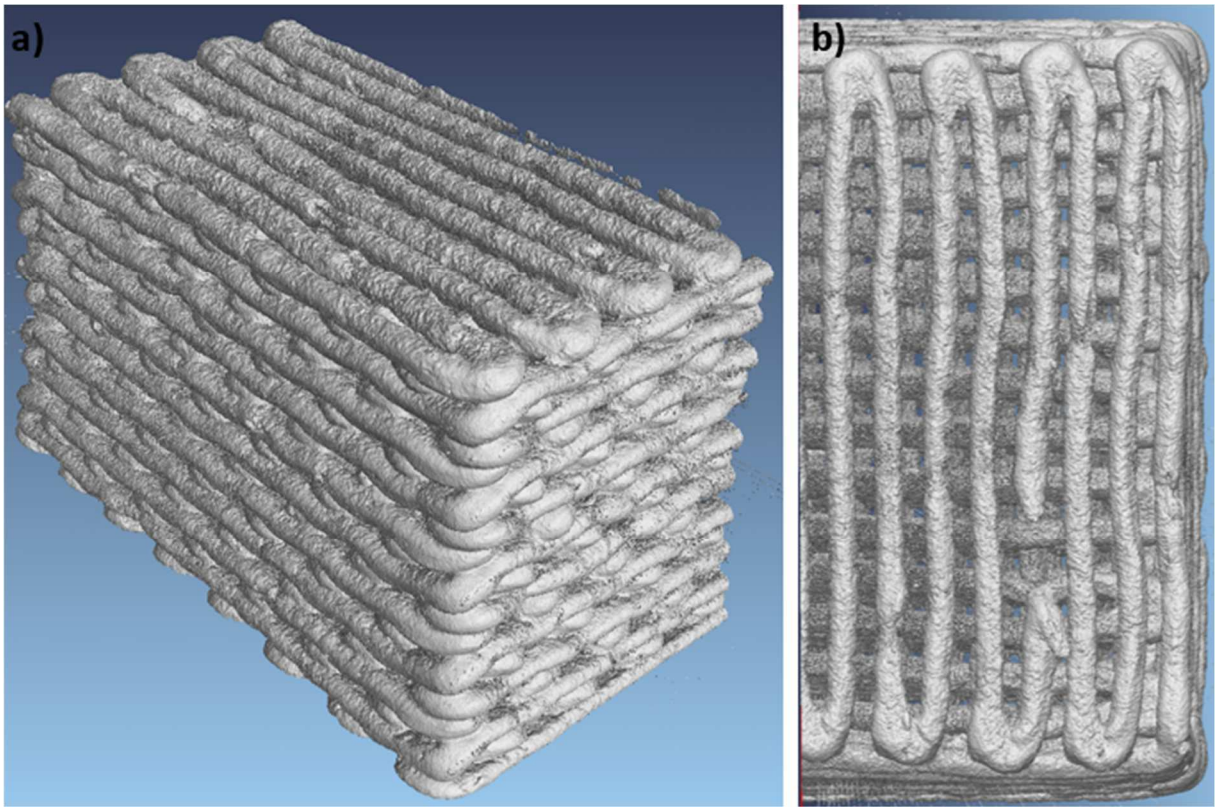

Figure 5.32 3D images obtained by micro-CT of a 47.5B-M scaffold: a) lateral view; b) top view (nominal strut diameter: 300 µm).

5.4.2 Mechanical properties

To be applied for bone restoration in load-bearing areas, bioactive glass scaffolds must present mechanical properties in the range of that of the bone where the implant is hosted. This is necessary for support of the healing bone and for proper load transfer from scaffold to bone and vice versa. So, the scaffolds shall have compressive strength in the range of 2-12 MPa [10].

Preliminary mechanical tests were conducted on the robocast scaffolds, in particular compression test along the vertical axis. The aim of the tests was double: to evaluate if the different porosity design, graded or monoporous, has any influence on the mechanical strength and to assess the Weibull modulus as index of repeatability of the whole fabrication process of the scaffolds.

The compressive test made on 20 graded scaffolds, belonging to the first series, allowed having a statistically relevant set of data, which was used to calculate the average compressive strength and the Weibull modulus. The average compressive strength resulted equal to 6.05 MPa (standard deviation= 2.58 MPa).

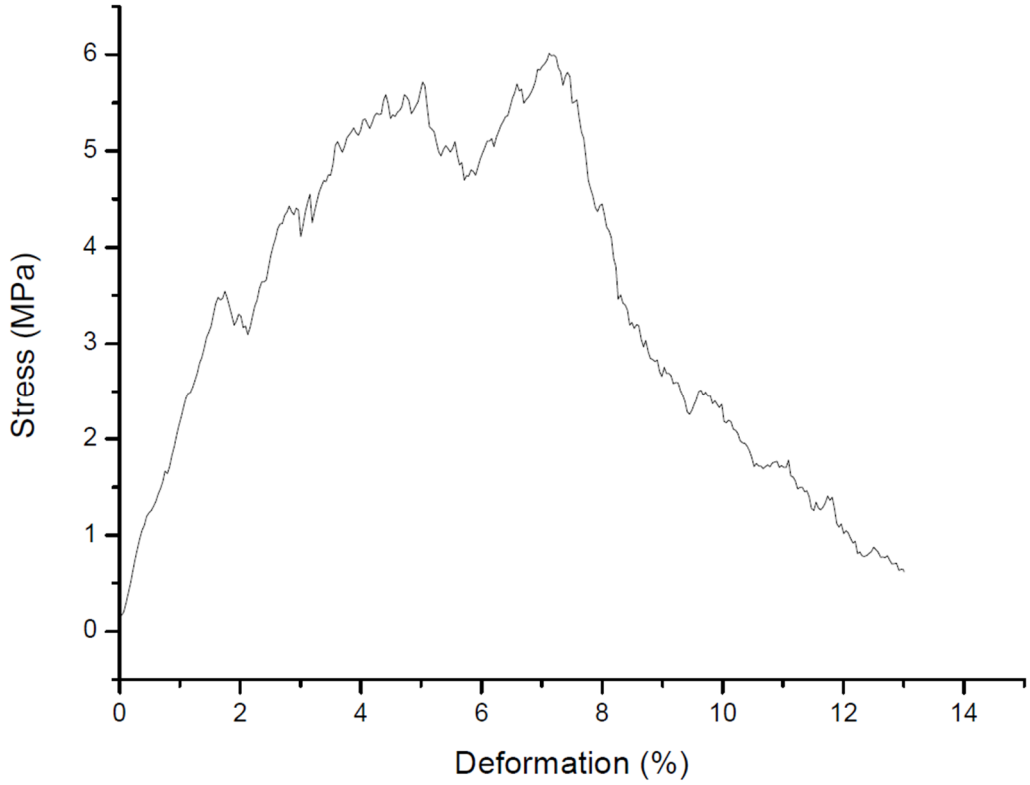

Figure 5.33 Example of stress vs deformation curve of a 47.5B-G scaffold (first series)

A typical stress-strain curve obtained during the compression test of the scaffolds is reported in **Figure 5.33**. The glass scaffold does not behave like a traditional bulky ceramic nor a ductile material, but its behaviour is typical of the cellular ceramics. This suggest that there were multiple fracture events during the compression, that generated the many peaks that can be seen in the curve. The weakest trabeculae broke first, then the strongest ones. This fact increases the fracture work, which can be estimated considering the area underneath the curve, leading to more resistant devices. It is helpful for load-bearing site since the scaffolds can withstand several different impacts without losing completely its integrity and strength. The multi-fracture theory is supported also by the fact that after the end of the test, the scaffolds appeared completely destroyed, only little pieces and powders remained.

The Weibull modulus was evaluated as described in section 4.4.2.2according to the following equation:

$$\ln\left(\ln\left(\frac{1}{1-P_f}\right)\right) = m\ln\left(\frac{\sigma}{\sigma_0}\right) = m\ln(\sigma) - m\ln(\sigma_0)$$

The data were plotted (**Figure 5.34**) and, by linear fitting through the method of the ordinary least squares, the value of m was calculated. It was assessed a value of 3.139 for the Weibull modulus, while the scale factor is equal to -6.

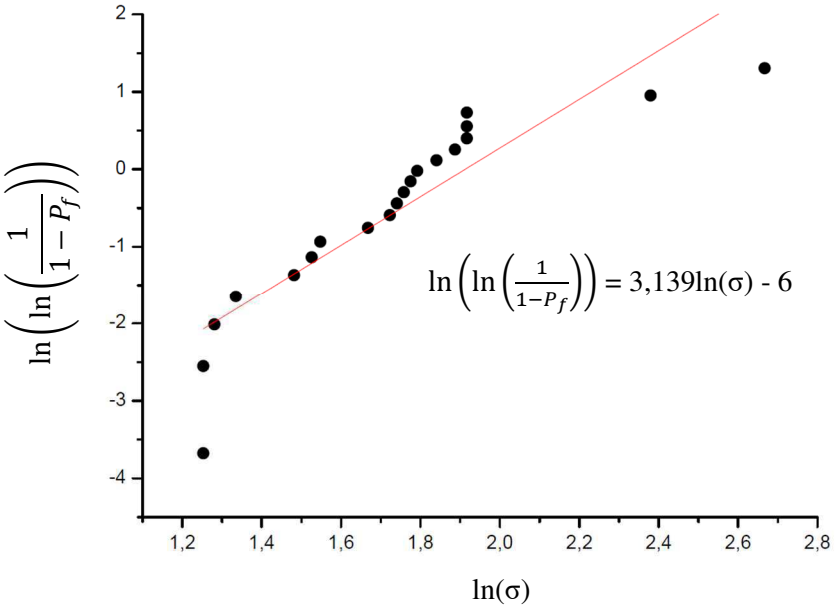

Figure 5.34 Weibull plot $\ln\left(\ln\left(\frac{1}{1-P_f}\right)\right)$ vs ln(σ) and equation of the straight line obtained by linear fitting of the data

Even though the compressive strength is relatively low compared to those of other scaffolds manufactured through solid freeform fabrication techniques [10], it is enough to match the resistance of the cancellous bone, making the scaffold suitable for load-bearing site repair. The Weibull modulus is not excellent, in fact the distribution of the strength value is quite large, ranging from 3.8 MPa to 14.4 MPa. Nevertheless, none of the scaffolds showed compressive strength lower than that of minimum value assessed for cancellous bone (1-2 MPa). The Weibull modulus of solid-freeform-fabricated porous hydroxyapatite, β-TCP and calcium polyphosphates scaffolds have been reported to be in the range of 3 to 9 if tested in compression [11] [12] [13].

It is worth to remember that the achievement of high mechanical strengths was not an aim of the present work. In fact, the sintering temperature was quite low, in order to maintain the amorphous structure of the 47.5B glass. As shown in section 5.4.1, this led to a low densification of the trabeculae and to the presence of a very large number of pores between particles, that can be considered as defects inside a ceramic matrix. The presence of pores has a great effect on the mechanical properties, decreasing them, since each defect can act as crack initiator. The presence of scaffolds that showed considerably higher strength with respect to the average suggested that, with further studies and optimization of the sintering process, better results, in term of mechanical properties, can be achieved.

The Weibull modulus is affected by two separate factors. One is the low densification achieved during the sintering process, which leaves a lot of defects between single particles. The second is related to the manufacturing process, especially to the air removal step during the ink fabrication. If air bubbles remain trapped within the ink, they will create large defects inside the trabeculae that can not be eliminated even by pushing the sintering process. These bubbles are randomly distributed inside the ink and, consequently, inside the scaffolds. Thus, it might happen that a large defect is present in a given scaffold and not in the one printed immediately after or before, thus changing the mechanical properties. Thus, the Weibull modulus, and the repeatability of the whole process, can be increased by optimizing the air removal. In literature there are proposed several different methods, instead of the manual one used for the developing of this thesis, such as the use of planetary centrifugal mixer [1], or much complex protocols involving the use of sonication [14]. Liu et al. [122] showed that the Weibull modulus of robocast 13-93 glass scaffolds can be increased up to 12.

The results from mechanical tests reported in this thesis suggest that 47.5B bioactive glass scaffolds produced by robocasting can be suitable for load-bearing site bone repair, but more complete characterization shall be object of further studies. In fact, the load during in vivo application is more

complex than simple compression, so it shall be suitable to perform flexural and compression along the X-Y axe tests.

Due to the lack of monoporous scaffolds belonging to the first series, the compressive strength of 47.5B-M scaffolds was tested by compression test on 5 scaffolds belonging to the second series. This will prevent possible comparison between the graded scaffolds tested before and those ones, since the denser structure can lead to increased mechanical properties.

The average compressive strength results equal to 9.94 MPa (standard deviation= 4.65 MPa). The large deviation is due to the fact that some high values were registered, such as 13 or 16 MPa, but also some lower ones, 5.6 MPa. This was opposite to what was expected, in relation to the results of the graded scaffolds. In fact, the monoporous design should be less dense, due to bigger porosity, thus also less resistant. But, as introduced before, the fact that the second series of scaffold is much densified with respect to the first one (**Table 5.7**) increased the mechanical properties.

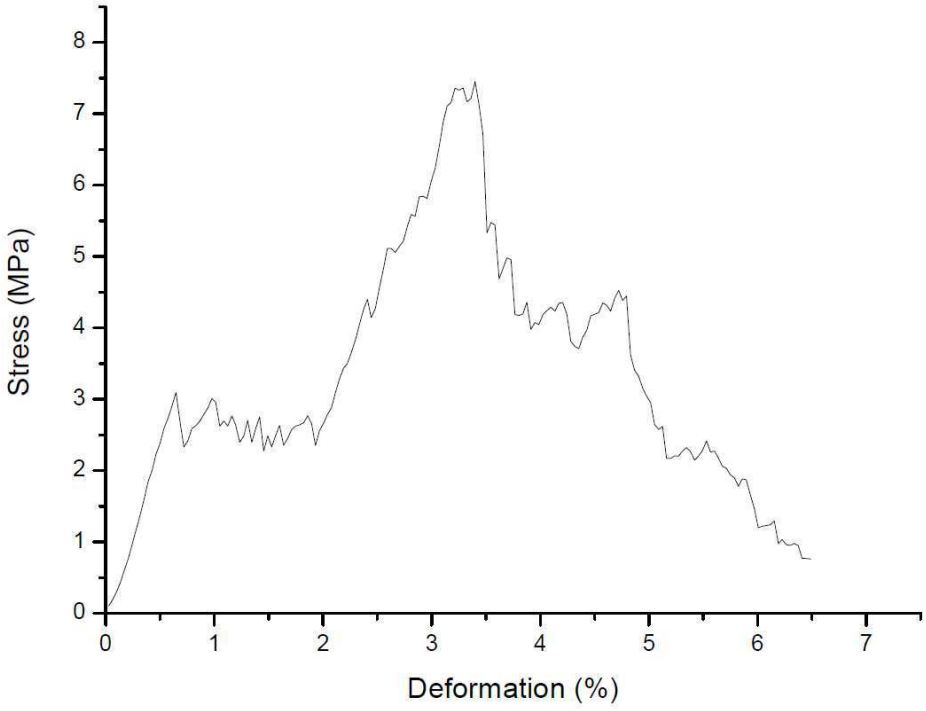

Figure 5.35 Example of a stress vs deformation curve of a 47.5B-M scaffold (second series)

As it is possible to see from the stress vs deformation curve (**Figure 5.35**), the fracture mechanisms were the same that are present in the 47.5B-G scaffolds belonging to the firs series. Since their strength is higher than the graded scaffolds, also the monoporous ones have proven to be potentially suitable for load-bearing application.

In order to have a comparison between the strength of the two different design, also some graded scaffolds belonging to the second series were tested. It was found that the compressive strength was equal to 7.53 MPa (standard deviation=3.86 MPa). The large distributions of the results obtained for the second-series 47.5B-M and 47.5B-G both do not allows to make any statement about possible differences between the two designs. Also, the results obtained for those scaffold are superimposable to the ones founded for the first-series 47.5B-G, so there is not significant differences between the two microstructures in terms of mechanical properties.

5.5 Bioactivity: in vitro evaluation

For stating that a glass has bioactive properties, it is necessary to prove that it can make HA precipitate onto its surface during implantation inside a living body. This behavior can be predicted also by in vitro experiment, through soaking into SBF [16]. One of the main points of the present work was to evaluate

the bioactivity of 47.5B glass scaffolds and to evaluate if the different porosity design plays some roles in the dissolution kinetics and on the HA precipitation.

All the experiments for the assessment of the scaffold bioactivity were performed onto scaffolds belonging to the firs-series manufactured, so it was possible to try making a comparison between the two designs, 47.5B-G and 47.5B-M, since the microstructure was the same in both types. The sample were prepared in the same way, by soaking them in SBF for the proper time with a glass mass to SBF volume ratio of 1.5. The bottles were kept in incubator at 37°C and agitated (100 rpm) for all the time.

5.5.1 Hydroxyapatite precipitation

The main indication of the bioactivity of a glass is the fact that HA precipitate onto its surface during implantation inside a living body or during immersion in solutions that simulate the body environment. In order to qualitatively evaluate the formation of a HA layer on the surface of the trabeculae of the scaffolds produced through robocasting, analyses were performed on the scaffolds that were soaked in SBF during the immersion tests (paragraph 4.4.3), in particular, XRD and SEM observation.

By performing XRD analyses on the whole scaffolds, which were soaked in SBF for different time points, it was possible to observe that HA precipitated on the surface of the scaffolds, through the evolution of the diffraction spectra. In particular, for both the scaffold designs, there was the disappearance of the amorphous halo typical of the glass and the appearance of the HA characteristic peaks. The two main peaks of the HA were detected, the highest at a position 2θ=31.795°, related to the crystalline plane with Miller indices (2 1 1), the other at 2θ=25.689, corresponding to the crystalline plane (0 0 2), data derived from powder diffraction file (PDF) database of X'Pert software (code no. 01-073-1731). These peaks are not sharp but have a quite broad appearance, suggesting that the HA formed on the scaffold struts has a nano-crystalline nature. The different spectra are shown in **Figure 5.36** and **Figure 5.37**.

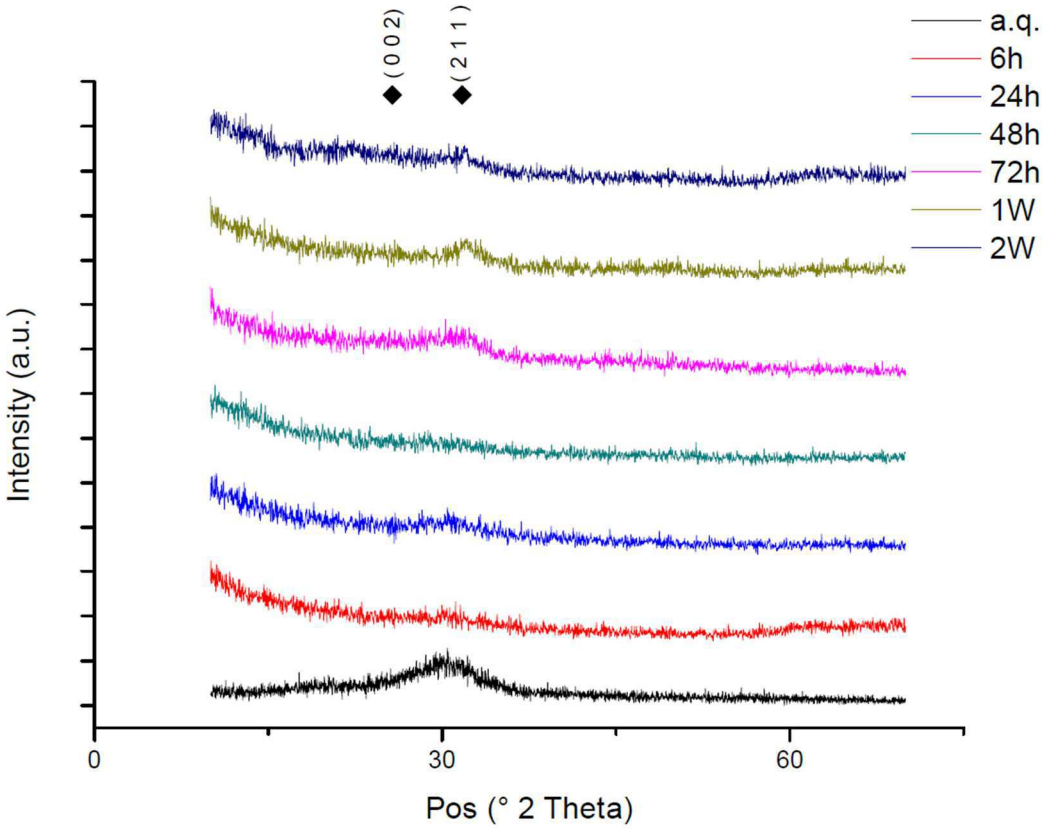

Figure 5.36 Diffraction spectra of 47.5B-G scaffolds after different immersion time in SBF. HA characteristic peaks are indicated by Miller indices (*h k l*). For comparison is also reported the diffraction spectra of 47.5B powders as quenched (a.q.)

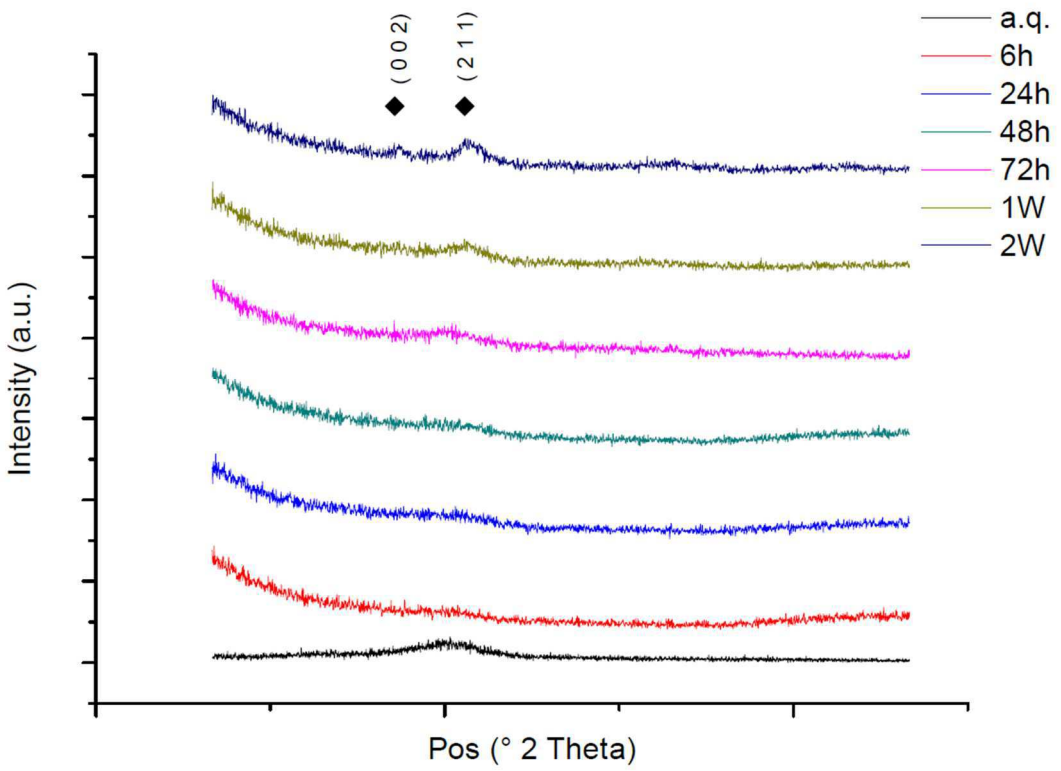

Figure 5.37 Diffraction spectra of 47.5B-M scaffolds after different immersion time in SBF. HA characteristic peaks are indicated by Miller indices (h k l). For comparison is also reported the diffraction spectra of 47.5B powders as quenched (a.q.)

It is not possible to perform any quantitative analysis, but XRD analyses have clearly proven that HA precipitated on both the scaffold types during immersion in SBF.

A better understanding of the in vitro bioactivity mechanism of the 47.5B scaffolds was obtained performing morphological and compositional analyses by SEM and EDS assisted by micro-CT imaging. So, it was possible to investigate the formation of the silica gel, the precipitation of the amorphous calcium-phosphate layer and the nucleation and growth of HA crystals. The EDS was useful to control the atomic ratio Ca/P, to check if the HA formed respected or not the stoichiometric value of 1.67.

For each time points the scaffolds were analyzed in order to obtain information on different levels, such as how the porosity evolved, whether or not the pore became closer or how the surface is modified by the interaction with the SBF. In order to do so, images at different magnitude were taken (500X, 1000X, and 2000/5000X) for each scaffold at different time points.

In figure **Figure 5.38a**, the formation of the silica-gel layer was assessed even for short time immersion, 6 h. It appeared homogeneous on all the surface and it covers all the particles underneath, smoothing the surfaces of the trabeculae. The morphology of the pores is unchanged. The cracks are due to gel drying after removal from SBF.

After 24 h, **Figure 5.38b**, the surface appears rougher and at higher magnification, 2000X and 10000X (**Figure 5.39**), it is possible to see that some large and irregular crystals formed on the glass surface. This newly-formed layer is composed by calcium and phosphorus and will be the precursor of HA. Very small grains were observed covering some areas on the surface, they can be HA nuclei that are already formed.

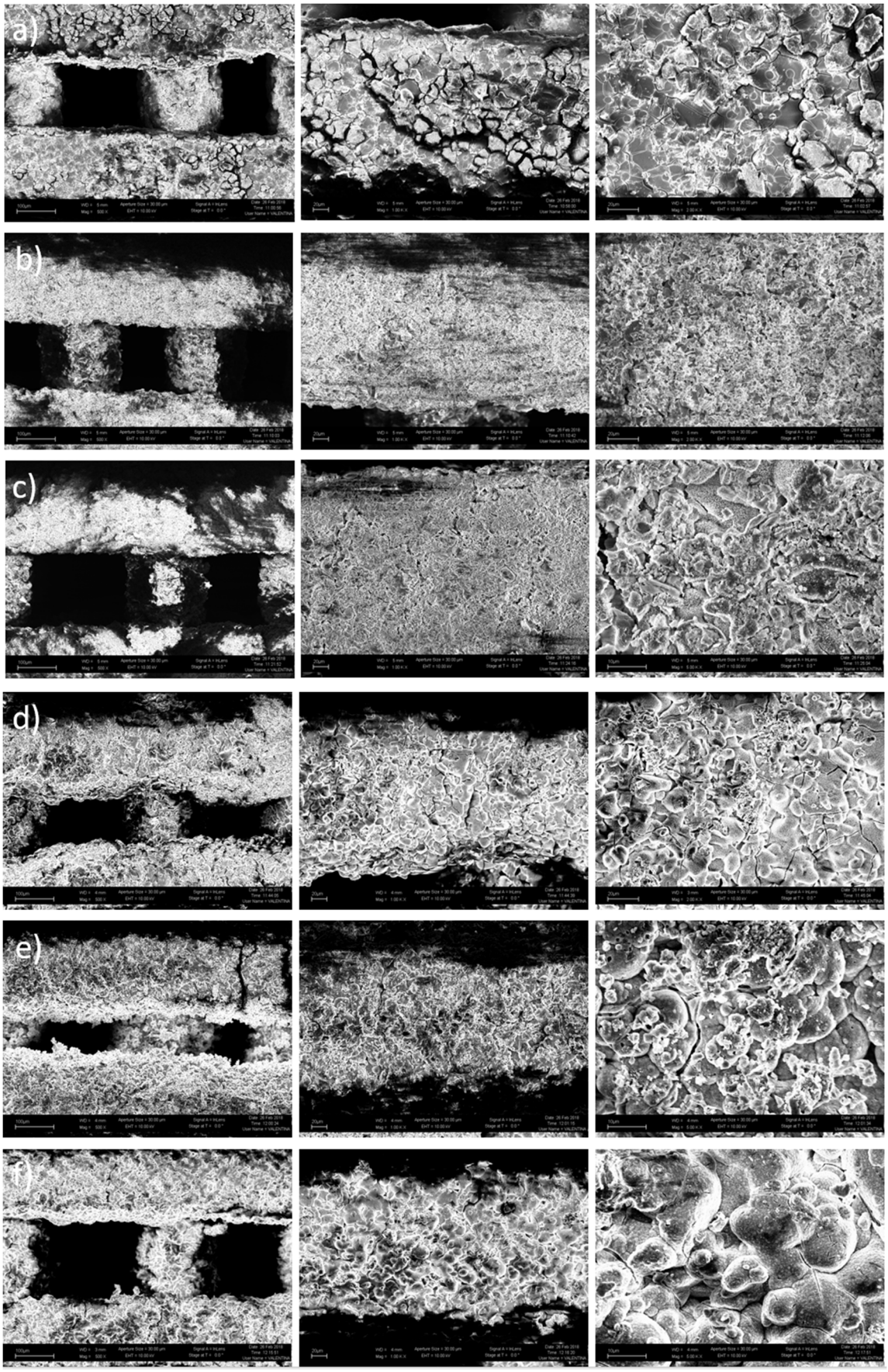

Figure 5.38 Morphological study of 47.5B-G scaffolds after immersion in SBF for different times: a) 6h (500X, 1000X, 2000X); b) 24h (500X, 1000X, 2000X); c) (500X, 1000X, 5000X); d) 72h (500X, 1000X, 2000X); e) 1w (500X, 1000X, 5000X); f) 2w (500X, 1000X, 5000X)

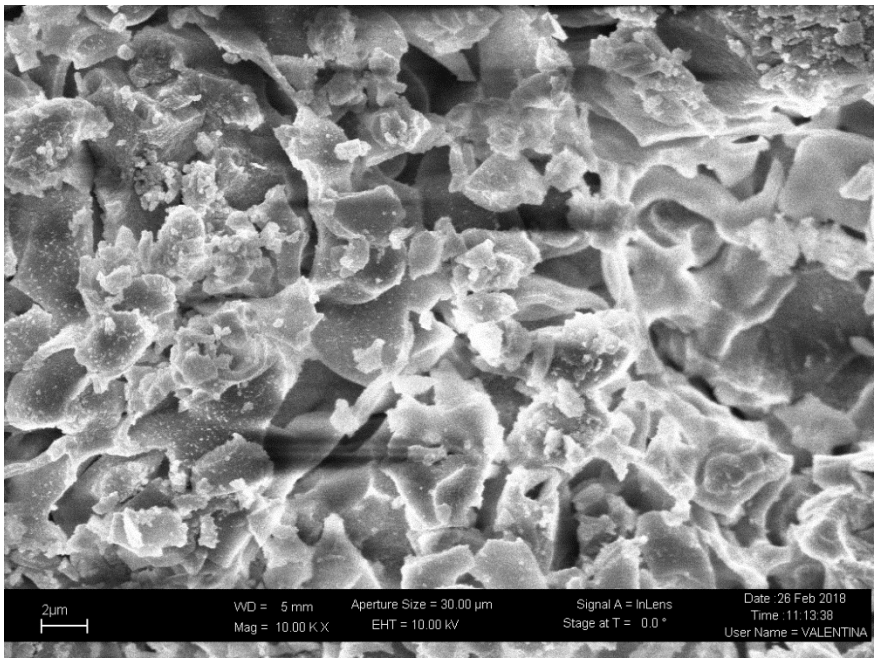

Figure 5.39 High-magnification image (10000X) of the surface of a 47.5B-G scaffold trabeculae after 24 h.

After 48 h (**Figure 5.38c**), the surface is homogeneously covered by acicular crystals and aggregates of them. Those are formed by crystallized HA that started growing on the surface. The cracked morphology of the silica-gel layer is still visible underneath the newly formed crystals (**Figure 5.40**).

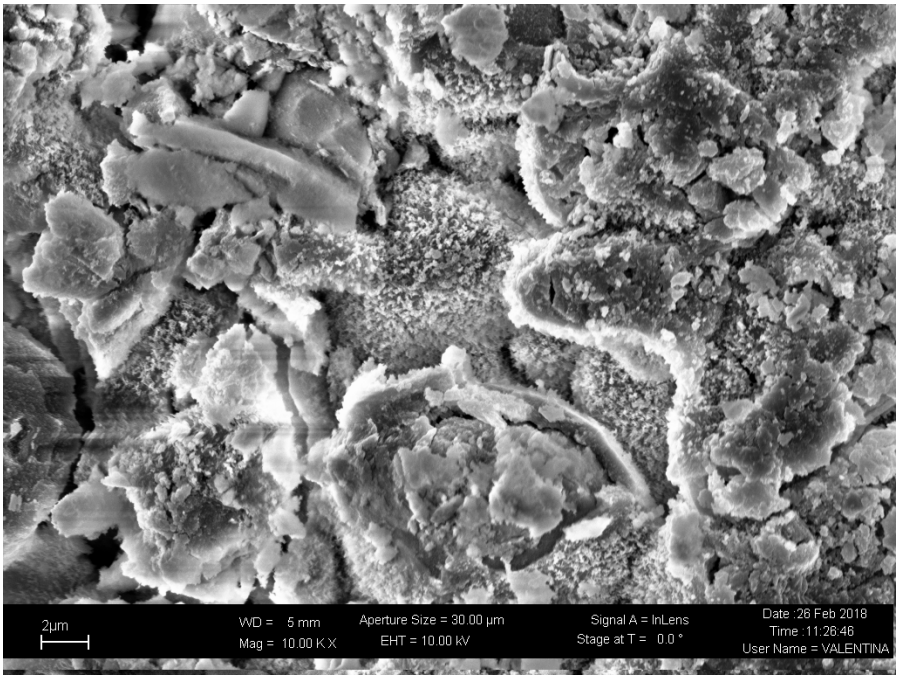

Figure 5.40 Surface of a trabeculae covered by acicular HA crystals after 48 h soaking in SBF (10000X)

After 72 h in SBF, the formation and growth of HA crystals took place all over the surface of the scaffolds and it is clearly visible at quite low magnification, such as 2000X (**Figure 5.38f**). They also started to aggregate, gaining the typical globular shape of HA. The precipitated layer was thicker and it reduced the width of the pores.

During the following two weeks the aggregation and the precipitation processes kept going (**Figure 5.38d-e**). In the end, all the surface of the trabeculae was covered by a continuous layer of crystalline

HA, which showed the characteristic “cauliflower” hierarchical shape. The larger globular crystals are composed by smaller ones (**Figure 5.41a**), and the surface of the latter is composed by nanometric HA spheres (**Figure 5.41b**).

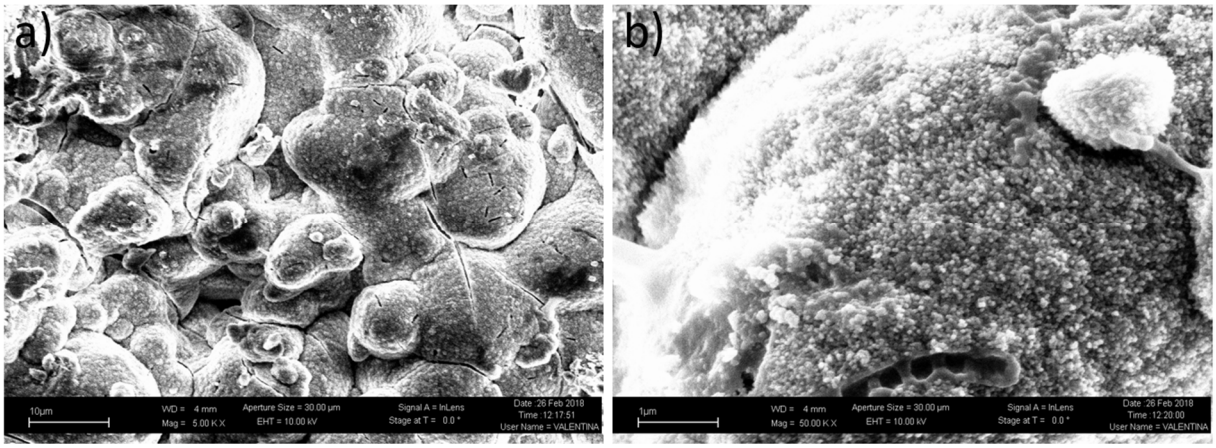

Figure 5.41 High magnification of 47.5B-G trabeculae after 2 weeks in SBF: a) 10000X; b) 50000X

The trabeculae of the specimens that were soaked two weeks seemed thinner with respect to the 1-week sample. Also, the morphology is more similar to the scaffold that was soaked for 72 hours, with smaller HA globular crystals. This could be due to a detachment of the HA layer that has growth during the first week. It may happen if the layer is not well attached to the glass surface or if it reaches a critical thickness, and the detachment can be stimulated by the dynamical condition of the test.

No increase in trabecular thickness was also observed through micro-CT analyses. In fact, the average rod dimension (256 μm) is comparable to the one obtained measuring the struts in the as sintered scaffolds (**Table 5.6**). The image obtained by micro-CT also showed also the presence of two different material phases with different densities. The higher-density phase is brighter with respect to the lower-density one (**Figure 5.42**). Some trabeculae are almost completely dark, while some others are very bright and. interestingly, most rods have a bright core and a dark outer coating. The external region of the rods (lower density) can be associated to reaction layers (silica gel, HA), while the core of the rods (higher density) corresponds to non-converted glass. The apparent density of the calcium-phosphate layer formed on the surface of the glass is relatively low due to the nanoporous nature of this newly-formed phase; however, its density may tend to increase over time as it progressively crystallizes to HA. These observations suggest that the in vitro bioactivity mechanism of these scaffolds is based on a progressive conversion of the glass to HA over time. This hypothesis is strongly supported by previous observation by other authors about robocast 13-93 glass scaffolds soaked in SBF [17]. Some additional considerations can be also presented. The fact that the three different types of trabeculae are present in well-defined areas within the scaffold suggest an inhomogeneous flow of SBF inside the scaffold and that, during the soaking time, the agitation was not enough to make the scaffold move and change position. So, the darker trabeculae were the one that did not touch the bottom of the bottle and received the highest SBF flow. Thus, the glass is almost totally converted into silica gel and HA; the very modest presence of an HA layer here is in accordance to the data recorded during the SEM observation (**Figure 5.41**) and to the hypothesis of a detachment of the HA precipitate during the first week and its consequent reprecipitation. On the lateral side of the scaffold, the trabeculae have a good ratio of glass conversion into silica glass and a well-defined HA layer. It is possible that the walls of the bottle somehow protected the scaffold, which lied in a corner of the bottle bottom during the immersion. The struts in the center and on the bottom of the scaffold are poorly converted due to bad or null flow of SBF within the scaffold. This might lead to a saturation of the solution and to prevent the ions from diffusing from the glass and from activating the bioactive mechanism.

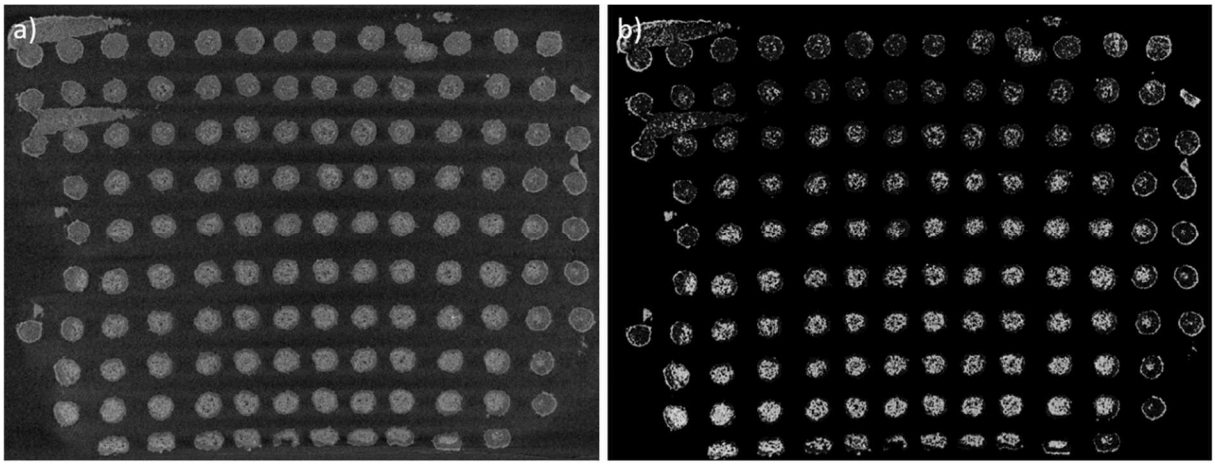

Figure 5.42 Cross-section of a 47.5B-G scaffold soaked into SBF for two weeks obtained by micro-CT: a) standard condition; b) augmented contrast.

A better understanding of the dissolution process of the glass and the HA precipitation was given through the chemical analyses performed by EDS. After 6 h (**Figure 5.43a**), the ratio of the peak intensity of all the elements (but the silicon) to the silicon peak is lower if compared to the one obtained observing the spectra of the as-sintered scaffold (**Figure 5.28**). This fact indicates that the dissolution of the glass, with the formation of the ion-depleted silica-gel layer, has already started. After 24 h (**Figure 5.43b**), the peaks related to Na and K disappeared and the one related to Mg is barely visible. It is possible that the signal came from under the depleted layer. Contrariwise, the Ca and P peaks increased due to the diffusion of calcium and phosphorous ions in the silica-gel layer. With longer immersion times, the intensity of those two peaks increased with respect to the others (**Figure 5.43c-d-e**), indicating the precipitation of more calcium and phosphorous on the scaffolds surface, and eventually the formation of crystalline HA. After two weeks the silica peak appeared again (**Figure 5.43f**). This is in accordance to the fact that the HA layer detached from the surface, exposing to the EDS analysis the material underneath the silica gel and HA layer formed after the removal of the apatite that precipitated firstly.

Another interesting thing, though, is the variation of the ratio between the atomic concentration of Ca and P. In fact, the first apatite that forms on the surface is usually lacking of calcium ions. Only after longer immersion time the stoichiometric Ca/P value of 1.67 is reached [18].

Table 5.11 Atomic concentration of Ca and P and their ratio evaluated on 47.5B-G scaffolds after SBF immersion for different times

Time point	Ca/P
6 h	2.08
24 h	1.09
48 h	1.05
72 h	1.03
1 w	1.33
2 w	3.18

The resulting ratios, calculated as the average of the Ca/P evaluated in three different areas of the sample, are reported in **Table 5.11**. At 6 h, the high Ca/P ratio could be due to the thinness of the silica-gel formed on the surface. Thus, the EDS detector received some signal also from the glass bulk underneath, where the Ca/P ratio is much higher than 1.67. Then the ratio slowly increased during time, as expected, approaching the stoichiometric one. The ratio observed after two weeks is extremely different from the expected one because it was affected from some signal coming from the bulk material and from experimental error due to the highly roughness of the surfaces.

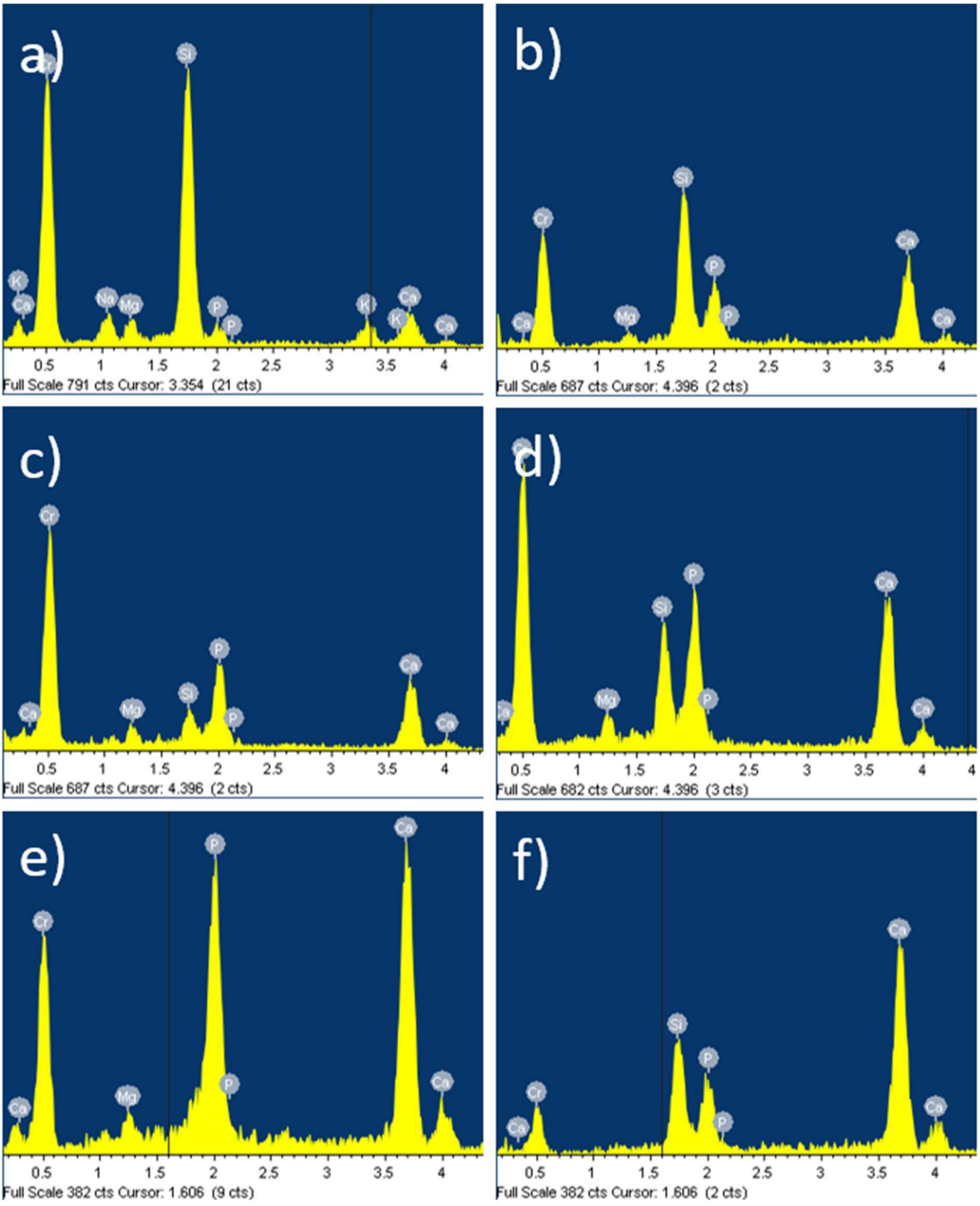

Figure 5.43 EDS spectra obtained from the analyses of 47.5B-G scaffolds after different immersion time in SBF: a) 6h; b) 24h; c) 48h; d)72h; e) 1w; f) 2w.

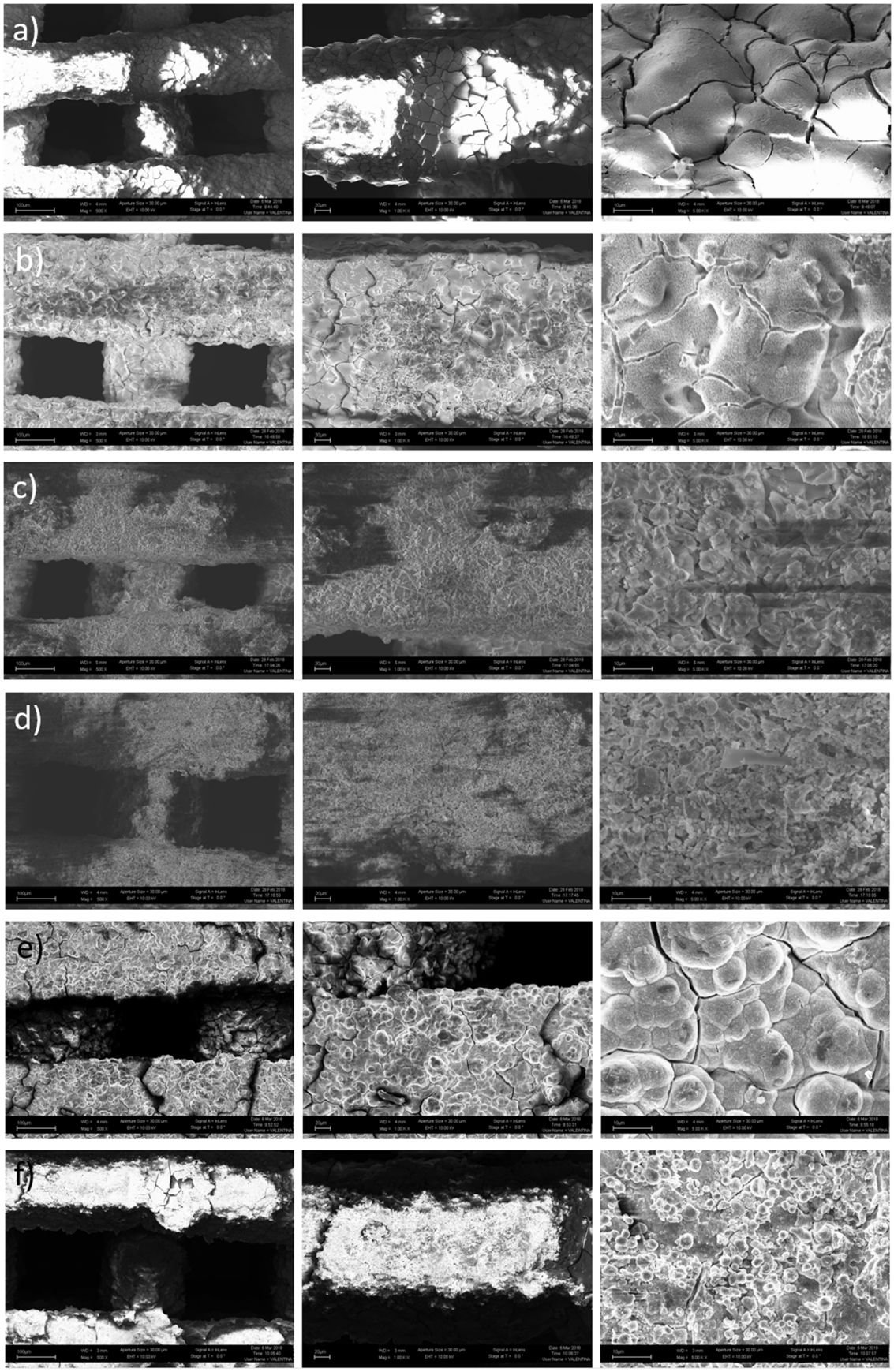

Figure 5.44 38 Morphological study of 47.5B-M scaffolds after immersion in SBF for different times: a) 6h (500X, 1000X, 5000X); b) 24h (500X, 1000X, 5000X); c) (500X, 1000X, 5000X); d) 72h (500X, 1000X, 5000X); e) 1w (500X, 1000X, 5000X); f) 2w (500X, 1000X, 5000X)

The morphological analysis of the monoporous scaffiolds after soaking into SBF did not reveal significant differences between them and the 47.5B-G ones. After six hours is possible to see the formation of the silica-gel (**Figure 5.44a**). The 24-hours soaked sample presented a surface that alternates areas where irregular crystals are preset (**Figure 5.44b**), which can be assessed to be the same Ca-P amorphous crystals observed also on the graded scaffold, and areas that are already well covered in small HA nuclei (**Figure 5.45**).

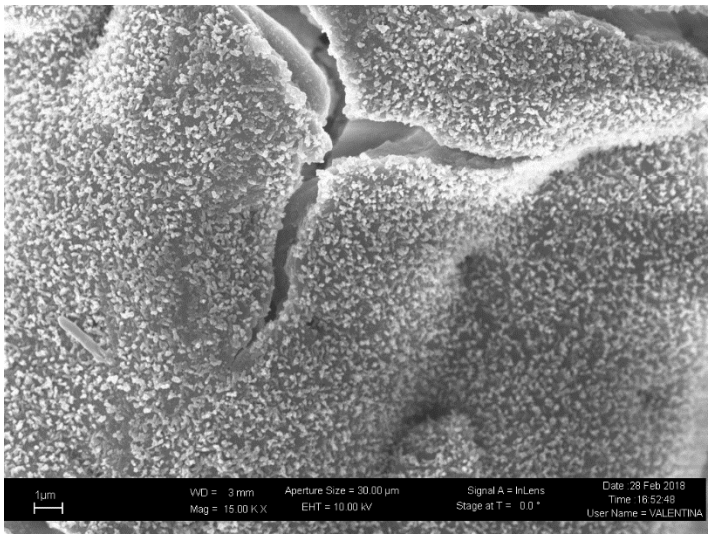

Figure 5.45 Surface of a 47.5B-M trabecula after 24h-soaking. It is homogeneously covered by small HA crystals (15000X)

The layer evolved in a similar manner, with respect to the other porosity design, by formation of acicular HA crystals that grown and joined together to form the large globular crystals typical of HA (**Figure 5.44c-d-e**). After 1 week, the struts are thicker and covered by large "cauliflower" HA aggregates. The surface of those aggregates is covered by nanometric HA spheres (**Figure 5.46**).

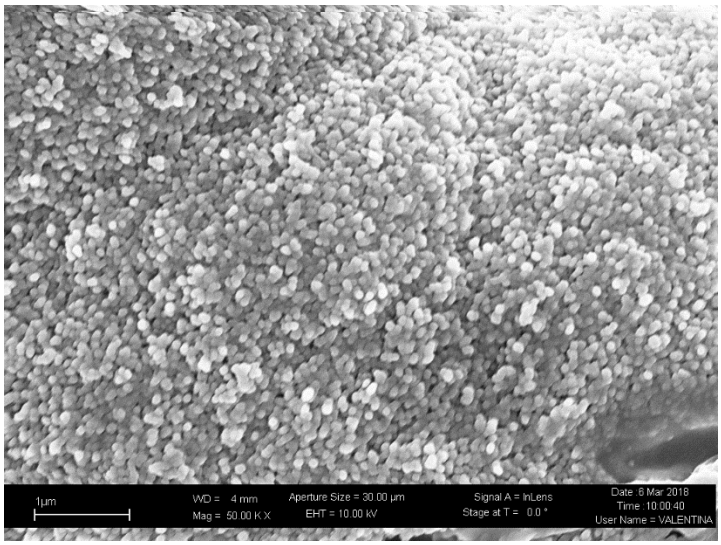

Figure 5.46 Nanometric HA spheres on the surface of a struts after 2-weeks (50000X)

After 2 weeks, no significant thickening of the rods is observed, meaning that the process of detachment of the HA layer, which happened on the graded scaffolds, toke place for those samples too. HA crystals precipitated again on the surfaces, but are smaller with respect to the ones that covered the 1-week specimen, as it is possible to see ad the 5000X magnification image in **Figure 5.44f**.

As in the case of the graded scaffold, the micro-CT analysis of the structure after two weeks highlighted the presence of three different compositions of the struts. Some are mostly converted into silica gel, with a thin layer of HA on the surface (**Figure 5.47**). Those are mostly on the upper part of the scaffold. Then

there are some rods, on the lateral sides of the scaffold, that present a quite thick HA coating and a converted core. The last type represents the trabeculae in the center of the scaffold which are almost unmodified.

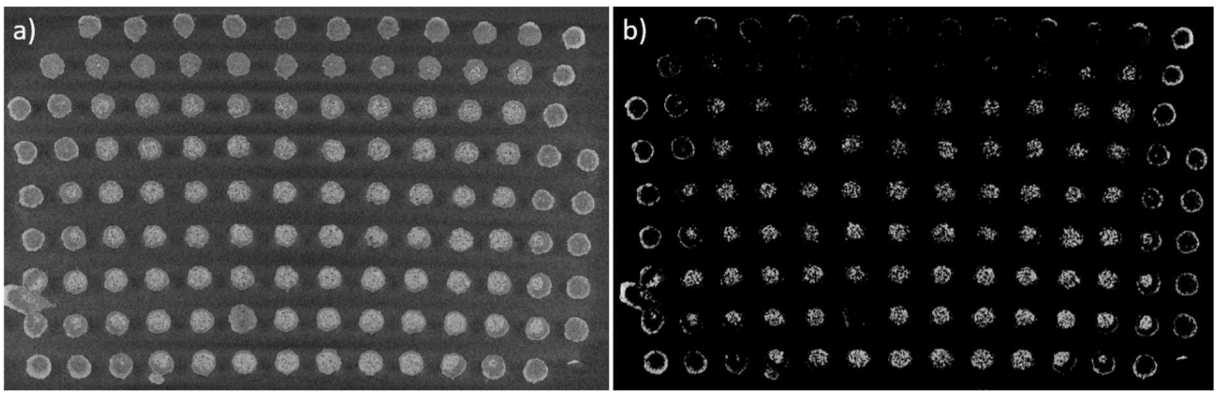

Figure 5.47 Cross-section of a 47.5B-G scaffold soaked into SBF for two weeks obtained by micro-CT: a) standard condition; b) augmented contrast.

The overall structure is very similar to the one observed for the graded scaffold (**Figure 5.42**), suggesting that in both the porosity design the SBF flow is similar and very limited in the center of the samples.

Furthermore, the similarities between the behavior of the two scaffold types are confirmed by the EDS analyses performed on the surface of the 47.5B-M scaffold (**Figure 5.48**). The consideration about the evolution of the surface chemistry of the scaffolds are the same that have been done for the 47.5B-G type. It is possible to see the formation of the ion-depleted silica gel layer after six hours (**Figure 5.48a**). Then the concentrations of calcium and phosphorus increased as the soaking time extended (**Figure 5.48b-c-d**), until the HA layer is thick enough to hide the presence of the silicon underneath after one week (**Figure 5.48e**). The spectrum of the two-week sample (**Figure 5.48f**) showed also the silicon peak due to the detachment mechanism for the outer HA layer, which was previously proposed.

The evolution of the atomic concentration ratio between Ca and P, shown in **Table 5.1**, is very similar to the one observed for the graded scaffold, with the ratio increasing when the immersion time is longer

Table 5.12 Atomic concentration of Ca and P and their ratio evaluated on 47.5B-M scaffolds after SBF immersion for different times

Time point	Ca/P
6 h	0.77
24 h	0.46
48 h	1.29
72 h	1.29
1 w	1.39
2 w	1.47

The ratio measured at 24 hours is lower than expected and it might be affected by some experimental errors during the measurement.

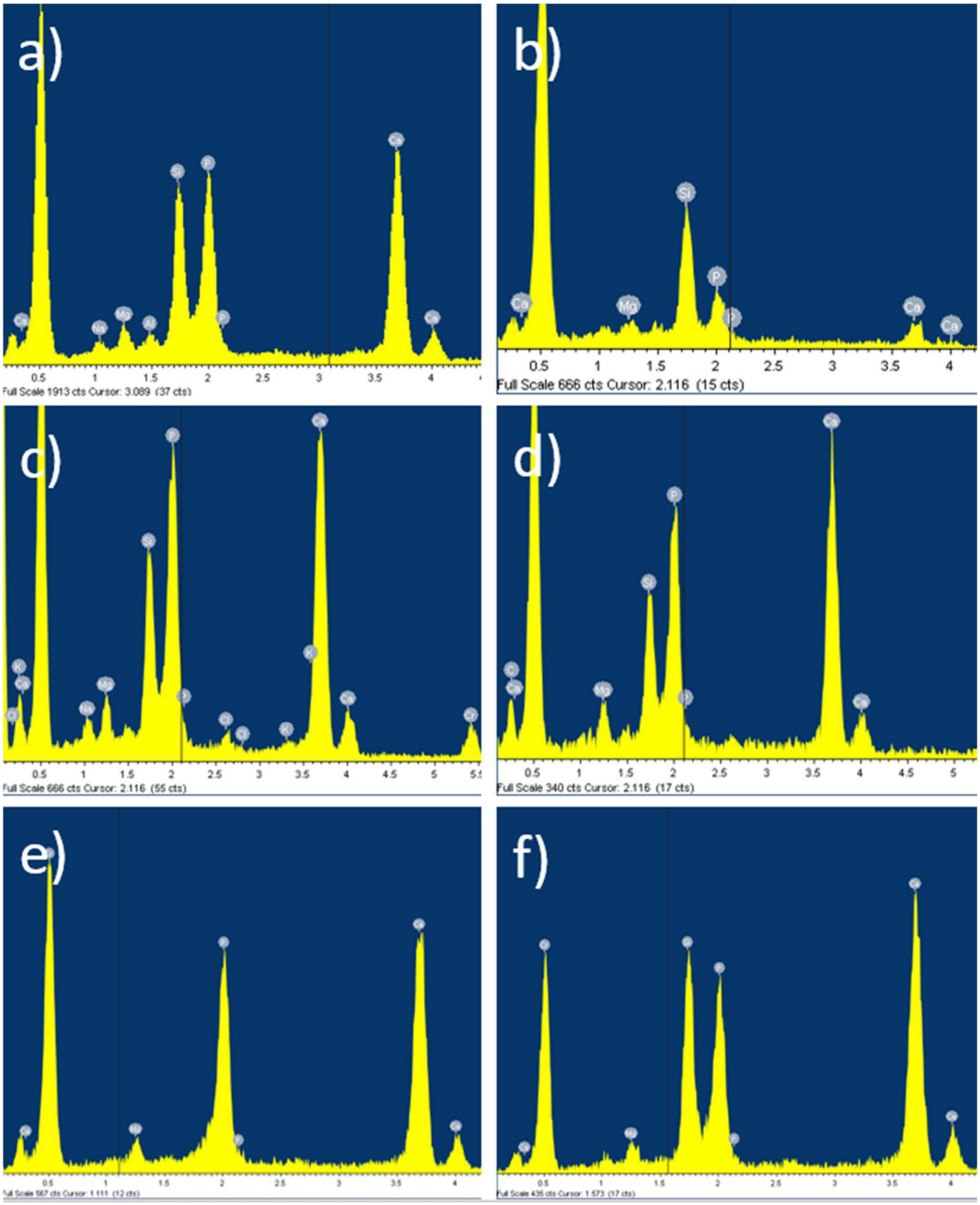

Figure 5.48 EDS spectra obtained from the analyses of 47.5B-M scaffolds after different immersion time in SBF: a) 6h; b) 24h; c) 48h; d)72h; e) 1w; f) 2w.

A section of the 47.5B-M, soaked for two weeks, was also observed to see if there is differential precipitation of HA from the core of the scaffold to the border. The thickness of the trabeculae seemed mostly unchanged, similar to the top struts (**Figure 5.49a**) and the HA layer covered them uniformly (**Figure 5.49b**), while the layer on the top rods was irregular and not uniform (**Figure 5.44f**). This might be related to the fact that the HA layer did not detached from the struts inside the scaffold, more protected from the SBF flow. However, the globular crystals of HA (**Figure 5.49c**) are smaller than the one observed on the top rods after 1 week (**Figure 5.44e**). This fact is in accordance to the hypothesis of a

limited SBF fluid within the scaffold core, resulting in lower refresh of the solution and saturation of it that lead to less HA precipitation.

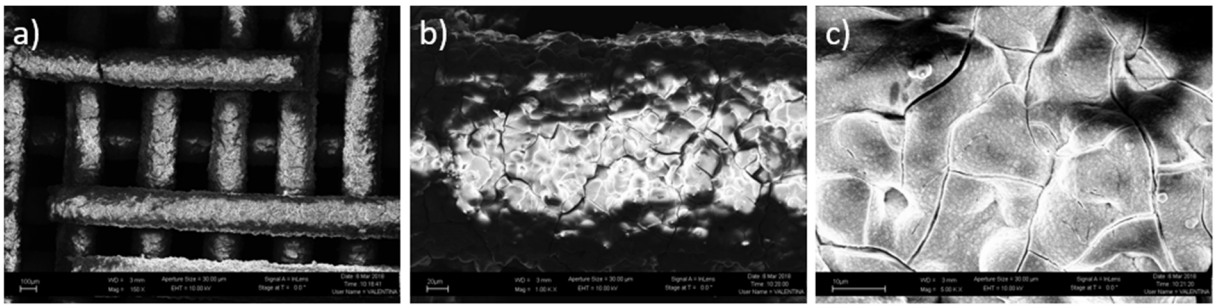

Figure 5.49 Horizontal section of 47.5B-M scaffold after two-week soaking in SBF: a)150X; b)1000X; c) 5000X

The morphological and chemical analyses carried on the 47.5B-G and 47.5B-M scaffolds, soaked for different time in SBF, did not allow to make quantitative statements about differences in the bioactivity of the two different scaffold types, therefore there is no chance to tell if a certain structure is more or less bioactive that the other one. Nevertheless, those analyses showed that both of the scaffolds are bioactive and promote the formation of a good and thick HA layer after short time (7 days). More information about the differences in bioactivity may come by forcing the SBF to flow through the structure, in order to have refresh of the solution also in the core of both the porosity designs.

5.5.2 Ionic dissolution

During the activation and the ongoing of the bioactivity mechanism of a bioactive glass, ions are released from the glass at the beginning and, afterwards, some of them, in particular calcium and phosphorus, will recombine and precipitate on the surface of the glass to form HA. Thus, following the evolution of the ionic concentration of different elements during dissolution test in SBF, it is possible to gain some additional information about the bioactivity mechanism. In particular, what is interesting about that for the developing of this thesis, greater changes in ionic concentration can be related to higher bioactivity. Comparing the values obtained by soaking the two different types of scaffolds, it might be possible to tell if this kind of porosity designs have some influences on the formation of the surface HA layer. This can be mainly related to the different solution flow inside the structure.

Due to the bioactivity mechanism of silicate bioactive glasses, such as 47.5B, it is expected that the concentrations of Na, K, Mg, and Si ions in the testing solution increase during time, while Ca and P shall decrease.

The SBF samples withdrawn from the bottles at each time points were analyzed by ICP-OES and the pH was measured. The concentration changes of the different ions released form the scaffold are shown in **Figure 5.50**. It has been chosen to plot the differences between the concentration of the ions in the solution with scaffolds immersed and pure SBF, used as blank, to show the actual trend of the ionic concentrations released from the scaffolds. Sodium is not reported because its concentration, extremely high within the SBF solution, oversaturated the detector.

The ionic dissolution test showed no significant differences between the dissolution of the graded and the monoporous scaffolds. The ion concentrations are in agreement with what expected. In particular, silicon concentration increased steadily within the first week, when the glass turned itself into silica gel releasing $Si(OH)_4$ and reaches the equilibrium after the glass is covered by HA, which avoids further exchange between the glass and the SBF. Calcium and phosphorus contents within the solution had an increasing and decreasing trend, respectively, all over the time. Specifically, the trend of phosphorus is indicative of the sequestration of phosphate ions from the solution, which means that calcium phosphate – and then HA - precipitates for all the soaking period. This is in good agreement with the SEM and micro-CT observation discussed in paragraph 5.5.1. The behavior of K and Mg concentration is in accordance with the evolution of the silica amount, showing dissolution of the glass within the first week when an almost steady state was reached. The evolution of the ionic concentration, especially the ones of Ca, Si and P, is in agreement with the values that can be fond in literature [19], relative to HA precipitation.

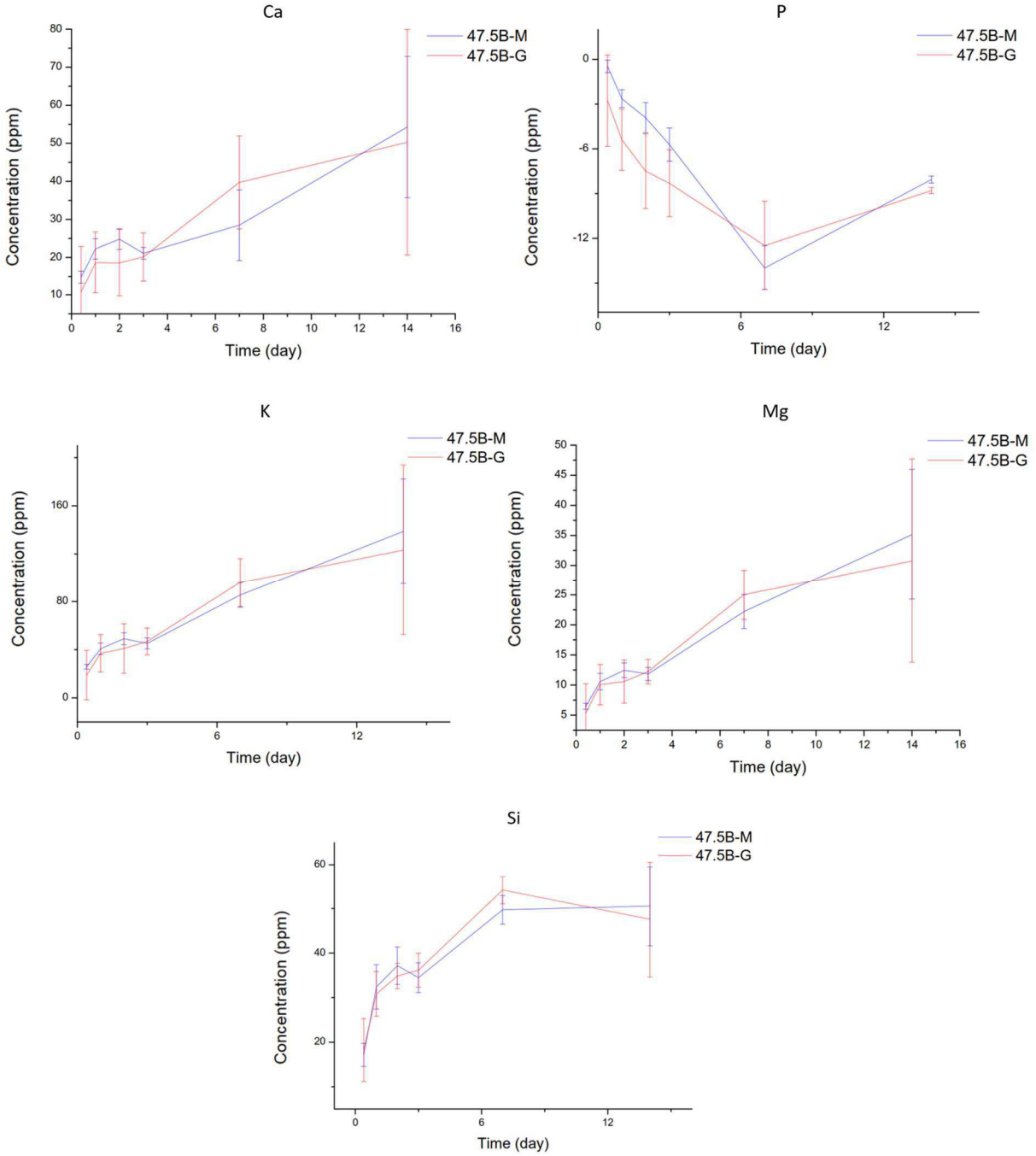

Figure 5.50 Ionic dissolution of bioactive glass scaffold, 47.5B-G and 47.5B-M, in SBF

The pH of the solutions containing the different samples was also measured, in order to have some more information about the scaffold reactivity. In fact, the pH variation is related to the ionic exchange between ions in the glass network and H^+ in the solution. The pH values measured, shown in **Figure 5.51**, showed a similar trend for both the scaffold design, with a rapid increase at short time and then a decrease of the slope of the curves. Since the pH is modified by the ionic exchange between the glass and the solution, once the HA layer starts to form and limit glass-SBF interaction, also the exchange rate decreases. A very little difference can be seen between the 47.5B-G and the 47.5B-M, since the former present value slightly higher than the latter. However, it has to be noticed that the difference in the error bars is lower than the instrument precision (0.02), so they might overlap. The pH of the SBF control was constant for all the time (7.40).

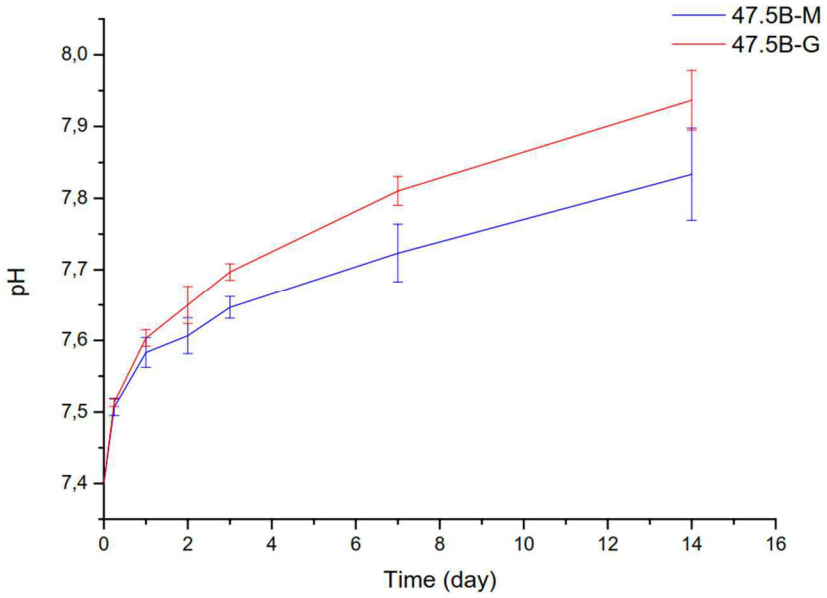

Figure 5.51 pH change of SBF during scaffold soaking

More investigations about the dissolution of the scaffolds were made using data obtained during the evaluation of the mechanical properties evolution. Samples were withdrawn from the bottles used for soaking the scaffolds and the solution was analyzed using ICP-OES. It was chosen not to perform direct confrontation between those value and the ones obtained before because of the different testing condition. The SBF was prepared in two different laboratories (the one used for the mechanical test at Politecnico, the other at TUT), the scaffold preparation was different and the dilution mean was not exactly the same. Anyway, the data collected from the last samples confirmed the absence of significant differences between the graded and the monoporous scaffolds. As it is possible to see in **Table 5.13**, the concentration values for the different ions are superimposable in the graded scaffolds samples and in the monoporous ones, for both 2 and 4 weeks of immersion time. The concentrations of all the ions increase with longer immersion time.

Table 5.13 Ionic dissolution of scaffold, graded and monoporous, soaked for 2 and4 weeks

Immersion time	Scaffold type	Concentration (ppm)									
		Ca		Mg		K		P		Si	
		Average	Std.dev.	Average	Std.dev.	Average	Std.dev.	Average	Std.dev.	Average	Std.dev.
2 weeks	47.5B-G	86.77	2.65	44.32	1.65	222	11.94	16.05	1.95	28.02	4.10
	47.5B-M	83.7	7.28	42.4	4.02	204.02	7.30	15.05	1.31	25.95	2.76
4 weeks	47.5B-G	96.1	5.65	54.1	1.7	251.35	5.44	9	0.42	36.3	0.99
	47.5B-M	101.1	10.76	53.97	13.40	246.8	11.11	4.73	1.65	45.9	4.81

The pH measured showed again no significant differences between the two scaffold types at 2 weeks, but a difference was registered after 4 weeks (**Table 5.14**).

The absence of differences between the two different porosity designs within 2 weeks can be related to the scarce flow of SBF within the core of the scaffolds. Thus, only the outer part of the scaffold, which is very similar in both the kinds, can react with the SBF. It is possible that for longer immersion times the center of the monoporous scaffolds can react more than the one of the graded due to bigger porosity that allows a little bit more of SBF flow.

Table 5.14 pH measured for graded and monoporous scaffold after 2 and 4 weeks

Immersion time	Scaffold type	pH	
		Average	Std.dev.
2 weeks	47.5B-G	7,78	0,05
	47.5B-M	7,78	0,05
4 weeks	47.5B-G	7,71	0,02
	47.5B-M	7,865	0,07

5.5.3 Mechanical properties evolution

When a scaffold is implanted in a load-bearing site, its duty is to be a template for the new bone growth but also it shall mechanically support the surrounding tissue, exactly as a healthy bone would have done. So, the mechanical properties of the scaffold need to be suitable at the moment of the implantation but also have not to decrease too fast during the healing time. In order to have an evaluation of the mechanical properties after implantation, the scaffolds were soaked in SBF for long time, 2 and 4 weeks, and then their compressive strength was assessed.

After being immersed, the scaffolds, all belonging to the first series, were washed with ethanol, dried and then tested by compression test. The results are reported in **Table 5.15**. The results are characterized by a large values distribution, which makes impossible to obtain a clear trend of the compressive strength over time. Furthermore, according to the data recorded in section 5.4.2, no significant difference between the graded and monoporous scaffolds was observed.

Table 5.15 Compressive strength (σ_C) of first-series scaffolds, 47.5B-G and 47.5B-M, after 2 and 4 weeks of immersion in SBF

	2 weeks		4 weeks	
	σ_C (MPa)	**Standard deviation (MPa)**	**σ_C (MPa)**	**Standard deviation (MPa)**
47.5B-G	9.94	7.80	10.44	8.18
47.5B-M	5.6	2.19	3.25	0.73

Despite the absence of differences within the value of compressive strength, the shape of the stress-deformation curve clearly changed after the soaking, after two weeks already and for both the scaffold types. The curve obtained are shown in **Figure 5.52**.

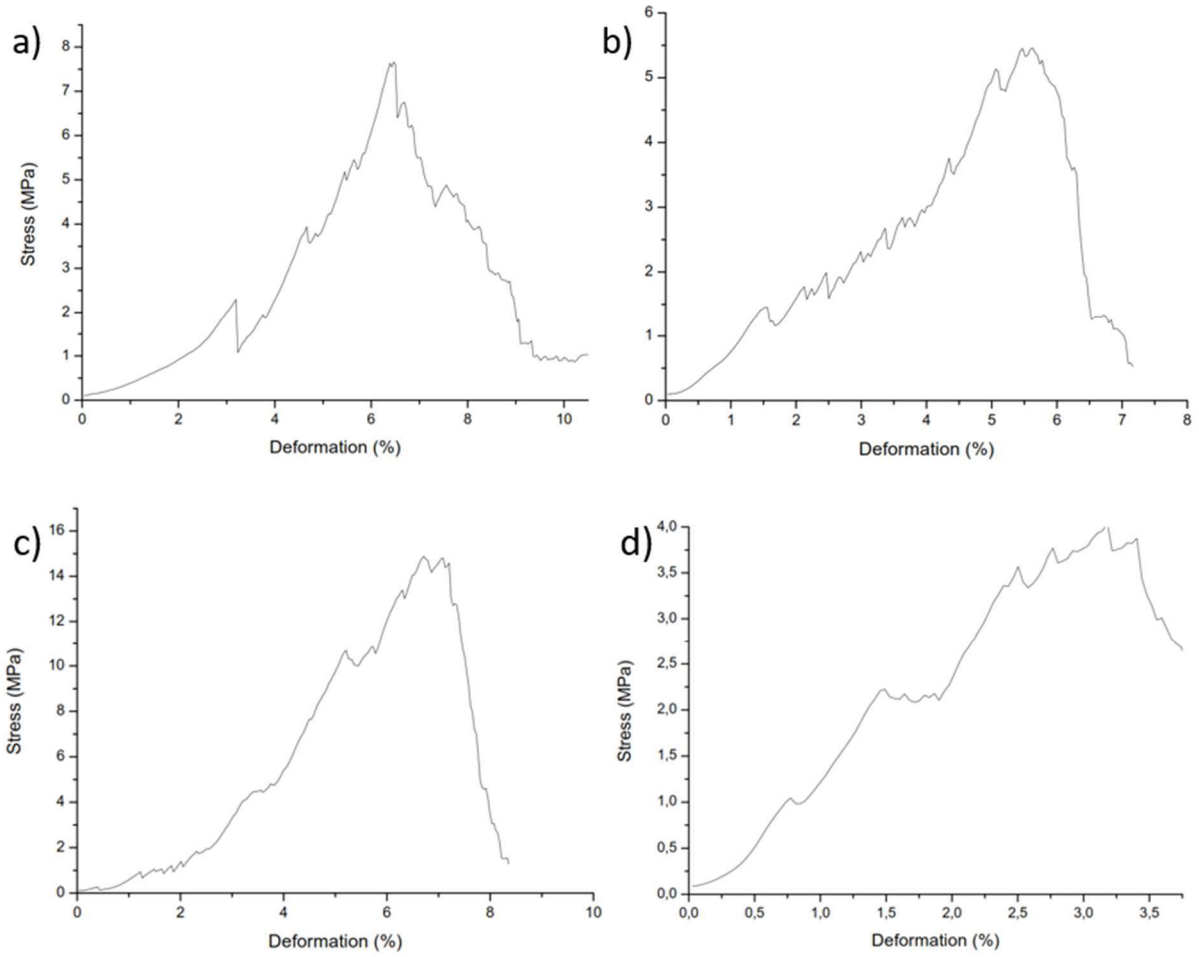

Figure 5.52 Compressive stress-deformation curves obtained for scaffolds soaked in SBF: a) 47.5B-G, 2 weeks; b) 47.5B-M, 2 weeks; c) 47.5B-G, 4 weeks; d) 47.5B-M, 4 weeks

Compared to the curves for as-sintered scaffolds (**Figure 5.33-35**), the scaffold behavior was more similar to brittle materials than to cellular ceramics. The ascendant trend of the curves is more linear and there are less peaks, indicating less fracture events within the samples. This behavior was already recorded in literature: for example, Liu et al. [122] discovered that robocast 13-93 glass scaffolds showed the same embrittlement after being soaked into SBF. Interestingly, in the same study, in vivo tests showed that the scaffolds acquired elastic properties after implantation, deforming themselves instead of scattering into pieces during compression tests. They also confirmed that the compressive strength of the scaffold decreases over time, but not in a drastic manner. This fact can explain why the results obtained during this work are so similar, other than the large values distribution. The values of compressive tests obtained after treatment in SBF are still lying within the typical range of cancellous bone and both types of prepared scaffolds are expected to be strong enough for ensuring adequate support to the regenerated tissue in an in vivo scenario.

5.6 Bibliography

[1] A. Nommeots-Nomm, P. Leeb and J. Jones, "Direct ink writing of highly bioactive glasses," *Journal of the European Ceramic Society,* p. http://dx.doi.org/10.1016/j.jeurceramsoc.2017.08.006, 2017.

[2] O. Peitl Filho, G. La Torre and L. Hench, "Effect of crystallisation on apatite-layer formation of bioactive glass 45S5," *Journal of Biomedical Materials Research,* vol. 30, pp. 509-514, 1996.

[3] E. Verné, O. Bretcanu, C. Balagna, C. Bianchi, M. Cannas, S. Gatti and Vi, "Early stage reactivity and in vitro behavior of silica-based bioactive glasses and glass-ceramics," *Journal of Material Science: Materials in Medicine,* vol. 20, pp. 75-87, 2008.

[4] M. Pascual, A. Duran and M. Prado, "A new method for determining fixed fiscosity points of glasses," *PHysics and Chemistry of Glasses,* vol. 46, pp. 512-520, 2005.

[5] M. N. Rahaman, Ceramic processing and sintering, II ed., CRC Press, 2003.

[6] M. Davis and I. Mitra, "Crystallization measurments usign DTA methods: applications to Zerodur," *Journal of America Chemistry Society,* vol. 86, pp. 1540-1546, 2003.

[7] Q. Fu, E. Saiz and A. Tomsia, "Direct ink writing of highly porous and strong glass scaffolds for load-bearing," *Acta Biomaterial,* vol. 7, pp. 3547-3554, 2011.

[8] L.-C. Gerhard and A. R. Boccaccini, "Bioactive Glass and Glass-Ceramic Scaffolds for Bone Tissue Engineering," vol. 3, pp. 3867-3910, 2010.

[9] V. Karageprogiu and D. Kaplan, "Porosity of 3D biomaterial scaffold and osteogenesis," *Biomaterials,* vol. 26, pp. 5474-5491, 2005.

[10] Q. Fu, E. Saiz, M. N. Rahaman and A. P. Tomsia, "Bioactive glass scaffold for bone tissue engineering: state of the art and future perspectives," pp. 1245-1256, 2011.

[11] P. Miranda, A. Pajares, E. Saiz, A. Tomsia and F. Guiberteau, "Mechanical properties of calcium phosphate scaffolds fabbricated by robocasting," *Journal of Biomedical Materials,* vol. 85, pp. 218-227, 2008.

[12] F. Martinez-Vazquez, F. Perera, P. Miranda, A. Pajares and F. Guiberteau, "Improving the compressive strenght of bioceramic robocast scaffolds by polymer infiltration," *Acta Biomater,* vol. 6, pp. 4361-4368, 2010.

[13] Y. Shanjani, Y. Hu, R. Pilliar and E. Toyserkani, "Mechanical characteristics of solid-freeform-fabricated porous calcium polyphosphate structures with oriented stacked layers," *Acta Biomater,* vol. 7, pp. 1788-1796, 2011.

[14] J. Franco, P. Hunger, M. Launey, A. Tomsia and E. Saiz, "Direct write assembly of calcium phosphate scaffolds using a water-based hydrogel," *Acta Biomaterialia,* vol. 6, pp. 218-228, 2010.

[15] X. Liu, M. Rahaman, G. Hilmas and B. Bal, "Mechanical properties of bioactive glass (13-93) scaffolds fabricated by robotic deposition for structural bone repair," *Acta Biomater,* vol. 9, pp. 7025-7034, 2013.

[16] T. Kokubo and H. Takadama, "How usefull is SBF in predicting in vivo bone bioactivity?," *Biomaterials,* vol. 27, pp. 2907-2915, 2006.

[17] X. Liu, M. Rahaman, G. Hilmas and B. B.S., "Mechanical properties of bioactive glass (13-93) scaffolds fabricated," vol. 9, pp. 7025-7034, 2013.

[18] F. Baino, M. Marshall, N. Kirk and C. Vitale-Brovarone, "Design, selection and characterization of novel glasses and glass-ceramics for use in prosthetic applications," *Ceramics International,* vol. 42, pp. 1482-1491, 2016.

[19] A. Nommeots-Nomm, S. Labbaf, A. Devlin, N. Todd, H. Geng, A. Solanki, H. Man Tang, P. Perdika, A. Pinna, F. Ejeian, O. Tsigkou, P. Lee, M. Esfahani, C. Mithcel and J. Jones, "Highly degradable porous melt-derived bioactive glass foam scaffolds for bone regeneration," *Acta Biomaterialia,* vol. 57, pp. 449-431, 2017.

6 Conclusion and future perspectives

This thesis was born with the aim to produce highly-bioactive, fully amorphous scaffolds for bone regeneration using bioactive glass and an innovative additive manufacturing technique, the robocasting. This technique was chosen because it offers the possibility of achieving very controlled and regular structure with a rather simple method. The feasibility of manufacturing scaffolds with porosity controlled at the smallest level suitable for bone regeneration (100 μm) was investigated, along with the possibility of obtaining structure with different pore size distributions. At last, a comparison between two different porosities design was tired, in term of bioactivity and mechanical properties.

Firstly, the thermal properties of the 47.5B glass, developed by prof. E. Verné at Politecnico di Torino, were completely characterized. In fact, it was necessary to understand its thermal behavior to optimize the sintering process. In order to avoid crystallization of the scaffolds during sintering, the crystallization of the glass was carefully investigated. The glass was shown to possess great sintering properties, in fact it has a wide range of possible temperatures for thermal treatment that do not lead to crystallization of the glass. The temperature chosen to sinter the scaffold during this work (600°C) is quite conservative and it might be increased, still maintaining the amorphous structure.

It was demonstrated that it is possible to obtain scaffolds with very small porosities, the smallest suitable for bone regeneration (≈100 μm), with a process that does not involve the use of ultra-fine powders, very thin nozzles and complex ink preparation. Similar dimensional results are present in literature, but they used much more complex processes, in terms of powder production and printer set-up. The powders used (φ<32 μm) are easily achievable by simple ball-milling, and, with respect to much smaller powder used in literature, their manipulation is more safe and requires less precautions for health. This is important if thinking about an industrial upscaling of the scaffold manufacturing, because it requires less complex manufacturing and less safety issues in the handling of the powders. Using bigger nozzles means that the printing process is less prone to interruptions caused by clogging of it, due to drying of the ink or aggregates into it. Since good results were achieved by a fully manual preparation of the ink, it is believed that better ones might be gained automating the process, at least in some part of it, such as the removal of the air bubbles.

The robocasting process has been proved, once the process parameters, i.e. ink composition, are optimized, to give high control on the dimensional features, with high repeatability of the process. It was also very easy to obtain different porosity design. Morphological and structural analyses confirmed the regularity of the scaffold structures and that pores with the desired size were obtained (≈200 μm and ≈100 μm). With those kind of pores two different scaffold types were obtained, one with pores that have the same dimensions (≈200 μm), the other with two-sized pores, smaller ones (≈100 μm) in the center of the structure and larger on the borders (≈200 μm). It was also possible to analyze the microstructure of the trabeculae, evaluating the sintering level. It was found that two microstructures were produced. The first showed a low level of sintering, as expected from the low sintering temperature. The particles were distinguishable and connected by sintering neck, forming a microporosity network inside the rods. The second microstructure, which appeared on scaffolds sintered during the last printing sessions, had a much denser structure, with a higher level of sintering. This fact might be related to some errors during the manufacturing process that were not possible to investigate due to lack of time. All the comparison made during the characterization of the scaffold properties consider only scaffold belonging to the first series.

Mechanical properties were not of specific interest during the developing of the present work, so the process, especially the sintering, was not optimized to obtain high strength. Nevertheless, it was interesting to test them in order to investigate if they can be used for load-bearing site applications. The resistance of the scaffold (6-9 MPa) has been proven to be in the range of the trabecular bone (0.1-16 MPa). Also, the Weibull modulus was investigated as index of repeatability of the manufacturing process. The modulus obtained by testing graded scaffold was modest (m=3.139) but in the range of the ones at disposal in literature for bioceramic scaffolds (3-9). The modulus can be increased by optimizing the manufacturing process, in particular the air removal from the ink. Also, a narrow result distribution might be obtained by increasing the sintering level. Thus, the defect size distribution within the

trabeculae will decrease and the void will be rounder, decreasing the stress intensification effect typical of sharp defects. Due to large distribution of compressive values obtained for all the scaffold tested, graded or monoporous, first or second series, no significant differences between the different scaffold types produced was detected. Deeper investigation about the effect of different porosity design could be necessary to improve the design process of 3D-printed scaffold, in order to obtain very controlled properties.

In vitro bioactivity of the scaffold was tested to investigate possible difference between the porosity design of the scaffolds. Morphological and chemical observations recorded no differences between the two types. In both the scaffolds there was a good precipitation of HA on the surface of the trabeculae and thick and dense layer of apatite formed on the glass surfaces. However, these analyses showed that only the outer part of the scaffolds was interested by SBF flow, leading to low reaction inside the core of the scaffolds, where there are the greater differences in porosity dimension.

The analyses of the ions released by the glass during the immersion in SBF, and the pH evolution of the solution, were in accordance to the results obtained by the morphological analyses of the scaffolds. In fact, they showed that there was ionic exchange between the glass and the solution and HA precipitation, concentration of Si, Ca, Mg, K and P evolved accordingly to literature. Also, the increase of the pH confirms that H^+ ions migrated from the solution to the glass. However, no differences between the graded and the monoporous scaffolds was recorded until soaking for 4 weeks. This was attributed to the scarce SBF flow within the scaffolds center, where there exist most differences between the two designs. During 4 weeks, some more reactions might happen in the core of the monoporous scaffolds due to larger porosity, with respect to the graded one.

The in vitro evolution of mechanical resistance of the scaffold was eventually tested. Due to large values distribution it was not possible to quantify the decreasing of the compressive strength of the scaffolds or tell what kind of scaffolds shown the worst worsening. Instead, it was seen that after immersion the scaffolds became more brittle, with more regular stress-deformation curves. This fact was already observed in literature. Anyway, also after 4 weeks in SBF, all the scaffolds have been proven suitable for load-bearing site application.

Some suggestions for the future developments of this research might be:

- Optimization of the scaffold printing process: the acceptable results obtained during this work can be increased by optimizing some step of the process. The repeatability and the final properties of the scaffold, in particular in mechanical properties, might be increased by pushing the air removal from the ink, maybe using some instrument, such as void pump. To control the temperature and the humidity of the environment were the ink is prepared and the scaffold are printed can lead to more constant final results. This will have effect mainly on the viscosity of the ink and on the drying and shrinkage of the scaffold during printing. The data suggest also that the sintering can be increased, while still avoiding the crystallization of the glass. Doing so, the mechanical properties might be increased.
- Study of the porosity design effect: once the process is optimized and the results obtained present a narrower distribution, deeper studies about the role of the porosity on the scaffold properties, such as mechanical or bioactivity, shall be conducted.
- Improved bioactivity tests: with the standard method, it was not possible to appreciate the differences of bioactivity caused by the different porosity designs because the core of the scaffold was very little interested by the test. Therefore, it seems necessary the development of novel test protocols, for 3D scaffolds, that possess the ability of stimulate the scaffold in its entirety, for example by forcing the SBF to flow through the structure.

Acknowledgements

First of all, I would like to thank prof. Enrica Vern for giving me opportunity of working about this topic and for making me flying to Finland.

My deeper and sincere thanks are addressed to Francesco Baino, that followed and guided me through the developing of this thesis, showing endless patient and availability for everything I needed.

Thanks to all the Glance group that received and helped me with daily lab work. In particular I would like to thank Domenico and Elisa, for making the work funnier.

Thank also to professor Jonathan Massera, from the Technological University of Tampere, for welcoming me during my staying abroad, and to all his group: Amy, for introducing me to the interesting world of robocasting, Ayush, Inari, Jenna and Gloria for sharing some lab time in the gray Finnish autumn.

A special thought goes to Lu, Matte and Lollo, that share with me the experience of being abroad for making our thesis, and who always stay close to me, making me feeling all their love even while being separate by a couple of oceans. I want to thank also all the wonderful people that made amazing the time spend at Politecnico: Marina, Andy, Cami, Alea, Aleo, Franz, Ale and all the others. My university experience wouldn't have been the same without you. And thanks to everyone shared time with me out of the classrooms: Pomi, Tato, Ica, Summa, Chiara e Ale.

Immense gratitude is for my family, that supported me all the way through those years, allowing me to make beautiful and important experience.

In the end, I would like to thank my girlfriend, Elisa, that was always close to me and never gave her support away from me. I love you.

Thanks to every one of you, this work wouldn't have been the same without each one.

Jacopo Barberi